Radiative Capture and Decays in *Ab Initio* Nuclear Theory

by

Peter Gysbers

B.Sc., McMaster University, 2017

A THESIS SUBMITTED IN PARTIAL FULFILLMENT
OF THE REQUIREMENTS FOR THE DEGREE OF

Doctor of Philosophy

in

THE FACULTY OF GRADUATE AND POSTDOCTORAL STUDIES
(Physics)

The University of British Columbia
(Vancouver)

March 2023

The following individuals certify that they have read, and recommend to the Faculty of Graduate and Postdoctoral Studies for acceptance, the thesis entitled:

Radiative Capture and Decays in *Ab Initio* Nuclear Theory

submitted by **Peter Gysbers** in partial fulfillment of the requirements for the degree of **Doctor of Philosophy** in **Physics**.

Examining Committee:

Petr Navrátil, Research Scientist, TRIUMF
Co-supervisor

Reiner Kruecken, Adjunct Professor, Physics and Astronomy, UBC
Co-supervisor

Mark Thachuk, Professor, Chemistry, UBC
University Examiner

Joanna Karczmarek, Professor, Physics and Astronomy, UBC
University Examiner

Mona Berciu, Professor, Physics and Astronomy, UBC
Supervisory Committee Member

Additional Supervisory Committee Members:

Rob Kiefl, Professor, Physics and Astronomy, UBC
Supervisory Committee Member

Fei Zhou, Professor, Physics and Astronomy, UBC
Supervisory Commitee Member

Abstract

Atomic nuclei exhibit many phenomena not limited to excited states, decays, reactions, and clustering. Nuclear processes control the evolution of stars and explain the abundances of chemical elements in the universe. Nuclear physics can be used to answer fundamental questions about underlying particle physics and cosmology, such as the symmetry between matter and antimatter or the nature of neutrinos. The discrepancy between theoretical predictions and observations motivates improved theory and can provide evidence for new physics. A predictive model of nuclei is needed as input for experimental tests and for astrophysical models.

Nuclei are complex strongly-interacting quantum many-body systems. Accurate theoretical techniques are required to predict the rate of nuclear decay processes, the cross section of nuclear reactions and the distribution of the emitted particles. *Ab initio* nuclear theory takes advantage of the recent rapid increase in computing power to calculate nuclear structure and reactions solely from realistic interactions between the constituent nucleons.

In this thesis, we first present beta-decay calculations using the *ab initio* no-core shell model. Our calculations provide an explanation for the quenching of Gamow-Teller beta-decays, provide nuclear structure corrections to the beta-spectrum necessary to interpret experiments seeking to find new physics and provide estimates for the hypothetical process of neutrinoless double-beta decay. Second, we present radiative capture calculations using the no-core shell model with continuum, an extension which places bound and scattering states on equal footing. The rate of radiative capture reactions in big bang nucleosynthesis is required to estimate the abundance of isotopes in the early universe. In addition, anomalies in recent radiative capture experiments claim the discovery of a new boson. Comparing to these experiments requires prediction of the distribution of electron-positron pairs produced by radiative capture.

Lay Summary

The components of the atomic nucleus are protons and neutrons. The numbers of these particles determine the characteristics of the nucleus. For example, adding one more proton or neutron can destabilize the nucleus and cause it to decay. There are many types of decays which emit different particles. From measurements of decay rates and decay products, we can refine our understanding of the known fundamental forces or find new forces.

Accurate theoretical predictions are needed which can be compared to observations. In this thesis, we use sophisticated computational techniques to predict the properties of many different nuclei and the rates of their varied decay modes. We also predict the rate of nuclear reactions corresponding to recent measurements with unexplained anomalies. The discrepancies between theory and experiment point the way towards refinement of theoretical models or may provide evidence for new physics.

Preface

This work is based on published and unpublished material. Chapter 1 introduces the field of nuclear physics, defines *ab initio* nuclear theory and outlines the thesis. Chapter 2, Chapter 3 and Chapter 4 are based on common literature and describe the mathematical and computational tools used in our calculations. Chapter 5 presents results which were originally published in [1–3], with the exception of Section 5.2.2 which is original unpublished material. Chapter 6 provides the theoretical basis for the following chapter. The first two sections are based on common literature, while the second two are original expository material. The first section of Chapter 7 presents results which were originally published in [4], while the second section presents original unpublished material.

- The results of Section 5.1.1 were previously published in

  [1] **P. Gysbers**, G. Hagen, J.D. Holt, G.R. Jansen, T.D. Morris, P. Navrátil, T. Papenbrock, S. Quaglioni, A. Schwenk, S.R. Stroberg, K.A. Wendt, Nat. Phys. **15** (5) (2019) 428–431.

  G.H., T.D.M. and T.P. performed the coupled-cluster calculations. G.R.J. computed three- nucleon forces for the coupled-cluster calculations. P.G., S.Q., P.N. and K.A.W. performed calculations for the two-body currents. P.N. developed the higher-precision chiral three- nucleon interactions used in this work and performed no-core shell model calculations. G.H. and T.D.M. derived and implemented the new formalism to incorporate higher- order excitations in coupled-cluster theory. S.R.S. and J.D.H. performed VS-IMSRG calculations. All authors discussed the results and contributed to the manuscript at all stages.

- The results of Section 5.1.2 were previously published in

  [2] A. Glick-Magid, C. Forssén, D. Gazda, D. Gazit, **P. Gysbers**, and P. Navrátil, Phys. Lett. B **832**, 137259 (2022).

  A. G. was the principal author of the manuscript. A. G. and D. G.(2) derived the expressions for the nuclear structure corrections. D. G.(1) and C. F. developed the

momentum-dependent operators. P. N. developed the formalism for translationally-invariant operators and densities. P. G. implemented and tested the operators in the no-core shell model. All authors discussed the results and edited the manuscript.

- The results of Section 5.2.1 were previously published in

  [3] S. Novario, **P. Gysbers**, J. Engel, G. Hagen, G. R. Jansen, T. D. Morris, P. Navrátil, T. Papenbrock, and S. Quaglioni, Phys. Rev. Lett. **126**, 182502 (2021).

  S. N. was the principle author of the manuscript. S. N., G. H., G. R. J., T. D. M. and T. P. performed the coupled cluster calculations and contributed to the development of improved coupled cluster methods and codes. J. E. provided the radial parts of the neutrino-less double beta decay matrix elements. P. G. implemented the double beta decay operators and performed the no-core shell model calculations with the assistance of P. N. and S. Q..

- The results of Section 5.2.2 are unpublished. This work was performed in collaboration with T. Miyagi, P. Navrátil, S. Quaglioni, J. Engel and S. R. Stroberg.

  J. E. provided the radial parts of the neutrino-less double beta decay matrix elements. P. G. implemented the double beta decay matrix operators and the SRG evolution of 3-body operators in the no-core shell model with assistance from P.N. and S.Q.. T.M. developed SRG evolution technology within the IMSRG with assistance from S.R.S.. Calculations were performed by P.G. and T.M..

- The results of Section 7.1 were previously published in

  [4] C. Hebborn, G. Hupin, K. Kravvaris, S. Quaglioni, P. Navrátil and **P. Gysbers**, Phys. Rev. Lett. **129** 042503 (2022).

  C. H. was the principal author of the manuscript, and further improved the capabilities of the NCSMC codes for two-nucleon projectiles. This was based on previous development by G.H., P.N. and S.Q. and assisted by K.K.. P.G. performed the SRG evolution of the electromagnetic operators and benchmarked the contributions to NCSMC transition matrix elements. All authors discussed the results and edited the manuscript.

Table of Contents

List of Tables

List of Figures

List of Abbreviations

$0\nu\beta\beta$ neutrino-less double beta decay

$2\nu\beta\beta$ two-neutrino double beta decay

2BC two-body current

3N three-nucleon

χ**EFT** chiral effective field theory

BSM beyond the Standard Model

CC Coupled-Cluster

CG Clebsch-Gordan

EFT effective field theory

F Fermi: a type of β-decay with $\Delta J = 0$

GT Gamow-Teller: a type of β-decay with $\Delta J = 1$

IMSRG In-Medium Similarity Renormalization Group

LEC low-energy constant

NCSM No-Core Shell Model

NCSMC No-Core Shell Model with Continuum

NME nuclear matrix element

NN nucleon-nucleon

OBDME one-body transition density matrix element

RGM resonating-group method

SD Slater Determinant

SM Standard Model

SRG Similarity Renormalization Group

Acknowledgements

I am thankful for the many individuals who helped me through this degree.

Of greatest influence was Petr Navrátil, who guided me through many projects, starting with a co-op position during my undergraduate degree. I am very grateful for Petr's patience and mentorship, lending technical expertise when I ran into problems and granting many opportunities to present my work and collaborate with other experts.

Special thanks to Sofia Quaglioni for inviting me to spend two summers as an intern at Lawrence Livermore National Lab (LLNL), that time was an excellent start to my degree. I really appreciate the continued support and encouragement.

Thank you to Reiner for chairing my committee, as well as to Rob, Mona and Fei for their excellent feedback.

This work would not be possible without collaboration with other scientists. I am very grateful to Ayala, Chloë, Sam, Michele and many others. I'd like to acknowledge everyone - past and present - in the TRIUMF theory department, especially the nuclear theory post-docs, with whom I could discuss research problems and learned a lot from. Thanks to Matteo, Takayuki, Anna, Mack, Lotta, Mehdi, and especially Angelo for guiding my first co-op project and explaining much of the nuclear theory basics.

Thanks to Olivia, Richard, Eric and Wojtek for encouraging exciting side-projects in quantum computing and machine learning. Thanks to all the theory students I've interacted with: Michael, Antoine, Riku, Callum, Kang, Mirko, David, Lindsay, Charlie and Javier. Shout-out to those I met at LLNL, esp. Evan, Matt, Ahsan, and Yijia and thank you to the many other people I've met along the way, through TRIUMF, the UBC Physics and Astronomy Department, the UBC AMS Waterpolo Club and UBC AMS Triathlon Club.

I acknowledge funding from National Science and Engineering Research Council of Canada, the US Department of Energy and the University of British Columbia. TRIUMF receives federal funding via a contribution agreement with the National Research Council of Canada. Computing support came from an INCITE Award at the Oak Ridge Leadership Computing Facility, from the LLNL Institutional Computing Grand Challenge program, from the Digital Research Alliance of Canada and the Oak cluster at TRIUMF.

Thank you to all of my family and friends for their encouragement and support throughout my education. Finally, thank you to Laura, for joining me on this adventure and pushing me through the final stretch, I'll value your support always.

Chapter 1

Introduction

1.1 Nuclear Structure and Reactions

Since its discovery by Rutherford in 1911, the atomic nucleus has been at the forefront of modern physics. Through increasingly sophisticated experiments, the internal structure of nuclei has been revealed. The nucleus was discovered to be built of discrete components: the nucleons (protons and neutrons).

The number of protons is Z, the atomic number, which controls the chemical properties of the atom (in a neutral atom there are also Z electrons). The total number of nucleons is A, the mass number, which differentiates "isotopes" (nuclei with the same Z but different A). Different isotopes have a differing number of neutrons N (since $A = Z + N$). For example, the element helium ($Z = 2$) is found in nature as isotopes with $N = 2$ (^{4}He) and $N = 1$ (^{3}He).

The nuclear chart (Figure 1.1) contains thousands of isotopes, each with its own spectrum of bound-state energies, shapes and sizes. Most nuclear states are unstable and decay or break-up into smaller nuclei or free nucleons. Decays emit radiation, as the nucleons fall to a lower energy configuration. For example, γ-decays emit photons while β-decays change the charge state by emitting electrons (or positrons). Emission of an entire ^{4}He nucleus is called α-decay. The rates of decay range across many orders of magnitude.

Nuclei can also transform through collisions with other nuclei. In the process of scattering they may undergo nuclear reactions: capturing nucleons, fusing together or breaking apart, releasing energy in the process. Nuclear reactions power the Sun and all other stars. All the chemical elements in the Earth were created in stars billions of years ago after many chains of reactions, building heavier and heavier nuclei.

The use of rare-isotopes has applications in materials science and medicine. For many years, it was not possible to explore the vast nuclear landscape and all the possible nuclear reactions that can occur. From the 1980s until the present the acceleration of short-lived nuclei has become possible allowing the study of exotic nuclei and nuclear reactions. Rare-

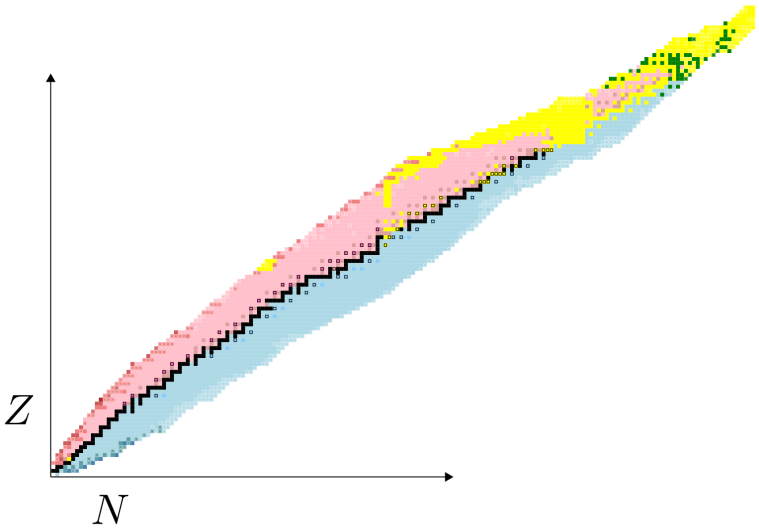

(a)

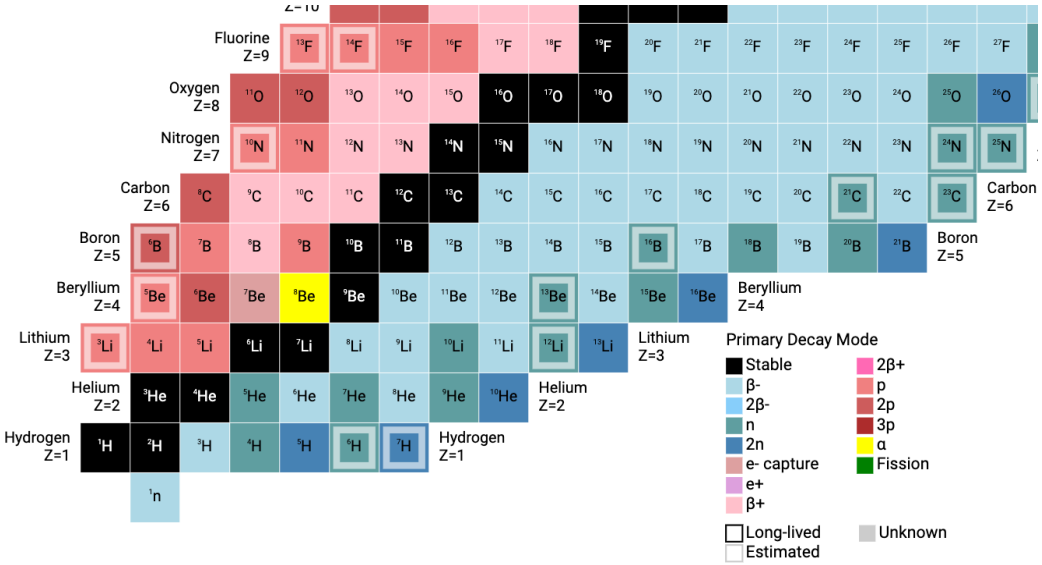

(b)

Figure 1.1: (a) The full chart of nuclides showing the observed isotopes arranged according to the number of protons (Z) and the number of neutrons (N). The isotopes coloured black do not decay, i.e. they are stable. The other isotopes are coloured according to their most dominant decay mode. Several thousand isotopes are shown but several thousand more are predicted to exist. "Existence" is generally defined as bound with respect to the strong force, i.e. decays are via electromagnetic or weak forces which act at a much longer time scale compared to the strong force. (b) A subset of the chart of nuclides, including only up to $Z = 9$ and $N = 18$. Figures adapted from [5] (which sources data from [6])

isotope production facilities have been constructed across the world including TRIUMF (Canada), FRIB (USA), RIKEN (Japan), GSI (Germany), GANIL (France) and ISOLDE at CERN (Switzerland).

In experiments, which attempt to emulate the highly ionized and high-temperature regime of stellar processes, it is extremely difficult to obtain the counts necessary to accurately measure nuclear reaction rates. Hence, predictive theories are needed to extrapolate beyond data. These theories are also needed to explain the vast collection of nuclear structure properties. In the past, simple models have been constructed to describe experimental observations. The liquid drop model was developed to account for trends in the binding energy of nuclei as a function of (A, Z). The deviations from this model motivated the more sophisticated shell model of Mayer and Jensen for which they won the Nobel prize.

A major goal of theoretical nuclear physics is to describe all of these phenomena from first principles. Recent advances in computing have enabled the study of nuclear properties in the low- and medium-mass regime, by the so-called "ab initio" methods: the no-core shell model [7], quantum Monte Carlo [8], coupled-cluster [9], and in-medium similarity renormalization group [10], to name a few. Their aim is to provide an accurate description of nuclear properties with controlled approximations and uncertainties starting from nucleons and the interactions between them.

Although the nucleons have internal structure (unlike, for example, the electron which appears to be an elementary particle), the nuclear interaction can be connected to a fundamental theory.

1.2 Elementary Particles and Interactions

The Standard Model of particle physics is the quantum field theory that classifies all of the known elementary particles and describes three of the four fundamental forces: the electromagnetic, weak and strong interactions[1]. This section is a summary, mostly based on [11, 12], see [13–16] for more details.

The particles of the Standard Model (shown in Figure 1.2) are categorized into two types, fermions and bosons, which obey different statistics. Fermions (quarks and leptons) make-up the bulk of the matter of the universe and follow Fermi-Dirac statistics. Two identical fermions cannot occupy the same quantum state (the Pauli exclusion principle) and hence collections of fermions take up volume. Bosons follow Bose-Einstein statistics and multiple bosons can occupy the same quantum state. Hence, collections of bosons can add coherently and act as force carriers between the fermions. Particles are identified as excitations (or "quanta") of their corresponding fields (e.g. an electron is an excitation of the electron field).

[1]The fourth force, gravity, has not yet been integrated and its inclusion is a very active area of physics research. However it is apparent that gravity acts in a "classical regime" and is not relevant at the energy scales discussed in this thesis.

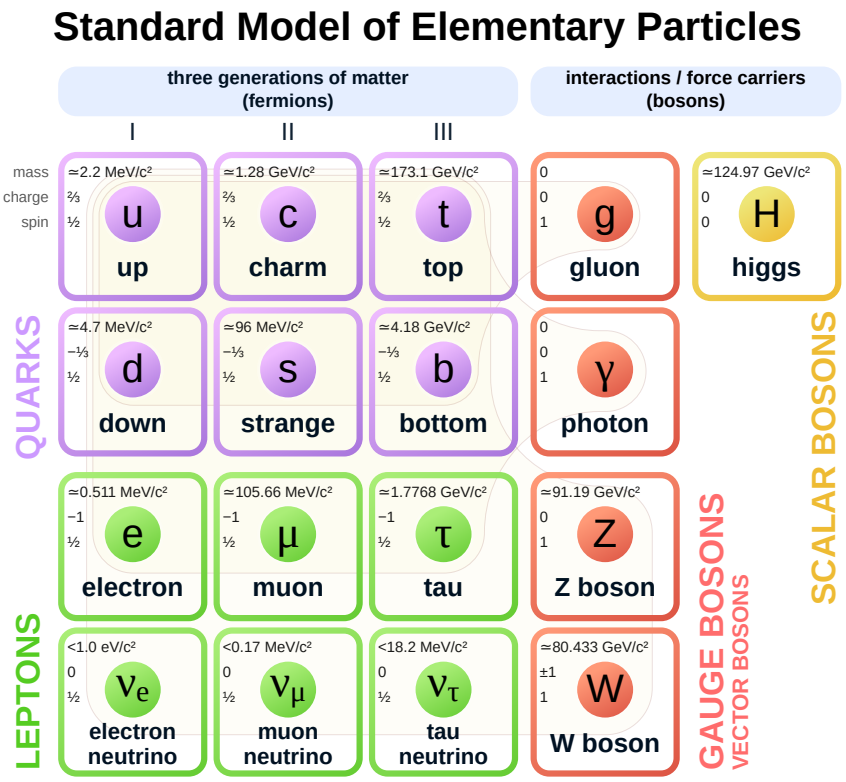

Figure 1.2: The Standard Model of elementary particles [17]: the 12 fundamental fermions and 5 fundamental bosons. Brown loops indicate which gauge bosons (red) couple to which fermions (purple and green). The value for "charge" reflected in figure is the electromagnetic charge. The mass values reflected in the figure are as of 2019 (periodic reevaluations are carried out by the Particle Data Group, see [18] for the latest).

Interactions between different particles can be constructed by combining together the fundamental vertices shown in Figure 1.3. Each vertex involves a coupling constant, and incoming and outgoing particles (fields). The photon field mediates the electromagnetic force and has a non-zero coupling with any field that has electric charge. The W and Z fields mediate the weak force, coupling with all the fundamental fermion fields and each other. The gluon fields mediate the strong force, coupling with quarks and the gluon field itself. The Higgs field couples to the masses of the other fundamental fields and itself.

In principle, the probability of any process is calculated by summing over all the relevant diagrams (with the required incoming and outgoing particles) using the Feynman rules extracted from the corresponding Lagrangian. In practice, this is only possible when the coupling constants at the vertices are small (e.g. in electromagnetism), where the contributions from complicated diagrams with large numbers of vertices and internal loops are suppressed. The theory of electron-photon interactions, quantum electrodynamics (QED),

has made the most precise predictions in all of theoretical physics[2]. The vast fields of chemistry and materials science depend on these interactions.

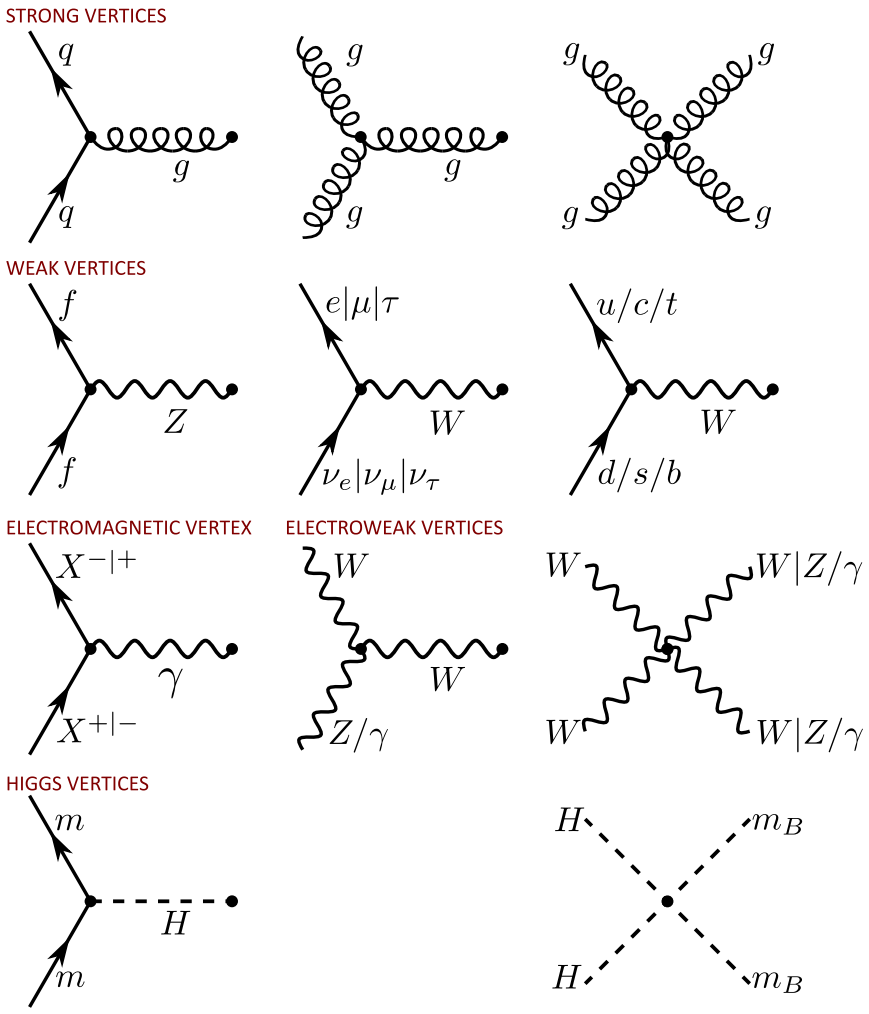

Figure 1.3: All vertices allowed in the Standard Model: q is any quark, g is a gluon, X is any charged particle, γ is a photon, f is any fermion, H is the Higgs, m is any particle with mass (with the possible exception of the neutrinos), m_B is any boson with mass. In diagrams with multiple particle labels separated by /, one particle label is chosen. In diagrams with particle labels separated by |, the labels must be chosen in the same order. For example, in the four boson electroweak case the valid diagrams are $WWWW$, $WWZZ$, $WW\gamma\gamma$, $WWZ\gamma$. Lines on the left correspond to incoming particles, while lines on the right are outgoing. The diagrams can be rotated such that an incoming particle becomes outgoing (or vice versa) resulting in conjugation of the corresponding field. The conjugate of each listed vertex (reversing the direction of arrows) is also allowed. Adapted from [20] and [21].

[2]The original theory used only the electromagnetic vertex of Figure 1.3. Modern predictions (as collected in [19]) include corrections from all the other vertices in the form of internal loops. At low energy, QED can be considered an effective field theory of the Standard Model.

A fundamental concept in physics is Noether's theorem, the idea that symmetries in the Lagrangian of a theory result in conserved quantities and conversely, every conservation law reflects an underlying symmetry. For example, energy and momentum conservation correspond to symmetries of translation in time and space respectively while angular momentum conservation corresponds to rotational symmetry. In special relativistic theories we also have invariance under boosts, i.e. Lorentz invariance. The combination of translations, rotations and boosts is called the Poincaré group. Particles appear as different representations of the Poincaré group. The simplest representation are one-component scalar fields, while the next simplest is a four-component Dirac spinor. The four components correspond to two spin states plus the two spin states of a distinct antiparticle. For example, the electron field is "spin-$\frac{1}{2}$" with four components: electrons with spin up and spin down, and anti-electrons ("positrons") with spin up and down. The spin corresponds to an intrinsic amount of angular momentum. Bosons have integer spin while fermions have half-integer spin.

The application of symmetries in particle physics invites the use of group theory which will be mentioned only in passing in this thesis. For example, the group of all rotations in three dimensions is $SO(3)$, it is closely related to the group $SU(2)$ which describes the symmetry of particle spin[3]. A spin-$\frac{1}{2}$ particle transforms under rotations according to the two-dimensional representation of $SU(2)$ (a spin-0 particle would transform under the one-dimensional representation and spin-1 under the three-dimensional, etc).

We associate with each particle several "charges", corresponding to so-called "internal symmetries" or "gauge symmetries". For example, electric charge can be associated with a $U(1)$ gauge symmetry, i.e. the dynamics of particles under the electromagnetic force can be described by a Lagrangian which is invariant to a $U(1)$ gauge transformation (in addition to Poincaré transformations). Additional symmetries one might expect are time reversal, parity ($\vec{r} \to -\vec{r}$) and charge conjugation (changing the sign of all internal charges, converting each particle into its antiparticle).

The forces of the Standard Model are based on symmetries of the gauge group $SU(3)_C \times SU(2)_L \times U(1)_Y$. The strong force is invariant under the $SU(3)_C$ gauge symmetry which corresponds to the so-called "colour-charge" of the quarks and gluons, hence the theory of this sector is termed quantum chromodynamics (QCD). The remaining $SU(2)_L \times U(1)_Y$ is termed the electroweak sector (a unified theory of electromagnetism and weak interactions).

The electroweak interaction is complicated, in fact weak processes violate parity and charge-conjugation (and likely time-reversal) symmetries. The quark and lepton fields are chiral, i.e. they have left-handed and right-handed particles. In the massless limit, chirality is equivalent to helicity and a right-(left-)handed particle is one whose spin and momentum are aligned (anti-aligned). Only left-handed fermions participate in weak interactions

[3]The difference is that a spinor under a rotation of 360° differs from the original spinor by a minus sign. A spinor is symmetric under a rotation of 720°.

and have charges (termed "weak isospin") under $SU(2)_L$. Both chiralities have a "weak hypercharge" under $U(1)_Y$ (which differs between left- and right-handed).

The electroweak gauge symmetry should forbid a Dirac mass term in the Lagrangian, which would mix left-handed and right-handed fields, but we observe fermions with mass in nature. A mechanism to generate mass for the charged fermions and weak gauge bosons is provided by the Higgs field. The Higgs field is a complex scalar field and the Lagrangian contains a peculiar potential. The minimum of the Higgs potential corresponds to a non-zero value of the field and so the local field about this minimum does not have the same symmetry, one of the two degrees of freedom becomes fixed (this is known as spontaneous symmetry breaking). The observed $W^{\pm}$, Z and photon are linear combinations between the $SU(2)_L$ and $U(1)_Y$ gauge fields. Interactions with the Higgs field play the role of a Dirac mass in the Lagrangian and so the measured masses of the fermions and weak gauge bosons are a function of coupling strengths and the vacuum expectation value of the Higgs field. The photon remains massless as it is the gauge field of a $U(1)$ subgroup of $SU(2)_L \times U(1)_Y$, the electric charge is a linear combination of the weak isospin and hypercharge. The discovery of the Higgs boson in 2012 [22, 23] was a very important confirmation of the Standard Model.

So far nuclei and nucleons have not yet been mentioned. They come about as an emergent phenomena of low-energy QCD. The QCD coupling strength between colour-charges does not decrease with distance resulting in the property of confinement, i.e. bare quarks are not observable but rather are constituents of colour-neutral composite particles (hadrons). We see in nature combinations of quarks: three quarks (baryons), or a quark and anti-quark pair (mesons). The physics of nuclei can be calculated at the level of the constituent nucleons with effective interactions connected to the underlying QCD.

1.3 Nucleons and Nuclear Forces

At low energies relevant for nuclear physics (in the tens of MeV far below the baryon mass scale $\Lambda_\chi \approx 1$ GeV), QCD is non-perturbative and thus very difficult to solve. While the technique of lattice QCD has been successful in describing hadronic spectra (possible states and their masses), calculations of two or more baryons are at present basically impossible using quarks and gluons as the degrees of freedom [24].

Consequently when calculating properties of atomic nuclei, we use nucleons and pions as the degrees of freedom. Nucleons are the baryons which consist only of the lightest quarks u and d: protons $p = uud$ and neutrons $n = udd$. Pions are the mesons: $\pi^+ = u\bar{d}$, $\pi^- = \bar{u}d$, $\pi^0 = \frac{1}{\sqrt{2}}\left(u\bar{u} - d\bar{d}\right)$. The quantum field theory of nucleons and pions is an "effective field theory" (EFT) of QCD.

The connection to QCD is achieved via chiral effective field theory (χEFT) [25]. χEFT has the same symmetries as QCD, in particular chiral symmetry which is spontaneously broken. In the limit of massless quarks, QCD is a chiral theory in which left- and right-

handed quarks can transform independently under flavour. The non-zero expectation value of the quark condensate due to the strong gluon interaction spontaneously breaks this symmetry. The symmetries that remain correspond to conserved isospin (see Section 2.4) and baryon number. Pions are generated in the theory as Nambu-Goldstone bosons [26].

χEFT describes interactions between nucleons by a hierarchy of terms consisting of pion exchanges and contact interactions [27, 28]. The mass of the pion $m_\pi \simeq 140$ MeV gives a "soft" scale, above which there is a mass gap to the next lightest meson, the rho ($m_\rho \approx 770$ MeV), giving a "hard" scale $\Lambda_\chi \approx m_\rho$. One can perturbatively expand the χEFT Lagrangian in powers of $Q \in \{\frac{p}{\Lambda_\chi}, \frac{m_\pi}{\Lambda_\chi}\}$, a simultaneous expansion in terms of the external three-momenta $|\vec{p}| = p$ and the pion mass [29]. The result is a finite set of diagrams at each order $(Q)^\nu$ (shown in Figure 1.4). The power of an irreducible diagram involving A nucleons with L loops is

$$\nu = -4 + 2A + 2L + \sum_i \Delta_i \,, \tag{1.1}$$

where each vertex i has dimension

$$\Delta_i = d_i + \frac{n_i}{2} - 2 \,, \tag{1.2}$$

and d_i is the number of derivatives and/or pion-mass insertions, while n_i denotes the number of nucleon fields (nucleon legs) involved in vertex i [29, 30].

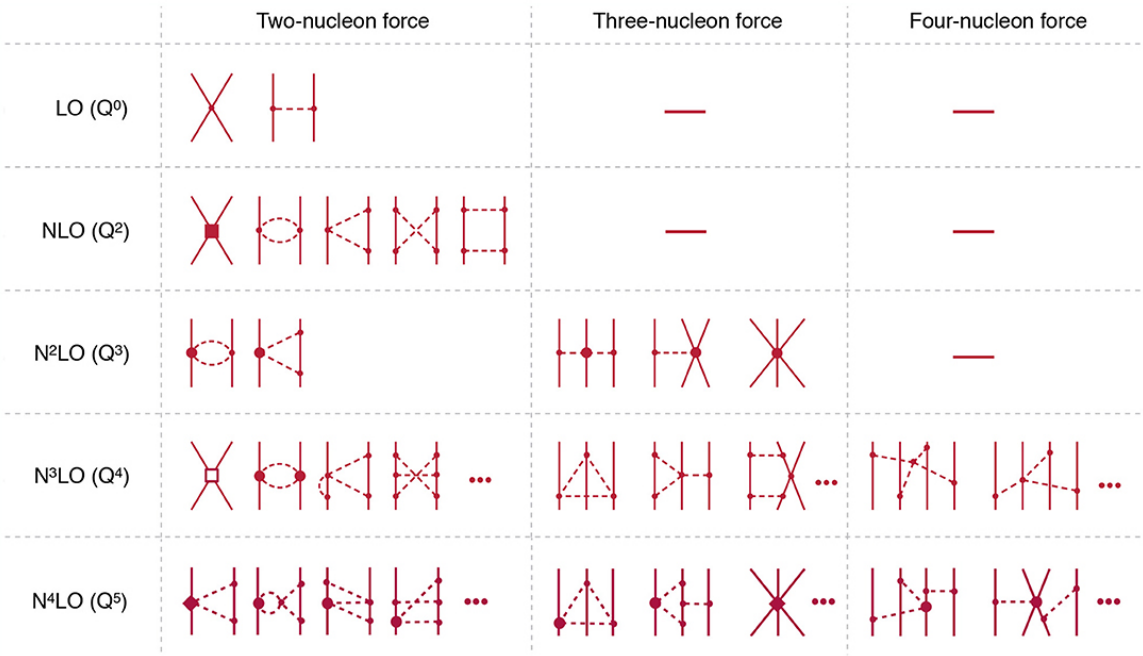

Figure 1.4: Hierarchy of nuclear forces in χEFT from [29]. Solid (dashed) lines denote nucleons (pions). The solid dots, filled circles, filled squares, filled diamonds, and open squares refer to vertices of dimension $\Delta_i = 0, 1, 2, 3$ and 4 respectively, as defined in (1.2).

χEFT contains parameters (low-energy constants or LECs) at each vertex, that are in principle calculable from QCD. However, at present these parameters are fitted to properties of few-nucleon systems (e.g. nucleon-nucleon scattering and properties (energies and decay rates) of the deuteron (^{2}H), triton (^{3}H) and Helium-3 (^{3}He). χEFT is systematically improvable as including higher-order terms result in increasingly small corrections. The importance of spin-orbit terms and tensor forces arise naturally in nucleon-nucleon (NN) interactions in χEFT. Three-nucleon (3N) and higher-body forces also naturally appear and are required to reproduce experiment.

Effective field theory techniques are also used to connect the nucleons to the other Standard Model interactions. The electric charge of the protons and magnetic moments of both nucleons allow the nucleons to interact electromagnetically. Hence, the nucleons in nuclei can rearrange to more energetically favourable configurations by emission of photons (γ-decay). The weak interaction allows the conversion of $u \leftrightarrow d$ quarks and therefore $n \leftrightarrow p$ nucleons by emission of W bosons (which quickly decay into a lepton and anti-neutrino, i.e. β-decay).

The Standard Model (SM) is an extremely precise theory but it does not explain everything, for example: gravity, dark matter and the properties of neutrinos. Nuclear physics can provide a test bed for beyond the Standard Model (BSM) theories as observed deviations from SM predictions of nuclear properties and reactions would provide evidence for new physics. However these predictions require reliable and accurate computational techniques such as *ab initio* methods.

1.4 The Nuclear Hamiltonian

Ab initio approaches start from a microscopic Hamiltonian of an A-nucleon system which includes the kinetic energy of each nucleon and a nuclear interaction. The interaction typically includes nucleon-nucleon (NN) and three-nucleon (3N) terms which are realistic in the sense that they reproduce few-nucleon data. In principle, higher many-nucleon contributions can be included but in general they are not needed.

The Hamiltonian is written as

$$H = \frac{1}{A} \sum_{i<j=1}^{A} \frac{(\vec{p}_i - \vec{p}_j)^2}{2m_N} + \sum_{i<j=1}^{A} V_{ij}^{NN} + \sum_{i<j<k=1}^{A} V_{ijk}^{3N} + \cdots , \tag{1.3}$$

where m_N is the nucleon mass[4] and $\vec{p}_i$ is the momentum of the i-th nucleon. The sum over $i < j$ prevents double-counting of identical pairs (i.e. $\sum_{i<j} = \frac{1}{2}\sum_{i\neq j}$). Since nuclei are self-bound, the kinetic energy term that appears is the intrinsic (relative) kinetic energy $T_{\rm rel}$, i.e. the difference between the total kinetic energy T and the kinetic energy of the

[4]In calculations we take the mass of the proton m_p and neutron m_n to be equal, and use the average nucleon mass: $m_N = \frac{1}{2}(m_p + m_n)$.

center of mass $T_{\rm CoM}$:

$$\begin{aligned} T_{\rm rel} =& T - T_{\rm CoM} \ , \\ \frac{1}{A}\sum_{i<j}\frac{(\vec{p}_i - \vec{p}_j)^2}{2m_N} =& \sum_i \frac{p_i^2}{2m_N} - \frac{P^2}{2m_N A} \ , \end{aligned} \tag{1.4}$$

where $\vec{P} = \sum_i \vec{p}_i$ is the total momentum. The electromagnetic interaction is included via the Coulomb force within V^{NN}, and applies only to pairs of protons. The nuclear interaction is more complicated.

Since the work of Yukawa in 1935, there has been evidence of the exchange of heavy particles. Since then, phenomenological forces have been fit to data e.g. meson exchange models such as CD-Bonn, Argonne V18, etc. However once QCD was discovered in the 1980s, these pictures needed to be connected. The pioneering work of Weinberg in 1990 [31] proposed to use χEFT to derive nucleon-nucleon forces from QCD as pion exchanges.

Using the underlying theory of QCD would require interactions between the constituent quarks but if we zoom out to the level of nucleons we are able to use an effective field theory. According to Weinberg [32], the steps of building an effective field theory are first, to identify the relevant degrees of freedom (in this case nucleons and pions) and second, to write down all possible interactions which preserve the underlying symmetries.

Nuclear interactions can be systematically derived in the framework of chiral effective field theory. The Lagrangian of QCD is expanded at low energy with protons, neutrons and pions as the degrees of freedom and arranged into a power series where the hierarchy between two-, three- and higher-body forces emerges naturally. The high-energy physics being left out is absorbed into the low-energy constants (LECs) which can be fitted to experimental data (in principle they could be computed via lattice QCD but despite much progress this is currently infeasible).

Effective field theories require choices in the regularization scheme and energy cutoff of the required integrals. Greater or fewer degrees of freedom can be used (e.g inclusion of the excited baryon state Δ or pion-less schemes). In principle, baryons and mesons with heavier quarks (e.g. strange) can be used, creating "hyper-nucleon" interactions.

The parametrization and fitting technique of nuclear forces are not unique. These choices create a zoo of theoretically equivalent forces but due to the change in the weighting of different LECs they may result in better predictions in different nuclei. This creates an obvious source of uncertainty in ab initio predictions but it is difficult to quantify without the ability to perform a single prediction with every available force. In practice to make new predictions we choose interactions with a good track record. The quantification of uncertainty due to the choice of nuclear force is a highly active area of research [33]. In principle χEFT will produce many-body interactions beyond three-body, but in this study we use only up to three body. The contribution of higher-body terms is generally small. *Ab*

initio calculations of very heavy systems have shown that NN+3N is sufficient [34].

The Hamiltonian is non-relativistic and hence we can use the framework of non-relativistic quantum mechanics. The properties of a system can be retrieved from the wavefunction, which is a solution to the Schrodinger equation. A nuclear Hamiltonian must conserve some symmetries, in particular intrinsic angular momentum and parity. Isospin (Section 2.4) is approximately conserved. The eigenstates of the Hamiltonian will be simultaneous eigenstates of the corresponding operators and hence the nuclear wavefunction will be labelled by J, π and M_T. The goal of *ab initio* nuclear theory is to find the nuclear wavefunction and then expectation values of operators will correspond to different observables.

1.5 Applications of Nuclear Theory

Ab initio nuclear theory provides insight to explain experimental results and can be combined with experiment to make predictions.

For example, theoretical calculations have recently been applied to solve the puzzle of nuclear beta decay quenching. Historically beta decay rates were observed to be systematically smaller than expected based on the rate of decay of free neutrons. This quenching effect can be explained by a better description of both the beta decay operator and the nuclear wavefunction. The operator contains a higher-order term in which the weak force acts on two nucleons simultaneously. *Ab initio* methods also include stronger correlations of nucleons compared to phenomenological shell models.

An accurate description of the nucleus is needed to find new physics in experiments involving nuclear systems. For example, nuclear structure can influence the distribution of momenta of outgoing electrons in beta decay. New experiments which measure the kinematics of the electrons must take into account these effects.

Another example is the hypothetical process of neutrino-less double beta decay. If measured the neutrino mass can be extracted from the decay lifetime using the nuclear matrix element from theory. The expected size of the nuclear matrix element influences which nuclei would be good candidates for measuring this yet-unseen decay mode. The observation of this process would expand the Standard Model by providing more information about neutrinos and could provide part of an explanation for matter-antimatter asymmetry in the universe.

Astrophysical quantities like cosmological isotopic abundances also require theoretical input. Reaction rates demand integrals over all energies but measurements are limited to discrete points. *Ab initio* nuclear theory has the potential to resolve conflicts between previous predictions and measurements of the cosmological lithium abundance.

Another cosmological mystery is dark matter. Proposed theories require new particles both to form the dark matter and to connect between the Standard Model and dark sector. Recent experiments report seeing the potential signature of a new particle with mass 17 MeV (the so-called X17 boson) which decays into an e^+e^- pair. This particle is emitted

during the decay of a ^{8}Be resonance in proton scattering experiments on ^{7}Li, i.e. the radiative capture reaction $^7\mathrm{Li}(p, e^+e^-)^8\mathrm{Be}$. A predictive nuclear model is needed to rule out a Standard Model effect and justify the claim.

1.6 Organization

This thesis is organized as follows:

- Chapter 2 introduces the mathematical tools necessary to build a nuclear wavefunction. This background provides the basis for the no-core shell model (NCSM) technique which can be used to compute the bound states of many light nuclei.

- Chapter 3 connects the Standard Model to expectation values of nuclear operators using nuclear decay as a motivating example.

- Chapter 4 describes the technique of Similarity Renormalization Group (SRG) which is a method in which unitary transformations are used to improve the Hamiltonian. This pre-processing step results in faster convergence of calculations. The NCSM is a computational method which scales poorly with the number of nucleons A and quickly becomes very expensive. While the amount of available computing power is continually increasing, the development of techniques which can improve results for the same amount of resources can be very useful.

- Chapter 5 presents the results of NCSM calculations. The NCSM was used to benchmark more approximate many-body methods, in this case "coupled-cluster" (CC) and "in-medium SRG" (IMSRG). All three *ab initio* methods were used to calculate the nuclear matrix elements for Gamow-Teller (GT) beta decays across a large range of nuclear masses and demonstrate that quenching is not observed in *ab initio* methods. The NCSM calculations demonstrate the power and necessity of SRG. NCSM calculations were also used to compute higher-order terms in the GT beta decay spectrum of $^6\mathrm{He} \to {}^6\mathrm{Li}$. These nuclear structure corrections will appear in future high-precision experiments and should not be mistaken for beyond the Standard Model physics. Finally, the NCSM was used again to benchmark CC and IMSRG in the calculation of neutrino-less double beta decay matrix elements.

- Chapter 6 introduces nuclear wavefunctions of unbound (continuum) systems and describes the method of no-core shell model with continuum (NCSMC). The NCSM is solely a bound state method and does not have the capability to describe the unbound states which occur in scattering and reactions. The NCSMC can describe both bound states and scattering states by including explicit cluster states. The scattering state amplitudes connect to cross sections of scattering processes and radiative capture reactions. The theory of electron-positron pair production in radiative capture is presented and compared to pair production in bound-state decays.

- Chapter 7 presents the application of NCSMC to the radiative capture reactions ^{4}He$(d,\gamma)^6$Li and ^{7}Li$(p,\gamma)^8$Be with extension to ^{7}Li$(p,e^+e^-)^8$Be. The first reaction has applications to ^{6}Li production in big bang nucleosynthesis.The second and third may be used to benchmark experiments in the search for BSM physics, in particular the claimed X17 boson.

Chapter 2

Many-Body Calculations

Note: The mathematical expressions in this chapter and the following will use natural units i.e. $\hbar = c = 1$. This means that masses are measured in MeV (rather than $\frac{\text{MeV}}{c^2}$). Distances are sometimes quoted in fm= 10^{-15}m (femtometre is often called "fermi" in nuclear physics after physicist Enrico Fermi). Momenta are quoted in either MeV or fm^{-1}, the conversion factor is $\hbar c$ =197.327 MeV fm [19].

2.1 The Quantum Harmonic Oscillator

A very simple picture of the nucleus is of independent nucleons influenced by a central potential. (One can imagine this coming about as the averaged interaction with all the other nucleons). One model of the mean nuclear potential is the harmonic oscillator potential: $V(r) \propto r^2 = \vec{r} \cdot \vec{r}$. This picture is clearly not the full story but introducing the process and solutions with this potential is a useful step towards a more realistic model.

We want to solve the time-independent Schrodinger equation:

$$H\psi = E\psi \ , \tag{2.1}$$

where we have the Hamiltonian, with kinetic energy T and potential energy V:

$$\begin{aligned} H =& T + V \ , \\ H =& \sum_{i=1}^{A} \left[\frac{p_i^2}{2m_N} + \frac{1}{2} m_N \Omega^2 r_i^2 \right] \ , \end{aligned} \tag{2.2}$$

with m_N the nucleon mass and Ω the harmonic oscillator frequency. Each particle labeled by i is independent in this model and solves a single-particle Hamiltonian:

$$H = \frac{p^2}{2m_N} + \frac{1}{2} m_N \Omega^2 r^2 \ . \tag{2.3}$$

The momentum is calculated through the gradient operator in quantum mechanics ($\vec{p} \rightarrow$

$-i\vec{\nabla}$) and so the momentum squared gives the Laplacian, i.e.

$$\frac{p^2}{2m_N} \to -\frac{\nabla^2}{2m_N} \,, \tag{2.4}$$

$$\begin{aligned}\nabla^2 =& \frac{1}{r^2}\frac{\partial}{\partial r}\left(r^2\frac{\partial}{\partial r}\right) + \frac{1}{r^2}\left(\frac{1}{\sin\theta}\frac{\partial}{\partial\theta}\left(\sin\theta\frac{\partial}{\partial\theta}\right) + \frac{1}{\sin^2\theta}\frac{\partial^2}{\partial\phi^2}\right) \,, \\ =& \frac{1}{r^2}\frac{\partial}{\partial r}\left(r^2\frac{\partial}{\partial r}\right) - \frac{L^2}{r^2} \,,\end{aligned} \tag{2.5}$$

where $\vec{L}$ is the angular momentum operator:

$$\vec{L} = \vec{r}\times\vec{p} = -i\vec{r}\times\vec{\nabla} = -i\left(\hat{\phi}\frac{\partial}{\partial\theta} - \hat{\theta}\frac{1}{\sin\theta}\frac{\partial}{\partial\phi}\right) \,. \tag{2.6}$$

The Hamiltonian is spherically symmetric and does not dependent on angles. This admits the separable solutions:

$$\psi(\vec{r}) = R_{n\ell}(r)Y_{\ell m}(\theta,\phi) \equiv \varphi_{n\ell m}(\vec{r}) \,, \tag{2.7}$$

where the angular wavefunction $Y_{\ell m}$ are the standard spherical harmonics [35]:

$$Y_{\ell m}(\theta,\phi) = \sqrt{\frac{(2\ell+1)}{4\pi}\frac{(\ell-|m|)!}{(\ell+|m|)!}}e^{im\phi}P_\ell^m(\cos\theta) \,, \tag{2.8}$$

and P_ℓ^m are the "associated Legendre polynomials". The spherical harmonics are eigenfunctions of the angular momentum operators:

$$L^2Y_{\ell m} = \ell(\ell+1)Y_{\ell m} \,, \tag{2.9}$$

$$L_zY_{\ell m} = mY_{\ell m} \,. \tag{2.10}$$

The ℓ determines the parity of the state, by $\pi = (-)^\ell$. ℓ can be zero or any positive integer and for each value of ℓ there are $2\ell+1$ possible values of m ($-\ell \le m \le \ell$).

The remaining piece is the radial Schrodinger equation:

$$\left\{\frac{1}{2m_Nr^2}\left[-\frac{\mathrm{d}}{\mathrm{d}r}\left(r^2\frac{\mathrm{d}}{\mathrm{d}r}\right) + \ell(\ell+1)\right] + \frac{m_N\Omega^2r^2}{2}\right\}R_{n\ell}(r) = E_{n\ell}R_{n\ell}(r) \,, \tag{2.11}$$

which has another set of solutions related to generalized Laguerre polynomials (A.32) [36]. n is any positive integer (or zero).

The radial and angular wavefunctions are normalized such that they form orthonormal bases of functions of their respective coordinates, i.e.

$$\int r^2\mathrm{d}rR_{n'\ell}(r)R_{n\ell}(r) = \delta_{nn'} \tag{2.12}$$

and

$$\int \mathrm{d}\cos\theta \mathrm{d}\phi Y^*_{\ell' m'}(\theta,\phi) Y_{\ell m}(\theta,\phi) = \delta_{\ell\ell'}\delta_{mm'} \ . \tag{2.13}$$

The combined solutions are labeled as $|n\ell m\rangle$, where

$$\langle \vec{r}|n\ell m\rangle = \varphi_{n\ell m}(\vec{r}) \ . \tag{2.14}$$

They are the eigenstates of the Hamiltonian operator:

$$H\,|n\ell m\rangle = E_{n\ell}\,|n\ell m\rangle \ , \tag{2.15}$$

and are orthonormal, i.e.

$$\begin{aligned}\langle n'\ell' m'|n\ell m\rangle =& \langle n'\ell' m'| \left(\int \mathrm{d}^3 r\,|\vec{r}\rangle\,\langle\vec{r}|\right)|n\ell m\rangle \\ =& \int \mathrm{d}^3\vec{r}\varphi^*_{n'\ell' m'}(\vec{r})\varphi_{n\ell m}(\vec{r}) \\ =& \delta_{nn'}\delta_{\ell\ell'}\delta_{mm'} \ .\end{aligned} \tag{2.16}$$

The energy depends only on the so-called "principal" quantum number $\tilde{N} = 2n + \ell$, $E_{n\ell} = E_{\tilde{N}} = \left(\tilde{N} + \frac{3}{2}\right)\Omega$. For reference, we can calculate the energy by evaluating the expectation value of the Hamiltonian by (2.15) or via an integral i.e.

$$\begin{aligned}\langle n'\ell' m'|\,H\,|n\ell m\rangle =& \int \mathrm{d}^3 r \varphi^*_{n'\ell' m'}(\vec{r}) \left(-\frac{\nabla^2}{2m_N} + \frac{1}{2}m_N\Omega^2 r^2\right)\varphi_{n\ell m}(\vec{r}) \\ =& E_{n\ell}\delta_{nn'}\delta_{\ell\ell'}\delta_{mm'} \ .\end{aligned} \tag{2.17}$$

The two components of this Hamiltonian are very similar:

$$\langle n'\ell' m'|\,T\,|n\ell m\rangle = \delta_{\ell\ell'}\delta_{mm'}\left(\left[2n+\ell+\frac{3}{2}\right]\delta_{nn'} + \left(\delta_{n,n'-1} + \delta_{n,n'+1}\right)\sqrt{(n+1)\left(n+\ell+\frac{3}{2}\right)}\right)\frac{\Omega}{2} \ , \tag{2.18}$$

$$\langle n'\ell' m'|\,V\,|n\ell m\rangle = \delta_{\ell\ell'}\delta_{mm'}\left(\left[2n+\ell+\frac{3}{2}\right]\delta_{nn'} - \left(\delta_{n,n'-1} + \delta_{n,n'+1}\right)\sqrt{(n+1)\left(n+\ell+\frac{3}{2}\right)}\right)\frac{\Omega}{2} \ . \tag{2.19}$$

This potential creates a "ladder" of equally separated states ("rungs" or "shells") which the nucleons can occupy. A model of the nucleus can be made by filling harmonic oscillator states, the most naive "shell model".

This filling must be limited by the fact that protons and neutrons are fermions with spin $\frac{1}{2}$ i.e. nucleons obey the Pauli exclusion principle (Fermi-Dirac statistics). For example, we can have 4 particles in the $\tilde{N} = 0$ shell (two protons and two neutrons, one of each has

spin $+\frac{1}{2}$ and $-\frac{1}{2}$). When a shell is filled like this, it is referred to as "closed" and energy is required to add a nucleon as it must go to the next higher shell. ^{4}He has this property and is more tightly bound than ^{5}He or ^{5}Li (both of which are in fact unbound).

The particular combinations of Z, N that are strongly bound compared to their neighbours in the nuclear chart are known as the "magic numbers" (2, 8, 20, 28, etc.). With respect to Z these correspond to helium, oxygen, calcium, nickel, etc. These are analogous to the numbers of electrons which fill the shells responsible for the periodic table in chemistry (2, 10, 18, 36, etc. correspond to the noble gases). These experimentally observed numbers were a motivation for the introduction of a "spin-orbit" term, described in Section 2.2.

The exact energy differences between shells depends on the shape of the nuclear potential. Historically phenomenological mean field models have been created, for example the Woods-Saxon potential [37], and were fitted to observed nuclear properties.

To create a truly first-principles approach, motivated by the Standard Model, our goal is to build the nucleus from the NN+3N interactions. The harmonic oscillator states $\varphi_{n\ell m}$ are still very useful as we can use a linear combination (of products) of these states as the solution to the true Hamiltonian (as we'll see in Section 2.7).

2.2 Spin and Angular Momentum Coupling

Nucleons are spin-$\frac{1}{2}$ particles, so a nucleon wavefunction should include a spinor χ, i.e.

$$\psi(\vec{r},\sigma) = \varphi_{n\ell m_\ell}(\vec{r})\chi_{sm_s}(\sigma) = \langle \vec{r}|n\ell m_\ell\rangle \langle\sigma|sm_s\rangle \ , \tag{2.20}$$

where the spinor is an eigenfunction of the spin operators:

$$S^2 |sm_s\rangle = s(s+1)|sm_s\rangle \ , \tag{2.21}$$

$$S_z |sm_s\rangle = m_s |sm_s\rangle \ . \tag{2.22}$$

We expect that the Hamiltonian is symmetric under rotations and reflections and so the total angular momentum and parity of a nuclear state, J^π, should be conserved. The total angular momentum operator is $\vec{J} = \vec{L} + \vec{S}$. The orbital angular momentum ℓ adds to the spin s such that the state has a total angular momentum quantum number j (this corresponds to the notation $(\ell s)j$). We should therefore use states with good j, created by combinations of (2.20) with the following expression (dropping n for brevity):

$$\begin{aligned} |(\ell s)jm\rangle &= \sum_{m_s m_\ell} \langle \ell m_\ell s m_s|(\ell s)jm\rangle \, |\ell m_\ell\rangle \, |sm_s\rangle \\ &= \sum_{m_s m_\ell} (\ell m_\ell s m_s|jm) \, |\ell m_\ell\rangle \, |sm_s\rangle \ . \end{aligned} \tag{2.23}$$

The coefficients $(\ell m_\ell s m_s|jm)$ are known as the Clebsch-Gordan (CG) coefficients.

The observed magic numbers motivated the presence of an attractive, single-particle spin-orbit term in the nuclear potential [38], i.e.

$$V_{so} = -v(r)\vec{L}\cdot\vec{S}\ . \tag{2.24}$$

The dot product between the spin and orbital momentum can be calculated via

$$\begin{aligned} 2\vec{L}\cdot\vec{S}\,|n\ell sjm\rangle &= \left(J^2 - L^2 - S^2\right)|n\ell sjm\rangle \\ &= \left[j(j+1) - \ell(\ell+1) - s(s+1)\right]|n\ell sjm\rangle \\ &= |n\ell sjm\rangle \cdot \begin{cases} \ell & s=\frac{1}{2}, j=\ell+\frac{1}{2} \\ (-(\ell+1)) & s=\frac{1}{2}, j=\ell-\frac{1}{2}\ . \end{cases} \end{aligned} \tag{2.25}$$

This shifts the energy of states with the highest ℓ and j in a shell down towards the next lower shell. If the coefficients $v_{n\ell} = \int \mathrm{d}r r^2 R_{n\ell}(r) R_{n\ell}(r) v(r)$ are strong enough ($E_{n\ell} = E_{\tilde{N}} - v_{n\ell} < \vec{L}\cdot\vec{S} >$), the experimentally observed magic numbers can be reproduced. For example, the harmonic oscillator alone produces the magic numbers: 2, 8, 20, 40, 70, etc. The spin-orbit term pushes states from $n=0$, $\ell=3$, $j=\frac{7}{2}$ down, with sufficient energy gap that these 8 states are labelled by a new magic number. States from higher energy levels are also rearranged, with the result: 2, 8, 20, 28, 50, etc. [39].

This addition to the nuclear potential was enough to make the single-particle shell model predictive, in the sense that the J^π of the ground state of a nucleus can be accurately predicted simply by filling the shells. However there remain many exceptions and the excited states of nuclei are not as easily predicted. To calculate these energies we need to work with a more realistic inter-nucleon interaction.

Since the interaction should depend on the relative position of pairs of particles $\vec{r}_1 - \vec{r}_2$, we would like to use two-nucleon wavefunctions. We can again use the CG coefficients to couple the individual angular momenta j_1 and j_2 to create states with good total angular momentum j, i.e.

$$|(j_1 j_2)jm\rangle = \sum_{m_1 m_2} (j_1 m_1 j_2 m_2 | jm)\,|j_1 m_1\rangle\,|j_2 m_2\rangle\ . \tag{2.26}$$

For 3N interactions we expect to need three-particle wavefunctions. The total operator would be $\vec{J} = \vec{J}_1 + \vec{J}_2 + \vec{J}_3$ which can be coupled by successive coupling of first $\vec{J}_{12} = \vec{J}_1 + \vec{J}_2$ and then $\vec{J} = \vec{J}_{12} + \vec{J}_3$, i.e.

$$\begin{aligned} |((j_1 j_2)j_{12} j_3)jm\rangle &= \sum_{m_3 m_{12}} (j_{12} m_{12} j_3 m_3 | jm)\,|(j_1 j_2)j_{12} m_{12}\rangle\,|j_3 m_3\rangle \\ &= \sum_{m_3 m_{12}} (j_{12} m_{12} j_3 m_3 | jm) \left[\sum_{m_1 m_2} (j_1 m_1 j_2 m_2 | j_{12} m_{12})\,|j_1 m_1\rangle\,|j_2 m_2\rangle\right] |j_3 m_3\rangle\ . \end{aligned} \tag{2.27}$$

But this is not unique, we could also couple $\vec{J}_1 + \vec{J}_{23}$ or $\vec{J}_{13} + \vec{J}_2$. The values of the quantum number j do not depend on the coupling order but the states corresponding to different coupling schemes are not the same [40]. To convert between these different bases we need the Wigner $6j$ symbol (A.11), the array with curly braces below:

$$|(j_1(j_2j_3)j_{23})jm\rangle = \sum_{j_{12}} (-)^{j_1+j_2+j_3+j} \hat{j}_{12}\hat{j}_{23} \left\{ \begin{array}{ccc} j_1 & j_2 & j_{12} \\ j_3 & j & j_{23} \end{array} \right\} |((j_1j_2)j_{12}j_3)jm\rangle \ . \tag{2.28}$$

2.3 Spherical Tensor Operators

The observable properties of a quantum state are extracted through the expectation values of operators i.e. the matrix element. For example, for an operator which depends only on the spatial coordinates, we have

$$\left\langle n'\ell'm' \right| O \left| n\ell m \right\rangle = \int \mathrm{d}^3 r \varphi^*_{n'\ell'm'}(\vec{r}) O(\vec{r}) \varphi_{n\ell m}(\vec{r}) \ . \tag{2.29}$$

The Hamiltonian is the operator corresponding to the energy. For example, single-nucleon energies come from the matrix elements ((2.17) again)

$$\left\langle n'\ell'm' \right| H \left| n\ell m \right\rangle = E_{n\ell} \delta_{nn'} \delta_{\ell\ell'} \delta_{mm'} \ . \tag{2.30}$$

It useful to transform any operator with dependence on the nucleon coordinates into an expansion over the spherical harmonics, i.e.

$$O(\vec{r}) = \sum_{\lambda\mu} O_{\lambda\mu}(\vec{r}) = \sum_{\lambda\mu} O_\lambda(r) Y_{\lambda\mu}(\theta, \phi) \ . \tag{2.31}$$

Each component $O_{\lambda\mu}$ is a component of a spherical tensor of rank λ. The Hamiltonian is a scalar (rank 0), since it has no dependence on the angular coordinates.

Another example is the Cartesian position vector $\vec{r} = (x, y, z)$ which can be converted into the so-called "covariant" components $r_\pm = \mp \frac{1}{\sqrt{2}} (x \pm iy)$ and $r_0 = z$ [40]. We have

$$r_\mu = \sqrt{\frac{4\pi}{3}} r Y_{1\mu}(\theta, \phi) \tag{2.32}$$

where $\mu = 0, \pm 1$ and $r = |\vec{r}|$. Therefore, the spherical components of the position vector form a spherical tensor of rank 1.

The Wigner-Eckart theorem [35] is a procedure which separates out the projection μ dependence to simplify calculations. We obtain the relation:

$$\left\langle j'm'\right| O_{\lambda\mu}\left|jm\right\rangle = (-)^{2\lambda}\hat{j'}^{-1}\left(jm\lambda\mu|j'm'\right)\left\langle j'\right|\left|O_\lambda\right|\left|j\right\rangle \ , \tag{2.33}$$

where the "hat" notation means $\hat{j} = \sqrt{2j+1}$ and the quantity $\langle j'|\,|O_\lambda|\,|j\rangle$ is the reduced matrix element (which contains the physics of the matrix element and is rotationally invariant). The CG coefficient immediately gives us selection rules, i.e. the matrix element is zero unless $\Delta(j'\lambda j)$ (the triangle condition: $|j'-j| \le \lambda \le j'+j$) and $m+\mu = m'$.

Complicated operators such as the electromagnetic interaction will be decomposed as a series of spherical tensor operators, as will be shown in Section 3.1. However, some operators are already a single irreducible tensor. For example, the identity 1 is a scalar, angular momentum $\vec{J}$ is a vector and $Y_{\lambda\mu}$ alone is a component of a rank λ tensor.

It is useful to list the reduced matrix elements of these [40]:

$$\left\langle j'\right|\left|1\right|\left|j\right\rangle = \delta_{jj'}\hat{j} \ , \tag{2.34}$$

$$\left\langle j'\right|\left|J\right|\left|j\right\rangle = \delta_{jj'}\hat{j}\sqrt{j(j+1)} \ , \tag{2.35}$$

$$\left\langle l'\right|\left|Y_L\right|\left|l\right\rangle = (-)^{l'}\frac{\hat{l'}\hat{L}\hat{l}}{\sqrt{4\pi}}\begin{pmatrix} l' & L & l \\ 0 & 0 & 0 \end{pmatrix} \ , \tag{2.36}$$

$$\left\langle \frac{1}{2}\right|\left|S\right|\left|\frac{1}{2}\right\rangle = \sqrt{\frac{3}{2}} \ , \tag{2.37}$$

where in (2.36) appears the $3j$ symbol (A.10).

As an example, (2.37) can be determined by combining (2.22) and (2.33), i.e.

$$\left\langle s'm'\right| S_z\left|sm\right\rangle = m\delta_{ss'}\delta_{mm'} \tag{2.38}$$

$$= \frac{(sm10|s'm')}{\hat{s}}\left\langle s'\right|\left|S\right|\left|s\right\rangle \ . \tag{2.39}$$

Setting $m = s = s'$ then:

$$s = \frac{(ss10|ss)}{\hat{s}}\left\langle s\right|\left|S\right|\left|s\right\rangle \ , \tag{2.40}$$

and for $s = \frac{1}{2}$:

$$\left\langle \frac{1}{2}\right|\left|S\right|\left|\frac{1}{2}\right\rangle = s\cdot\hat{s}\cdot\frac{1}{(ss10|ss)} = \frac{1}{2}\cdot\sqrt{2}\cdot\frac{1}{\sqrt{\frac{1}{3}}} = \sqrt{\frac{3}{2}} \ . \tag{2.41}$$

A standard notation for $s = \frac{1}{2}$ is to relate $\vec{S} = \frac{\vec{\sigma}}{2}$, where σ_i are the standard Pauli matrices

(see Section A.1). The result is

$$\left\langle \frac{1}{2}\right| |\sigma| \left|\frac{1}{2}\right\rangle = \sqrt{6}\,. \tag{2.42}$$

When using a coupled basis, we may still need to compute expectation values of operators which are also coupled, i.e.

$$O_{\lambda\mu} = [O_{\lambda_1} \otimes O_{\lambda_2}]_{\lambda\mu} = \sum_{\mu_1\mu_2} (\lambda_1\mu_1\lambda_2\mu_2|\lambda\mu)\, O_{\lambda_1\mu_1} O_{\lambda_2\mu_2}\,. \tag{2.43}$$

The reduced matrix elements, where O_{λ_1} acts on the j_1, j_1' space and O_{λ_2} acts on the j_2, j_2' space, are calculated via [41]

$$\left\langle j_1' j_2'; j'\right| |O_\lambda| \, |j_1 j_2; j\rangle = \hat{j}'\hat{\lambda}\hat{j} \left\{ \begin{array}{ccc} j_1' & j_2' & j' \\ j_1 & j_2 & j \\ \lambda_1 & \lambda_2 & \lambda \end{array} \right\} \left\langle j_1'\right| |O_{\lambda_1}| \, |j_1\rangle \left\langle j_2'\right| |O_{\lambda_2}| \, |j_2\rangle \,. \tag{2.44}$$

The array in brackets is the Wigner $9j$ symbol (A.13). When $\lambda = 0$ then $9j$ reduces to a $6j$ (see A.14), i.e.

$$\left\langle j_1' j_2'; j'\right| |[O_L P_L]_0| \, |j_1 j_2; j\rangle = \delta_{j'j} \, (-)^{j_2'+j'+j_1} \left\{ \begin{array}{ccc} j_1' & j_2' & j' \\ j_2 & j_1 & L \end{array} \right\} \left\langle j_1'\right| |O_L| \, |j_1\rangle \left\langle j_2'\right| |P_L| \, |j_2\rangle \,. \tag{2.45}$$

An example is the spin-orbit term in the Hamiltonian, which is a scalar product between vectors:

$$\left\langle \ell' s'; j'\right| \left| \left[\vec{L}\cdot\vec{S}\right]_0 \right| \ell s; j\rangle = \delta_{j'j} \, (-)^{s'+j'+\ell} \left\{ \begin{array}{ccc} \ell' & s' & j' \\ s & \ell & 1 \end{array} \right\} \left\langle \ell'\right| |L| \, |\ell\rangle \left\langle s'\right| |S| \, |s\rangle \,. \tag{2.46}$$

We may also have operators which act only on a subspace. For example, we may need to calculate just σ for state $|(\ell s)j\rangle$ by using the same formula (2.44), setting $O_{\lambda_1} = 1$ ($\lambda_1 = 0$, $\lambda = \lambda_2 = 1$) (again a zero in the $9j$ gives a $6j$ (A.14)). Therefore:

$$\begin{aligned} \left\langle \ell' \frac{1}{2}; j'\right| |\sigma| \left|\ell \frac{1}{2}; j\right\rangle &= \left\langle \frac{1}{2}\right| |\sigma| \left|\frac{1}{2}\right\rangle \delta_{\ell\ell'} \hat{j}\hat{j}' \, (-)^{\ell'+j'+\frac{3}{2}} \left\{ \begin{array}{ccc} \frac{1}{2} & \frac{1}{2} & 1 \\ j & j' & \ell \end{array} \right\} \\ &= \sqrt{6}\delta_{\ell\ell'} \hat{j}\hat{j}' \, (-)^{\ell'+j'+\frac{3}{2}} \left\{ \begin{array}{ccc} \frac{1}{2} & \frac{1}{2} & 1 \\ j & j' & \ell \end{array} \right\} . \end{aligned} \tag{2.47}$$

One last (and defining) property of spherical tensors is how they transform under rotations. A rotation in three-dimensional Cartesian space induces a unitary transformation on angular momentum eigenstates $|jm\rangle$ in the Hilbert space of dimension $2j+1$ [41].

The matrix elements of such a transformation (for a rotation $\mathcal{R}$ about the Euler angles α, β and γ) are the Wigner D-matrices, i.e.

$$\left\langle jm' \right| \mathcal{R}(\alpha,\beta,\gamma) \left| jm \right\rangle \equiv D^{j}_{m'm}(\alpha,\beta,\gamma) \; . \tag{2.48}$$

State vectors transform according to

$$\mathcal{R} \left| jm \right\rangle = \sum_{m'} D^{j}_{m'm} \left| jm' \right\rangle \; , \tag{2.49}$$

and correspondingly the spherical tensor operators which act on those state vectors transform as

$$\mathcal{R} O_{\lambda\mu} \mathcal{R}^{\dagger} = \sum_{m'} O_{\lambda m'} D^{\lambda}_{m'\mu} \; . \tag{2.50}$$

See Section A.3 for more details.

2.4 Isospin

Because of the very close masses of the proton and neutron, these particles can be modeled as the two projections of a two state system, i.e. a spinor χ. This approximate symmetry is known as isospin. The proton and neutrons are eigenstates of the isospin operator τ with quantum number $t = \frac{1}{2}$. Our convention is that protons have projection $m_t = \frac{1}{2}$ and neutrons $m_t = -\frac{1}{2}$.

Analogous to Section 2.3, operators can be separated into spherical tensor operators acting in isospin space. Rank-0 operators are known as "isoscalar" and have no isospin dependence. Rank-1 operators that depend on τ (τ_z or $\tau_\pm$) are "isovector".

A single-nucleon basis therefore consists of the states

$$\begin{aligned} \langle \vec{r}\sigma\tau | n\ell j m m_t \rangle =& \varphi_{n\ell j m m_t}(\vec{r},\sigma,\tau) \\ =& \sum_{m_\ell m_s} (\ell m_\ell s m_s | jm) \, \varphi_{n\ell m_\ell}(\vec{r}) \chi_{s m_s}(\sigma) \chi_{t m_t}(\tau) \; , \end{aligned} \tag{2.51}$$

where $s = \frac{1}{2}$ and $t = \frac{1}{2}$ is implicit in the first line. In the following sections we often use a collective index $\alpha = \{n\ell j m m_t\}$.

Spin-$\frac{1}{2}$ particles transform under rotations in physical space according to the two-dimensional representation of the group $SU(2)$. In the case of isospin-$\frac{1}{2}$, the particles transform under rotations in an abstract "isospin space" [11]. This is an internal symmetry corresponding to the invariance of the nuclear force with respect to quark "flavour" i.e. the type of quarks engaged in an interaction. Interactions between any pair of quarks or linear combinations of quarks are identical. The full symmetry would be the group $SU(6)$ (as there are 6 quark flavours) but this symmetry is explicitly broken by the widely differing

masses of the quarks. The up and down quarks are sufficiently close in mass that they form a very good approximation of the subgroup $SU(2)$. We can assign $u(d)$ the isospin projection $+\frac{1}{2}(-\frac{1}{2})$, hence the combinations $p = uud$ and $n = udd$ have $+\frac{1}{2}$ and $-\frac{1}{2}$ respectively.

Spin and isospin both combine according to the rules of angular momentum addition using the CG coefficients (2.23). To be explicit, for spin-$\frac{1}{2}$, let $|\uparrow\rangle = \left|s = \frac{1}{2}, m = \frac{1}{2}\right\rangle$ and $|\downarrow\rangle = \left|s = \frac{1}{2}, m = -\frac{1}{2}\right\rangle$. With two spinors $(\chi^{(1)}\chi^{(2)})$ we have the four combined states: $|\uparrow\uparrow\rangle$, $|\uparrow\downarrow\rangle$, $|\downarrow\uparrow\rangle$ and $|\downarrow\downarrow\rangle$. They are eigenstates of the combined spin projection operator $S_z = S_z^{(1)} + S_z^{(2)} = \frac{1}{2}\left(\sigma_z^{(1)} + \sigma_z^{(2)}\right)$, i.e. they have the eigenvalues 1, 0, 0, and -1 respectively (as $m = m_1 + m_2$).

The total spin corresponds to the operator:

$$S^2 = \left(\vec{S}^{(1)} + \vec{S}^{(2)}\right) \cdot \left(\vec{S}^{(1)} + \vec{S}^{(2)}\right) = \left(S^{(1)}\right)^2 + \left(S^{(2)}\right)^2 + 2\vec{S}^{(1)} \cdot \vec{S}^{(2)} \,. \tag{2.52}$$

The first two terms return eigenvalues of the total single-particle spin and will each be always $\frac{3}{4}$ e.g. $(S^{(1)})^2\chi^{(1)}\chi^{(2)} = \left(\frac{3}{4}\chi^{(1)}\right)\chi^{(2)} = \frac{3}{4}\chi^{(1)}\chi^{(2)}$. The last term can be calculated via $\vec{S}^{(1)} \cdot \vec{S}^{(2)} = \frac{1}{4}\left(\sigma_x^{(1)}\sigma_x^{(2)} + \sigma_y^{(1)}\sigma_y^{(2)} + \sigma_z^{(1)}\sigma_z^{(2)}\right)$, using the action of the Pauli matrices (Section A.1) which may flip the spins: $\sigma_x(\uparrow,\downarrow) = (\downarrow,\uparrow)$, $\sigma_y(\uparrow,\downarrow) = (-i\downarrow, i\uparrow)$ and $\sigma_z(\uparrow,\downarrow) = (\uparrow,-\downarrow)$. For example:

$$\begin{aligned}
\vec{S}^{(1)} \cdot \vec{S}^{(2)} |\uparrow\downarrow\rangle &= \frac{1}{4}\left[\left(\sigma_x^{(1)}\uparrow\right)\left(\sigma_x^{(2)}\downarrow\right) + \left(\sigma_x^{(1)}\uparrow\right)\left(\sigma_x^{(2)}\downarrow\right) + \left(\sigma_x^{(1)}\uparrow\right)\left(\sigma_x^{(2)}\downarrow\right)\right] \\
&= \frac{1}{4}\left[(\downarrow)(\uparrow) + (i\downarrow)(-i\uparrow) + (\uparrow)(-\downarrow)\right] \\
&= \frac{1}{4}\left[2|\downarrow\uparrow\rangle - |\uparrow\downarrow\rangle\right] \,.
\end{aligned} \tag{2.53}$$

It follows for the other states:

$$\vec{S}^{(1)} \cdot \vec{S}^{(2)} \begin{pmatrix} |\uparrow\uparrow\rangle \\ |\uparrow\downarrow\rangle \\ |\downarrow\uparrow\rangle \\ |\downarrow\downarrow\rangle \end{pmatrix} = \frac{1}{4}\begin{pmatrix} |\uparrow\uparrow\rangle \\ 2|\downarrow\uparrow\rangle - |\uparrow\downarrow\rangle \\ 2|\uparrow\downarrow\rangle - |\downarrow\uparrow\rangle \\ |\downarrow\downarrow\rangle \end{pmatrix} \,. \tag{2.54}$$

$|\uparrow\uparrow\rangle$ and $|\downarrow\downarrow\rangle$ are eigenstates of the total spin, e.g. $S^2|\uparrow\uparrow\rangle = \frac{1}{4}(3+3+2)|\uparrow\uparrow\rangle = 2|\uparrow\uparrow\rangle$. They are therefore spin-1 states ($|sm\rangle = |11\rangle$ and $|1-1\rangle$ respectively) as $s(s+1) = 2 \implies s = 1$. The remaining two states must be mixed to create eigenstates, i.e. $|10\rangle = \frac{1}{\sqrt{2}}(|\uparrow\downarrow\rangle + |\downarrow\uparrow\rangle)$ (spin-1) and $|00\rangle = \frac{1}{\sqrt{2}}(|\uparrow\downarrow\rangle - |\downarrow\uparrow\rangle)$ (spin-0). The necessary coefficients in the linear combinations, coupling two spin-$\frac{1}{2}$ to spin-1 or spin-0, are exactly the CG coefficients: $(\frac{1}{2}m_1\frac{1}{2}m_2|sm)$. A pair of spin-$\frac{1}{2}$ particles therefore can form four orthogonal states which are eigenstates of the total spin, a symmetric triplet with total 1 and an antisymmetric singlet with total 0.

An identical argument follows for isospin, i.e. $s \to t, \sigma \to \tau$ (τ_i are the same Pauli

matrices as σ_i for spin but acting in isospin space). A pair of isospin-$\frac{1}{2}$ particles can be arranged into an isospin-1 symmetric triplet and an isospin-0 antisymmetric singlet. Combined with spin, two nucleons have sixteen possible states. However, due to the necessary anti-symmetry of fermions, if we have a symmetric function of the spatial coordinates, the allowed states can only be in the combinations (symmetric spin, anti-symmetric isospin) or (anti-symmetric spin, symmetric isospin) e.g. (spin 1, isospin 0) or (spin 0, isospin 1). The explicit condition for anti-symmetry of two-nucleon states is $(-)^{\ell+s+t} = -1$. Likewise three-nucleon states have spin and isospin of $\frac{1}{2}$ or $\frac{3}{2}$ and must be anti-symmetrized.

2.5 Many-Body States

The naive way to model a system of A particles would be to assemble a many-body state as the direct product of single-particle wavefunctions $\varphi_{\alpha_i}(\vec{x}_i)$ ($\alpha_i = n_i\ell_i j_i m_i m_{ti}$, $\vec{x}_i = \vec{r}_i\sigma_i\tau_i$) i.e. $\phi_{\alpha_1\cdots\alpha_A}(\vec{x}_1,\cdots,\vec{x}_A) = \langle\vec{x}_1\cdots\vec{x}_A|\alpha_1\cdots\alpha_A\rangle = \varphi_{\alpha_1}(\vec{x}_1)\cdots\varphi_{\alpha_A}(\vec{x}_A)$. However this method cannot be correct as the states do not have the anti-symmetric exchange property of fermions. To enforce the Pauli principle we must have $\phi_{\alpha_1\alpha_2}(\vec{x}_1,\vec{x}_2) = -\phi_{\alpha_1\alpha_2}(\vec{x_2},\vec{x_1})$. Two fermions should not be in the same state or at the same position, i.e. $\phi_{\alpha\alpha}(\vec{x}_1,\vec{x}_2) = 0 = \phi_{\alpha_1\alpha_2}(\vec{x},\vec{x})$.

We can enforce the Pauli principle by assembling states $|\phi_\alpha\rangle$, normalized such that $\langle\phi_\alpha|\phi_\alpha\rangle = 1$, through Slater determinants, i.e.

$$\langle\vec{x}_1\cdots\vec{x}_A|\phi_\alpha\rangle = \langle\vec{x}_1\cdots\vec{x}_A|\alpha_1\cdots\alpha_A\rangle_{SD} = \frac{1}{\sqrt{A!}}\begin{vmatrix}\varphi_{\alpha_1}(\vec{x}_1) & \cdots & \varphi_{\alpha_A}(\vec{x}_1)\\ \vdots & \ddots & \vdots\\ \varphi_{\alpha_1}(\vec{x}_A) & \cdots & \varphi_{\alpha_A}(\vec{x}_A)\end{vmatrix}. \tag{2.55}$$

Slater determinant (SD) states allow us to use the formalism of creation and annihilation operators ("second quantization"). The algebraic relations of these operators precisely capture the desired anti-symmetry.

We start with a vacuum state $|0\rangle$ (no particles). The operator $a_i^\dagger$ creates a state which has a particle with index i (i.e. with the quantum numbers α_i). However if that index is already occupied we get zero. Similarly the operator a_i destroys a particle with index i but returns zero if that index is already empty. This is summarized by

$$\begin{aligned} a_i^\dagger|0\rangle &= |i\rangle\ , \quad a_i^\dagger|i\rangle = 0\ ,\\ a_i|i\rangle &= |0\rangle\ , \quad a_i|0\rangle = 0\ , \end{aligned} \tag{2.56}$$

with the algebraic properties:

$$\{a_i, a_j\} = 0\ ,\ \left\{a_i^\dagger, a_j^\dagger\right\} = 0\ , \quad \left\{a_i, a_j^\dagger\right\} = \delta_{ij}\ , \tag{2.57}$$

where the curly braces denote the anti-commutator: $\{a,b\} = ab + ba$. The Slater-determinant

state is exactly recovered by successive application of creation operators, i.e.

$$|\alpha_1 \cdots \alpha_A\rangle_{SD} = a^\dagger_{\alpha_1} \cdots a^\dagger_{\alpha_A} |0\rangle \ . \tag{2.58}$$

The calculation of many-body operators is greatly simplified by this formalism. If we have a spherical tensor operator which acts on the coordinates of a single nucleon, we can evaluate the expectation value for the entire nucleus by summing over all of the single-nucleon expectation values. The rank and projection of an operator $O_{\lambda\mu}$ are transferred to a pair of creation and annihilation operators, i.e.

$$O_{\lambda\mu} = \sum_{\alpha\beta} \langle\alpha| O_{\lambda\mu} |\beta\rangle \, a^\dagger_\alpha a_\beta \ , \tag{2.59}$$

$$O_\lambda = -\sum_{ab} \langle a| |O_\lambda| |b\rangle \, \hat{\lambda}^{-1} \left(a^\dagger_a \tilde{a}_b\right)_\lambda \ , \tag{2.60}$$

where the labels a, b include $n\ell j$ (in contrast to α, β: $n\ell jm$). A phase is added to the annihilation operator such that it obeys the correct tensor transformation properties: $\tilde{a}_{jm} = (-)^{j-m} a_{j-m}$ [42].

If we have the SD wavefunctions $|\psi_f\rangle$ and $|\psi_i\rangle$ then the reduced many-body transition matrix element is simply

$$\langle\psi_f| |O_\lambda| |\psi_i\rangle = -\sum_{ab} \langle a| |O_\lambda| |b\rangle \, \hat{\lambda}^{-1} \langle\psi_f| \left|\left(a^\dagger_a \tilde{a}_b\right)_\lambda\right| |\psi_i\rangle \ . \tag{2.61}$$

The $\langle\psi_f| \left|\left(a^\dagger_a \tilde{a}_b\right)_\lambda\right| |\psi_i\rangle$ term is referred to as the one-body transition density matrix element (OBDME). The only components of the OBDME which will be non-zero are those in which $|\psi_i\rangle$ and $|\psi_f\rangle$ don't have state b occupied and have state a empty respectively.

Some operators are more complicated and intrinsically depend on the coordinates of more than one nucleon at a time. One clear example is double-beta decay (explained in Section 3.2.3) In this case there are two protons in the final state where there were two neutrons in the initial state. Such operators are two-body operators and are computed via

$$\langle\psi_f| O_{\lambda\mu} |\psi_i\rangle = \sum_{\alpha\beta\gamma\delta} \langle\alpha\beta| O_{\lambda\mu} |\gamma\delta\rangle \langle\psi_f| a^\dagger_\alpha a^\dagger_\beta a_\delta a_\gamma |\psi_i\rangle \ . \tag{2.62}$$

These can be computed with coupled pairs of nucleons via the two-body density matrix elements (TBDME) $\langle\psi_f| \left|\left[\left[a^\dagger_a a^\dagger_b\right]_{J_{ab}} [\tilde{a}_c \tilde{a}_d]_{J_{cd}}\right]_\lambda\right| |\psi_i\rangle$, i.e.

$$\langle\psi_f| |O_\lambda| |\psi_i\rangle = -\frac{1}{4} \sum_{abcd} D_{ab} D_{cd} \hat{\lambda}^{-1} \langle ab; J_{ab}| \left|O^\lambda\right| |cd; J_{cd}\rangle \langle\psi_f| \left|\left[\left[a^\dagger_a a^\dagger_b\right]_{J_{ab}} [\tilde{a}_c \tilde{a}_d]_{J_{cd}}\right]_\lambda\right| |\psi_i\rangle \ , \tag{2.63}$$

where $D_{ab} = \sqrt{1 + \delta_{ab}}$ appears because $|ab; J_{ab}\rangle$ are orthonormalized [43].

Similarly for three-body operators (in particular the 3N force), we have

$$\langle\psi_f|\, O_{\lambda\mu}\,|\psi_i\rangle = \sum_{\alpha\beta\gamma\delta\epsilon\kappa} \langle\alpha\beta\gamma|\, O_{\lambda\mu}\,|\delta\epsilon\kappa\rangle \,\langle\psi_f|\, a^\dagger_\alpha a^\dagger_\beta a^\dagger_\gamma a_\kappa a_\epsilon a_\delta\,|\psi_i\rangle \ .$$

It is far too memory intensive to store three-body densities and so the matrix elements are generally computed "on-the-fly".

2.6 Intrinsic Coordinates

The nuclear Hamiltonian should describe the physics intrinsic to the nucleus. The harmonic oscillator Hamiltonian (2.2) has an external potential which cannot be physical. The true Hamiltonian (1.3) must use coordinates which are measured from the center of mass i.e. $\vec{r}_i \to \vec{r}_i - \vec{R}$ (where $\vec{R} = \frac{1}{A}\sum_i \vec{r}_i$) and $\vec{p}_i \to \vec{p}_i - \frac{1}{A}\vec{P}$ (where $\vec{P} = \sum_i \vec{p}_i$). Alternatively the Hamiltonian can use relative coordinates (i.e. T that depends on $p_i - p_j$ and V_{NN} that depends on $r_i - r_j$). The nuclear force should naturally depend only on the relative positions of nucleons and cannot be easily calculated otherwise as the center of mass position is not known a priori.

However we can still use the harmonic oscillator states to build up the nuclear wavefunction because they have very useful transformation properties. The center of mass dependence factors exactly [44]. We may use harmonic oscillator states which are functions of the relative coordinates. We choose to use the following set of so-called "Jacobi" coordinates:

$$\begin{aligned}
\vec{\xi}_0 =& \sqrt{\frac{1}{A}}\,[\vec{r}_1 + \cdots + \vec{r}_A] = \sqrt{A}\vec{R}\ , && (2.64)\\
\vec{\xi}_1 =& \sqrt{\frac{1}{2}}\,[\vec{r}_1 - \vec{r}_2]\ , \\
\vec{\xi}_2 =& \sqrt{\frac{2}{3}}\left[\frac{1}{2}\,(\vec{r}_1 + \vec{r}_2) - \vec{r}_3\right]\ , \\
&\vdots \\
\vec{\xi}_{A-1} =& \sqrt{\frac{A-1}{A}}\left[\frac{1}{A-1}\,(\vec{r}_1 + \vec{r}_2 + \cdots + \vec{r}_{A-1}) - \vec{r}_A\right]\ . && (2.65)
\end{aligned}$$

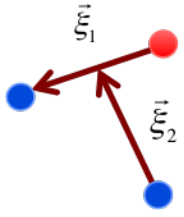

Figure 2.1: Schematic diagram of the Jacobi coordinates with three particles.

A many-particle state may be created simply by coupling harmonic oscillator states

that depend on each coordinate i.e. $\varphi_{n_1\ell_1 m_1}(\vec{\xi}_1)\varphi_{n_2\ell_2 m_2}(\vec{\xi}_2)\cdots\varphi_{n_{A-1}\ell_{A-1}m_{A-1}}(\vec{\xi}_{A-1})$. For example, a two particle basis may use only the ξ_1 coordinate and coupled spin and isospin, i.e.

$$\left\langle \vec{\xi}_1\sigma_1\sigma_2\tau_1\tau_2 \middle| n\ell sjmtm_t \right\rangle = \sum_{m_\ell m_s} (\ell m_\ell s m_s|jm)\,\varphi_{n\ell m_\ell}(\vec{\xi}_1)\,(\chi(\sigma_1)\chi(\sigma_2))_{sm_s}\,(\chi(\tau_1)\chi(\tau_2))_{tm_t}\ . \tag{2.66}$$

Additional particles have a coordinate that depends on their position relative to the center of mass of the other particles. $\vec{\xi}_2$ adds dependence on $\vec{r}_3$ but relative to $\frac{1}{2}(\vec{r}_1+\vec{r}_2)$ as shown in Figure 2.1. For three particles, we have to couple $\varphi_{n\ell sj}(\vec{\xi}_1)$ and $\varphi_{\mathcal{N}\mathcal{L}\mathcal{J}}(\vec{\xi}_2)$, i.e.

$$\left\langle \vec{\xi}_1\vec{\xi}_2\sigma_1\sigma_2\sigma_3 \middle| (n\ell sj\mathcal{N}\mathcal{L}\mathcal{J})NJM \right\rangle = \sum_{m\mathcal{M}} (jm\mathcal{J}\mathcal{M}|JM)\,\varphi_{n\ell sjm}(\vec{\xi}_1)\varphi_{\mathcal{N}\mathcal{L}\mathcal{J}\mathcal{M}}(\vec{\xi}_2) \tag{2.67}$$

where $N = 2n+\ell+2\mathcal{N}+\mathcal{L}$. Implicitly, we are adding along with $\vec{\xi}_2$ another spin-$\frac{1}{2}$ for σ_3 and we should also couple isospin: $\left\langle \tau_1\tau_2\tau_3 \middle| (t\tfrac{1}{2})T \right\rangle$.

In order to maintain anti-symmetry we need a specific combination of states, i.e.

$$|NiJT\rangle = \sum (n\ell sjt; N\mathcal{L}\mathcal{J}||NiJT)\,|n\ell sjt; N\mathcal{L}\mathcal{J}; JT\rangle \tag{2.68}$$

where we have another set of numbers $(n\ell sj; N\mathcal{L}\mathcal{J}||NiJT)$, the "coefficients of fractional parentage" (CFPs). There is a straightforward algorithm for constructing states of many particles with Jacobi coordinates and obtaining the CFPs [45]. An A-body state is a simple extension onto an $(A-1)$-state. However, as A increases this becomes much more expensive than a SD basis (and is not often done at $A \geq 7$ [46]). The set of indices i increases with N.

The connection between Slater determinant and Jacobi-coordinate bases comes from the Talmi-Moshinsky transformation [44]. With two nucleons the relation is

$$\sum_{m_1m_2} (\ell_1 m_1 \ell_2 m_2|\mathcal{L}\mathcal{M})\,\varphi_{n_1\ell_1m_1}(\vec{r}_1)\varphi_{n_2\ell_2m_2}(\vec{r}_2) = \sum_{n\ell mNLM} (n\ell NL\mathcal{L}|n_1\ell_1n_2\ell_2\mathcal{L})_{\frac{\mu_2}{\mu_1}} \times (\ell mLM|\mathcal{L}\mathcal{M})\,\varphi_{n\ell m}(\vec{\xi}_1)\varphi_{NLM}(\vec{\xi}_0)\ . \tag{2.69}$$

The quantities $(n\ell NL\mathcal{L}|n_1\ell_1n_2\ell_2\mathcal{L})_{\frac{\mu_2}{\mu_1}}$ are the so-called harmonic oscillator brackets for two particles of mass ratio $\frac{\mu_2}{\mu_1}$ (in this case 1) [47].

We have a choice of which basis to use, single-nucleon SD or Jacobi. In either case we have to solve an equivalent equation.

2.7 Solving the Schrodinger Equation

We may calculate the wavefunction of a nucleus by using an ansatz which is a linear combination of an (infinite) orthonormal basis, i.e.

$$|\psi\rangle = \sum_{\alpha} c_{\alpha} |\phi_{\alpha}\rangle \ , \tag{2.70}$$

where $\langle\phi_{\alpha}|\phi_{\beta}\rangle = \delta_{\alpha\beta}$.

We may find an approximate solution by using a finite basis. This can be done by solving the eigenvalue problem:

$$H |\psi_{\lambda}\rangle = E_{\lambda} |\psi_{\lambda}\rangle \ , \tag{2.71}$$

where we must calculate all the matrix elements:

$$H_{\beta\alpha} = \langle\phi_{\beta}| H |\phi_{\alpha}\rangle \ . \tag{2.72}$$

Through the variational principle, adding additional states to the basis will always improve the agreement between the lowest energy and the true ground state (if the trial wavefunction has any overlap with the ground state). The ground state $|\psi_0\rangle$ corresponds to the set of coefficients $c^{(0)}$ which minimize the energy, i.e.

$$\begin{aligned} E_0 &= \langle\psi_0| H |\psi_0\rangle \\ &= \sum_{\beta} c_{\beta}^{(0)*} \langle\phi_{\beta}| H \sum_{\alpha} c_{\alpha}^{(0)} |\phi_{\alpha}\rangle \\ &= \sum_{\alpha\beta} c_{\beta}^{(0)*} c_{\alpha}^{(0)} \langle\phi_{\beta}| H |\phi_{\alpha}\rangle \ . \end{aligned} \tag{2.73}$$

The next excited state has the minimal energy of states formed from the space orthogonal to the ground state. The next has minimal energy orthogonal to the first two. And so on...

2.8 The No-Core Shell Model

The no-core shell model (NCSM) is an *ab initio* technique which uses an expansion over a many-body harmonic oscillator basis to construct a many-nucleon wavefunction [7].

The goal is to find the solutions of the Schrodinger equation (1.3) (i.e. the eigenvectors of H (2.71)). These solutions will be eigenstates with good $J^{\pi}M_T$ quantum numbers (approximate T) and eigenvalues E_{λ}, i.e.

$$\left|\Psi_{A\lambda}^{J^{\pi}TM_T}\right\rangle = |A\lambda J^{\pi}TM_T\rangle \ , \tag{2.74}$$

where

$$H\,|A\lambda J^\pi T M_T\rangle = E_\lambda\,|A\lambda J^\pi T M_T\rangle\ . \tag{2.75}$$

The strategy of the NCSM is to find the coefficients of an ansatz wavefunction. The basis is made up of SD states of single particle harmonic oscillator states or harmonic oscillator states with Jacobi coordinates. The eigenstates are a sum over configurations, i.e.

$$|A\lambda J^\pi T M_T\rangle = \sum_{N_{\rm ex}=0}^{N_{\rm max}} \sum_{\alpha} c^{J^\pi T M_T}_{\lambda N_{\rm ex}\alpha}\,|A N_{\rm ex}\alpha J^\pi T M_T\rangle\ . \tag{2.76}$$

The label $N_{\rm ex}$ denotes the total number of excitations of nucleons above the lowest Pauli-allowed configuration. As the nucleons are in harmonic oscillator states, the excitation level for the i-th nucleon corresponds to its principal quantum number: $\tilde{N}_i = 2n_i + \ell_i$. The minimum configuration has $N_{\rm ex} = N_{\rm min}$ ($N_{\rm max} = 0$) determined by the Pauli principle, e.g. in ^{4}He all nucleons may be in $\tilde{N} = 0$, therefore $N_{\rm min} = 0$, but for ^{6}Li, there must be at least one proton and one neutron in $\tilde{N} = 1$ therefore $N_{\rm min} = 2$ (see Figure 2.2). Hence

$$N_{\rm ex} = \sum_i^A \tilde{N}_i - N_{\rm min}\ . \tag{2.77}$$

The label $\alpha = \{\alpha_1 \cdots \alpha_A\}$ denotes the configuration of nucleons with that $N_{\rm ex}$. For example, $N_{\rm ex} = 2$ includes all possible combinations of two nucleons excited by +1 level and one nucleon excited by +2. The sum over $N_{\rm ex}$ is restricted by parity to either an even or odd sequence. The number of configurations grows exponentially with $N_{\rm ex}$ and A. This is the main limitation for computation.

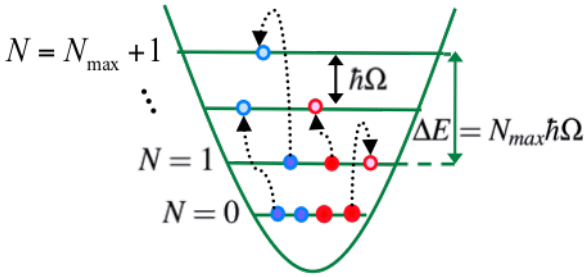

Figure 2.2: Truncation diagram for the NCSM. As an example, the solid circles indicate the lowest Pauli configuration of ^{6}Li. Here "N" corresponds to the harmonic oscillator excitation level ($\tilde{N}$ in the text).

The matrix elements of the kinetic energy can be easily computed analytically using (2.18). The matrix elements of the interaction from chiral effective field theory are computed via numerical integrals of the radial harmonic oscillator wavefunctions e.g. $\langle n'\ell'|\,V\,|n\ell\rangle =$

$\int r^2 \mathrm{d}r R^*_{n\ell}(r) V(r) R_{n\ell}(r)$. A useful property of harmonic oscillator states is that they are eigenfunctions of the Fourier transform [48], sometimes the matrix elements are easier to calculate in momentum space i.e. $\langle n'\ell'| V |n\ell\rangle = \int p^2 \mathrm{d}p R^*_{n\ell}(p) V(p) R_{n\ell}(p)$.

There is a compromise in the choice of basis between the scaling of the basis size with A versus the ease of removal of the center of mass. The Jacobi ξ are defined in an anti-symmetric way and therefore an A-nucleon eigenstate described by $A-1$ intrinsic coordinates can be directly related to an eigenstate expanded in the Slater determinant basis using (2.69), omitting spin and isospin, i.e.

$$\langle \vec{r}_1 \cdots \vec{r}_A | \psi \rangle_{SD} = \left\langle \vec{\xi}_1 \cdots \vec{\xi}_{A-1} \middle| \psi \right\rangle \varphi_{000}(\vec{\xi}_0) \ . \tag{2.78}$$

When using the Jacobi coordinates, center of mass motion does not contribute at all to the eigenenergies or eigenstates. However when using SD states, the excitation of the center of mass state $\varphi_{NLM}(\xi_0)$ can create spurious eigenstates that can appear at similar energy to real states. To remove the ambiguity between physical and spurious states the method of Lawson projection is used [49]. A term is added to the Hamiltonian controlled by the parameter $\beta \sim 1-10$ which pushes eigenstates with the center of mass in an excited state to a higher energy above the physically relevant states, i.e.

$$H = T_{\mathrm{rel}} + V + \beta \left(H_{\mathrm{CoM}} - \frac{3}{2}\Omega \right) \ , \tag{2.79}$$

where

$$H_{\mathrm{CoM}} = \frac{P^2}{2 m_N A} + \frac{m_N A \Omega R^2}{2} \ , \tag{2.80}$$

T_{rel} is defined in (1.4) and V consists of the remaining terms in (1.3).

The main computational hurdle of the NCSM is the diagonalization of a very large sparse matrix. The Lanczos procedure is an effective tool as it finds the extremal eigenvalues (and corresponding eigenstates) first (which are most physically relevant) [50]. The Hamiltonian is block-diagonal. For each $J^\pi T$ block, we have a matrix with respect to the $|N\alpha\rangle$ ($|N\alpha J^\pi T\rangle$) states, schematically:

$$H = \begin{pmatrix} \langle 00| H |00\rangle & \langle 00| H |10\rangle & \langle 00| H |11\rangle \cdots & \langle 00| H |N_{\max}\alpha_{\max}\rangle \\ \vdots & \ddots & & \vdots \\ & & & \langle N_{\max}\alpha_{\max}| H |N_{\max}\alpha_{\max}\rangle \end{pmatrix} \ . \tag{2.81}$$

The expansion has two input parameters which must be chosen to do a calculation, $N_{\max}$ and the oscillator frequency Ω. The predictions of any NCSM calculation will have some theoretical uncertainty based on the variation with respect to these parameters. For a given A value there will be a value of Ω which gives the lowest ground state energy.

Generally the largest possible $N_{\max}$ is used, but by computing at a succession of values we can determine whether our calculation is converged. An uncertainty of the ground state energy can be given based on an ad hoc extrapolation to an infinite basis by fitting the parameters (E_∞,a,b) of an exponential function, i.e.

$$E(N_{\max}) = E_\infty + ae^{-bN_{\max}} \ . \tag{2.82}$$

A fundamental limitation of the NCSM is that for finite $N_{\max}$ the asymptotics of weakly bound states cannot be correctly reproduced and the properties of continuum states ($E > 0$) cannot be calculated. This is because the states of the harmonic oscillator states fall to zero very quickly past the oscillator length. This is addressed with the extension NCSMC described in Section 6.2.

2.9 Static Nuclear Properties and Many-Body Operators

The wavefunction of the nucleus contains all the information needed to predict observable quantities. Each observable property corresponds to the expectation value of an operator.

One example is the size of the nucleus. The spatial extent of a single particle can be directly determined from the projection of the particle's state on the spatial coordinates, i.e. $\langle r|i\rangle = \psi_i(r)$. The mass density distribution should be simply $\psi^*(\vec{r})\psi(\vec{r})$, normalized such that $\langle\psi|\psi\rangle = \int \mathrm{d}^3r\psi^*(\vec{r})\psi(\vec{r}) = 1$. To determine, for example, the average radius we insert the squared-radius operator:

$$< r^2 >= \langle\psi|\, r^2\, |\psi\rangle = \int \mathrm{d}^3r\psi^*(\vec{r})r^2\psi(\vec{r}) \ . \tag{2.83}$$

The average radius is $\bar{r} = \sqrt{< r^2 >}$, as we require a scalar operator $r^2 = \vec{r}\cdot\vec{r}$ to calculate a scalar quantity. $< \vec{r} >$ will give the dipole moment (for protons).

For a many-body state $|\phi_\alpha\rangle$, the notation $\langle\phi_\alpha|\phi_\alpha\rangle$ implies that we integrate over all the nucleon coordinates ($\vec{x}_i = \vec{r}_i\sigma_i\tau_i$) i.e. $\int \mathrm{d}\xi = \int \prod_i^A \mathrm{d}^3r_i \sum_{m_s,m_t}$ such that

$$\langle\phi_\alpha|\phi_\alpha\rangle = \int \mathrm{d}\xi\phi^*_\alpha(\vec{x}_1,\cdots,\vec{x}_A)\phi_\alpha(\vec{x}_1,\cdots,\vec{x}_A) = 1 \ . \tag{2.84}$$

In the impulse approximation, we also attach to any operator a sum, the matter density operator $\rho_m(\vec{r}) = \sum_i^A \delta(\vec{r}-\vec{r}_i)$ and integrate over d^3r. A many-nucleon operator is then reduced to a sum of single-nucleon operators. The normalization factor is the mass number, i.e.

$$\langle\phi_\alpha|\, \rho_m(\vec{r})\, |\phi_\alpha\rangle = \int \mathrm{d}\xi \int \mathrm{d}^3r\phi^*_\alpha(\vec{x}_1,\cdots,\vec{x}_A)\sum_j^A \delta(\vec{r}-\vec{r}_j)\phi_\alpha(\vec{x}_1,\cdots,\vec{x}_A) = A \ . \tag{2.85}$$

The matter radius of a nucleus is:

$$\langle\phi_\alpha|\, r_m^2\, |\phi_\alpha\rangle = \frac{1}{A}\int \mathrm{d}\xi \int \mathrm{d}^3 r \phi_\alpha^*(\vec{x}_1,\cdots,\vec{x}_A) r^2 \sum_j^A \delta(\vec{r}-\vec{r}_j)\phi_\alpha(\vec{x}_1,\cdots,\vec{x}_A)\ , \tag{2.86}$$

using the operator:

$$r_m^2 = \frac{1}{A}\int \mathrm{d}^3 r \sum_i^A r^2 \delta(\vec{r}-\vec{r}_i)\ . \tag{2.87}$$

where $\vec{r}$ is taken relative to the center of mass. It is common to write this directly in the form

$$r_m^2 = \frac{1}{A}\sum_i^A r_i^2. \tag{2.88}$$

If we want to count only the protons (neutrons) we use the isospin projection operator $\frac{1+\tau_{zi}}{2}$ ($\frac{1-\tau_{zi}}{2}$). The point proton and neutron radius operators are then

$$r_p^2 = \frac{1}{Z}\sum_i^A \frac{1+\tau_{zi}}{2} r_i^2\ , \tag{2.89}$$

$$r_n^2 = \frac{1}{N}\sum_i^A \frac{1-\tau_{zi}}{2} r_i^2\ . \tag{2.90}$$

In the above, for the operators we should have used coordinates with respect to the center of mass i.e. $\vec{r}_i - \vec{R}$. Typically these are rewritten into a two-body form proportional to $\vec{r}_i - \vec{r}_j$, which are then used with the two-body transition densities [51], e.g. the matter radius (2.88) would be

$$\begin{aligned} r_m^2 =& \frac{1}{A}\sum_i \left(\vec{r}_i - \vec{R}\right)\cdot\left(\vec{r}_i - \vec{R}\right) \\ =& \frac{1}{A^2}\sum_{i<j} (\vec{r}_i - \vec{r}_j)^2\ . \end{aligned} \tag{2.91}$$

We would then integrate over only the internal coordinates, i.e. $\int \mathrm{d}\xi = \int \prod_{i=1}^{A-1} \mathrm{d}^3\xi_i \sum_{m_s,m_t}$.

Some operators can be easily converted to two-nucleon relative coordinates. Different operators may have a different scaling factors depending whether they depend on the spatial coordinates versus for example spin [51]. It depends whether we are summing A nucleons, $\frac{A(A-1)}{2}$ pairs of nucleons or $\frac{A(A-1)(A-2)}{6}$ triplets.

The orbital angular momentum operator with coordinates defined with respect to the

center of mass can be converted as

$$\begin{aligned}\vec{L} =& \sum_i (\vec{r}_i - \vec{R}) \times (\vec{p}_i - \frac{1}{A}\vec{P}) \\ =& \frac{1}{A}\sum_{i<j} (\vec{r}_i - \vec{r}_j) \times (\vec{p}_i - \vec{p}_j) \ . \end{aligned} \tag{2.92}$$

However, when the single-nucleon spin operator $\vec{s}$ is upgraded to a two-nucleon coupled spin, we need a different A-dependent scaling factor, i.e.

$$\begin{aligned}\vec{S} =& \sum_i \vec{s}_i \\ =& \frac{1}{A-1}\sum_{i<j} (\vec{s}_i + \vec{s}_j) \quad . \end{aligned} \tag{2.93}$$

General operators (i.e. spherical tensor operators) which depend on the single-nucleon coordinates (and momenta) can be evaluated with Jacobi coordinate basis states by using translationally invariant transition densities and replacing the coordinates in tandem with applying appropriate scaling (when using a harmonic oscillator basis). The standard SD matrix elements (2.61) contain center of mass contamination, i.e. the matrix elements:

$$\begin{aligned}{}_{SD}\left\langle A\lambda_f J_f \right| \left| O_\lambda \right| \left| A\lambda_i J_i \right\rangle_{SD} =& -\frac{1}{\hat{\lambda}} \sum_{1,2} \left\langle n_1 l_1 j_1 \right| \left| O_\lambda(\vec{r},\sigma) \right| \left| n_2 l_2 j_2 \right\rangle \\ & \times {}_{SD}\left\langle A\lambda_f J_f \right| \left| \left(a^\dagger_{n_1 l_1 j_1} \tilde{a}_{n_2 l_2 j_2} \right)_\lambda \right| \left| A\lambda_i J_i \right\rangle_{SD} \ . \end{aligned} \tag{2.94}$$

However, eigenstates in the SD basis may still be used with the matrix elements of the eigenstates in the Jacobi basis and translationally-invariant densities, to compute the translationally invariant matrix elements:

$$\begin{aligned}\left\langle A\lambda_f J_f \right| \left| O_\lambda \right| \left| A\lambda_i J_i \right\rangle =& -\frac{1}{\hat{\lambda}} \sum \left\langle nlj \right| \left| O_\lambda(-\sqrt{\frac{A-1}{A}}\vec{\xi},\sigma) \right| \left| n'l'j' \right\rangle \\ & \times \left(M^\lambda \right)^{-1}_{nljn'l'j',n_1 l_1 j_1 n_2 l_2 j_2} \\ & \times {}_{SD}\left\langle A\lambda_f J_f \right| \left| \left(a^\dagger_{n_1 l_1 j_1} \tilde{a}_{n_2 l_2 j_2} \right)_\lambda \right| \left| A\lambda_i J_i \right\rangle_{SD} \ , \end{aligned} \tag{2.95}$$

where $\vec{\xi}$ is short-hand for $\vec{\xi}_{A-1}$ (2.65) and the sum is over all quantum numbers which do not appear on the left. The transformation matrix M^λ is defined in [52] and combines with the OBDME to form a translationally invariant quantity. The general strategy is to replace $\vec{r} \to \sqrt{\frac{A-1}{A}}\vec{\xi}$ and $\vec{\nabla}_r \to -\sqrt{\frac{A-1}{A}}\vec{\nabla}_\xi$.

2.10 Charge and Current Densities of the Nucleus

To calculate the charge density distribution $\rho(\vec{r})$ of the nucleons, we again use $\frac{1+\tau_{zi}}{2}$ to select only the protons, i.e. with the operator:

$$\rho(\vec{r}) = e\sum_{i=1}^{A}\frac{1+\tau_{zi}}{2}\delta(\vec{r}-\vec{r}_i)\ . \tag{2.96}$$

For generality we can evaluate the expectation of the operator acting between two different nuclear eigenstates $|i\rangle$ and $|f\rangle$ (which are linear combinations of the basis states $|\phi_\alpha\rangle$), i.e.

$$\langle f|\,\rho(\vec{r})\,|i\rangle = e\sum_{j}^{A}\frac{1+\tau_{zj}}{2}\int \mathrm{d}\xi\psi_f^*(\vec{x}_1,\cdots,\vec{x}_A)\delta(\vec{r}-\vec{r}_j)\psi_i(\vec{x}_1,\cdots,\vec{x}_A)\ . \tag{2.97}$$

The total charge is normalized to Z, i.e.

$$\langle f|\,\rho\,|i\rangle = \int \mathrm{d}^3r\,\langle f|\,\rho(\vec{r})\,|i\rangle = Z\delta_{fi}\ . \tag{2.98}$$

The nucleons are moving within the nucleus. This creates a charged "convection current" density $\vec{j}_c$ which can be summarized via the velocity distribution of the protons, using $\vec{v} = \frac{\vec{p}}{m_N} \to \frac{-i\vec{\nabla}}{m_N}$, i.e.

$$\vec{j}_c(\vec{r}) = e\sum_{i}\frac{1+\tau_{zj}}{2}\left(\frac{\vec{p}_i\delta(\vec{r}-\vec{r}_i)+\delta(\vec{r}-\vec{r}_i)\vec{p}_i}{2m_N}\right)\ . \tag{2.99}$$

Because $\vec{p}$ and δ do not commute, we must use the symmetric combination [53, 54]. The result for many-nucleon states is

$$\langle f|\,\vec{j}_c(\vec{r})\,|i\rangle = -ie\sum_{j}\frac{1+\tau_{zj}}{2m_N}\int \mathrm{d}\xi\psi_f^*(\vec{x}_1,\cdots,\vec{x}_A)\vec{\nabla}_j\psi_i(\vec{x}_1,\cdots,\vec{x}_A)\ . \tag{2.100}$$

There are corrections to the current due to the presence of charged exchange particles (pions) in χEFT which will be discussed later (Section 3.1.2 and Section 3.2.1).

The divergence free part of the current can be separated out and described as the curl of a magnetization, i.e.

$$\vec{j}_c(\vec{r}) = \vec{j}(\vec{r}) + \vec{\nabla}\times\vec{\mu}_\ell(\vec{r})\ , \tag{2.101}$$

defining $\vec{j} = \vec{j}_c - \vec{\nabla}\times\vec{\mu}_\ell$, where $\vec{\nabla}\cdot\vec{j} = \vec{\nabla}\cdot\vec{j}_c$. The magnetization comes from the component of the protons motion contributing to their angular momentum i.e. it is proportional to the

orbital angular momentum operator $\vec{L}$ and can be written as

$$\vec{\mu}_\ell(\vec{r}) = \frac{e}{2m_N}\sum_i^A \frac{1+\tau_{zi}}{2}\left(\frac{\vec{L}_i\delta(\vec{r}-\vec{r}_i)+\delta(\vec{r}-\vec{r}_i)\vec{L}_i}{2}\right) . \tag{2.102}$$

The nucleons also have intrinsic magnetic moments due to their internal structure. Part of the magnetization is simply a sum over the individual magnetic moments: protons $\vec{\mu}_p = g_p\mu_N\vec{\sigma}$ and neutrons $\vec{\mu}_n = g_n\mu_N\vec{\sigma}$, proportional to spin with the corresponding g factors: $g_p = 2.793$ and $g_n = -1.913$, in units of the nuclear magneton $\mu_N = \frac{e}{2m_N}$, i.e.

$$\vec{\mu}_s(\vec{r}) = \sum_i^A \mu_i\delta(\vec{r}-\vec{r}_i)\vec{\sigma}_i , \tag{2.103}$$

$$\mu_i = \mu_N\left(\frac{1+\tau_{zi}}{2}g_p + \frac{1-\tau_{zi}}{2}g_n\right) . \tag{2.104}$$

The intrinsic magnetization is a clear example of the isoscalar/isovector breakdown of an operator. It can be rearranged, i.e.

$$\mu_i = \mu^{IS} + \mu_i^{IV} , \tag{2.105}$$

$$\mu^{IS} = \frac{1}{2}\left(g_p + g_n\right) , \tag{2.106}$$

$$\mu_i^{IV} = \frac{\tau_{zi}}{2}\left(g_p - g_n\right) . \tag{2.107}$$

The total electromagnetic current operator is then

$$\vec{\mathcal{J}}(\vec{r}) = \vec{j}_c(\vec{r}) + \vec{\nabla}\times\vec{\mu}_s(\vec{r}) = \vec{j}(\vec{r}) + \vec{\nabla}\times\left(\vec{\mu}_s(\vec{r}) + \vec{\mu}_\ell(\vec{r})\right) . \tag{2.108}$$

The charge and current determine the interaction between the nucleus and the electromagnetic field. As will be discussed in Section 3.1, a nucleus may change state by interaction with the electromagnetic field. The charge and current distribution can be decomposed into spherical tensor operators (multipoles) as in (2.31) and their interaction with a classical electromagnetic field defines the static electric (E) and magnetic (M) moment operators [54]:

$$M^E_{\lambda\mu}(\vec{r}) = r^\lambda Y_{\lambda\mu}(\Omega_r)\rho(\vec{r}) , \tag{2.109}$$

$$M^M_{\lambda\mu}(\vec{r}) = \left(\vec{\mu}_s(\vec{r}) + \frac{1}{\lambda+1}\vec{r}\times\vec{j}_c(\vec{r})\right)\cdot\vec{\nabla}r^\lambda Y_{\lambda\mu}(\Omega_r) . \tag{2.110}$$

The multipole order is limited to $\lambda \geq 0$ for E and $\lambda \geq 1$ for M.

Chapter 3

Electroweak Decays of Nuclei

According to Fermi's Golden Rule [11], the rate of a decay is proportional to the product of the "amplitude" $\mathcal{M}$ for the process (corresponding to a nuclear matrix element) and the available phase space volume (all possible final states and combinations of momentum). The general formula for the decay rate Γ of an initial particle of mass M_I to N particles is:

$$\Gamma_{1\to N} = \frac{\mathcal{S}}{2M_I} \bar{\sum_i} \sum_f \int |\mathcal{M}|^2 \prod_{F=1}^{N} \frac{\mathrm{d}^3 p_F}{(2\pi)^3 2E_F} \,, \tag{3.1}$$

where i and f label available internal states of the initial particle I and final outgoing particles F, respectively. $\mathcal{S}$ is the symmetry factor that corrects for double-counting of identical particles in the final state, it gets a factor $1/n!$ for each group of n identical particles [11].

The bar on the first sum $\bar{\sum}$ means an average, as an initial state may be in superposition of quantum numbers. For example, in an unpolarized collection of spin-$\frac{1}{2}$ particles, the projections $+\frac{1}{2}$ and $-\frac{1}{2}$ are equally likely and so we average by dividing by two. For particles with total angular momentum J the projection M may vary from $-J$ to J and so $\bar{\sum}_M = \frac{1}{2J+1} \sum_M$.

The infinitesimal phase space volume for a particle of 4-momentum $P = (E, \vec{p})$ is $\frac{\mathrm{d}^4 P}{(2\pi)^4}$. The 4-momentum phase-space is reduced to 3-momentum by the constraint that initial and final momenta be "on-shell" ($P^2 = m^2 = E^2 - p^2$ and $E \geq 0$), i.e.

$$\begin{aligned} \int \frac{\mathrm{d}^4 P}{(2\pi)^4} 2\pi \delta(E^2 - p^2 - m^2)\theta(E) &= \int \frac{\mathrm{d}E \mathrm{d}^3 p}{(2\pi)^4} \frac{2\pi}{2\sqrt{p^2+m^2}} \delta(E - \sqrt{p^2+m^2}) \\ &= \int \frac{\mathrm{d}^3 p}{(2\pi)^3 2E} \,. \end{aligned} \tag{3.2}$$

The amplitude (or matrix element) will depend on the interaction of the initial and final quantum fields of the process. For forces that can be described by a perturbative theory, the interactions can be understood as a hierarchy of diagrams as laid out by Feynman

(originally for QED [55]). The Feynman rules can be derived from the Standard Model (or EFT) Lagrangian. Each particle is represented by a line and the interactions are represented by a vertex (the connection between lines). A simplified version of the rules is as follows:

1. For each incoming particle we insert a wavefunction $|I\rangle$. For each outgoing particle we have a conjugate wavefunction $\langle F|$.
   - leptons (such as electrons and neutrinos) are described by Dirac spinors $u^s(p)$ with spin s
   - photons are described by a polarization vector $\vec{e}_\lambda(\vec{q})$
2. At each vertex we insert the coupling constant and operator corresponding to the interaction. In addition we have a δ over the 4-momenta going into and out of the vertex. Some examples:
   - For elementary particles the vertex is extremely simple, e.g. for an electron interacting with a photon we have $ie\gamma^\mu$ where e is the charge coupling constant ($e^2 = 4\pi\alpha$, $\alpha \simeq \frac{1}{137}$), γ^μ is a Dirac gamma matrix
   - For nuclei we have a more complicated operator. As we will see in Section 3.1, the interaction of a nucleus and a photon can be wrapped into the nuclear current operator $\mathcal{J}_\mu(q)$. In principle, the current should have additive contributions from each nucleon but the vertices should take into account the internal structure [53]. See Section B.3 for more details.
3. Finally, if necessary, we add a propagator for particles corresponding to any internal lines and integrate over the internal phase space.
   - For photons, insert $-\frac{i\eta_{\mu\nu}}{q^2}$ and integrate over $\int \frac{\mathrm{d}^4 q}{(2\pi)^4}$

The vertex factors arise from interaction terms in the Lagrangian of a theory while the propagators come from the "free" terms [11].

3.1 Electromagnetism: γ Decay

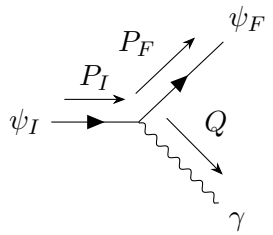

Figure 3.1: The Feynman diagram and kinematics for photon emission.

Electromagnetic interactions are relevant to nuclear reactions (especially radiative capture) but here we first present the formalism for bound-bound decays.

In a gamma decay we have a one particle in the initial state (the initial nucleus) and two particles in the final state (a different nuclear state and a photon). The leading order ("tree level") Feynman diagram corresponding to this process is shown in Figure 3.1. A physical (massless) photon with 4-momentum $Q = (\omega, \vec{q})$ is limited by the condition $|\vec{q}| = \omega$ and has two possible polarizations $\lambda = \pm 1$.

The γ-decay rate for a nucleus at rest with mass M_I ($P_I = (M_I, \vec{0})$) is

$$\Gamma = \frac{1}{2M_I} \bar{\sum_i} \sum_f \sum_\lambda \int \left| \mathcal{M}_{FI}^{\lambda Q} \right|^2 \frac{\mathrm{d}^3 q}{(2\pi)^3 2\omega} \frac{\mathrm{d}^3 p_F}{(2\pi)^3 2E_F} \ . \tag{3.3}$$

The rate depends on an average over possible initial states and a sum over the possible final states (including an integral over the final phase space).

We have the initial state with the nucleus in state $|I\rangle$ and no photons $|0\rangle$. The final state is $|F\rangle$ with a photon state $|Q\lambda\rangle$. The strength of the interaction between the photon field and the nucleus is the expectation value between these states of the overlap of quantum fields over all space, i.e.

$$\mathcal{M}_{FI}^{\lambda Q} = \langle F; Q\lambda | \int \mathrm{d}^4 x A_\mu(x) \mathcal{J}^\mu(x) \left| I; 0 \right\rangle \ . \tag{3.4}$$

Due to gauge invariance we can set the scalar part of the radiation field to 0, i.e. choose $A = (0, \vec{A})$. $\mathcal{J} = (\rho, \vec{\mathcal{J}})$ is the nuclear current operator which extracts the distribution of electromagnetic charge and currents in the nucleus. Since the states can be factorized ($\langle F | \langle Q\lambda |$ and $|I\rangle |0\rangle$), the operators act separately on the nuclear and photon spaces ($\langle Q\lambda | A_\mu(x) |0\rangle$ and $\langle F | \mathcal{J}^\mu(x) |I\rangle$). The above assumes first-order perturbation theory because the coupling constant (the proton charge) e is small. Here e is absorbed into the definition of the nuclear current. Because the quantum states are eigenstates of their respective Hamiltonians, the time dependent parts of the wavefunctions are exponential: $\psi_a(\vec{x}, t) = \langle \vec{x} | a \rangle \, e^{-iE_a t}$, and so the integral over time will give a δ for the energies i.e. $\int \mathrm{d}t e^{i\omega t} = 2\pi\delta(\omega)$. Therefore:

$$\begin{aligned} \mathcal{M}_{FI}^{\lambda Q} =& \int \mathrm{d}t e^{iE_F t} e^{i\omega t} e^{-iE_I t} \int \mathrm{d}^3 x \langle F | \langle Q\lambda | \vec{A}(\vec{x}) \cdot \vec{\mathcal{J}}(\vec{x}) |I\rangle |0\rangle \\ =& 2\pi\delta(E_F + \omega - E_I) \int \mathrm{d}^3 x \langle Q\lambda | \vec{A}(\vec{x}) |0\rangle \cdot \langle F | \vec{\mathcal{J}}(\vec{x}) |I\rangle \ . \end{aligned} \tag{3.5}$$

The photon field has the form [13, 56]:

$$\vec{A}(\vec{x}) = \int \frac{\mathrm{d}^3 k}{(2\pi)^3 2\omega_k} \sum_{\lambda'} \left(\vec{e}_{\lambda'}(\vec{k}) e^{i\vec{k}\cdot\vec{x}} a_{\lambda'}(\vec{k}) + \vec{e}^*_{\lambda'}(\vec{k}) e^{-i\vec{k}\cdot\vec{x}} a^\dagger_{\lambda'}(\vec{k}) \right) \ , \tag{3.6}$$

where we have the creation and annihilation operators $a^\dagger_\lambda$, a_λ with commutation relations for bosons: $\left[a_\lambda(\vec{q}), a^\dagger_{\lambda'}(\vec{k})\right] = 2\omega_q \delta_{\lambda\lambda'}(2\pi)^3\delta^3(\vec{q}-\vec{k})$ with $\omega_q = \omega = |\vec{q}|$ and $\omega_k = |\vec{k}|$. $\vec{e}_\lambda(\vec{k})$ are polarization vectors with $\lambda = \pm 1$. They satisfy $\vec{e}_\lambda \cdot \vec{e}^*_{\lambda'} = \delta_{\lambda\lambda'}$ and $\vec{e}^*_\lambda = (-1)^\lambda \vec{e}_{-\lambda}$. The final state is then $\langle Q\lambda| = \langle \vec{q}\lambda| = \langle 0| a_\lambda(\vec{q})$ and only the $a^\dagger$ term of $\vec{A}$ survives, i.e.

$$\begin{aligned}\langle \vec{q}\lambda|\, \vec{A}(\vec{x})\, |0\rangle =& \langle 0|\, a_\lambda(\vec{q}) \int \frac{\mathrm{d}^3k}{(2\pi)^3 2\omega_k} \sum_{\lambda'} \vec{e}^*_{\lambda'}(\vec{k}) e^{-i\vec{k}\cdot\vec{x}} a^\dagger_{\lambda'}(\vec{k})\, |0\rangle \\ =& \vec{e}^*_\lambda(\vec{q}) e^{-i\vec{q}\cdot\vec{x}} \ . \end{aligned} \tag{3.7}$$

The nuclear states can be factorized into an intrinsic state and a center of mass wave [53], i.e.

$$\begin{aligned}|I\rangle =& |P_I, i\rangle = \sqrt{2E_I} e^{i\vec{p}_I\cdot\vec{R}}\, |i\rangle \ , \\ |F\rangle =& |P_F, f\rangle = \sqrt{2E_F} e^{i\vec{p}_F\cdot\vec{R}}\, |f\rangle \ , \end{aligned} \tag{3.8}$$

where the normalization treats the nucleus as a generalized Dirac spinor. The matrix element of $\langle F|\, \vec{\mathcal{J}}(\vec{x})\, |I\rangle$ is evaluated as an integral over the spatial center of mass coordinates $\vec{R}$ and all of the nucleon intrinsic coordinates summarized by ξ. Inserting (3.7) and (3.8) the integral in (3.5) is

$$\begin{aligned}&\int \mathrm{d}^3x\, \langle \vec{q}\lambda|\, \vec{A}(\vec{x})\, |0\rangle \cdot \langle F|\, \vec{\mathcal{J}}(\vec{x})\, |I\rangle \\ =& \int \mathrm{d}^3x \int \mathrm{d}\xi \int \mathrm{d}^3R \left\langle F\middle|\xi, \vec{R}\right\rangle \left[e^{-i\vec{q}\cdot\vec{x}} \vec{e}^*_\lambda \cdot \vec{\mathcal{J}}(\vec{x})\right] \left\langle \xi, \vec{R}\middle| I\right\rangle \\ =& \sqrt{2E_I 2E_F} \int \mathrm{d}\xi \int \mathrm{d}^3R\, \langle f|\xi\rangle\, e^{-i\vec{p}_F\cdot\vec{R}} \left[\int \mathrm{d}^3x e^{-i\vec{q}\cdot\vec{x}} \vec{e}^*_\lambda \cdot \vec{\mathcal{J}}(\vec{x})\right] e^{i\vec{p}_I\cdot\vec{R}}\, \langle \xi|i\rangle \ . \end{aligned} \tag{3.9}$$

We may change variables $\vec{x}' = \vec{x} - \vec{R}$ to evaluate the matrix element with operators of intrinsic coordinates (as in Section 2.9 and Section 2.10). The current operator should be translationally invariant and the integration over $\vec{R}$ returns δ, i.e.

$$\begin{aligned}&\int \mathrm{d}\xi \int \mathrm{d}^3R\, \langle f|\xi\rangle\, e^{-i\vec{p}_F\cdot\vec{R}} \left[\int \mathrm{d}^3x' e^{-i\vec{q}\cdot(\vec{x}'+\vec{R})} \vec{e}^*_\lambda(\vec{q}) \cdot \vec{\mathcal{J}}(\vec{x}'+\vec{R})\right] e^{i\vec{p}_I\cdot\vec{R}}\, \langle \xi|i\rangle \\ =& \int \mathrm{d}\xi\, \langle f|\xi\rangle \left[\int \mathrm{d}^3R e^{-i(\vec{p}_F - \vec{p_I} + \vec{q})\cdot\vec{R}}\right] \left[\int \mathrm{d}^3x' e^{-i\vec{q}\cdot\vec{x}'} \vec{e}^*_\lambda(\vec{q}) \cdot \vec{\mathcal{J}}(\vec{x}')\right] \langle \xi|i\rangle \\ =& (2\pi)^3 \delta(\vec{p}_I - \vec{p}_F - \vec{q})\, \langle f|\, \vec{e}^*_\lambda(\vec{q}) \cdot \vec{\mathcal{J}}(\vec{q})\, |i\rangle \ . \end{aligned} \tag{3.10}$$

The matrix element contains the standard nuclear current transition operator (the Fourier transform of the spatial charged current density operator of Section 2.10):

$$\vec{\mathcal{J}}(\vec{q}) = \int \mathrm{d}^3r e^{-i\vec{q}\cdot\vec{r}} \vec{\mathcal{J}}(\vec{r}) \ . \tag{3.11}$$

Inserting (3.9) and (3.10) into (3.5) we have the amplitude for gamma-decay:

$$\mathcal{M}_{FI}^{\lambda Q} = (2\pi)^4 \delta^4(P_I - P_F - Q)\sqrt{2E_I 2E_F}\,\langle f|\,\vec{e}^{\,*}_\lambda(\vec{q})\cdot\vec{\mathcal{J}}(\vec{q})\,|i\rangle\ . \tag{3.12}$$

We use the property $[\delta(x)]^2 = \frac{\delta(x)}{(2\pi)^4}$ and $E_I = M_I$ and the decay rate becomes:

$$\begin{aligned}\Gamma =& \frac{1}{2M_I}\bar{\sum_i}\sum_f\sum_\lambda\int(2\pi)^4\delta^4(P_I - P_F - Q)2M_I 2E_F\left|\langle f|\,\vec{e}^{\,*}_\lambda(\vec{q})\cdot\vec{\mathcal{J}}(\vec{q})\,|i\rangle\right|^2\frac{\mathrm{d}^3q}{(2\pi)^3 2\omega}\frac{\mathrm{d}^3p_F}{(2\pi)^3 2E_F}\\ =& \bar{\sum_i}\sum_f\sum_\lambda\int\left|\langle f|\,\vec{e}^{\,*}_\lambda(\vec{q})\cdot\vec{\mathcal{J}}(\vec{q})\,|i\rangle\right|^2\frac{\mathrm{d}^3q}{(2\pi)^3 2\omega}2\pi\delta(M_I - E_F - \omega)\ .\end{aligned} \tag{3.13}$$

3.1.1 Multipole Decomposition of Electromagnetic Current

The electromagnetic current operators $\mathcal{J}(\vec{q}) = (\rho, \vec{\mathcal{J}})$ (sometimes called "form factors" or "response functions"), needed to evaluate the rate, are the Fourier transforms of the spatial charge and current distributions of the nucleus ($\rho(\vec{r})$ and $\vec{\mathcal{J}}(\vec{r})$ defined in Section 2.9). The charge density operator is defined by

$$\rho(\vec{q}) = \int \mathrm{d}^3 r e^{-i\vec{q}\cdot\vec{r}}\rho(\vec{r})\ . \tag{3.14}$$

The plane wave $e^{-i\vec{q}\cdot\vec{r}}$ has a straight-forward decomposition into spherical tensor operators, i.e.

$$e^{-i\vec{q}\cdot\vec{r}} = 4\pi\sum_{JM}(-i)^J j_J(qr)Y_{JM}(\Omega_r)Y^*_{JM}(\Omega_q) \tag{3.15}$$

with $J \geq 0$, $-J \leq M \leq J$. To simplify later equations we combine the Bessel function and spherical harmonic into the useful quantity:

$$M_{JM}(q,\vec{r}) = j_J(qr)Y_{JM}(\Omega_r). \tag{3.16}$$

The charge density operator is then

$$\rho(\vec{q}) = 4\pi\sum_{JM}(-i)^J Y^*_{JM}(\Omega_q)\int \mathrm{d}^3 r M_{JM}(q,\vec{r})\rho(\vec{r}) \tag{3.17}$$

$$= 4\pi\sum_{JM}(-i)^J Y^*_{JM}(\Omega_q)\mathcal{C}_{JM}(q)\ , \tag{3.18}$$

which defines the "Coulomb multipole operator"

$$\mathcal{C}_{JM}(q) = \int \mathrm{d}^3 r M_{JM}(q,\vec{r})\rho(\vec{r})\ . \tag{3.19}$$

This is simplified by setting $e_z = \hat{q}$ (then only $M = 0$ contributes as $Y_{LM}(\theta_q = 0) = \frac{\hat{L}}{\sqrt{4\pi}}\delta_{M0}$), i.e.

$$\rho(q) = \sqrt{4\pi}\sum_J (-i)^J \hat{J}\mathcal{C}_{J0}(q);\,. \tag{3.20}$$

This also means that the operators don't need to be written in terms of $\vec{q}$, but depend on $q = |\vec{q}|$.

A vector operator like the current can be spanned by the polarization vectors, including the longitudinal, $\vec{e}_0 = \vec{e}_z$, in addition to the transverse, $\vec{e}_{\pm 1} = \mp\frac{1}{\sqrt{2}}(\vec{e}_x \pm i\vec{e}_y)$. Using this basis, the current can be decomposed as

$$\vec{\mathcal{J}}(q) = \sum_\lambda \mathcal{J}(q,\lambda)\vec{e}^*_\lambda\,. \tag{3.21}$$

The components of the current density operator are then

$$\begin{aligned}\mathcal{J}(q,\lambda) =& \vec{e}_\lambda \cdot \vec{\mathcal{J}}(q)\\ =& \int \mathrm{d}^3 r e^{-i\vec{q}\cdot\vec{r}}\vec{e}_\lambda \cdot \vec{\mathcal{J}}(\vec{r})\\ =& \int \mathrm{d}^3 r \left(4\pi\sum_{JM}(-i)^J j_J(qr)Y_{JM}(\Omega_r)Y^*_{JM}(\Omega_q)\right)\vec{e}_\lambda\cdot\vec{\mathcal{J}}(\vec{r})\,.\end{aligned} \tag{3.22}$$

The spherical vector harmonics, which are defined as

$$\vec{Y}_{JLM}(\Omega) = \sum_{m\lambda}(Lm1\lambda|JM)\,Y_{Lm}(\Omega)\vec{e}_\lambda\,, \tag{3.23}$$

can be combined with the Bessel functions to form

$$\vec{M}_{JLM}(q,\vec{r}) = j_L(qr)\vec{Y}_{JLM}(\Omega_r)\,, \tag{3.24}$$

and then with the vector current, to obtain the quantity:

$$M_{JLM}(q) = \int \mathrm{d}^3 r j_L(qr)\vec{Y}_{JLM}(\Omega_r)\cdot\vec{\mathcal{J}}(r)\,. \tag{3.25}$$

Using the inverse relation for vector spherical harmonics:

$$Y_{JM}(\Omega)\vec{e}_\lambda = \sum_{Lm}(JM1\lambda|Lm)\,\vec{Y}_{LJm}(\Omega)\,, \tag{3.26}$$

the components can be simplified (preemptively swapping $J \leftrightarrow L$), i.e.

$$\begin{aligned}\mathcal{J}(q,\lambda) =& 4\pi \sum_{LM} (-i)^L Y^*_{LM}(\Omega_q) \int \mathrm{d}^3 r j_L(qr) \left(\sum_{Jm} (LM1\lambda|Jm)\, \vec{Y}_{JLm}(\Omega_r) \right) \cdot \vec{\mathcal{J}}(\vec{r}) \\ =& 4\pi \sum_{LM} (-i)^L \frac{\hat{L}\delta_{M0}}{\sqrt{4\pi}} \sum_{Jm} (LM1\lambda|Jm) \int \mathrm{d}^3 r \vec{M}_{JLm}(q,\vec{r}) \cdot \vec{\mathcal{J}}(r) \\ =& \sqrt{4\pi} \sum_{LJ} (-i)^L \hat{L}\, (L01\lambda|J\lambda)\, M_{JL\lambda}(q) \,. \end{aligned} \tag{3.27}$$

We have two cases: $\lambda = 0$ and $\lambda = \pm 1$. For $\lambda = 0$ we have

$$\mathcal{J}(q,0) = \sqrt{4\pi} \sum_{LJ} (-i)^L \hat{L}\, (L010|J0)\, M_{JL0}(q) \,. \tag{3.28}$$

Alternatively, we can use

$$e^{-iqz} = \sqrt{4\pi} \sum_{J=0} (-i)^J \hat{J} M_{J0}(q,\vec{r}) \,, \tag{3.29}$$

then

$$\begin{aligned} e^{-i\vec{q}\cdot\vec{r}}\vec{e}_0 =& e^{-iqz}\vec{e}_0 \\ =& \frac{i}{q}\vec{\nabla} e^{-iqz} \\ =& \sqrt{4\pi} \sum_{J=0} (-i)^J \hat{J} \frac{i}{q} \vec{\nabla} M_{J0}(q,\vec{r}) \,. \end{aligned} \tag{3.30}$$

The result is

$$\mathcal{J}(q,0) = \sqrt{4\pi} \sum_{J} (-i)^J \hat{J} \mathcal{L}_{J0}(q) \,, \tag{3.31}$$

where we have the "longitudinal multipole operator"

$$\mathcal{L}_{JM}(q) = \int \mathrm{d}^3 r \frac{i}{q} \left(\vec{\nabla} M_{JM}(q,\vec{r}) \right) \cdot \vec{\mathcal{J}}(r) \,. \tag{3.32}$$

For $\lambda = \pm 1$ we do the sum over L, which is limited to $\{J-1, J, J+1\}$ by the CG coefficients

(evaluated via (A.9)), i.e.

$$\begin{aligned}\mathcal{J}(q,\lambda) =&\sqrt{4\pi}\sum_{J=1}\left[(-i)^{J-1}(J\hat{-}1)\,(J-101\lambda|J\lambda)\,M_{JJ-1\lambda}(q)\right.\\&\left.+(-i)^{J}\hat{J}\,(J01\lambda|J\lambda)\,M_{JJ\lambda}(q)+(-i)^{J+1}(J\hat{+}1)\,(J+101\lambda|J\lambda)\right]\\=&\sqrt{2\pi}\sum_{J=1}(-i)^{J}\left[i\sqrt{J+1}M_{JJ-1\lambda}(q)-\lambda\sqrt{2J+1}M_{JJ\lambda}(q)-i\sqrt{J}M_{JJ+1\lambda}(q)\right]\ .\end{aligned}\tag{3.33}$$

An equivalent relation is

$$e^{-i\vec{q}\cdot\vec{r}}\vec{e}_\lambda =\sqrt{2\pi}\sum_{J=1}(-i)^{J}\left(i\sqrt{J+1}\vec{M}_{JJ-1\lambda}(q,\vec{r})-\lambda\sqrt{2J+1}\vec{M}_{JJ\lambda}(q,\vec{r})-i\sqrt{J}\vec{M}_{JJ+1\lambda}(q,\vec{r})\right)\ .\tag{3.34}$$

Using the identity [56]:

$$\frac{1}{q}\vec{\nabla}\times\vec{M}_{JJM} =-i\sqrt{\frac{J}{2J+1}}\vec{M}_{JJ+1M}+i\sqrt{\frac{J+1}{2J+1}}\vec{M}_{JJ-1M}\ ,\tag{3.35}$$

the expression is further simplified, i.e.

$$\mathcal{J}(q,\lambda=\pm1) =\sqrt{2\pi}\sum_{J=1}(-i)^{J}\hat{J}\left(\mathcal{T}^{E}_{J\lambda}-\lambda\mathcal{T}^{M}_{J\lambda}\right)\ ,\tag{3.36}$$

which defines the "transverse electric multipole operators":

$$\mathcal{T}^{E}_{JM}(q)=\int \mathrm{d}^3r\frac{1}{q}\left(\vec{\nabla}\times\vec{M}_{JJM}(q,r)\right)\cdot\vec{\mathcal{J}}(r)\tag{3.37}$$

and the "transverse magnetic multipole operators":

$$\mathcal{T}^{M}_{JM}(q)=\int \mathrm{d}^3r\vec{M}_{JJM}(q,r)\cdot\vec{\mathcal{J}}(r)\ .\tag{3.38}$$

Real photons are limited to $\lambda=\pm1$. The relevant operator for photon emission (as in (3.13)) is then

$$\begin{aligned}\langle f|\,\vec{e}^{\,*}_\lambda\cdot\vec{\mathcal{J}}(\vec{q})\,|i\rangle&=\langle f|\,(-1)^{\lambda}\vec{e}_{-\lambda}\cdot\vec{\mathcal{J}}(\vec{q})\,|i\rangle\\&=-\langle f|\sum_{J}(-i)^{J}\sqrt{2\pi}\hat{J}\left[\mathcal{T}^{E}_{J-\lambda}(q)+\lambda\mathcal{T}^{M}_{J-\lambda}(q)\right]|i\rangle\ .\end{aligned}\tag{3.39}$$

3.1.2 Approximations

In the long-wavelength approximation ($qr \ll 1$), the Bessel functions can be expanded as

$$j_\ell(qr) = \frac{(qr)^\ell}{(2\ell+1)!!}\left\{1 - \frac{\frac{1}{2}(qr)^2}{2\ell+3} + \cdots\right\} , \tag{3.40}$$

where $(2\ell+1)!!$ denotes a "double factorial" (i.e. for odd n: $n!! = n(n-2)\cdots 3\cdot 1$).

This leads to a decomposition in terms of the multipole operators we already defined in Section 2.9 (integrating 2.109 and 2.110):

$$M^E_{JM} = \sum_i^A e\frac{1+\tau_{zi}}{2} r_i^J Y_{JM}(\Omega_i) , \tag{3.41}$$

$$M^M_{JM} = \sum_i^A \left(2\mu_i \vec{S}_i + \frac{1}{J+1}\mu_N \frac{1+\tau_{zi}}{2}\vec{L}_i\right)\cdot\vec{\nabla}_i\left(r_i^J Y_{JM}(\Omega_i)\right) . \tag{3.42}$$

The Coulomb operators can then be approximated by

$$\mathcal{C}_{JM}(q) \approx \frac{q^J}{(2J+1)!!} M^E_{JM} . \tag{3.43}$$

Another approximation uses the conservation of vector current:

$$\vec{\nabla}\cdot\vec{\mathcal{J}} = \frac{\mathrm{d}\rho}{\mathrm{d}t} . \tag{3.44}$$

Substituting the time evolution operator, evaluated between energy eigenstates, we have

$$< \frac{\mathrm{d}\rho}{\mathrm{d}t} > = < -i\,[H,\rho] > = -i < \omega\rho > , \tag{3.45}$$

where $\omega = E_f - E_i$ and $< \cdots > = \langle f|\cdots|i\rangle$. This is known as Siegert's theorem [57] and with this relation the longitudinal multipoles can be replaced. First using integration by parts to move the gradient, i.e.

$$\begin{aligned}\mathcal{L}_{JM}(q) =& \frac{i}{q}\int \mathrm{d}^3 r \vec{\nabla} M_{JM}(q,r)\cdot\vec{\mathcal{J}}(r) \\ =& -\frac{i}{q}\int \mathrm{d}^3 r M_{JM}(q,r)\vec{\nabla}\cdot\vec{\mathcal{J}}(r) \\ =& -\frac{\omega}{q}\mathcal{C}_{JM}(q) .\end{aligned} \tag{3.46}$$

The transverse electric can first be directly related to the longitudinal, i.e.

$$\mathcal{T}^E_{JM}(q) = \sqrt{\frac{J+1}{J}}\mathcal{L}_{JM}(q) - i\sqrt{\frac{2J+1}{J}} M_{JJ+1M}(q) . \tag{3.47}$$

Then making use of Siegert's theorem, and neglecting the second term of (3.35) (in which the integral (3.25) will have an extra factor of qr), we have

$$\mathcal{T}^E_{JM}(q) \approx -\frac{\omega}{q}\sqrt{\frac{J+1}{J}}\mathcal{C}_{JM}(q) \tag{3.48}$$

$$=\frac{\omega q^{J-1}}{(2J+1)!!}\sqrt{\frac{J+1}{J}}M^E_{JM}\ . \tag{3.49}$$

The transverse magnetic operator can be approximated as

$$\mathcal{T}^M_{JM}(q) \approx \frac{q^J}{(2J+1)!!}\sqrt{\frac{J+1}{J}}M^M_{JM}\ . \tag{3.50}$$

In all of the above we have focused on the tree-level diagram of a photo-nucleus interaction. However there are higher order diagrams. The size of the electromagnetic coupling e makes any additional photon vertices small and therefore we neglect them in this study. But there are additional diagrams coming from the χEFT description of the nuclei. The photon is not simply interacting with the nucleons but also with the charged pions being exchanged. Siegert's theorem helps with this for the electric multipoles, as the pions will contribute to the current $\mathcal{J}$ and the continuity equation (3.44) makes the matrix element only depend on the charge ρ. However for magnetic multipoles we do expect contribution from meson-exchange currents (MECs). There has been some effort in the literature to derive and compute the two-body operators corresponding to the MECs (e.g. [58]). The overall effect is on the order of 10% in some nuclei.

In this study we include only $E1$, $M1$ and $E2$ and neglect two-body exchange currents.

3.1.3 Final Formula and Selection Rules

If we insert (3.39) into (3.3), the rate of decay of an excited nuclear state is

$$\Gamma =\frac{e^2}{2J_i+1}\sum_{M_i}\sum_{M_f}\sum_{\lambda}\int\frac{\mathrm{d}^3q}{(2\pi)^3 2\omega}2\pi\delta(M_I-E_F-\omega)$$
$$\times\left|\langle J_fM_f|\sqrt{2\pi}\sum_{J=1}^{\infty}(-i)^J\hat{J}\left[\mathcal{T}^E_{J-\lambda}(q)+\lambda\mathcal{T}^M_{J-\lambda}(q)\right]|J_iM_i\rangle\right|^2\ , \tag{3.51}$$

where the coupling constant is explicitly removed from the current operators. The integral measure is $\mathrm{d}^3q=\omega^2\mathrm{d}\omega\mathrm{d}\Omega$ and so we can use the δ to integrate $\mathrm{d}\omega$, i.e.

$$\int\frac{\omega^2\mathrm{d}\omega}{2\omega}\delta(M_I-E_F-\omega)=\frac{\omega}{2}f_r\ , \tag{3.52}$$

where on the right ω is fixed to the value M_I-E_F and f_r is the recoil factor $f_r=(1-\frac{\omega}{M_F})^{-1}$ (which takes into account the motion of the final nucleus $E_F\simeq M_F+\frac{P_F^2}{2M_F}$).

CG coefficients are inserted in order to use the reduced transition matrix elements $T^{\sigma}_{J} = \langle J_f | \, | \mathcal{T}^{\sigma}_{J} | \, | J_i \rangle$ where the σ and σ' can take the values 0 or 1, corresponding to electric or magnetic respectively. The sum over the Ms in the CGs gives $\delta_{JJ'}$, using (A.7) to reorder the CGs, i.e.

$$
\begin{aligned}
&\sum_{M_i}\sum_{M_f}\sum_{\lambda}\left|\langle J_f M_f|\sum_{J}(-i)^J\hat{J}\left[\mathcal{T}^{E}_{J-\lambda}(q)+\lambda\mathcal{T}^{M}_{J-\lambda}(q)\right]|J_i M_i\rangle\right|^2 \\
=&\sum_{M_i}\sum_{M_f}\sum_{\lambda}\left(\sum_{J\sigma}(-i)^J\hat{J}\hat{J}_f^{-1}\left(J_i M_i J-\lambda|J_f M_f\right)\lambda^{\sigma}T^{\sigma}_{J}\right)\left(\sum_{J'\sigma'}(-i)^{J'}\hat{J}'\hat{J}_f^{-1}\left(J_i M_i J'-\lambda|J_f M_f\right)\lambda^{\sigma'}T^{\sigma'}_{J'}\right)^* \\
=&\sum_{\lambda}\sum_{J\sigma}\sum_{J'\sigma'}\sum_{M_i}\sum_{M_f}(-)^{J_i-M_1}\frac{\hat{J}_f}{\hat{J}}\left(J_f M_f J_i-M_i|J-\lambda\right)(-)^{J_i-M_1}\frac{\hat{J}_f}{\hat{J}'}\left(J_f M_f J_i-M_i|J'-\lambda\right) \\
&\times(-i)^J\hat{J}\hat{J}_f^{-1}\lambda^{\sigma}T^{\sigma}_{J}(-i)^{-J'}\hat{J}'\hat{J}_f^{-1}\lambda^{\sigma'}T^{\sigma'*}_{J'} \\
=&\sum_{\lambda}\sum_{J\sigma\sigma'}\lambda^{\sigma+\sigma'}T^{\sigma}_{J}T^{\sigma'*}_{J'} \\
=&2\sum_{J\sigma}|T^{\sigma}_{J}|^2
\end{aligned}
\tag{3.53}
$$

where the sum over λ fixes $\sigma = \sigma$', i.e.

$$\sum_{\lambda}\lambda^{\sigma+\sigma'} = 2\delta_{\sigma\sigma'}\ . \tag{3.54}$$

After integrating over the angles $\int \mathrm{d}\Omega = 4\pi$ and replacing $e^2 = 4\pi\alpha$, the final rate is

$$\Gamma_{fi} = \frac{8\pi\alpha\omega}{2J_i+1} f_r \sum_{J\sigma}|T^{\sigma}_{J}|^2\ . \tag{3.55}$$

The selection rules for a decay (displayed in Table 3.1) are enforced by the reduced matrix elements. A decay will be dominated by the transition type furthest to the left in the table. Higher multipoles are "forbidden" in the sense that their rates are suppressed by additional factors of ω^2. For example, $1^- \to 0^+$ will be an "allowed" E1 transition and forbidden for M2 (still possible but suppressed). Similarly, for $1^+ \to 0^+$, M1 transitions are allowed and E2 are forbidden.

	σJ			
	E1	M1	E2	M2
ΔJ	$0, 1$ (except $0 \to 0$)		$0, 1, 2$ (except $0 \to 0, 1, \frac{1}{2} \to \frac{1}{2}$)	
$\Delta\pi$	yes	no		yes

Table 3.1: The selection rules for allowed γ-decay transitions. For a given ΔJ and $\Delta\pi$ the furthest left multipole in the table will be dominant.

3.2 Weak Interactions: β Decay

A γ-decay changes only the internal configuration of the nucleus (observed by a change of the energy and possibly angular momentum and parity) but it remains the same isotope. A β-decay is a type of process which changes the nucleon make-up i.e. $(A, Z) \to (A, Z \pm 1)$, changing the isotope but remaining an "isobar". A neutron within the nucleus decays to a proton by emission of an electron and anti-neutrino. The electron is referred to as a β^- particle. In some nuclei it is possible to have β^+ decay where a proton decays to a neutron by emission of a positron and neutrino. In this thesis we reduce the scope to β^-decays.

A β-decay is a $1 \to 3$ decay (corresponding to the Feynman diagram in Figure 3.2a), i.e. we have the rate

$$\Gamma = \frac{1}{2M_I} \bar{\sum_i} \sum_f \sum_{s\bar{s}} \int \left|\mathcal{M}_{FI}^{s\bar{s}}(K)\right|^2 \frac{\mathrm{d}^3 k}{(2\pi)^3 2E} \frac{\mathrm{d}^3 \bar{k}}{(2\pi)^3 2\bar{E}} \frac{\mathrm{d}^3 P_F}{(2\pi)^3 2E_F} \,, \tag{3.56}$$

where $K = k + \bar{k}$ with k for the electron and $\bar{k}$ for the anti-neutrino. The amplitude must contain $\delta(P_F + K - P_I)$ which can be used to do the integral over $\mathrm{d}^3 P_F$. To get the rate, we sum over the outgoing lepton spins and integrate over their momenta (usually neglecting the neutrino mass). This is a somewhat involved process which will not be described here, see [11] for details. The kinematics of an analogous process (electron-positron pair production) will be discussed in Section 6.4.

The Standard Model describes β decay through an interaction between quarks and leptons via W boson exchange as shown in Figure 3.2b. The flavour of the quarks changes and the W carries the resulting difference in charge. The weak interaction is described by a so-called "V-A" theory meaning that the interactions have both vector (V) and axial-vector (A) contributions.

We can successively apply EFT to simplify this diagram. First, we can consider the W as acting on the nucleon as a whole rather than at the quark level (Figure 3.2c). The vertex factor for a $W-$lepton or $W-$quark interaction contains the "V-A" operator $\gamma^\mu(1-\gamma_5)$. For nucleons this must be upgraded with form factors $F_V(K^2)$ and $F_A(K^2)$: $\gamma^\mu \left(F_V - F_A\gamma_5\right)$ to account for the internal structure, where $F_V(0) \equiv g_V \simeq 1$ and $F_A(0) \equiv g_A \simeq 1.27$.

Second, the mass of the W boson is much heavier than the relevant scale ($m_W \simeq$80 GeV). The original diagram depends on two vertices each with a $\frac{-g}{2\sqrt{2}}$ coupling as well as the propagator of the massive particle $\sim \frac{1}{K^2 + m_W^2}$. The large mass allows us to drop the K (as $m_W^2 \gg K^2$) and replace the internal line in the diagram with a contact interaction (Figure 3.2d). The resulting lepton-nucleon coupling depends on the square of the quark/lepton-level coupling and the mass [54], i.e.

$$\frac{G}{\sqrt{2}} = \frac{g^2}{8m_W^2} \,, \tag{3.57}$$

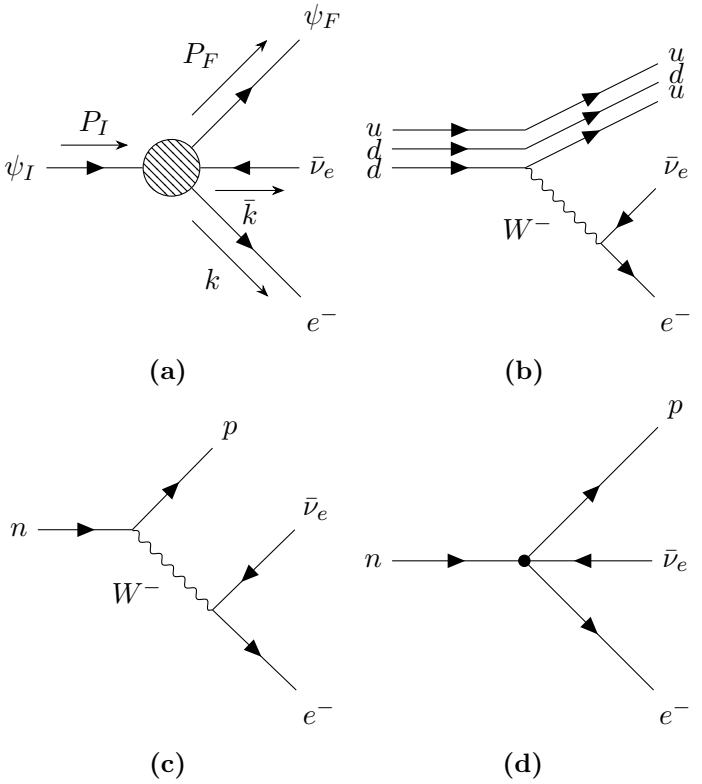

Figure 3.2: The leading order Feynman diagrams for a β^- decay at different levels of EFT. Solid lines represent fermions (nucleons, quarks and leptons). Wavy lines represent bosons (the W). (a) The diagram for a nuclear decay including the kinematics. The circle at the vertex represents an effective operator. (b) The diagram for β decay including the W boson at the level of quarks. (c) The diagram for β decay including the W boson at the level of nucleons. (d) The diagram for β decay at the level of nucleons, where the dot represents an effective operator.

where G is the "Fermi" constant which takes the value 1.1663787×10^{-5} GeV^{-2} [19]. It was measured first through nuclear β decay and the relation between g and m_W was later reverse-engineered through more sophisticated experiments.

The final step is to sum over the single-nucleon operators and we get a current operator evaluated between the initial and final nucleus wavefunctions just like in (3.12) (Figure 3.2a).

Schematically, the amplitude of the diagram in the W picture (Figure 3.2c) is

$$\mathcal{M} \sim \int \frac{\mathrm{d}^4 K}{(2\pi)^4} \left((2\pi)^4 \delta(k + \bar{k} - K) \langle e\bar{\nu}| \frac{g}{2\sqrt{2}} \gamma^\mu (1 - \gamma_5) |0\rangle \right) \times \frac{\left(\eta_{\mu\nu} - \frac{K_\mu K_\nu}{m_W^2}\right)}{K^2 + m_W^2} \left((2\pi)^4 \delta(P_F + K - P_I) \langle p| \gamma^\mu \left(g_V - g_A \gamma_5\right) |n\rangle \right) , \tag{3.58}$$

which becomes (Figure 3.2a):

$$\mathcal{M} \sim \frac{G}{\sqrt{2}}(2\pi)^4 \delta(P_F + k + \bar{k} - P_I) \ell_\mu \langle f | \mathcal{J}_W^\mu | i \rangle \ , \tag{3.59}$$

where ℓ is the lepton current defined through the Feynman rules by

$$\ell_\mu = \bar{u}_s(k) \gamma_\mu (1 - \gamma_5) \nu_{\bar{s}}(\bar{k}) \tag{3.60}$$

and $\mathcal{J}_W^\mu$ is the nuclear current operator for the weak interaction.

Just like in (3.4) this comes from the integral of interacting fields. We have the lepton field:

$$\mathcal{K}(\vec{x}) = \int \frac{\mathrm{d}^3 k}{(2\pi)^3 2E_k} \sum_s \left[a_{ks} u^s(\vec{k}) e^{i\vec{k}\cdot\vec{x}} + b_{ks}^\dagger v^s(-\vec{k}) e^{-i\vec{k}\cdot\vec{x}} \right] \ , \tag{3.61}$$

where a ($b^\dagger$) create leptons (anti-leptons) described by Dirac spinors u (v) with momentum k and helicity s. The amplitude is then

$$\begin{aligned} \mathcal{M}_{FI}^{s\bar{s}} =& \left\langle F; ks\bar{k}\bar{s} \right| \frac{G}{\sqrt{2}} \int \mathrm{d}^4 x \mathcal{K}_\mu(x) \mathcal{J}_W^\mu(x) \left| I; 0 \right\rangle \\ =& \frac{G}{\sqrt{2}} 2\pi \delta(E_F + E + \bar{E} - E_I) \int \mathrm{d}^3 x \left\langle ks\bar{k}\bar{s} \right| \mathcal{K}_\mu(\vec{x}) \left| 0 \right\rangle \left(4E_I E_F \langle f | \mathcal{J}_W^\mu(\vec{x}) | i \rangle \right) \ , \end{aligned} \tag{3.62}$$

where

$$\left\langle ks\bar{k}\bar{s} \right| \mathcal{K}_\mu(\vec{x}) \left| 0 \right\rangle = \ell_\mu e^{-i\vec{q}\cdot\vec{x}} \ . \tag{3.63}$$

Combining these, the rate is

$$\Gamma \propto \bar{\sum_i} \sum_f \sum_{s\bar{s}} \frac{G^2}{2} \left| \ell \cdot \langle f | \left(\mathcal{J}^V + \mathcal{J}^A \right) | i \rangle \right|^2 \times (\text{phase space factor}) \ . \tag{3.64}$$

The weak-nucleon interaction is exactly analogous to the electromagnetic interaction with two exceptions:

1. In addition to a vector component, the current operator also has an axial-vector component.

   Exactly like electromagnetic theory, we can use a multipole expansion. This time every operator has two components $\mathcal{C}_W \to \mathcal{C}^V + \mathcal{C}^A$, etc.

2. It can be charge-changing[1] (i.e. decays via $W^\pm$).

[1] The weak force also contains a neutral current (corresponding to the Z boson) but that will not be discussed here.

A β decay requires the current to be charge-changing so we attach the isospin operator:

$$\mathcal{J}_W^{\pm} = \frac{\tau_{\pm}}{2}\left(\mathcal{J}^V + \mathcal{J}^A\right) \ . \tag{3.65}$$

The summed squared matrix element is then (45.17 in [54]):

$$\begin{aligned}
&\frac{1}{2J_i+1}\sum_{M_i}\sum_{M_f}|\mathcal{M}|^2 \\
=&\frac{G^2}{2}\frac{4\pi}{2J_i+1}\times \\
&\left[\frac{1}{2}\sum_{\lambda=\pm1}\ell_\lambda\ell_\lambda^*\sum_{J\geq1}\left|\langle J_f|\left|\lambda\mathcal{T}_J^M+\mathcal{T}_J^E\right||J_i\rangle\right|^2\right. \\
&+\sum_{J\geq0}\ell_z\ell_z^*\left|\langle J_f||\mathcal{L}_J||J_i\rangle\right|^2+\ell_0\ell_0^*\left|\langle J_f||\mathcal{C}_J||J_i\rangle\right|^2 \\
&\left.-\left(\ell_z\ell_0^*\langle J_f||\mathcal{L}_J||J_i\rangle\langle J_f||\mathcal{C}_J||J_i\rangle+h.c.\right)\right] ,
\end{aligned} \tag{3.66}$$

where we use the covariant components of $\ell_\mu = (\ell_0, \ell_1, \ell_{-1}, \ell_z)$.

The vector part of the weak nuclear current is the same operator as the electromagnetic nuclear current (conserved vector current (CVC) theory [54]). Therefore in the same way, the longitudinal multipoles can be removed by relating them to the Coulomb multipoles just like in Section 3.1.2. However the axial-vector current is not conserved and must explicitly contain longitudinal multipoles. The sum over lepton spins will create different kinematic dependence on each nuclear operator (as we will see in Section 6.4).

3.2.1 Leading-Order Beta Decay Operators and Two-Body Currents

The long-wavelength approximation ($|\vec{K}| \to 0$) leads to a great reduction in the number of non-zero multipole operators [54]. The only remaining terms are $\mathcal{C}^V$ and $\mathcal{T}^{A,E}$. The leading order terms of these operators correspond to two types of "allowed" decays.

Decays which do not change the nuclear angular momentum are so-called Fermi (F) decays and correspond to the operator:

$$\mathcal{C}_{00}^{V\pm} = \frac{1}{\sqrt{4\pi}}\sum_i^A \tau_{\pm} \ . \tag{3.67}$$

In these decays $\Delta J = 0$, meaning the electron and anti-neutrino must couple to total spin $S = 0$.

Decays which do change nuclear angular momentum are so-called Gamow-Teller (GT) decays. In this case $\Delta J = 1$, meaning the electron and anti-neutrino must couple to total

spin $S = 1$. The corresponding operator is

$$\mathcal{T}^{A,E\pm}_{1M} = \sqrt{2}\mathcal{L}^{A,\pm}_{1M} = \frac{i}{\sqrt{6\pi}} g_A \sum_i^A \tau_\pm \sigma_{1M} \ . \tag{3.68}$$

Experimentally certain nuclei (i.e. particular states of nuclei) may decay primarily by one operator or the other. As in Section 3.1 there are selection rules. Only first-forbidden β decays change parity. In this study, we focus on allowed GT decays where parity is conserved.

Higher order diagrams emerge from χEFT in the same way as in electromagnetism. Two nucleons may simultaneously contribute to the matrix elements through a pion exchange or a contact operator [57]. The additional operator corresponding to these terms is termed a two-body current (2BC). The 2BC is related to the nuclear force, as the pion exchange and 3N contact term share LECs [59, 60].

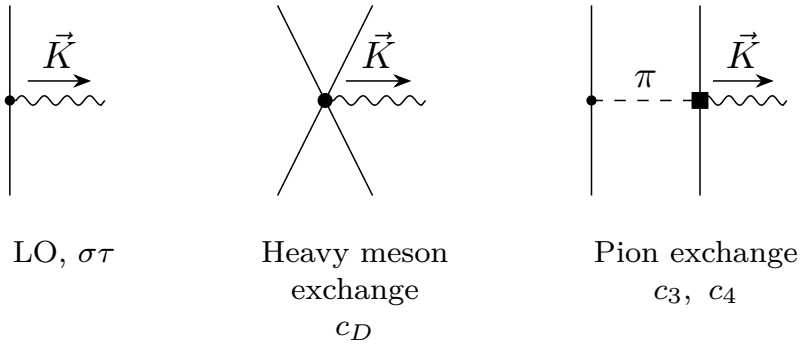

Figure 3.3: Diagrammatic representations of terms that contribute to the axial-vector charge-changing current up to N^2LO in the limit $\vec{K} \to 0$. Solid lines represent nucleons while wavy lines represent the W boson. The left-most diagram yields the standard (one-body) $\sigma\tau$ transition operator, the other diagrams form the leading 2BC.

3.2.2 The GT Beta Decay Spectrum

To leading order, the GT decay rate depends on $\mathcal{L}^A$ (3.68). Experiments are starting to reach the level of precision where corrections to this approximation are necessary in theoretical predictions.

Assuming a neutrino with zero mass, $\bar{k} = \bar{E}$, the phase space can be easily integrated

over the neutrino momentum. The rate is proportional to this phase space factor, i.e.

$$\begin{aligned}\Gamma &\propto \int \frac{\mathrm{d}^3k}{(2\pi)^3}\frac{\mathrm{d}^3\bar{k}}{(2\pi)^3}\delta(E_F - E_I - E - \bar{E}) \\ &= \int \frac{k^2\mathrm{d}k\mathrm{d}\Omega_k}{(2\pi)^3}\frac{\bar{E}^2\mathrm{d}\bar{E}\mathrm{d}\Omega_{\bar{k}}}{(2\pi)^3}\delta(E_{max} - E - \bar{E}) \\ &= \int \frac{kE\mathrm{d}E\mathrm{d}\Omega_k\mathrm{d}\Omega_{\bar{k}}}{(2\pi)^6}\left(E_{max} - E\right)^2 \ , \end{aligned} \tag{3.69}$$

where $E = \sqrt{k^2 + m_e^2}$, $\mathrm{d}E = \frac{E}{k}\mathrm{d}k$ and $E_{max} = E_F - E_I$.

The full expression for the differential distribution of electrons is

$$\begin{aligned}\frac{\mathrm{d}\Gamma_{fi}}{\mathrm{d}E\frac{\mathrm{d}\Omega_k}{4\pi}\frac{\mathrm{d}\Omega_{\bar{k}}}{4\pi}} =& \frac{4}{\pi^2}(E_{max} - E)^2 kEC_{corr}\mathcal{F}(Z,E)\left|\langle f|\left|\mathcal{L}^A\right||i\rangle\right|^2 \\ &\times 3\left(1 + \delta_1^\beta\right)\left(1 + a_{\beta\nu}\vec{\beta}\cdot\hat{\nu} + b_F\frac{m_e}{E}\right) \ . \end{aligned} \tag{3.70}$$

The Fermi function $\mathcal{F}(Z,E)$ takes into account Coulomb distortion [61] of the electron's wavefunction and C_{corr} contains non-nuclear corrections (e.g. finite size effects). Here $\vec{\beta} = \frac{\vec{k}}{E}$, with $\vec{k}$ and E the momentum and energy of the emitted electron and $\hat{\nu}$ is the unit vector for the direction of the momentum of the emitted anti-neutrino. The V-A structure of the weak interaction in the Standard Model implies that for a Gamow-Teller transition the angular correlation coefficient $a_{\beta\nu}$ has the value of $-\frac{1}{3}$ while the "Fierz interference" term b_F is expected to be 0. The deviations from this expectation are denoted δ_a^β and δ_b^β defined by $a_{\beta\nu} = -\frac{1}{3}\left(1 + \delta_a^\beta\right)$ and $b_F^\beta = \delta_b^\beta$ respectively.

The presence of a beyond the Standard Model interaction could induce a non-zero value in the δs. However this must be differentiated from Standard Model effects e.g. the finite momentum transfer, higher-order transition operators and nuclear structure. The Standard Model corrections δ_1^β, δ_a^β and δ_b^β are related to ratios of the leading $\mathcal{L}_1^A$ operator with additional multipole operators ($\mathcal{C}_1^A$ and $\mathcal{T}_1^{V,M}$, see [2, 62] for more details).

3.2.3 Double-Beta Decay

When the energy of the adjacent $(Z \pm 1)$ nucleus is too high (such that single beta decay is kinematically forbidden) it may still be possible to double-beta decay, if the nucleus of the $Z \pm 2$ isobar has low enough energy.

This process has been observed [63] with a very low rate. Since two neutrinos are produced, this is known as $2\nu\beta\beta$. Like single β decay, it has two modes, Fermi and Gamow-Teller which are products of the same single-beta-decay operators. A difference is that the matrix element must also include a sum over intermediate virtual states of the nucleus and a corresponding energy dependent weighting.

Given the unknown nature of neutrinos, the mass of the neutrino has yet to be incorporated into the Standard Model, it may be possible that the neutrino is its own anti-particle.

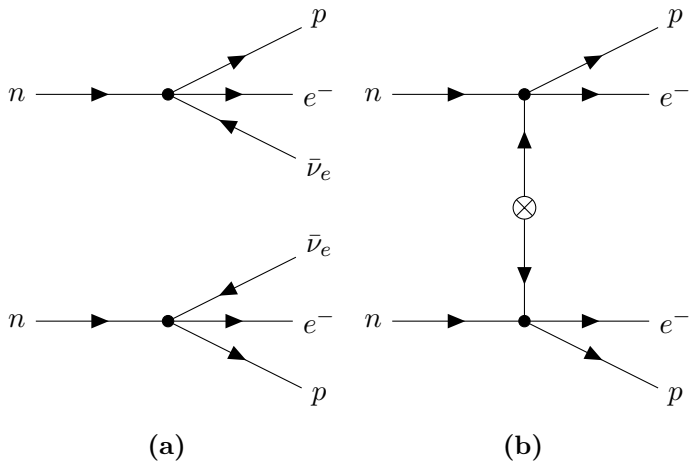

Figure 3.4: Feynman diagrams for (a) two-neutrino double-beta decay ($2\nu\beta\beta$) and (b) neutrino-less double-beta decay ($0\nu\beta\beta$).

If neutrinos are "Majorana" it would be possible to observe a different process, $0\nu\beta\beta$, if the two neutrinos annihilate. The kinematics of the electrons would be used to differentiate this mode. The ratio between the total energy of the emitted electrons in $2\nu\beta\beta$ and the available nuclear transition energy is a continuum between 0 and 1, peaked at $\frac{1}{3}$, while in $0\nu\beta\beta$ the peak would be at 1 [64].

Neutrino-less double-beta decay is a hypothetical process. If discovered it would provide evidence of lepton number violation and determine the Majorana character of neutrinos. It is expected to be extremely rare. The rate of this decay depends on the neutrino mass and hence can be used to determine the mass; however, the nuclear matrix element is required to compute it. The halflife formula is

$$[T^{0\nu}_{1/2}]^{-1} = G^{0\nu}|M^{0\nu}|^2 \left(\frac{\langle m_\beta \beta\rangle}{m_e}\right)^2 , \tag{3.71}$$

where $G^{0\nu}$ is a phase-space factor (an integral over the possible outgoing electron momenta), m_e the electron mass and $\langle m_{\beta\beta}\rangle$ is the effective neutrino mass [65]. The quantity of interest that will be computed here is the nuclear matrix element $M_{0\nu}$.

In principle, the matrix element can be computed through multipole decomposition of the weak current and chiral effective theory. However its derivation is beyond the scope of this thesis. The leading order operator consists of four contributions (the Gamow-Teller [GT], Fermi [F], Tensor [T] and contact [C]), and so the total operator is

$$M^{0\nu} = M^{0\nu}_{GT} + M^{0\nu}_{F} + M^{0\nu}_{T} + M^{0\nu}_{C} . \tag{3.72}$$

Each component has different spin dependence and can be derived by connecting a neutrino potential to χEFT [66]. The existence of the contact is a relatively recent theoretical

discovery [67]. For now we will neglect it, its inclusion is a very active area of research [68].

The operator takes the following form:

$$M_x = H_x y_x \tau_1^+ \tau_2^+ \ , \tag{3.73}$$

where the spin dependence of the operator is contained within

$$y_x = \begin{cases} 1 & \text{if } x = F \ , \\ \sigma_1 \cdot \sigma_2 & \text{if } x = GT \ , \\ \sqrt{\frac{24\pi}{5}} Y_2(\hat{r}) S_{12} & \text{if } x = T \ , \end{cases} \tag{3.74}$$

where $S_{12} = 3(\vec{\sigma}_1 \cdot \hat{r})(\vec{\sigma}_2 \cdot \hat{r}) - \vec{\sigma}_1 \cdot \vec{\sigma}_2$.

H_x depends on the relative coordinate $r = \xi_1$ and is input through harmonic oscillator radial matrix elements of a neutrino potential, i.e.

$$H_x(r) = \frac{2R}{\pi} \int \mathrm{d}q \frac{q \cdot f_x(qr) h_x(q^2)}{q + E_0^{\mathrm{cl}}} \ , \tag{3.75}$$

with the approximate nuclear radius $R = A^{\frac{1}{3}} r_0$ ($r_0 = 1.2$ fm). The f_x are Bessel functions, i.e.

$$f_x = \begin{cases} j_0 & \text{if } x = F, GT \ , \\ j_2 & \text{if } x = T \ , \end{cases} \tag{3.76}$$

and the h_x are form factors to correct for the finite size of the nucleons. For example, h_F depends on the vector form factor g_V and a "finite-size cutoff" parameter Λ_V:

$$h_F(q^2) = \frac{g_V}{\left(1 + \frac{q^2}{\Lambda_V}\right)^2} \ . \tag{3.77}$$

The h_{GT} and h_T are more complicated (depending on g_A, Λ_A, m_π, $m_{p,n}$ and $\mu_{p,n}$) and are not shown for brevity. They are tabulated in [69], following the derivations of [65] and [70]. H_x contains the radius R which could also be computed with *ab initio* techniques but in our application of this operator (benchmarks with other models) that would introduce more model dependence. This form of the operator makes use of the "closure" approximation to remove the sum over virtual nuclear states. The appropriate closure energy E_0^{cl} will be different for different nuclei as we are averaging over the states of the particular intermediate isotope [71].

It is important to note that by definition the $0\nu\beta\beta$ operator must depend on two-nucleon coordinates. Therefore it is implemented using a coupled isospin basis. It must be a rank-2

isotensor with projection ± 2, i.e.

$$\begin{aligned}\left\langle t_1' t_2'; t' m_t' \right| \left[\tau_1 \tau_2\right]^2_{-2} \left| t_1 t_2; t m_t \right\rangle &= \left(t m_t T M_T | t' m_{t'} \right) \hat{t}'^{-1} \left\langle t_1' t_2'; t' m_t' \right| \left| \left[\tau_1 \tau_2\right]^2 \right| \left| t_1 t_2; t m_t \right\rangle \\ &= (112 - 2|1 - 1)\, \hat{1}^2 \left\{ \begin{array}{ccc} \frac{1}{2} & \frac{1}{2} & 1 \\ \frac{1}{2} & \frac{1}{2} & 1 \\ 1 & 1 & 2 \end{array} \right\} \left\langle \frac{1}{2} \right| |\tau| \left| \frac{1}{2} \right\rangle^2 . \end{aligned} \tag{3.78}$$

Of course $\left\langle \frac{1}{2} \right| |\tau| \left| \frac{1}{2} \right\rangle = \sqrt{6}$, the same as $\left\langle \frac{1}{2} \right| |\sigma| \left| \frac{1}{2} \right\rangle$.

Chapter 4

Similarity Renormalization Group

In a basis expansion technique, the elements of the Hamiltonian matrix which inhibit convergence the most are those that connect high and low energy i.e. the off-diagonal elements. The method of Similarity Renormalization Group (SRG) applies a unitary transformation which is designed to suppress these elements. Effectively it reduces the resolution of the interaction, so that short-distance (high-energy) features are removed but low-energy observables are unchanged [72].

A nuclear interaction with a strong short-distance component is often referred to as "hard", hence applying SRG creates a "soft" interaction. The original Hamiltonian is referred to as "bare" and after SRG the "evolved" Hamiltonian should have the same expectation values (energies) but they will converge more rapidly with respect to the model-space size (the parameter N_{max} in NCSM calculations).

In this section technique of SRG evolution is summarized. The implementation of general SRG-evolved operators of three-nucleons in the NCSM contributed to the results presented in Section 5.2.2.

4.1 Softening Potentials with Flow Equations

The nuclear Hamiltonian itself is not observable thus one can apply an arbitrary unitary transformation without changing observable quantities. The Hamiltonian is taken to be a function of a continuous parameter s, i.e.

$$H(s) = U(s)HU^{\dagger}(s) \; , \tag{4.1}$$

where U is a unitary transformation parameterized by s ($U(s)U^{\dagger}(s) = U^{\dagger}(s)U(s) = 1$). The parameter s sets the amount of renormalization. $s = 0$ is the original "bare" Hamiltonian:

$$H(s=0) = H, \; U(s=0) = 1 \; . \tag{4.2}$$

The evolution of the Hamiltonian is carried out by choosing a generator $\eta(s)$ and integrating the flow equation:

$$\frac{\mathrm{d}H(s)}{\mathrm{d}s} = [\eta(s), H(s)] \ , \tag{4.3}$$

from $s = 0$ up to a finite value of s.

The choice of generator depends on the application, in this work we choose a commutator with the kinetic energy: $\eta(s) = m_N^2[T, H(s)]$ [73]. The parameter s must have units that are the inverse [-4] of those of the generator [+4] (in natural units). Typically the results are presented with respect to $\lambda = s^{-1/4}$, as λ then has units of momentum (fm^{-1}). $\lambda = \infty$ corresponds to the bare Hamiltonian. A typical stopping point for s is $\lambda = 2\mathrm{fm}^{-1}$ ($\simeq 400$ MeV), this corresponds to roughly twice the Fermi energy of the nucleons in the nucleus and is an arbitrary but reasonable separation between high- and low-energy.

It is also possible to find a flow equation for $U(s)$ as well, i.e.

$$\frac{\mathrm{d}U}{\mathrm{d}s} = \eta(s)U(s) \ , \tag{4.4}$$

but in practice this is not necessary. Historically calculations only evolved H. We may calculate $U(s)$ from eigenvectors of $H(0)$ and $H(s)$ ($|\psi(0)\rangle$ and $|\psi(s)\rangle$ respectively), i.e.

$$U(s) = \sum_i |\psi_i(s)\rangle \langle\psi_i(0)| \ . \tag{4.5}$$

An important point is that the Hamiltonian is defined in a two- (or three-) nucleon space. It is upgraded to the form in (1.3) by summing over all pairs (triplets) in the A-body system. We perform SRG on the two- (three) body space and so the eigenvectors mentioned in (4.5) will be two- (three-) nucleon states. After upgrading the A-body space and solving the A-body Hamiltonian we will have A-nucleon eigenstates so there exists an A-body version of $U(s)$ but it is impractical to compute.

Another note is that there is an ambiguity in the relative phase of the two eigenstates $|\psi(s)\rangle$ and $|\psi(0)\rangle$ that cannot be determined uniquely by the diagonalization of $H(s)$ and $H(0)$ respectively. Since we expect that SRG will only affect short-range terms and not produce a drastic change to the wavefunction, the relative phase is chosen such that $\langle\psi_i(0)|\psi_i(s)\rangle \geq 0$.

The choice of generator determines how the structure of the Hamiltonian is modified. Since the kinetic energy is tri-diagonal in the harmonic oscillator basis, using it in the generator forces the Hamiltonian to evolve towards being (tri-)diagonal. This is schematically shown in Figure 4.1.

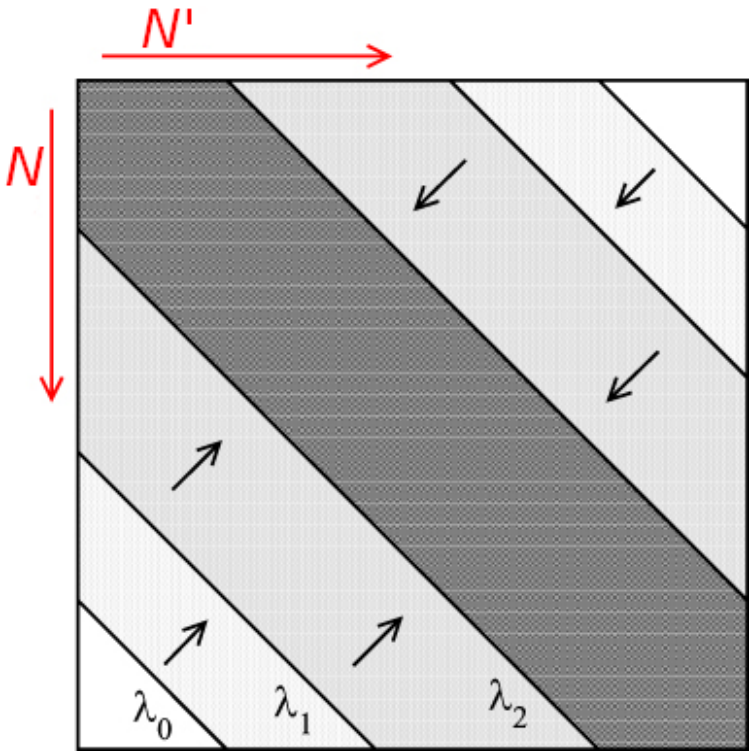

Figure 4.1: A schematic representation of the effect of SRG evolution on the Hamiltonian matrix. The matrix elements are arranged according to the total number of harmonic oscillator excitations N (corresponding to $\tilde{N} = 2n + \ell$ in the text). At successively smaller stopping points, $\lambda_0 > \lambda_1 > \lambda_2$, the matrix elements near the diagonal become larger compared to those further from the diagonal. Adapted from [72]

4.2 SRG Evolution of Operators

When the transformed Hamiltonian is used in a many-body calculation the resulting eigenfunctions will be different but the eigenvalues should be the same (due to unitarity). Other observables have corresponding operators that should also be evolved and the result should be the same between the evolved and unevolved wavefunction [74], i.e.

$$\langle\psi|\, O\, |\psi\rangle = \langle\psi(s)|\, O(s)\, |\psi(s)\rangle \tag{4.6}$$

There is an analogous flow equation to (4.3) for operators:

$$\frac{\mathrm{d}O(s)}{\mathrm{d}s} = [\eta(s), O(s)]\ , \tag{4.7}$$

but if we extract the transformation $U(s)$ we can calculate $O(s)$ directly in the 2- (3-) nucleon space, i.e.

$$O(s) = U(s) O U^{\dagger}(s)\ . \tag{4.8}$$

4.2.1 Induced Many-Body Terms

SRG transformations induce higher-body terms in operators (including the Hamiltonian) and these need to be included in order to maintain unitarity [75]. These terms will be missing if the evolution is carried out in a few-body space i.e. evolution in two-body coordinates will be missing three-body terms. A two-body potential in the Hamiltonian will produce a three-body term if evolved in three-body coordinates. This occurs as spectator nucleons will be linked through the repeated product with the generator.

One way to see this is to write the operator in terms of creation and annihilation operators ($a^\dagger$,a respectively) [75]. Schematically (suppressing indices and sums):

$$\langle O \rangle = \left\langle O^{(1)} \right\rangle a^\dagger a + \left\langle O^{(2)} \right\rangle a^\dagger a^\dagger a a + \left\langle O^{(3)} \right\rangle a^\dagger a^\dagger a^\dagger a a a \tag{4.9}$$

The product of two one-body pieces (i.e. $a^\dagger a$ with $a^\dagger a$) will result in a two-body piece $a^\dagger a^\dagger a a$ (after normal ordering).

Another way to see this is to differentiate $O = O_{12} + O_{13} + O_{23} + O_{123}$ explicitly with respect to s and compare to the flow equation calculated in each subspace [76], i.e.

$$\begin{aligned} \frac{\mathrm{d}O}{\mathrm{d}s} =& \frac{\mathrm{d}O_{12}}{\mathrm{d}s} + \frac{\mathrm{d}O_{13}}{\mathrm{d}s} + \frac{\mathrm{d}O_{23}}{\mathrm{d}s} + \frac{\mathrm{d}O_{123}}{\mathrm{d}s} \\ =& \left[[T, H], O \right] & (4.10) \\ =& \left[[T_{12}, V_{12}] + [T_{13}, V_{13}] + [T_{23}, O_{23}] + [T, V_{123}], O \right] \ , & (4.11) \end{aligned}$$

where O_{12} is a two-body operator operating on particles 1 and 2 and O_{123} is an irreducible 3-body piece. The s-dependence of H, V and O operators is implied here. Each two-body part results from the sub-equation:

$$\frac{\mathrm{d}O_{ij}}{\mathrm{d}s} = \left[[T_{ij}, V_{ij}], O_{ij} \right] \ , \tag{4.12}$$

where, even though we have three particles, the dependence on the third coordinate T_k commutes ($T = T_{ij} + T_k$, where $T = \sum^3 \frac{p_i^2}{2m_N} = \frac{q^2}{2m_N} + \frac{3k^2}{4m_N}$, $q = p_i - p_j$, $k = \frac{2}{3}\left[p_k - \frac{1}{2}(p_i + p_j)\right]$). If we cancel the ij terms on both sides then

$$\begin{aligned} \frac{\mathrm{d}O_{123}}{\mathrm{d}s} =& \left[[T_{12}, V_{12}], (O_{13} + O_{23} + O_{123}) \right] + \{123 \to 132\} \\ &+ \{123 \to 231\} + \left[[T, V_{123}], O_{123} \right] \ . & (4.13) \end{aligned}$$

Even if $H_{123} = V_{123} = 0$ and $O_{123}(s = 0) = 0$, a non-zero O_{123} will be induced through the evolution as $\frac{\mathrm{d}O_{123}}{\mathrm{d}s}$ will be non-zero.

4.2.2 Calculations of SRG-evolved Operators

The induced terms need to be separated out in order to be used. The irreducible 2- and 3-body components must be embedded into the many-body separately as they have different scaling factors with the total nucleon number (due to combinatorics, see Section 2.9). The evolution is carried out separately in each space and then the two-body total is subtracted from the three-body after embedding.

To make the notation clear:

$$O^{(1)} = \sum_{ij} \langle i| O |j\rangle \, a_i^\dagger a_j \ , \tag{4.14}$$

$$O^{(2)} = \sum_{ijkl} \langle ij| O |kl\rangle \, a_i^\dagger a_j^\dagger a_l a_k \ , \tag{4.15}$$

$$\left[O^{(1)}\right]^{(2)} = \sum_{ijkl} \langle i| O |k\rangle \, \langle j|l\rangle \, a_i^\dagger a_j^\dagger a_l a_k \ , \tag{4.16}$$

$$O^{(3)} = \sum_{ijklmn} \langle ijk| O |lmn\rangle \, a_i^\dagger a_j^\dagger a_k^\dagger a_n a_m a_l \ , \tag{4.17}$$

$$\left[O^{(2)}\right]^{(3)} = \sum_{ijklmn} \langle ij| O |lm\rangle \, \langle k|n\rangle \, a_i^\dagger a_j^\dagger a_k^\dagger a_n a_m a_l \ . \tag{4.18}$$

Two-body evolution of a two-body operator is calculated from a two-body unitary, i.e.

$$O^{(2)}(s) = U^{(2)}(s) O^{(2)} U^{\dagger(2)}(s) \ . \tag{4.19}$$

The irreducible three-body induced operator is isolated by subtracting the two-body evolved operator from the operator evolved in three-body space:

$$O^{(3)}(s) = U^{(3)}(s) \left[O^{(2)}\right]^{(3)} U^{\dagger(3)}(s) - \left[U^{(2)}(s) O^{(2)} U^{\dagger(2)}(s)\right]^{(3)} \ . \tag{4.20}$$

In principle evolution should be carried out in every subspace up to A-body as schematically shown in Figure 4.2 but here we truncate at three-body. Generally a hierarchy of importance is expected in the induced terms, i.e. higher-body terms are smaller. The size of the missing terms can be determined by the variation of the parameter s. In addition, $U^{(3)}$ will depend on three-body interactions in the Hamiltonian if they are included.

In the two- and three-body level the Hamiltonian is a block-diagonal operator in terms of the quantum numbers J, π and T for total angular momentum, parity and isospin respectively. The Hamiltonian and therefore the unitarity transformation U can be computed independently for each $J\pi T$ channel. Some operators connect blocks with different spin and/or isospin. The operator must then be evolved by multiplying the corresponding

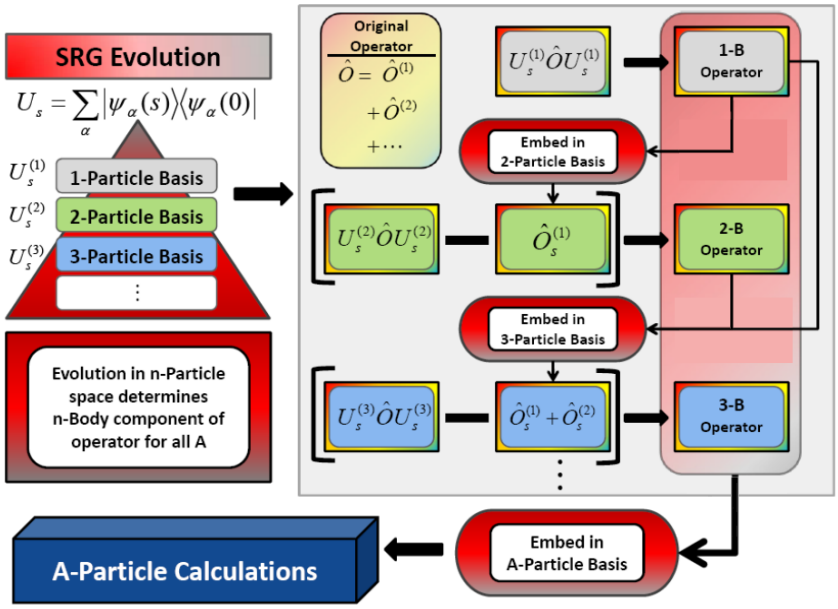

Figure 4.2: The process of preparing an operator for an A-particle calculation. A diagrammatic summary of Section 4.2.2. Adapted from [72]

blocks on either side, i.e.

$$\left\langle J'^{\pi'}T' \middle| O(s) \middle| J^\pi T \right\rangle = \left\langle J'^{\pi'}T' \middle| U^{J'\pi'T'}(s) O U^{\dagger J\pi T}(s) \middle| J^\pi T \right\rangle \ . \tag{4.21}$$

The additional expense of calculating the SRG evolution is not prohibitive as it is carried out in the two-, or three-nucleon space in which the potential is formulated. While computationally expensive at the few-body level, the benefit is seen at the much more expensive many-body level. In addition, since 3N forces are included in the calculation anyway, the cost of including 3N induced terms is not insurmountable.

SRG is performed with the Jacobi basis which may use a basis with much higher N_{max} compared to the SD basis in the two- and three- body spaces. In this basis the numerical calculations of evolution are more precise. In the two-body space we can include up to $N_{max} = 300$ but in the three- we use $N_{max} \in \{30 - 50\}$ with lower N_{max} for higher J blocks.

In summary, the workflow of an NCSM calculation for a two-body operator with SRG is as follows:

1. Choose an NN + 3N Hamiltonian ($H^{(2)} + H^{(3)}$).
2. Solve (4.3) for $H_s^{(2)}$.
3. Extract $U_s^{(2)}$ and apply to $O^{(2)}$.
4. Solve (4.3) for $\left[H^{(2)} + H^{(3)}\right]_s^{(3)}$.

5. Extract $U_s^{(3)}$ and apply to $\left[O^{(2)}\right]^{(3)}$.

6. Subtract $O_s^{(2)}$ from $\left[O^{(2)}\right]_s^{(3)}$to obtain $O_s^{(3)}$.

7. Embed $\left[H^{(2)}\left(+H^{(3)}\right)\right]_s$ into A-body and solve for A-body eigenstates.

8. Calculate $< O_s >=< O_s^{(2)} > + < O_s^{(3)} >$.

In our terminology, using only $H_s^{(2)}$ is the NN result, $\left[H^{(2)}\right]_s^{(3)}$ is the NN+3N induced, and $\left[H^{(2)} + H^{(3)}\right]_s^{(3)}$ is the NN+3N full.

Chapter 5

NCSM Results

5.1 Beta Decay

Beta decay is the dominant decay mode of many nuclei in the nuclear chart (blue and pink in Fig. 1.2), hence it is an important testing ground for comparing nuclear models to experiment. The discrepancies between calculations and observations motivate ever more sophisticated theoretical techniques.

One such discrepancy is the historical difference between theoretical predictions and experimental observations. This is known as the quenching problem. A decay within a nucleus is observed to be less likely than expected based on free neutron decay. For Gamow-Teller decays, phenomenological models can easily match the decay rate if the parameter g_A (in (3.68)) in calculations is modified ("quenched") by a factor of about 0.75.

In Section 5.1.1, we address quenching by using more accurate operators in *ab initio* methods. Part of the quenching can be explained by inclusion of higher-order operators e.g. two-body currents (2BCs) where the presence of pions in the nucleus modifies the nuclear transition operator. In addition, the accuracy of the operator's expectation values requires that the operator be SRG-evolved consistently with the input Hamiltonian.

Future discrepancies may arise as experiments improve their precision beyond that of theoretical predictions. In order to keep up, calculations must begin including corrections to the leading order β decay operator.

In Section 5.1.2, we address the search for beyond the Standard Model (BSM) physics in measurements of β-decay spectra. In particular, we calculate the nuclear structure corrections that must be anticipated in order to identify BSM effects in measurements of the $^6\mathrm{He} \to {}^6\mathrm{Li}$ decay.

5.1.1 SRG and 2BC in GT Decay

In our paper [1], we computed β-decay rates for nuclei across the nuclear chart. We chose strong GT transitions for which quenching should dominate, rather than nuclei like ^{14}C in

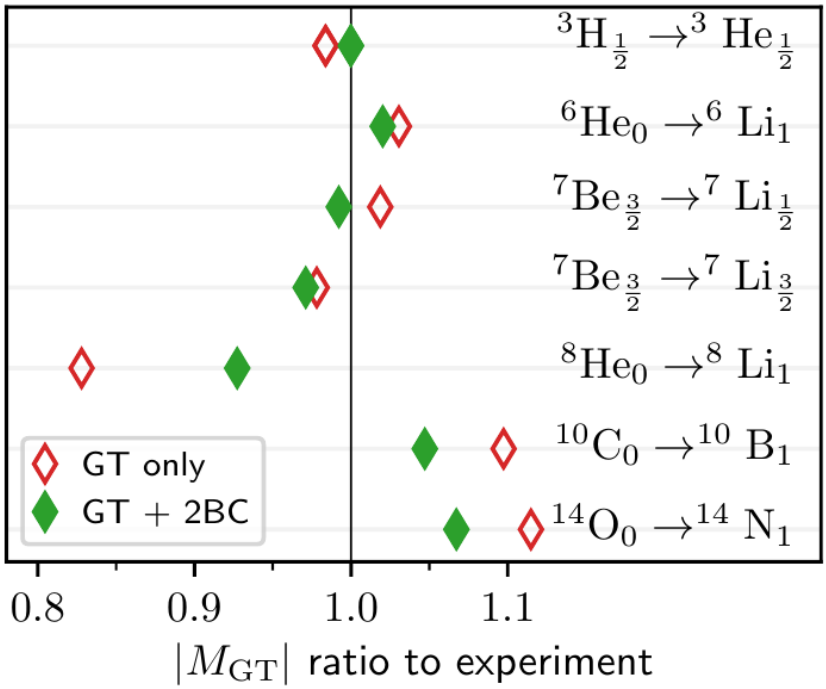

Figure 5.1: Theory-to-experiment ratio for the Gamow-Teller matrix elements of six strong transitions in light nuclei for the NN-N^{4}LO+3N$_{lnl}$ interaction developed in [1]. The subscripts in the legend denote the total angular momenta of the parent and daughter states. All initial states are ground states. In the case ^{3}H $\rightarrow$ ^{3}He,^{6}He $\rightarrow$ ^{6}Li and ^{7}Be $\rightarrow$ ^{7}Li$_{\frac{3}{2}}$, the daughter nucleus is in its ground state, while the ^{7}Be $\rightarrow$ ^{7}Li$_{\frac{1}{2}}$,^{8}He $\rightarrow$ ^{8}Li$_1$ and ^{10}C $\rightarrow$ ^{10}B$_1$ are decays to the first excited state of the daughter nucleus, and the ^{14}O $\rightarrow$ ^{14}N$_1$ is a decay to the second excited state of ^{14}N. Hollow symbols correspond to results obtained with the standard Gamow-Teller $\sigma\tau$ operator, and full symbols include 2BC. The results are converged to within 3% with respect to the model-space size. This uncertainty is slightly larger than the marker size and is not shown for transparency. Figure reproduced from [1].

which fine-tuned cancellations occur.

In light nuclei, we applied the NCSM to compute nuclear wavefunctions and the β-decay transition matrix elements. These calculations contributed to an understanding of the effect of two-body currents (2BCs) in the decay. Figure 5.1 shows the result of inclusion of 2BCs compared to the leading order operator (3.68).

The two-body currents which can be derived from χEFT [57, 60] share parameters with the 3N terms in the Hamiltonian. In fact the low-energy constant c_D was fit using the ^{3}H $\rightarrow$ ^{3}He decay including 2BCs (which is precisely why that result agrees so well with experiment) [60].

The Gamow-Teller beta decay operator is a good example of SRG in action. Figure 5.2 shows the effect of two-nucleon SRG on the GT operator in two different transitions. The

leading order GT operator (3.68) is denoted as "$\sigma\tau$". As the interactions used in calculating the wavefunctions were evolved, it is necessary to consistently evolve the operators. Not evolving the operator consistently results in the dotted lines which have a large spread with respect to the evolution parameter of the input Hamiltonian. This spread is significantly reduced when the operator is evolved (the dashed line).

The inclusion of the higher order operator improves agreement with experiment, resulting in the solid lines of Figure 5.2. The lack of spread with respect to λ indicates that the effect of three-nucleon terms will be small enough to neglect. This is because the dominant term (GT) is a one-body operator and its two-body induced contribution is already small. The three-body induced term will be smaller and the two-body current (a two-body operator) is already relativity small, and so will also have a small induced term.

The decrease due to the 2BCs is not entirely consistent, for example in ^{8}He the matrix element increases, it is only when looking across the nuclear chart that this trend is seen. The NCSM was used to verify the effects of the 2BC in light nuclei and benchmark the operators for more approximate *ab initio* methods like coupled-cluster (CC) and in-medium similariy renormalization group (IMSRG). The CC and IMSRG techniques were used to calculate the matrix elements for much heavier nuclei. These more approximate methods were used to calculate GT rates across a wide range of nuclear masses. Figure 5.3 shows IMSRG calculations for many-medium mass nuclei as compared to experiment and phenomenological shell model calculations. The overall theory vs experiment slope was greatly improved towards 1.

The strongest GT transition is tin-100 (^{100}Sn) which, while difficult to compute with *ab initio* techniques due to its large size, is a good candidate for coupled-cluster calculations because it is doubly-magic ($Z = N = 50$). Figure 5.4 shows the GT matrix element of ^{100}Sn computed with CC for a number of nuclear interactions. The inclusion of the 2BCs reduces the size of the transition strength giving an equivalent result to phenomenological models where a quenching factor was applied.

With *ab initio* methods the quenching factor becomes unnecessary. Two-body currents in combination with an *ab initio* description of the nuclei explain the observed quenching of the GT strength across the nuclear chart.

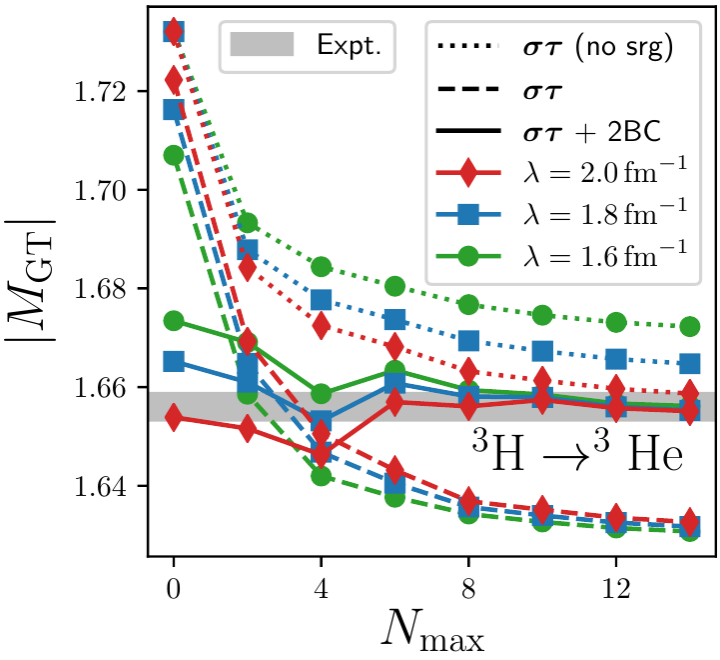

(a)

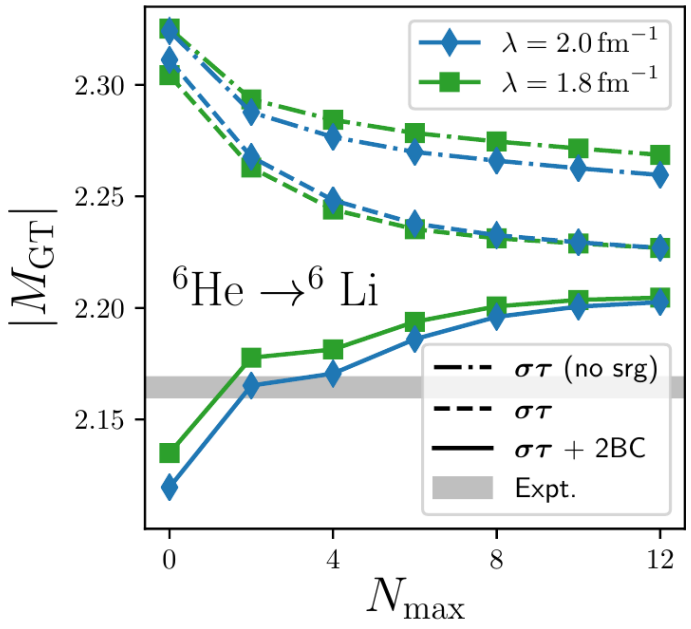

(b)

Figure 5.2: Convergence of the ^{3}H $\rightarrow$ ^{3}He (a) and ^{6}He $\rightarrow$ ^{6}Li (b) Gamow-Teller matrix elements with respect to the NCSM basis size for three values of the SRG evolution parameter λ. Dashed and full lines show results obtained with one-body only and one- plus two-body operators respectively. The NN-N^{4}LO+3N$_{lnl}$ interaction was used with both the interaction and transition operators consistently SRG evolved. The dotted and dash-dotted lines show results obtained with the same SRG evolved interaction using only the one-body operator without any SRG evolution. The shadow bands represent the experimental values with their uncertainties. Figure reproduced from [1].

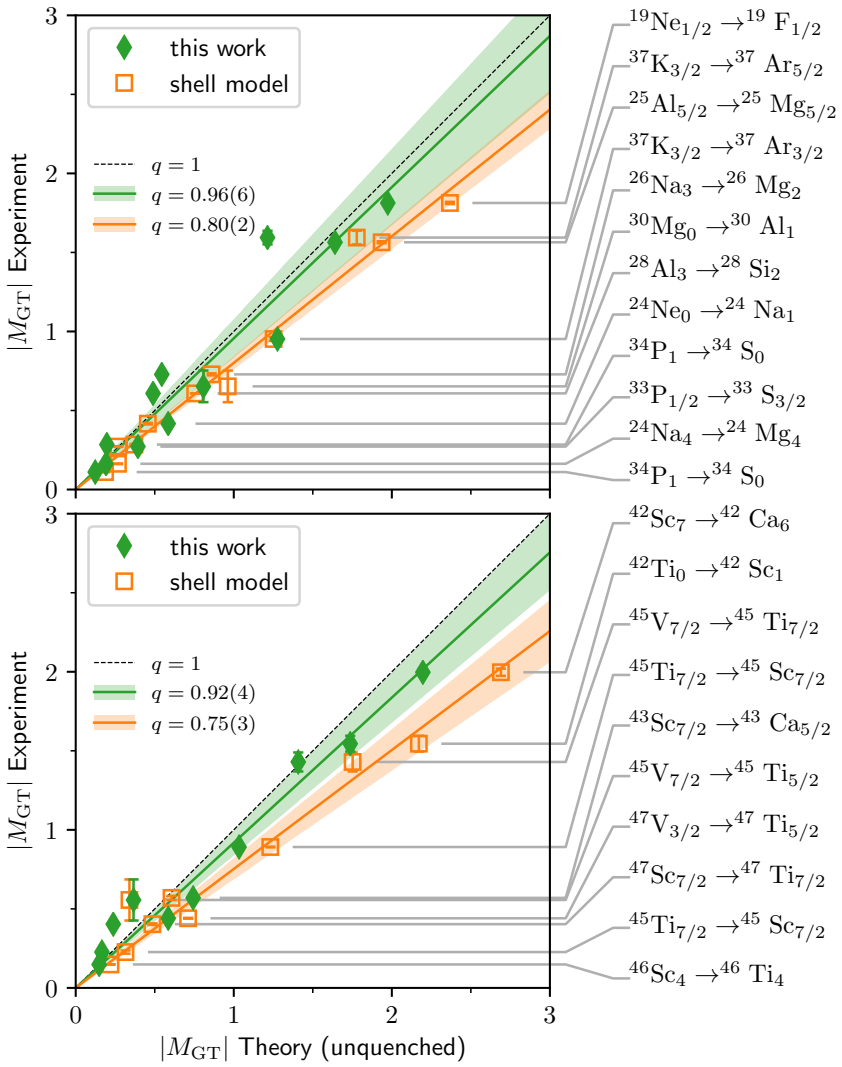

Figure 5.3: Comparison of experimental [77] and theoretical Gamow-Teller matrix elements for medium-mass nuclei. Plots of the Gamow-Teller matrix elements: *sd*-shells (top) and *pf*-shells (bottom). Theoretical results were obtained using phenomenological shell-model interactions [78, 79] with an unquenched standard Gamow-Teller $\sigma\tau$ operator (open orange squares) and using VS-IMSRG approach with the NN-N^{4}LO+3N$_{lnl}$ interaction and consistently evolved Gamow-Teller operator plus 2BCs (filled green diamonds). The linear fit show the resulting quenching factor q given in the panels, and shaded bands indicate one standard deviation from the average quenching factor. Experimental uncertainties, taken from [77], are shown as vertical error bars. Figure reproduced from [1].

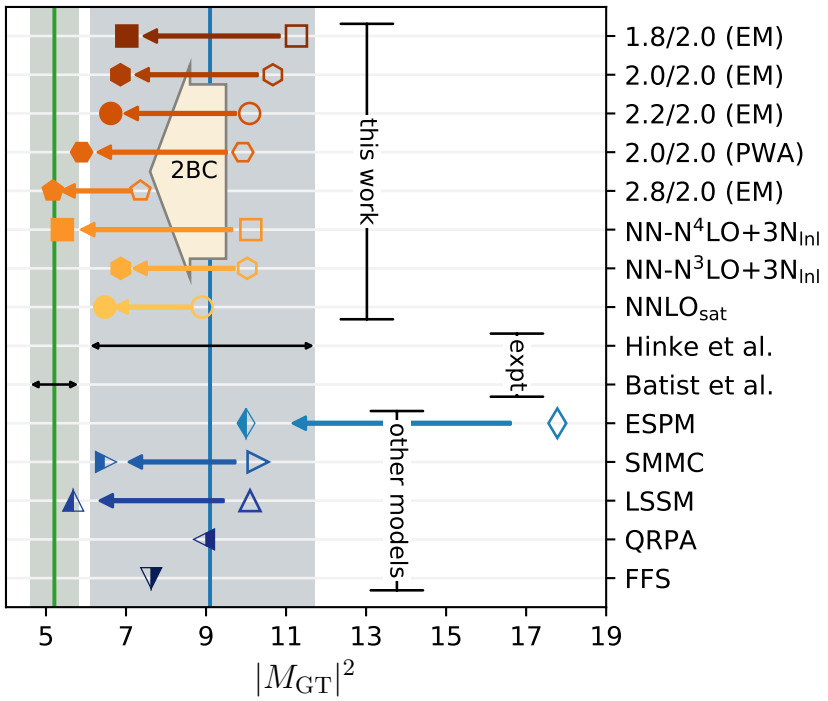

Figure 5.4: Comparison of the Gamow-Teller strength $|M_{GT}|^2$ for the β-decay of ^{100}Sn calculated in [1] compared to data [80], systematics [81], and other models (extreme single-particle model (ESPM), shell-model Monte-Carlo (SMMC), large-space shell-model (LSSM), quasiparticle random-phase approximation (QRPA) and finite Fermi systems (FFS)) from [80]. Open symbols represent results obtained with the standard Gamow-Teller operator ($\sigma\tau$), filled symbols also include two-body currents (2BCs) and partially filled symbols show values following from the multiplications of the computed Gamow-Teller strength by the square of a phenomenological quenching factor. Each of our ^{100}Sn calculations carries a conservatively estimated uncertainty of about 10% (not shown to avoid overcrowding the figure). Figure reproduced from [1].

5.1.2 Precision Beta Decay

In the previous section, *ab initio* techniques were used to improve agreement between experimental observations and theoretical predictions from the Standard Model (SM). These calculations are approaching the precision needed to differentiate between the SM and new beyond the Standard Model (BSM) physics.

β-decay observables are sensitive to interference between currents of SM particles and hypothetical BSM particles. Such couplings are proportional to $\left(\frac{v}{\Lambda}\right)^2$ where $v \approx 174$ GeV is the SM vacuum expectation value and Λ is the new physics energy scale. A coupling on the order of 10^{-4} would suggest new physics at a scale beyond the reach of current particle accelerators. Such small deviations from the SM demand high-precision theoretical calculations of β-decay observables with quantified uncertainties.

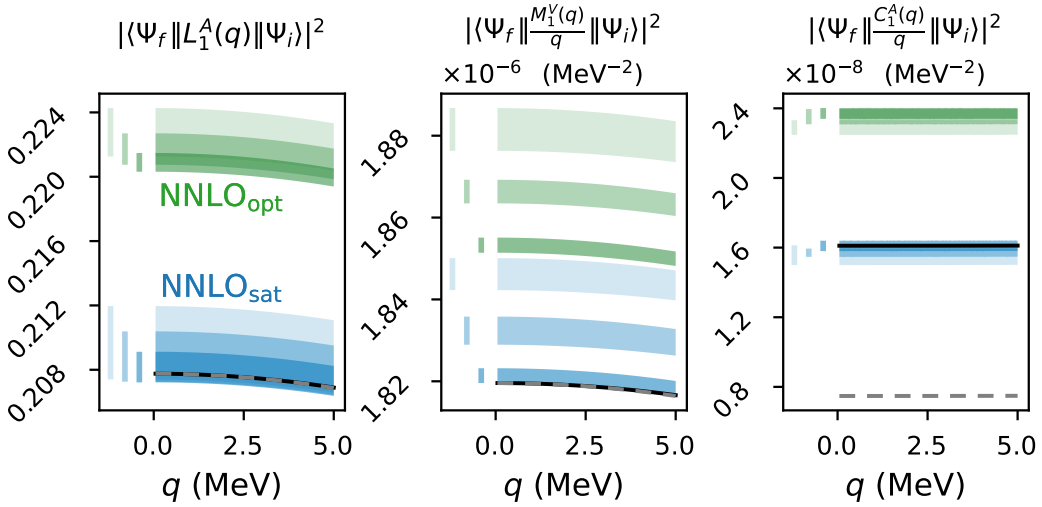

Figure 5.5: Dependence of nuclear matrix elements on the NCSM model-space parameters and nuclear Hamiltonians. The light to dark bands correspond to $N_{\rm max} = 8, 10, 12$ for the NNLO$_{\rm sat}$ (blue) interaction and $N_{\rm max} = 10, 12, 14$ for the NNLO$_{\rm opt}$ (green) interaction. The width of the bands show the variation with HO frequency $\hbar\Omega = 16, 20, 24$ MeV. The solid (dashed) line shows the result with the NNLO$_{\rm sat}$ interaction at $N_{\rm max} = 12$, $\hbar\Omega = 20$ MeV computed with translationally-invariant (standard) one-body densities. Figure reproduced from [2].

In our paper [2], as a feasibility study, we computed β-decay observables of the pure Gamow-Teller transition ^{6}He$(0^+) \to {}^6$Li(1^+). These are very light nuclei for which NCSM calculations are very tractable, in addition there are several ongoing experimental campaigns to make very precise measurements with per-mil accuracy.

We used technology developed in [82] to evaluate q dependent current operators in the NCSM. We calculated the wavefunctions of ^{6}He and ^{6}Li with the NCSM with two different nucleon-nucleon forces (NNLO$_{opt}$[83] and NNLO$_{sat}$[84]). We computed the transition matrix elements for several multipole operators. For this transition the contribution of 2BCs is small enough that they can be neglected (within the error budget of other quantities).

Figure 5.5 shows the transition matrix elements for the axial Coulomb and axial longitudinal nuclear operators ($\mathcal{C}_1^A$ and $\mathcal{L}_1^A$ respectively (see Section B.3)) and the vector transverse magnetic nuclear operator $\mathcal{T}_1^{V,M}$ (referred to as "M_1^V" in the figure). We estimated uncertainty bands for each nuclear force by varying the NCSM parameters: Ω and N_{max}. In addition, we compared the results of computing the transition matrix element in the standard way (2.94) and using translationally invariant densities (2.95). Figure 5.6 shows similar uncertainty bands for the components of the nuclear operators (in terms of the "basic" multipole operators given in Section B.4).

It is clear that there is greater dependence on the choice of nuclear interaction than on the NCSM parameters. We also found that the transition matrix elements are sensitive to

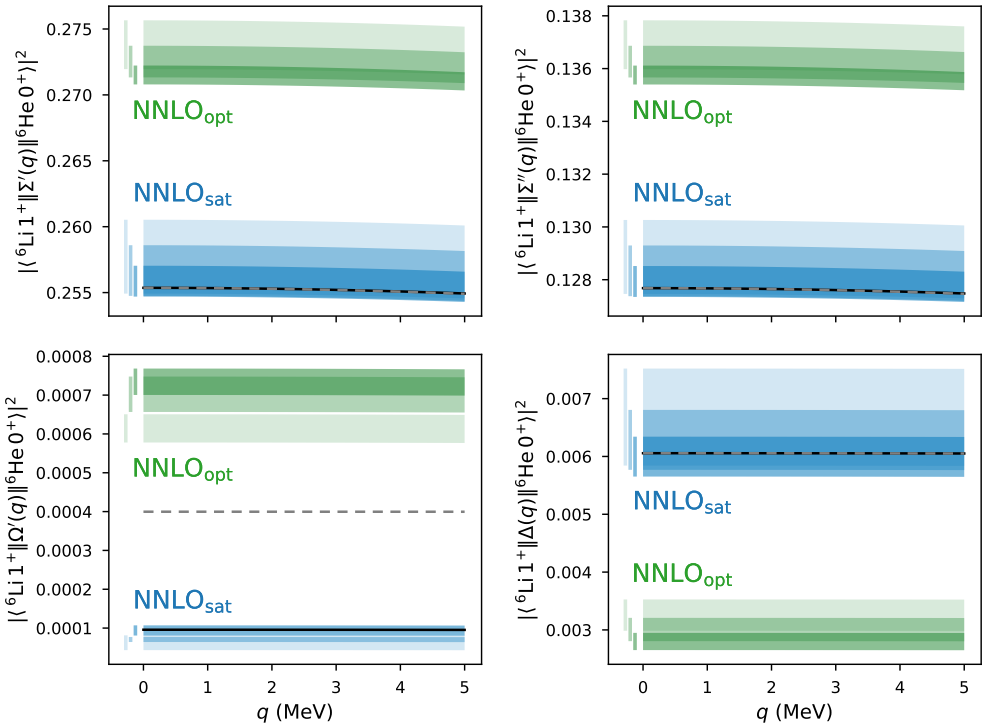

Figure 5.6: Dependence of nuclear matrix elements on the NCSM model space parameters and nuclear Hamiltonians. Light, medium, and heavy filled bands correspond to $N_{\max} = 8, 10, 12$ for the NNLO$_{\rm sat}$ interaction including 3NF (blue bands), and $N_{\max} = 10, 12, 14$ for the NNLO$_{\rm opt}$ interaction with only 2NF (green bands). The width of the bands show the variation with HO frequency $\hbar\Omega = 16, 20, 24$ MeV. The solid (dashed) line shows the result with the NNLO$_{\rm sat}$ interaction at $N_{\max} = 12$, $\hbar\Omega = 20$ MeV computed with translationally-invariant (standard) one-body densities. Figure reproduced from [2].

contamination by the center of mass. The gradient operator induces spurious center of mass effects. The most sophisticated description of this transition is the $N_{max} = 12$, $\hbar\Omega = 20$ MeV, NNLO$_{sat}$ calculation with translationally invariant densities.

The total energy dependent corrections to the β spectrum are pictured in Figure 5.7. The total spectrum corresponds to the partially integrated rate (3.70) i.e. $\frac{\mathrm{d}\Gamma_{fi}}{\mathrm{d}E}$. Overall we find that the Standard Model corrections do differ from zero and must be accounted for in experiments to differentiate from BSM effects. The corrections correspond to 1% of the spectrum and a 2% correction to the angular correlation.

Our prediction for the Fierz term is q-independent at leading order and has the value $b_F = -1.52(18) \times 10^{-3}$. The term $b_F \frac{m_e}{E}$ should therefore make a non-zero appearance in the spectrum and imitates BSM physics at the TeV scale. Our theoretical prediction carries a cumulative uncertainty of less than 15% i.e. the Fierz term has a predicted value on the order of 10^{-3} with an uncertainty of 10^{-4}, so experiments at 10^{-4} precision must certainly

take into account these calculations.

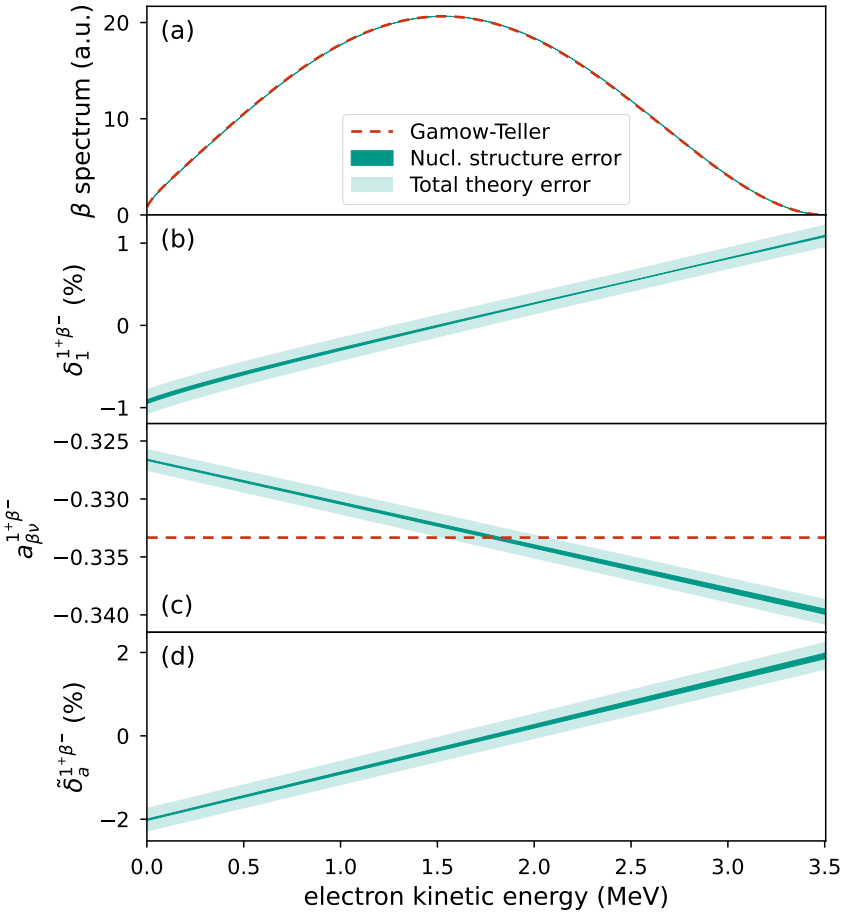

Figure 5.7: (a) Calculated energy dependence of the spectrum of ^{6}He β-decay, in arbitrary units. Dashed line is the pure GT spectrum, while the filled bands include nuclear-structure dependent corrections. (b) The residual nuclear structure correction $\delta_1^{1^+\beta^-}$ compared to the pure GT spectrum. (c) Energy dependence of the angular correlation $a_{\beta\nu}$. Dashed line corresponds to the SM value, $a_{\beta\nu}^{\rm GT} = -1/3$. (d) Relative size of the $\tilde{\delta}_a^{1^+\beta^-}$ correction. The width of the dark filled bands shows the variation with the employed nuclear Hamiltonian and NCSM model space parameters for HO frequency $\hbar\Omega = 16, 20, 24$ MeV, $N_{\rm max} = 8, 10, 12$ $(10, 12, 14)$ using the NNLO$_{\rm sat}$ (NNLO$_{\rm opt}$) interaction, using translationally-invariant one-body densities. The width of the light filled band shows the total estimated theory error. Figure reproduced from [2].

5.2 Neutrino-less Double Beta Decay

Neutrino-less double-β decay is a hypothetical process in which a nucleus undergoes two simultaneous β decays but emits no neutrinos, as discussed in Section 3.2.3. The observation of this decay would provide evidence of a lepton-number violating process and identify the neutrino as a Majorana particle, thus providing insights towards the origin of the matter-

antimatter symmetry in the universe and the neutrino mass. Current experiments have established a lower limit on the lifetime of about 10^{26} years [85–87] and sensitivity will be improved by several orders of magnitude further in the coming years.

Essential for planning and interpreting these experiments are the nuclear matrix elements (NMEs) that relate the decay lifetime to the neutrino mass scale (3.71). These matrix elements are not known and cannot be measured. Theoretical computations based on different models and techniques lead to factors of 3 to 5 in predicting these numbers. Further complication is the recent discovery that within χEFT, the standard decay operator must be supplemented by a contact operator of uncertain strength [67]. Efforts are underway to compute this contact from QCD and better understand its impact.

The candidate nuclei for experimentally measuring $0\nu\beta\beta$ decay e.g. ^{48}Ca [88, 89] are heavy and cannot be computed with the NCSM using current computing resources. Therefore numerical methods with additional levels of approximation are needed. Calculations of fictitious decays of lighter nuclei are still of value, as they can be compared to the NCSM as a benchmark. In realistic scenarios these decays would not be detectable as they would be swamped by single beta decays or would be energetically forbidden.

5.2.1 Coupled-Cluster Benchmarks

Our recent paper [3] presents calculations of the $^{48}\text{Ca} \rightarrow {}^{48}\text{Ti}$ decay via $0\nu\beta\beta$. This was calculated with the coupled-cluster method (CC). NCSM calculations were used to gauge the quality of coupled-cluster in several light nuclei by calculation of fictitious decays. Using several interactions, we calculated the NME for $0\nu\beta\beta$ using the closure energy of 5 MeV (defined in Section 3.2.3).

In Figure 5.8, the NCSM NMEs are compared to the CC NMEs. The coupled-cluster method approximates a nuclear state with an expansion over particle-hole excitations of nucleons with respect to a particular reference state. Each calculation requires a choice of reference state. The CC results are shown as two pairs. Each pair corresponds to a different reference state. The first (second) point with each pair show CCSD (CCSDT-1) approximations, corresponding to the inclusion of singles+doubles [90] (singles+doubles+triples [91, 92]) excitations. The error bar on the NCSM results corresponds to the extrapolation to infinite model space. These results demonstrate that if the coupled-cluster calculations choose the correct reference state and go to triples excitations, their calculations are comparable to NCSM.

The coupled-cluster method has much better scaling with A than the NCSM. This allows it to calculate the $0\nu\beta\beta$ matrix element for ^{48}Ca which is a promising experimental candidate [88, 89]. A comparison of the $^{48}\text{Ca} \rightarrow {}^{48}\text{Ti}$ NME with various phenomenological methods (and the *ab initio* method IMSRG+GCM [94]) is shown in 5.9. While the ground state of ^{48}Ca is spherical, that of ^{48}Ti is deformed. The error band corresponds to the choice of deformed vs spherical CC reference state. Based on the benchmarks against the

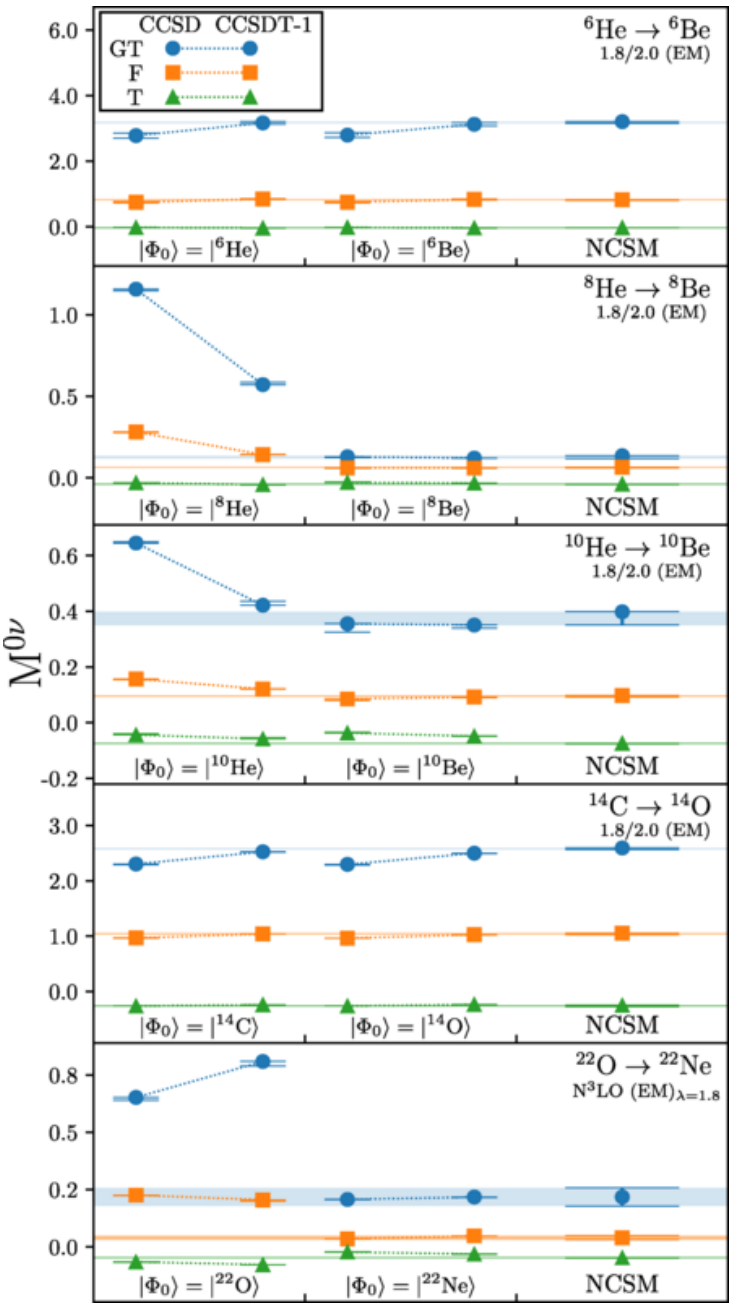

Figure 5.8: Comparison of the $0\nu\beta\beta$ nuclear matrix element in several light nuclei computed with the coupled cluster method and the no-core shell model. The first two columns correspond to different choices for the coupled-cluster reference state, and results for the CCSD and CCSDT-1 approximations are shown in each. The error bars indicate the uncertainties coming from variations with the model-space size. Each case utilizes the 1.8/2.0(EM) interaction [93] except for $^{22}\text{O} \rightarrow {}^{22}\text{Ne}$ which disregards the three-nucleon forces to more rapidly converge the NCSM results. Figure reproduced from [3].

NCSM, we would expect the CC prediction using a deformed reference state to be the most accurate.

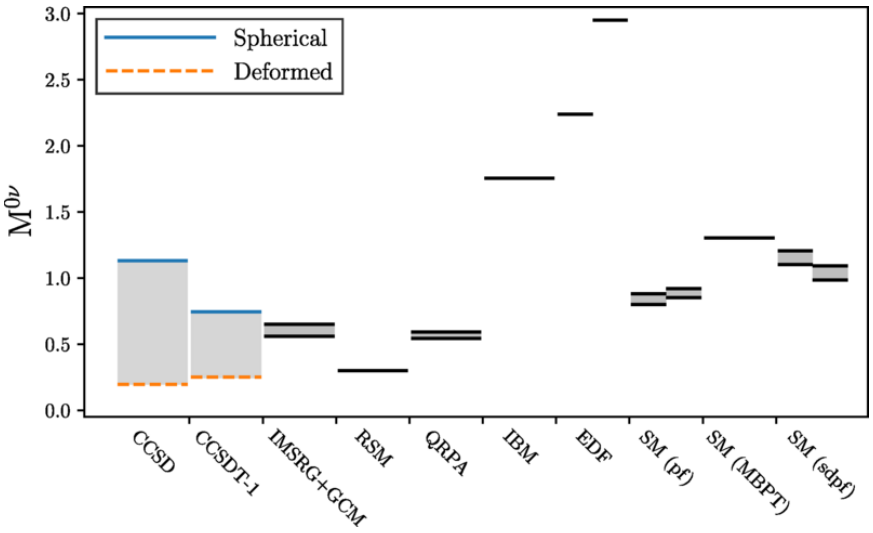

Figure 5.9: Comparison of the NME for the $0\nu\beta\beta$ decay of ^{48}Ca, calculated within various approaches. The coupled-cluster results use both the CCSD and CCSDT-1 approximations with both the spherical and deformed reference states. For IMSRG+GCM [94], the double bars show the effects of uncertainty in model-space size; otherwise they show those of uncertainty in short-range correlation functions. The other results are the realistic shell model [95], the quasiparticle random phase approximation [96], the interacting boson model [97], various energy-density functionals [98, 99] and phenomenological shell models [66, 71, 100, 101]. Figure reproduced from [3].

5.2.2 VS-IMSRG Benchmarks

The same calculations with a different nuclear force was carried out for a similar suite of light nuclei and the operators were consistently SRG-evolved. This was compared with the technique of VS-IMSRG ("valence space in-medium SRG"), which has an additional unitary transformation on top of regular SRG [10]. VS-IMSRG, like coupled-cluster, is also capable of calculating the ^{48}Ca decay.

SRG calculations were carried out at both the two- and three-body level. As $0\nu\beta\beta$ is a two-body operator, it was expected that the three-body induced term would be bigger (compared to that of single beta decay). However our finding is that the three-body induced effect is quite small. The spread with λ is not always improved relative to two-body evolution and the overall contribution is very small. Some examples are shown in Figure 5.10 and Figure 5.11.

Figure 5.10 demonstrates the matrix element for light mirror nuclei where the isospin changes by $\Delta T = 0$. This is a hypothetical mode because single-β decays are possible and in the case of ^{6}He $\rightarrow$ ^{6}Be the change in charge is enough that the new nucleus would be

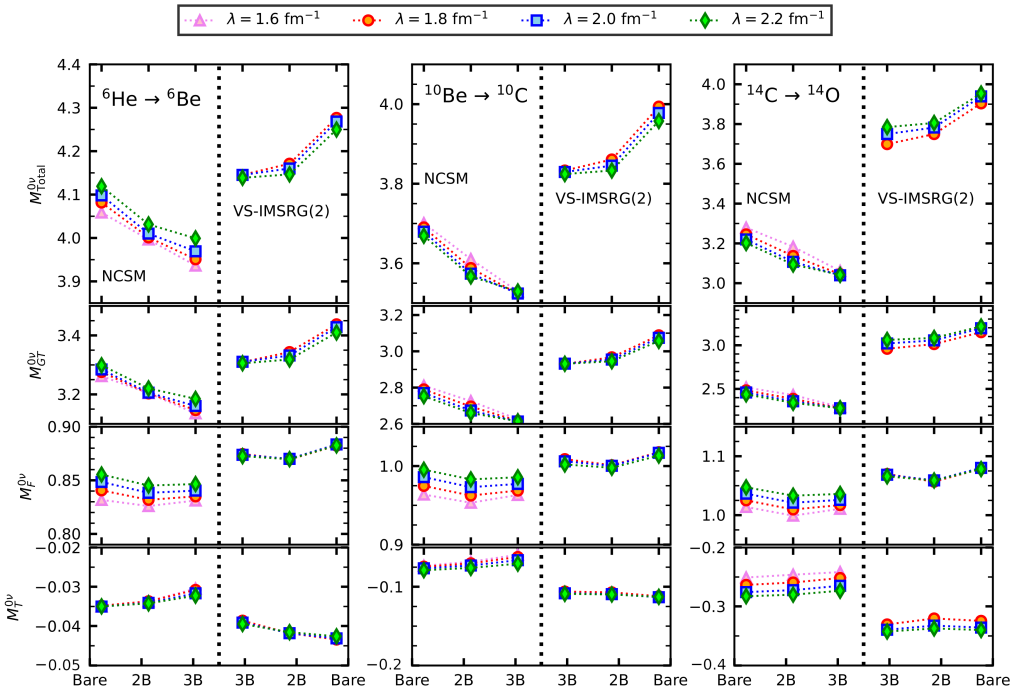

Figure 5.10: Nuclear matrix elements of the neutrino-less double-beta decay transitions with $\Delta T = 0$. From left to right, columns correspond to the transitions: $^{6}\text{He}(0^+_1) \rightarrow {}^{6}\text{Be}(0^+_1)$, $^{10}\text{Be}(0^+_1) \rightarrow {}^{10}\text{C}(0^+_1)$ and $^{14}\text{C}(0^+_1) \rightarrow {}^{14}\text{O}(0^+_1)$. The numerical calculations use the parameters $\hbar\Omega = 20$ MeV and $N_{max} = 8$ ($e_{max} = 12$) in the NCSM (IMSRG). The NCSM calculation at $A = 14$ uses an additional approximation known as "importance truncation" [102] to obtain a result at $N_{max} = 8$.

unbound due to Coulomb repulsion (see Figure 1.1). Figure 5.11 shows the more realistic case of $\Delta T = 2$ which corresponds to the situation in experimental candidates. The matrix elements here are significantly smaller.

Overall, the spread in λ becomes smaller as the 2N-induced and 3N-induced contributions are included, indicating the 4N induced term is less important. A few exceptions are observed i.e. the $M^{0\nu}_{GT}$ term for NCSM in ^{6}He and IMSRG in ^{14}C. This benchmark indicates an difference of about 3, 8, 20% for A=6, 10, 14 respectively. According to a previous study, the $A = 14$ difference is especially large due to neglected triples in VS-IMSRG [94], inclusion of these in progress [103].

These results indicate some deficiencies in the IMSRG for smaller nuclei. Generally NCSM agrees with the couple-cluster method (with the deformed basis) which has been found to give smaller $0\nu\beta\beta$ matrix elements than the IMSRG [94]. Overall, *ab initio* calculations with different methods are relatively consistent and report smaller matrix elements than phenomenological models possibly reproducing a quenching-like effect.

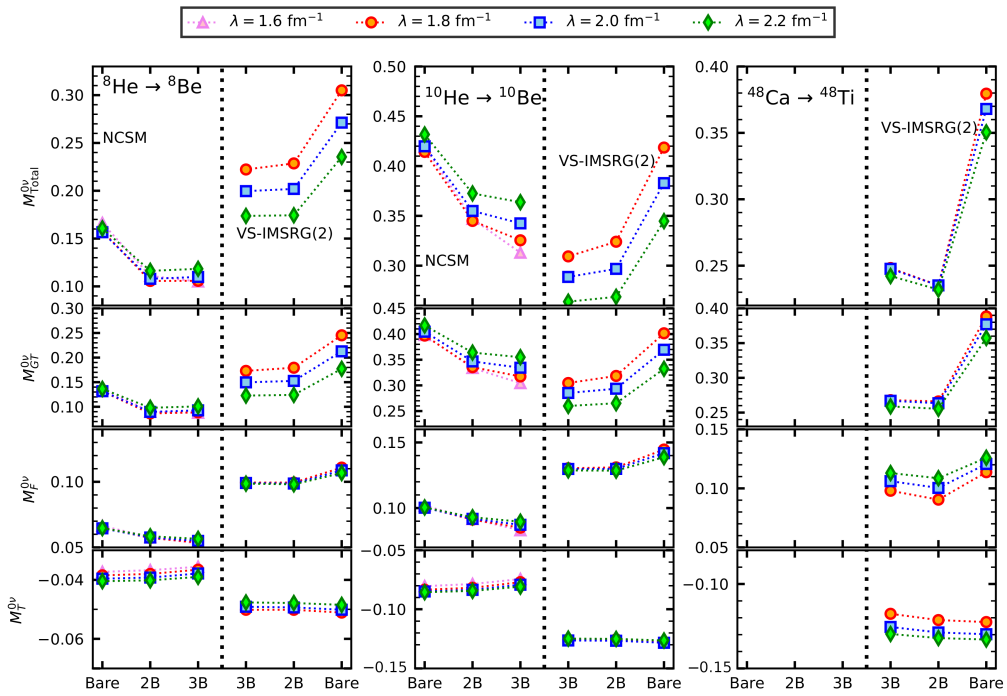

Figure 5.11: Nuclear matrix elements of the neutrino-less double-beta decay transitions with $\Delta T = 2$. From left to right, columns correspond to the transitions: $^{8}\text{He}(0^{+}_{1}) \rightarrow {}^{8}\text{Be}(0^{+}_{1})$, $^{10}\text{He}(0^{+}_{1}) \rightarrow {}^{10}\text{Be}(0^{+}_{1})$ and $^{48}\text{Ca}(0^{+}_{1}) \rightarrow {}^{48}\text{Ti}(0^{+}_{1})$. The numerical calculations use the parameters $\hbar\Omega = 20$ MeV, except $\hbar\Omega = 16$ MeV for $A = 48$, and $N_{max} = 8$ ($e_{max} = 12$) in the NCSM (IMSRG).

Chapter 6

Scattering and Reactions of Nuclei

Calculations of continuum phenomena like nuclear reactions, for example, radiative capture and photo-disintegration are important for the study of astrophysics. Nuclear reactions drive the life and death of stars but many of the reactions involved occur at energies where counting rates are too low to be reached by experiment. A predictive theory is needed to extrapolate to that domain from higher energy experiments (e.g. $^{12}\mathrm{C}(\alpha,\gamma)^{16}\mathrm{O}$ measurements at TRIUMF [104]) and therefore provide reliable input to astrophysical models.

The basis expansion of the NCSM is made of square-integrable states which must go to zero at large distances. Weakly-bound states require the description of this far-distance behaviour and so are difficult to construct, needing many more high-energy excitations. Unbound states such as resonances and scattering states are impossible to reproduce.

The no-core shell model with continuum (NCSMC) [105] is a many-body method which provides a unified description of bound states and continuum dynamics. To introduce this technique, we will first discuss the general theory of scattering and reactions.

6.1 Scattering Theory

Ignoring the internal structure of the particles, a two-particle collision (between a projectile with mass M_P and a target with mass M_T) can be simplified to a one variable problem as the reaction should not depend on the overall center of mass motion. We can solve for the wavefunction of the system as a function of only the relative position.

We expect that the initial state of scattering is a plane wave: e^{ikz}, and the final state should be a spherical wave: $\frac{e^{ikr}}{r}$, where $k = \sqrt{2\mu E}$ is the wavenumber, E is the available kinetic energy and μ is the reduced mass of the system:

$$\mu = \frac{M_P M_T}{M_P + M_T} \,. \tag{6.1}$$

We look for solutions with the ansatz [36]

$$\psi(r,\theta) \approx \mathcal{N}\left(e^{ikz} + f(\theta)\frac{e^{ikr}}{r}\right) , \tag{6.2}$$

where $\mathcal{N}$ is a normalization factor.

The differential cross section is the observable which can be measured in an experiment, where a beam impinges on a target. It is defined as the proportionality constant $D(\theta)$ between the number of particles $\mathrm{d}N$ entering the infinitesimal area $\mathrm{d}\sigma$ and scattering into the infinitesimal solid angle $\mathrm{d}\Omega$ (see Figure 6.1). i.e.

$$D(\theta) = \frac{1}{\mathcal{L}}\frac{\mathrm{d}N}{\mathrm{d}\Omega} = \frac{\mathrm{d}\sigma}{\mathrm{d}\Omega} , \tag{6.3}$$

where $\mathcal{L}$ is the luminosity (the number of incident particles per unit area per unit time).

The probability $\mathrm{d}P$ is the probability density $|\psi|^2$ times the infinitesimal volume $\mathrm{d}V$. Conservation of probability equates the initial and final probabilities, for particles with speed v, in time $\mathrm{d}t$ to relate the cross section to the wavefunction, i.e.

$$\begin{aligned}
\mathrm{d}P_I =& \mathrm{d}P_F , \\
|\psi_I|^2\,\mathrm{d}V =& |\psi_F|^2\,\mathrm{d}V , \\
|\mathcal{N}|^2\, v\mathrm{d}t\mathrm{d}\sigma =& |\mathcal{N}|^2\,\frac{|f|^2}{r^2} v\mathrm{d}t r^2\mathrm{d}\Omega , \\
\frac{\mathrm{d}\sigma}{\mathrm{d}\Omega} =& |f(\theta)|^2 .
\end{aligned} \tag{6.4}$$

Hence $f(\theta)$ is the scattering amplitude, the probability amplitude of elastic scattering in the direction θ. The normalization $\mathcal{N}$ cancels out so in the following we will set it to 1.

We must solve the Schrodinger equation for $\psi(r,\theta)$, giving $f(\theta)$ from which we can directly extract the scattering cross sections. We can't use Fermi's golden rule because the nuclear interaction is not weak, but it will apply to electromagnetic transitions as will be shown in Section 6.3. If we already knew the wavefunction we could extract the scattering amplitude via an integral [106], i.e.

$$f(\theta) = \frac{\mu}{2\pi}\int e^{ikr} V(r)\psi(r)\mathrm{d}^3 r , \tag{6.5}$$

but we will instead calculate it directly as a solution to the Schrodinger equation.

6.1.1 Partial Wave Analysis

Due to conservation of angular momentum (and parity) different channels scatter independently. Correspondingly the Schrodinger equation with a spherically symmetric potential admits separable solutions $\psi(\vec{r}) = R_\ell(r)Y_{\ell m}(\theta,\phi)$, $u_\ell(r) = rR_\ell(r)$ satisfies the radial equa-

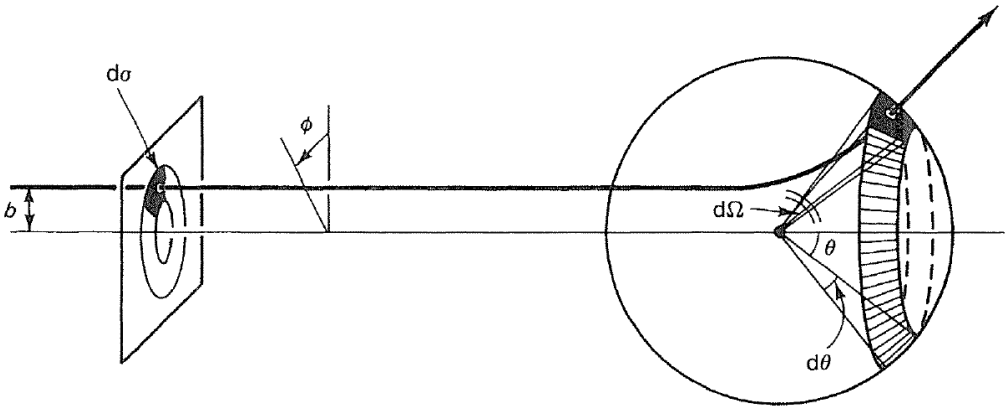

Figure 6.1: A particle incident on area $\mathrm{d}\sigma$ scatters into the solid angle $\mathrm{d}\Omega$. b is the impact parameter, the distance by which the incident particle would have missed the scattering center, had it continued on its original trajectory. Figure reproduced from [11].

tion:

$$\left[\frac{\mathrm{d}^2}{\mathrm{d}r^2} - \frac{\ell(\ell+1)}{r^2} - 2\mu V(r) + k^2\right] u_\ell = 0 \,. \tag{6.6}$$

Each channel ℓ gives a different $u_\ell(r)$. The $Y_{\ell m}(\theta,\phi)$ are again the spherical harmonics (2.8).

In the far field ($r \to \infty$), the interaction $V(r)$ and the centrifugal term $\frac{\ell(\ell+1)}{r^2}$ go to zero and the spherical wave solves

$$\left[\frac{\mathrm{d}^2}{\mathrm{d}r^2} + k^2\right] u_\ell = 0 \,. \tag{6.7}$$

In the intermediate region (assuming $V(r)$ goes to zero more quickly than the centrifugal $\frac{\ell(\ell+1)}{r^2}$ potential) we have the equation:

$$\left[\frac{\mathrm{d}^2}{\mathrm{d}r^2} - \frac{\ell(\ell+1)}{r^2} + k^2\right] u_\ell = 0 \,, \tag{6.8}$$

which admits the Bessel function solutions $R_\ell(r) = j_\ell(kr), n_\ell(kr)$ which can behave like a outgoing spherical wave when combined. We therefore expect a solution to be a linear combination:

$$\psi(r,\theta,\phi) = \sum_{\ell m} \left(A_{\ell m} j_\ell(kr) + B_{\ell m} n_\ell(kr)\right) Y_{\ell m}(\theta,\phi) \,. \tag{6.9}$$

Only $m = 0$ can contribute due to the cylindrical symmetry of the system, i.e.

$$\psi(r,\theta) = \sum_{\ell} \left(A_\ell j_\ell(kr) + B_\ell n_\ell(kr)\right) P_\ell(\cos\theta) \,, \tag{6.10}$$

where $P_\ell(\cos\theta)$ are the Legendre polynomials (coming from $Y_\ell^0(\theta,\phi) = \frac{\hat{\ell}}{\sqrt{4\pi}} P_\ell(\cos\theta)$).

A plane wave is made from a combination of only j_ℓ (since n_ℓ is not finite at the origin),

i.e.

$$e^{ikz} = \sum_\ell i^\ell (2\ell+1) j_\ell(kr) P_\ell(\cos\theta) \ , \tag{6.11}$$

which can be expressed as a combination of an incoming spherical wave I_ℓ and an outgoing spherical wave O_ℓ via:

$$e^{ikz} = \sum_\ell i^\ell (2\ell+1) \frac{i}{2} \frac{1}{kr} \left(I_\ell(kr) - O_\ell(kr)\right) P_\ell(\cos\theta) \ , \tag{6.12}$$

where

$$I_\ell(kr) = kr \left(n_\ell(kr) - i j_\ell(kr)\right) \ , \tag{6.13}$$

$$O_\ell(kr) = kr \left(n_\ell(kr) + i j_\ell(kr)\right) \ . \tag{6.14}$$

The wavefunction is often expressed in the form:

$$\psi(r,\theta) = \sum_\ell i^\ell (2\ell+1) \frac{i}{2} \frac{1}{kr} \left(I_\ell(kr) - S_\ell O_\ell(kr)\right) P_\ell(\cos\theta) \tag{6.15}$$

where S_ℓ is the "S-matrix element" (not yet a true matrix but will be generalized into one in Section 6.1.3). The I_ℓ, O_ℓ asymptotically go to $i^\ell e^{-ikr}$, $i^{-\ell} e^{ikr}$ respectively. Therefore we can match to our expected asymptotic solution:

$$\begin{aligned}
f(\theta)\frac{e^{ikr}}{r} =& \psi(r,\theta) - e^{ikz} \\
=& \sum_\ell i^\ell (2\ell+1) \frac{i}{2} \frac{1}{kr} \left(I_\ell(kr) - S_\ell O_\ell(kr)\right) P_\ell(\cos\theta) \\
& - \sum_\ell i^\ell (2\ell+1) \frac{i}{2} \frac{1}{kr} \left(I_\ell(kr) - O_\ell(kr)\right) P_\ell(\cos\theta) \\
=& \sum_\ell i^\ell (2\ell+1) \frac{i}{2} \frac{1}{kr} \left([I_\ell - I_\ell] + (1 - S_\ell) O_\ell\right) P_\ell(\cos\theta) \ , \\
f(\theta) =& \sum_\ell (2\ell+1) \frac{i}{2k} \left(1 - S_\ell\right) P_\ell(\cos\theta) \ .
\end{aligned} \tag{6.16}$$

This can be again redefined in terms of the "partial-wave amplitudes":

$$a_\ell = \frac{1}{2ik} \left(S_\ell - 1\right) \ . \tag{6.17}$$

With the incoming plane wave explicit, our wavefunction solution looks like:

$$\psi(r,\theta) = e^{ikz} + \sum_\ell \hat{\ell}^2 a_\ell \frac{e^{ikr}}{r} P_\ell(\cos\theta) \ , \tag{6.18}$$

and we can identify:

$$f(\theta) = \sum_{\ell} \hat{\ell}^2 a_\ell P_\ell(\cos\theta) \ . \tag{6.19}$$

The problem of finding $f(\theta)$ has now been transferred to the problem of finding a_ℓ, which is generally done by finding the solutions to the interior wavefunction (where the potential $V(r)$ dominates) using a different method and then using matching conditions at some $r = a$. This is the principle behind the R-matrix method described later in this section and in Section 6.2.2.

The scattering amplitude and S-matrix can be reparametrized using the phase shift δ_ℓ, i.e.

$$a_\ell = \frac{1}{2ik}\left(e^{2i\delta_\ell} - 1\right) = \frac{1}{k} e^{i\delta_\ell} \sin\delta_\ell \ , \tag{6.20}$$

$$S_\ell = e^{2i\delta_\ell} \ . \tag{6.21}$$

The phase shift is the only effect of the central potential on a spherical wave, i.e. due to conservation of probability the incoming and outgoing spherical wavefunctions can only differ by a phase, the factor $e^{2i\delta_\ell}$ [36].

6.1.2 Coulomb Scattering

In nuclear scattering the incident particles have electric charge. This means the interaction includes the Coulomb potential: $V_C(r) = \frac{q_1 q_2}{r}$. Since this $V(r)$ potential does not drop off more quickly than the centrifugal term, we can no longer use the Bessel functions.

In this case we have the equation:

$$\left[\frac{\mathrm{d}^2}{\mathrm{d}r^2} - \frac{\ell(\ell+1)}{r^2} - \frac{2k\eta}{r} + k^2\right] u = 0 \tag{6.22}$$

where $\eta = \frac{\mu q_1 q_2}{k} = \frac{q_1 q_2}{v}$ is the Sommerfeld parameter. The incoming and outgoing waves now depend on η i.e. $I_\ell(\eta, kr)$ and $O_\ell(\eta, kr)$ respectively, where $I_\ell = G_\ell + iF_\ell$ and $O_\ell = G_\ell - iF_\ell$. $F_\ell(\eta, kr)$ and $G_\ell(\eta, kr)$ are the Coulomb functions [107, 108], which reduce to $krj_\ell(kr)$, $krn_\ell(kr)$ at $\eta = 0$.

The Coulomb wave solution analogous to the plane-wave (6.12) is:

$$\psi_C(r,\theta) = \sum_{\ell} i^\ell (2\ell+1) \frac{i}{2} \frac{1}{kr} \left(I_\ell(\eta, kr) - O_\ell(\eta, kr)\right) P_\ell(\cos\theta) \ . \tag{6.23}$$

The asymptotic scattering states have the following form:

$$\psi_C(r,\theta) = e^{i[kz + \eta \ln k(r-z)]} + f_C(\theta) \frac{e^{i[kr - \eta \ln 2kr]}}{r} \ , \tag{6.24}$$

where $f_C = \frac{1}{2ik}\sum_\ell \hat{\ell}^2 P_\ell(\cos\theta)\left[e^{2i\sigma_\ell(\eta)}-1\right]$ and $\sigma_\ell(\eta) = \arg\Gamma(\ell+1+i\eta)$. f_C has the more compact expression [109]

$$f_C = \frac{1}{2k\sin^2\frac{\theta}{2}} e^{2i\left(\sigma_0 - \eta\ln\sin\frac{\theta}{2}\right)} \ . \tag{6.25}$$

The presence of an additional short-range potential in addition to the Coulomb potential adds a second term to the asymptotic wavefunction, i.e.

$$\psi(r,\theta) = \psi_C(r,\theta) + f(\theta)\frac{e^{i[kr-\eta\ln 2kr]}}{r} \ . \tag{6.26}$$

The coefficient $f(\theta)$ is now a "Coulomb-distorted amplitude"[107, 109] which has an S-matrix element with an additional Coulomb phase σ_ℓ, i.e.

$$f(\theta) = \frac{1}{2ik}\sum_\ell \hat{\ell}^2 e^{2i\sigma_\ell}\left(S_\ell - 1\right) P_\ell(\cos\theta) \ . \tag{6.27}$$

Analogous to (6.15) the asymptotic wavefunction is:

$$\psi(r,\theta) = \sum_\ell i^\ell (2\ell+1)\frac{i}{2}\frac{1}{kr} e^{i\sigma_\ell}\left(I_\ell(\eta,kr) - S_\ell O_\ell(\eta,kr)\right) P_\ell(\cos\theta) \tag{6.28}$$

The total elastic differential cross section will be the combination:

$$\frac{\mathrm{d}\sigma}{\mathrm{d}\Omega} = |f_C + f|^2 \ . \tag{6.29}$$

The matching condition used to find the wavefunction is the inverse logarithmic derivative (at $r = a$). This defines R-matrix element

$$R_\ell = \frac{1}{a}\frac{u_\ell^{(int)}(ka)}{u_\ell^{(int)\prime}(ka)} = \frac{1}{a}\frac{u_\ell^{(ext)}(ka)}{u_\ell^{(ext)\prime}(ka)} \ , \tag{6.30}$$

where $u_\ell^{(int)}$ denotes the radial part of the interior wavefunction, numerically integrated, and $u_\ell^{(ext)}$ is the radial component of the exterior wavefunction (6.28), i.e.

$$u_\ell^{(ext)} = \frac{i}{2}\left[I_\ell - S_\ell O_\ell\right] \ . \tag{6.31}$$

The matching conditions allows us to solve for S_ℓ:

$$S_\ell = \frac{I_\ell - aR_\ell I_\ell'}{O_\ell - aR_\ell O_\ell'} \ . \tag{6.32}$$

In practice the resolution of all radial equations is not computationally feasible and we must truncate at some ℓ. Thankfully, phase shifts are strongly suppressed by the centrifugal

term when $\frac{\ell(\ell+1)}{a^2} \gg k^2$ [110]. Experimentally high ℓ states will also be suppressed by screening of the Coulomb potential [106].

6.1.3 Multi-channel Scattering and Reactions

The nuclear reaction may change the composition of the colliding particles, i.e. the final internal states of the projectile and target may be different than their initial internal states. When the incoming particles are composite particles they may have many internal states. The different combinations of internal states as well as different mass partitions (i.e. a different number of nucleons in each nucleus) can be collected under the term "channels". Each channel $|\nu\rangle$ can be thought of as two internal wavefunctions ϕ coupled together [109], i.e.

$$|\nu\rangle = \left[\left[\phi^{(1)}_{\nu S_1} \otimes \phi^{(2)}_{\nu S_2}\right]^{(S)} \otimes Y_L(\Omega_{r_\nu})\right]^{(J^\pi M)} , \tag{6.33}$$

where $\vec{r}_\nu$ is the relative coordinate between the center of mass of the two clusters. The system with a total A nucleons is split between two clusters with A_1 and A_2 nucleons respectively (where of course $A_1 + A_2 = A$) and so the coordinate $\vec{r}_\nu$ is defined by

$$\vec{r}_\nu = (r_\nu, \theta_{r_\nu}, \phi_{r_\nu}) = \frac{1}{A_1}\sum_{i=1}^{A_1} \vec{r}_i - \frac{1}{A_2}\sum_{j=A_1+1}^{A} \vec{r}_j \ . \tag{6.34}$$

The total angular momentum J, projection M and parity π must be conserved and so there will be a different set of ν and corresponding equations for each $J^\pi M$. The $J^\pi M$ labels will be suppressed in much of the following. The stationary scattering wavefunction with entrance channel ν_i will look like:

$$\left|\Psi^{J^\pi M}_{\nu_i}\right\rangle = \sum_\nu \mathcal{A}\,|\nu\rangle\,\frac{u_{\nu\nu_i}(r_\nu)}{r_\nu} , \tag{6.35}$$

where $\mathcal{A}$ is the anti-symmetrization operator (with respect to exchanges of nucleons between the clusters [111]). The radial part $u_{\nu\nu_i}$ must have the asymptotic form:

$$u_{\nu\nu_i}(r_\nu) = \frac{i}{2\sqrt{v_\nu}}\left[\delta_{\nu\nu_i} I_\nu(\eta_\nu, k_\nu r_\nu) - S_{\nu\nu_i} O_\nu(\eta_\nu, k_\nu r_\nu)\right] , \tag{6.36}$$

and solves the Schrodinger equation:

$$\left[\frac{\mathrm{d}^2}{\mathrm{d}r^2} - \frac{\ell(\ell+1)}{r^2} - 2\mu_\nu V + k_\nu^2\right] u_{\nu\nu_i}(r) - 2\mu_\nu \sum_{\nu'} \int \mathrm{d}r' W_{\nu\nu'}(r,r') u_{\nu'\nu_i}(r') = 0 \ . \tag{6.37}$$

$W_{\nu\nu'}$ is a non-local potential that occurs due to the necessary anti-symmetrization $W_{\nu\nu'} = \langle\nu|\,\delta(r_\nu - r) V \mathcal{A} \delta(r_{\nu'} - r')\,|\nu'\rangle - \langle\nu|\,V\,|\nu'\rangle\,\delta_{\nu\nu'}\delta(r - r')$ [109]. The wavenumber is $k_\nu =$

$\sqrt{2\mu_\nu(E-E_\nu)}$ where E_ν is the threshold for the channel ν. The relative velocity is $v_\nu = k_\nu/\mu_\nu$ and the normalization $v_\nu^{-\frac{1}{2}}$ keeps the S-matrix unitary.

The S-matrix becomes $S_{\nu\nu_i}$ which will have dimensions corresponding to the number of initial channels and the number of available channels. This leads to the definition of the diagonal phase shifts δ_ν: $S_{\nu\nu} = e^{2i\delta_\nu}$ and the eigen-phase shifts δ_λ where $e^{2i\delta_\lambda}$ are the eigenvalues of S. The S-matrix must be block-diagonal with respect to the total angular momentum J and parity π. The off-diagonal S-matrix elements where ν and ν_i have different mass partitions would correspond to nuclear reactions. Off-diagonal matrix elements with the same mass partitions but different internal states would be deemed inelastic scattering.

Colliding systems in the entrance channel ν (now denoting just the mass partition and internal states labeled by total spin S_1, S_2) can have different initial orientations M_1 and M_2. When those projections are selected, we have an asymptotic form analogous to (6.26), i.e.

$$\psi_{\nu M_1 M_2}(r,\theta) = \psi_C(r,\theta)\phi^{(1)}_{\nu M_1}\phi^{(2)}_{\nu M_2} + \sum_{\nu' M_1' M_2'} \frac{e^{i(k_{\nu'}r - \eta_{\nu'}\ln 2k_{\nu'}r)}}{r} f^{\nu M_1 M_2}_{\nu' M_1' M_2'}(\theta)\phi^{(1)}_{\nu' M_1'}\phi^{(2)}_{\nu' M_2} \ . \tag{6.38}$$

This wavefunction can also be constructed by summing over coupled channels (6.33), i.e.

$$\psi_{\nu M_1 M_2}(r,\theta) = \frac{\sqrt{4\pi}}{k_\nu} \sum_{J\pi} \sum_{SL} \hat{L} e^{i\sigma_L} \left(S_1 M_1 S_2 M_2 | SM\right) \left(L0SM|JM\right) \psi_{\nu J^\pi M}(r,\theta) \ , \tag{6.39}$$

with $M = M_1 + M_2$. The projection of L must be zero due to the cylindrical symmetry about the beam.

Scattering and reaction rates will depend on the partial amplitudes $f^{\nu M_1 M_2}_{\nu' M_1' M_2'}$ which further depend on the multi-channel S-matrix (6.36), i.e.

$$\begin{aligned} f^{\nu M_1 M_2}_{\nu' M_1' M_2'}(\theta) = & \frac{\sqrt{4\pi}}{k} \sum_{J\pi} \sum_{SL} \sum_{S'L'} \hat{L} e^{i(\sigma_L + \sigma_{L'})} \left(S_1 M_1 S_2 M_2 | SM\right) \\ & \times \left(L0SM|JM\right) \left(S_1' M_1' S_2' M_2' | S' M'\right) \left(S' M' L' M - M' | JM\right) \\ & \times \left(\delta_{\nu\nu'}\delta_{SS'}\delta_{LL'} - S_{\nu' S' L', \nu S L}\right) Y_{L'(M-M')}(\theta) \ . \end{aligned} \tag{6.40}$$

A cross section is proportional to the square of the scattering amplitudes and we average over initial orientations and sum over final orientations. For elastic scattering, the initial and final channels are the same and we have a pure Coulomb term:

$$\frac{\mathrm{d}\sigma_{\nu\to\nu}}{\mathrm{d}\Omega} = \frac{1}{\hat{S}_1 \hat{S}_2} \sum_{M_1 M_2} \sum_{M_1' M_2'} \left| f_C(\theta)\delta_{M_1 M_1'}\delta_{M_2 M_2'} + f^{\nu M_1 M_2}_{\nu M_1' M_2'}(\theta) \right|^2 \ . \tag{6.41}$$

For inelastic scattering, or a reaction, we have

$$\frac{\mathrm{d}\sigma_{\nu\to\nu'}}{\mathrm{d}\Omega} = \frac{1}{\hat{S}_1^2\hat{S}_2^2}\sum_{M_1M_2}\sum_{M_1'M_2'}\left|f^{\nu M_1M_2}_{\nu' M_1'M_2'}(\theta)\right|^2 \ . \tag{6.42}$$

6.1.4 Cluster States from NCSM

The internal quantum numbers of the clusters can be included through the NCSM. A two-cluster state with total angular momentum J, parity π and isospin T can be described by:

$$\left|\Phi^{J^\pi T}_{\nu r}\right\rangle = \left[\left(\left|A_1\lambda_1 S_1^{\pi_1}T_1\right\rangle\left|A_2\lambda_2 S_2^{\pi_2}T_2\right\rangle\right)^{(sT)}Y_\ell(\theta_{r_\nu},\phi_{r_\nu})\right]^{(J^\pi T)}\frac{\delta(r-r_\nu)}{rr_\nu} \ . \tag{6.43}$$

The intrinsic (internally anti-symmetric) wavefunctions of the clusters are $|A_1\lambda_1 S_1^{\pi_1}T_1\rangle$ and $|A_2\lambda_2 S_2^{\pi_2}T_2\rangle$. They are individually eigenstates (i.e. NCSM solutions denoted by λ) of the A_1- and A_2-nucleon Hamiltonians respectively. The brackets denote implicitly the angular momentum coupling of S_1S_2 to s and $s\ell$ to J and the isospin coupling T_1T_2 to T. The intrinsic cluster quantum numbers and the quantum numbers denoting different partial waves are grouped together into the single index $\nu = \{A_1\lambda_1 S_1^{\pi_1}T_1; A_2\lambda_2 S_2^{\pi_2}T_2; s\ell\}$.

In the technique known as the resonating-group method (RGM), or "NCSM/RGM" [112], these states are used as a basis to construct an A-nucleon wavefunction for a given entrance channel ν_i, i.e.

$$\left|\Psi^{J^\pi T}_{\nu_i}\right\rangle = \sum_\nu\int \mathrm{d}r r^2\frac{\gamma^{J^\pi T}_{\nu\nu_i}(r)}{r}\mathcal{A}_\nu\left|\Phi^{J^\pi T}_{\nu r}\right\rangle \ . \tag{6.44}$$

The $\gamma^{J^\pi T}_{\nu\nu_i}(r)$ are the variational amplitudes of the relative motion between the clusters. The operator $\mathcal{A}_\nu$ is the inter-cluster anti-symmetrizer. It depends on the ν because it will depend on the mass partitioning.

In this basis the A-nucleon Schrodinger equation can be mapped to a one-dimensional coupled-channel equation for the amplitudes:

$$\sum_\nu\int \mathrm{d}r r^2\left[\mathcal{H}^{J^\pi T}_{\nu'\nu}(r',r) - E\mathcal{N}^{J^\pi T}_{\nu'\nu}(r',r)\right]\frac{\gamma^{J^\pi T}_{\nu\nu_i}(r)}{r} = 0 \ , \tag{6.45}$$

where $\mathcal{H}$ and $\mathcal{N}$are the integration kernels of the Hamiltonian and norm respectively. They are simply the matrix elements connecting the basis states, i.e.

$$\mathcal{H}_{\nu'\nu}(r',r) = \left\langle\Phi_{\nu' r'}\right|\mathcal{A}_{\nu'}H\mathcal{A}_\nu\left|\Phi_{\nu r}\right\rangle \ , \tag{6.46}$$

$$\mathcal{N}_{\nu'\nu}(r',r) = \left\langle\Phi_{\nu' r'}\right|\mathcal{A}_{\nu'}\mathcal{A}_\nu\left|\Phi_{\nu r}\right\rangle \ . \tag{6.47}$$

In practice, the kernels are calculated by discretizing the cluster states as an expansion over harmonic oscillator states, i.e.

$$|\Phi_{\nu r}\rangle = \sum_{n=0}^{N_{rel}} R_{n\ell}(r)\,|\Phi_{\nu n}\rangle \ , \tag{6.48}$$

where

$$|\Phi_{\nu n}\rangle = \left[(|A_1\lambda_1 I_1^{\pi_1} T_1\rangle\,|A_2\lambda_2 I_2^{\pi_2} T_2\rangle)^{(sT)}\,Y_\ell(\theta_{r_\nu},\phi_{r_\nu})\right]^{(J^\pi T)} R_{n\ell}(r_\nu) \ , \tag{6.49}$$

and the number of harmonic oscillator excitations N_{rel} used is comparable to the parameter N_{max} of the internal NCSM states [111].

The Hamiltonian can be factorized into intrinsic parts H_1, H_2 acting on the A_1, A_2 clusters separately plus part which depends only on the relative coordinate, i.e.

$$H = H_{\rm rel}(r) + H_1 + H_2 \ , \tag{6.50}$$

where

$$H_{\rm rel}(r) = T_{\rm rel}(r) + \bar{V}_C(r) + V_{loc} \ , \tag{6.51}$$

$T_{\rm rel}(r)$ is the relative kinetic energy between the clusters, $\bar{V}_C(r) = \frac{e^2 Z_{1\nu} Z_{2\nu}}{r}$ is the average Coulomb potential ($Z_{1\nu}$ and $Z_{2\nu}$ are the charge numbers of the clusters of channel ν). $V_{\rm loc}$ is the short-range part of inter-cluster potential, i.e. the nuclear interaction summing the over the nucleon pairs ij with i in 1 and j in 2 and triplets ijk with ij in 1 and k in 2 (and i in 1 and jk in 2). The long-range Coulomb term is subtracted i.e. $V_{loc} = V_{NN+3N} - \bar{V}_C$.

Despite the similarity, the $\gamma_{\nu\nu_i}$ amplitudes do not represent a wavefunction. However, we can define the function $\chi_{\nu\nu_i}(r)$ which is [113], i.e.

$$\frac{\chi_{\nu\nu_i}(r)}{r} = \sum_{\nu'} \int {\rm d}r' r'^2 \mathcal{N}^{\frac{1}{2}}_{\nu\nu'}(r,r') \frac{\gamma_{\nu'\nu_i}(r')}{r'} \ . \tag{6.52}$$

It solves a Schrodinger equation analogous to (6.37):

$$\begin{aligned} &\frac{1}{2\mu_\nu}\left\{-\frac{1}{r^2}\frac{\rm d}{{\rm d}r}\left(r^2\frac{\rm d}{{\rm d}r}\right) + \frac{\ell(\ell+1)}{r^2} + V_C(r)\right\}\frac{\chi_{\nu\nu_i}(r)}{r} \\ &+ \sum_{\nu'}\int {\rm d}r' r'^2 W_{\nu\nu'}(r,r')\frac{\chi_{\nu'\nu_i}(r')}{r'} = (E - E_\nu)\,\frac{\chi_{\nu\nu_i}(r)}{r} \ , \end{aligned} \tag{6.53}$$

where μ_ν is the reduced mass in channel ν and $E_\nu = E_{\lambda_1} + E_{\lambda_2}$ is the threshold at which channels containing $|\lambda_1\rangle\,|\lambda_2\rangle$ become open.

When scattering is possible (at energies $E > E_\nu$), the asymptotic form of χ (in the

region where $W = 0$) should be the same as (6.36) i.e.

$$\chi^{(ext)}_{\nu\nu_i}(r) = \frac{i}{2\sqrt{v_\nu}} \left[\delta_{\nu\nu_i} I_\ell(\eta_\nu, kr) + S_{\nu\nu_i} O_\ell(\eta_\nu, kr)\right] \ . \tag{6.54}$$

When $E < E_\nu$, the radial Schrodinger equation has the asymptotic solutions which are the Whittaker functions $W_\ell(\eta_\nu, kr)$, i.e.

$$\chi^{(ext)}_{\nu}(r) = C_\nu W_\ell(\eta_\nu, kr) \ , \tag{6.55}$$

with C_ν the asymptotic normalization constant. A discrete set of these solutions exist giving bound states of the A-nucleon system. Note the lack of second index ν_i, as it applies only to the scattering states.

The solutions are found by an R-matrix method, analogous to that mentioned in Section 6.1.2. The internal wavefunction is discretized by expansion over a convenient basis, in particular a Lagrange mesh [114]. Then the matching conditions are implemented with the introduction of a Bloch operator $\mathcal{L}_\nu$ into the Schrodinger equation:

$$\begin{aligned} \frac{1}{2\mu_\nu} \left\{ -\frac{1}{r^2}\frac{\mathrm{d}}{\mathrm{d}r}\left(r^2 \frac{\mathrm{d}}{\mathrm{d}r}\right) + \frac{\ell(\ell+1)}{r^2} + V_C(r) - (E - E_\nu) \right\} \frac{\chi^{(int)}_{\nu\nu_i}(r)}{r} \\ + \sum_{\nu'} \int \mathrm{d}r' r'^2 W_{\nu\nu'}(r, r') \frac{\chi^{(int)}_{\nu'\nu_i}(r')}{r'} + \mathcal{L}_\nu \frac{\chi^{(int)}_{\nu\nu_i}(r)}{r} = \mathcal{L}_\nu \frac{\chi^{(ext)}_{\nu\nu_i}(r)}{r} \ , \end{aligned} \tag{6.56}$$

where, with matching radius a,

$$\mathcal{L}_\nu = \frac{1}{2\mu_\nu} \delta(r - a) \left(\frac{\mathrm{d}}{\mathrm{d}r} - \frac{B_\nu}{r}\right) \ , \tag{6.57}$$

and B_ν is an arbitrary parameter, tuned depending whether a scattering or bound solution is sought. See [115] for details.

6.2 The No-Core Shell Model with Continuum

6.2.1 A Unified Basis

A generalized cluster expansion can be used to describe both bound states and scattering states of an A-nucleon system on an equal footing.

We write a new ansatz which is a superposition of discrete energy eigenstates of the A-nucleon system and continuous cluster states of A_1-, A_2-nucleon states, i.e.

$$\left|\Psi^{J^\pi T}_{A\nu_i}\right\rangle = \sum_\lambda c^{J^\pi T}_{\lambda\nu_i} \left|A\lambda J^\pi T\right\rangle + \sum_\nu \int \mathrm{d}r r^2 \frac{\gamma^{J^\pi T}_{\nu\nu_i}(r)}{r} \mathcal{A}_\nu \left|\Phi^{J^\pi T}_{\nu r}\right\rangle \ . \tag{6.58}$$

The combined wavefunction contains the NCSM eigenstates of the full A-nucleon system in the first term. The second term is the RGM wavefunction described in Section 6.1.4. Multiple NCSM calculations are needed to construct this basis and often fewer than the number of all possible NCSM eigenstates are included, but generally only the subset corresponding to the energy region of interest are needed. Finding the unknown coefficients $c^{J^\pi T}_{\lambda\nu_i}$ and amplitudes $\gamma^{J^\pi T}_{\nu\nu_i}(r)$ then allows us to construct realistic wavefunctions which can be used to predict observable properties of the nuclear system.

6.2.2 Solving the NCSMC

Schematically, the Schrodinger equation in the NCSMC looks like

$$\begin{pmatrix} H & h \\ h & \mathcal{H} \end{pmatrix} \begin{pmatrix} c \\ \gamma \end{pmatrix} = E \begin{pmatrix} I & g \\ g & \mathcal{N} \end{pmatrix} \begin{pmatrix} c \\ \gamma \end{pmatrix} . \tag{6.59}$$

Making the conversion $\gamma \to \chi$ via (6.52) (known as orthogonalization) this becomes:

$$\begin{pmatrix} \mathcal{E} & \bar{h} \\ \bar{h} & \bar{\mathcal{H}} \end{pmatrix} \begin{pmatrix} c \\ \chi \end{pmatrix} = E \begin{pmatrix} \delta & \bar{g} \\ \bar{g} & \Delta \end{pmatrix} \begin{pmatrix} c \\ \chi \end{pmatrix} . \tag{6.60}$$

As the NCSM states are already eigenstates the upper left of the left-hand side is $\mathcal{E}_{\lambda\lambda'} = E_\lambda \delta_{\lambda\lambda'}$ while the upper left of the right hand side is $\delta_{\lambda\lambda'}$. The diagonal norm kernel with the orthogonalized cluster states is $\Delta_{\nu\nu'}(r,r') = \delta_{\nu\nu'}\frac{\delta(r-r')}{rr'}$.

The Hamiltonian kernel in the orthogonal basis is

$$\bar{\mathcal{H}}_{\nu\nu'}(r,r') = \sum_{\mu\mu'} \int\int \mathrm{d}y \mathrm{d}y' y^2 y'^2 \mathcal{N}^{-\frac{1}{2}}_{\nu\mu}(r,y) \mathcal{H}_{\mu\mu'}(y,y') \mathcal{N}^{-\frac{1}{2}}_{\mu'\nu'}(y',r') . \tag{6.61}$$

The remaining off-diagonal blocks are the coupling-kernels:

$$\bar{g}_{\lambda\nu}(r) = \sum_{\nu'} \int \mathrm{d}r' r'^2 \left\langle A\lambda \right| \mathcal{A} \left| \phi_{\nu' r'} \right\rangle \mathcal{N}^{-\frac{1}{2}}_{\nu'\nu}(r',r) , \tag{6.62}$$

known as the cluster form factor, and

$$\bar{h}_{\lambda\nu}(r) = \sum_{\nu'} \int \mathrm{d}r' r'^2 \left\langle A\lambda \right| H\mathcal{A} \left| \phi_{\nu' r'} \right\rangle \mathcal{N}^{-\frac{1}{2}}_{\nu'\nu}(r',r) , \tag{6.63}$$

the coupling form factor.

Just as in the RGM we can use an R-matrix method. The addition of the A-nucleon NCSM states adds additional terms to the discretized RGM equations and upgrades the Bloch operator $\mathcal{L}$ to a matrix of zeros with the RGM $\mathcal{L}$ in the lower right [111]. We are left

with a diagonalization problem:

$$\left(\bar{H}+\mathcal{L}\right)\begin{pmatrix}\bar{c}\\ \bar{\chi}\end{pmatrix}=E\begin{pmatrix}\bar{c}\\ \bar{\chi}\end{pmatrix}\,, \tag{6.64}$$

with $\bar{H}=N^{-\frac{1}{2}}\begin{pmatrix}\mathcal{E} & \bar{h}\\ \bar{h} & \bar{\mathcal{H}}\end{pmatrix}N^{-\frac{1}{2}}$, $\begin{pmatrix}\bar{c}\\ \bar{\chi}\end{pmatrix}=N^{+\frac{1}{2}}\begin{pmatrix}c\\ \chi\end{pmatrix}$, $N=\begin{pmatrix}\delta & \bar{g}\\ \bar{g} & \Delta\end{pmatrix}$.

6.2.3 Transition Matrix Elements

The transition matrix elements of operators connecting NCSMC states will be a sum of the internal transitions (operators acting on each cluster) and the operator acting on the relative motion. Similarly to (6.50), operators can be separated into parts:

$$O=O^{(1)}+O^{(2)}+O^{(\mathrm{rel})}(r_\nu)\,, \tag{6.65}$$

which act on the projectile, target and relative motion respectively.

For electromagnetic operators of rank K, the component of the operator acting on the relative motion $O_K^{(\mathrm{rel})}$ will depend on the effective charge $q^\sigma_{\nu K}$. This is because the coordinates of the protons in the clusters differs a little from the center of mass of the clusters. In the first cluster $r_{p\in Z_1}=\frac{-A_2}{A}r_\nu$ and the second $r_{p\in Z_2}=\frac{A_1}{A}r_\nu$ [116]. For example:

$$q^\sigma_{\nu K}=\begin{cases}Z_{1\nu}\left(\frac{A_2}{A}\right)^K+Z_{2\nu}\left(-\frac{A_1}{A}\right)^K & \text{if } \sigma=E(\text{exact for } K=1)\,,\\ \frac{1}{A}\left(Z_{1\nu}\left(\frac{A_2}{A_1}\right)+Z_{2\nu}\left(\frac{A_1}{A_2}\right)\right) & \text{if } \sigma=M(K=1)\,.\end{cases} \tag{6.66}$$

The electric and magnetic multipole operators are then

$$M^\sigma_K=\begin{cases}M_K^{E(1)}+M_K^{E(2)}+q^E_{\nu K}er_\nu^K Y_K(\Omega_{r_\nu}) & \text{if } \sigma=E(\text{exact for } K=1)\,,\\ M_K^{M(1)}+M_K^{M(2)}+q^M_{\nu K}\mu_N\sqrt{\frac{3}{4\pi}}L_{r_\nu} & \text{if } \sigma=M(K=1)\,.\end{cases} \tag{6.67}$$

After we solve the NCSMC for the coefficients c_λ and γ_ν, we then assemble the transition

matrix elements by inserting the expansions on each side, i.e.

$$\begin{aligned}\left\langle \psi_{fA}^{J_f\pi_f T_f} \right| |O_K| \left| \psi_{iA}^{J_i\pi_i T_i} \right\rangle = &\sum_{\lambda_i\lambda_f} c^*_{\lambda_f} c_{\lambda_i} \left\langle A\lambda_f J_f\pi_f T_f \right| |O_K| \left| A\lambda_i J_i\pi_i T_i \right\rangle \\ &+ \sum_{\lambda_f\nu} c^*_{\lambda_f} \int \mathrm{d}r r^2 \left\langle A\lambda_f J_f\pi_f T_f \right| |O_K \mathcal{A}_\nu| \left| \phi_{\nu r}^{J_i\pi_i T_i} \right\rangle \frac{\gamma_{\nu\nu_i}(r)}{r} \\ &+ \sum_{\lambda_i\nu'} c_{\lambda_i} \int \mathrm{d}r r^2 \frac{\gamma_{\nu'\nu_f}(r)}{r} \left\langle \phi_{\nu' r}^{J_f\pi_f T_f} \right| |\mathcal{A}_{\nu'} O_K| \left| A\lambda_i J_i\pi_i T_i \right\rangle \\ &+ \sum_{\nu\nu'} \int \mathrm{d}r r^2 \int \mathrm{d}r' r'^2 \frac{\gamma_{\nu'\nu_f}(r)}{r} \left\langle \phi_{\nu' r}^{J_f\pi_f T_f} \right| |\mathcal{A}_{\nu'} O_K \mathcal{A}_\nu| \left| \phi_{\nu r'}^{J_i\pi_i T_i} \right\rangle \frac{\gamma_{\nu\nu_i}(r')}{r'} \,. \end{aligned} \tag{6.68}$$

The first term is simply the NCSM matrix elements of the full operator. For the other terms we insert the operator components. Evaluations of $O^{(i)}$ will require insertions of completeness over the internal states $\sum_j |A_i\lambda_j\rangle \langle A_i\lambda_j|$, resulting in a combination of the internal matrix elements and the coupling kernels. The last term is expressed in terms of the norm kernels.

6.3 Radiative Capture

Radiative capture is a type of fusion nuclear reaction in which two nucleons collide and form a larger bound nucleus and the extra energy is released through a photon. "Radiative" since radiation is emitted and "capture" because the projectile is captured by the target nucleus. Figure 6.2 shows this process diagrammatically.

When interactions between particles are weak then again Fermi's Golden Rule can be applied. For example, when there are two particles in the initial state with 4-momenta $P_1 = (E_1, \vec{p}_1)$ and $P_2 = (E_2, \vec{p}_2)$ the cross section is [11]:

$$\sigma = \frac{S}{v} \frac{1}{2E_1 2E_2} \bar{\sum_i} \sum_f \int |\mathcal{M}|^2 \prod_{F=1}^{N} \frac{\mathrm{d}^3 p_F}{(2\pi)^3 2E_F} \,. \tag{6.69}$$

The amplitude $\mathcal{M}$ contains the transition matrix element for the interaction that induces a transition between the initial and final states. An addition to (3.1), is the incoming relative velocity v:

$$v = \frac{\sqrt{P_1^2 P_2^2 - m_1^2 m_2^2}}{E_1 E_2} \,. \tag{6.70}$$

In a radiative capture reaction $T(P,\gamma)F$, we calculate the cross section for a $2 \to 2$

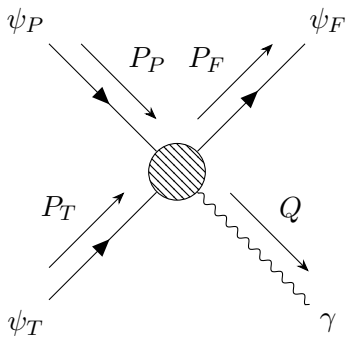

Figure 6.2: The Feynman diagram and kinematics for radiative capture.

process, i.e.

$$\mathrm{d}\sigma = \frac{1}{v}\frac{1}{4E_P E_T}\bar{\sum_i}\sum_f\sum_\lambda \left|\mathcal{M}_{FI}^{\lambda Q}\right|^2 \frac{\mathrm{d}^3 q}{(2\pi)^3 2\omega}\frac{\mathrm{d}^3 p_F}{(2\pi)^3 2E_F} \ . \tag{6.71}$$

The amplitude is very similar to (3.3), but the initial state is two clusters: the target T and projectile P. The average over initial states is an average over the angular momenta of both clusters (target $|s_T m_T\rangle$ and projectile $|s_P m_P\rangle$), i.e. $\bar{\sum_i} = \frac{1}{\hat{s}_P^2 \hat{s}_T^2}\sum_{m_P m_T}$. The sum over final states $|J_f M_f\rangle$ is $\sum_f = \sum_{M_f}$.

Similarly to (3.12), the amplitude is

$$\mathcal{M}_{FI}^{\lambda Q} = (2\pi)^4 \delta(P_P + P_T - P_F - Q)\,\langle f|\,\vec{e}_\lambda^{\,*}\cdot\vec{\mathcal{J}}(q)\,|i\rangle\, 8E_F E_P E_T \ . \tag{6.72}$$

Cancelling the $2E$ factors and doing the final state integral, the cross section is then

$$\mathrm{d}\sigma = \frac{e^2}{v}\frac{\mathrm{d}^3 q}{(2\pi)^3 2\omega} 2\pi\delta(E_F - E_I - \omega)\bar{\sum_i}\sum_f\sum_\lambda \left|H_\lambda^{fi}\right|^2 \ , \tag{6.73}$$

where

$$H_\lambda^{fi} = \langle f|\,\vec{e}_\lambda^{\,*}\cdot\vec{\mathcal{J}}(\vec{q})\,|i\rangle \ . \tag{6.74}$$

Implicit in the definition of the multipole operators is that the λ polarizations are transverse to $\vec{q}$, the direction of the photon. However the projection of the spherical tensor operator should be defined in the same coordinates as the quantum states it acts on. In a reaction, we define the angular momentum projection of the nuclear states with respect to the relative velocity (i.e. the direction of the beam). This requires us to rotate the operators (or states) using the Wigner D-matrices (Section A.3).

In principle, if the initial bound state in γ decay were polarized with respect to some axis, the differential decay rate would require a rotation of the operator to change basis

from the axes set by measurement of the photon to the axes set by the polarization [54].

The set of coordinates defined relative to $\hat{z}$ along the beam is the "$\hat{v}$-frame", the set of coordinates defined relative to $\hat{z}$ along the photon is the "$\hat{q}$-frame". In our case, the direction of the photon is described by the polar coordinates (θ_q, ϕ_q) in the $\hat{v}$-frame. The corresponding rotation $\hat{v} \to \hat{q}$ is $\mathcal{R}(\phi_q, \theta_q, -\phi_q)$ [117]. The state $|i\rangle$ in the $\hat{q}$-frame is $|i\rangle_q = \mathcal{R}(\phi_q, \theta_q, -\phi_q)\,|i\rangle_v$, related by a rotation operator to the state $|i\rangle$ in the $\hat{v}$-frame. The matrix element is expanded over multipole operators via (3.39) in the $\hat{q}$-frame. In order to use states in the $\hat{v}$-frame we apply the rotation operators. Using (A.19) and (A.29) the result contains the D-matrices, i.e.

$$\begin{aligned}
\langle f|_q\, \vec{e}^*_\lambda \cdot \vec{\mathcal{J}}(q)\,|i\rangle_q &= \langle f|_v\, \mathcal{R}^\dagger(\phi_q, \theta_q, -\phi_q) \vec{e}^*_\lambda \cdot \vec{\mathcal{J}}^\dagger(q) \mathcal{R}(\phi, \theta, -\phi)\,|i\rangle_v \\
&= \langle f|_v\, \mathcal{R}^\dagger(\phi_q, \theta_q, -\phi_q) \sum_{jm} (-i)^j \sqrt{2\pi}\hat{j}\left[\mathcal{T}^E_{j-\lambda}(q) + \lambda \mathcal{T}^M_{j-\lambda}(q)\right] \mathcal{R}(\phi, \theta, -\phi)\,|i\rangle_v \\
&= \langle f|_v\, \mathcal{R}(-\phi_q, -\theta_q, \phi_q) \sum_{jm} (-i)^j \sqrt{2\pi}\hat{j}\left[\mathcal{T}^E_{j-\lambda}(q) + \lambda \mathcal{T}^M_{j-\lambda}(q)\right] \mathcal{R}^\dagger(-\phi, -\theta, \phi)\,|i\rangle_v \\
&= \langle f|_v \sum_{jm} (-i)^j \sqrt{2\pi}\hat{j}\left[\mathcal{T}^E_{jm}(q) + \lambda \mathcal{T}^M_{jm}(q)\right] D^j_{m-\lambda}(-\phi_q, -\theta_q, \phi_q)\,|i\rangle_v \ .
\end{aligned} \tag{6.75}$$

In the following manipulations we use $|i\rangle = |i\rangle_v$ and so we insert into (6.74) the operator:

$$\vec{e}^*_\lambda \cdot \vec{\mathcal{J}}(q) = \sum_{jm} (-i)^j \sqrt{2\pi}\hat{j}\left[\mathcal{T}^E_{jm}(q) + \lambda \mathcal{T}^M_{jm}(q)\right] D^j_{m-\lambda}(-\phi_q, -\theta_q, \phi_q) \ . \tag{6.76}$$

The initial state can be expanded over a coupled basis, i.e. we combine (6.39) and (6.43):

$$|\nu_i m_P m_T\rangle = \frac{\sqrt{4\pi}}{k_{\nu_i}} \sum_{JLS} \hat{L} e^{i\sigma_L} (s_P m_P s_T m_T | SM)\,(L0SM|JM)\,|\nu_i LSJM\rangle \ . \tag{6.77}$$

$|\nu_i LSJM\rangle$ represent scattering states in a coupled basis (e.g. NCSMC states $\left|\psi^{J^\pi M}_{A\nu_i}\right\rangle$) where here ν_i describes the mass partition and internal states.

The sum in (6.73) can be expanded

$$\begin{aligned}
\bar{\sum_i} \sum_f \sum_\lambda \left|H^{fi}_\lambda\right|^2 = &\frac{1}{\hat{s}^2_P \hat{s}^2_T} \sum_{m_P m_T} \sum_{M_f} \sum_\lambda \left(\langle J_f M_f | \sum_{\sigma jm} D^j_{m-\lambda} \left[\sqrt{2\pi}\hat{j}\lambda^\sigma (-i)^j \mathcal{T}^\sigma_{jm}\right] |s_P m_P s_T m_T\rangle \right) \\
&\times \left(\langle J_f M_f | \sum_{\sigma' j' m'} D^{j'}_{m'-\lambda} \left[\sqrt{2\pi}\hat{j}'\lambda^\sigma (-i)^{j'} \mathcal{T}^{\sigma'}_{j'm'}\right] |s_P m_P s_T m_T\rangle \right)^* \ ,
\end{aligned} \tag{6.78}$$

where $\sigma = (0, 1)$ corresponding to (E,M) respectively and the ν_i labels and θ_q, ϕ_q are

suppressed.

First, we substitute (6.77) ($|s_P m_P s_T m_T\rangle = |\nu_i m_P m_T\rangle$), using the replacement: $X^{\sigma}_{jm} = \frac{\sqrt{4\pi}}{k}\sqrt{2\pi}\hat{j}\lambda^{\sigma}(-i)^j \mathcal{T}^{\sigma}_{jm}$, i.e.

$$\begin{aligned}\hat{s}_P^2\hat{s}_T^2\bar{\sum_i}\sum_f\sum_\lambda\left|H^{fi}_\lambda\right|^2 = &\sum_{m_P m_T}\sum_{M_f}\sum_\lambda\Bigg\{\langle J_f M_f|\sum_{\sigma jm} D^j_{m-\lambda}X^\sigma_{jm}\\ &\times\sum_{LSJ}\hat{L}e^{i\sigma_L}\left(s_P m_P s_T m_T|SM\right)\left(L0SM|JM\right)|LSJM\rangle\Bigg\}\\ &\times\Bigg\{\langle J_f M_f|\sum_{\sigma' j' m'} D^{j'}_{m'+\lambda}X^{\sigma'}_{j'm'}\\ &\times\sum_{L'S'J'}\hat{L}'e^{i\sigma_{L'}}\left(s_P m_P s_T m_T|S'M\right)\left(L'0S'M'|J'M'\right)\left|L'S'J'M'\right\rangle\Bigg\}^*.\end{aligned} \tag{6.79}$$

We make use of the sum over m_P, m_T (A.4):

$$\sum_{m_P m_T}\left(s_P m_P s_T m_T|SM\right)\left(s_P m_P s_T m_T|S'M\right) = \delta_{SS'}\sum_M, \tag{6.80}$$

and the Wigner-Eckart theorem (2.33):

$$\langle J_f M_f|\,X^\sigma_{jm}\,|LSJM\rangle = \hat{J}_f^{-1}\left(JMjm|J_f M_f\right)\langle J_f|\left|X^\sigma_j\right||LSJ\rangle\ . \tag{6.81}$$

Defining $X^{\sigma j}_{J_f LSJ} = \langle J_f|\left|X^\sigma_j\right||LSJ\rangle$ and making use of (A.31) with $m = m'$, we have

$$\begin{aligned}\hat{s}_P^2\hat{s}_T^2\bar{\sum_i}\sum_f\sum_\lambda\left|H^{fi}_\lambda\right|^2 = &\hat{J}_f^{-2}\sum_{M_f}\sum_\lambda\sum_{\sigma jm}\sum_{LSJM}\sum_{\sigma' j'}\sum_{L'J'}\hat{L}\hat{L}'e^{i(\sigma_L-\sigma_{L'})}\\ &\times X^{\sigma j}_{J_f LSJ}X^{\sigma' j'*}_{J_f L'SJ'}\sum_K(-)^{m+\lambda}\left(jmj'-m|K0\right)\left(j-\lambda j'\lambda|K0\right)D^K_{00}\\ &\times\left(L0SM|JM\right)\left(L'0SM|J'M\right)\left(JMjm|J_f M_f\right)\left(J'Mj'm|J_f M_f\right)\ .\end{aligned} \tag{6.82}$$

We identify $D^K_{00}(-\phi,-\theta,\phi)$ as the Legendre polynomial $P_K(\cos\theta_q)$. The sums over m and M produce $6j$s by making use of (A.7) and (A.12) repeatedly, i.e.

$$\begin{aligned}&\sum_M\sum_m(-)^m\left(jmj'-m|K0\right)\left(L0SM|JM\right)\left(L'0SM|J'M\right)\left(JMjm|J_f M_f\right)\left(J'Mj'm|J_f M_f\right)\\ &=(-)^{S-J_f}\,\hat{J}_f^2\hat{J}\hat{J}'\begin{Bmatrix}J & J' & K\\ j' & j & J_f\end{Bmatrix}\begin{Bmatrix}J & J' & K\\ L' & L & S\end{Bmatrix}\left(L0L'0|K0\right)\ .\end{aligned} \tag{6.83}$$

The remaining sum over projections is $\sum_{M_f} = \hat{J}_f^2$. And so converting X back to T and

using the shorthand $T^{\sigma j}_{J_f LSJ} = \langle J_f | \left| \mathcal{T}^\sigma_j \right| | LSJ \rangle$, we have

$$\begin{aligned}
\hat{s}_P^2 \hat{s}_T^2 \bar{\sum_i} \sum_f \sum_\lambda \left| H^{fi}_\lambda \right|^2 =& \hat{J}_f^2 \sum_\lambda \sum_{\sigma j} \sum_{LSJ} \sum_{\sigma' j'} \sum_{L' J'} \hat{L}\hat{L}' e^{i(\sigma_L - \sigma_{L'})} X^{\sigma j}_{J_f LSJ} X^{\sigma' j' *}_{J_f L' S J'} \\
& \times \sum_K P_K \, (-)^{S - J_f + \lambda} \, \hat{J}\hat{J}' \left\{ \begin{array}{ccc} J & J' & K \\ j' & j & J_f \end{array} \right\} \left\{ \begin{array}{ccc} J & J' & K \\ L' & L & S \end{array} \right\} \\
& \times \left(L 0 L' 0 | K 0 \right) \left(j - \lambda j' \lambda | K 0 \right) \\
=& \frac{8\pi^2}{k^2} \hat{J}_f^2 \sum_{\sigma j \sigma' j'} \sum_{S L L' J J' J} \left(\sum_\lambda (-)^\lambda \left(j - \lambda j' \lambda | K 0 \right) \lambda^{\sigma + \sigma'} \right) \\
& \times (-i)^{j - j'} \hat{L}\hat{L}' e^{i(\sigma_L - \sigma_{L'})} T^{\sigma j}_{J_f LSJ} T^{\sigma' j' *}_{J_f L' S J'} \sum_K P_K \\
& \times (-)^{S - J_f} \, \hat{j}\hat{j}' \hat{J}\hat{J}' \left\{ \begin{array}{ccc} J & J' & K \\ j' & j & J_f \end{array} \right\} \left\{ \begin{array}{ccc} J & J' & K \\ L' & L & S \end{array} \right\} \left(L 0 L' 0 | K 0 \right) \, .
\end{aligned} \tag{6.84}$$

This can be simplified, similarly to (3.54), with:

$$\begin{aligned}
\sum_\lambda \lambda^{\sigma + \sigma'} (-)^\lambda \left(j - \lambda j' \lambda | K 0 \right) =& (-)^1 \left(j - 1 j' 1 | K 0 \right) + (-)^{\sigma + \sigma' - 1} \left(j 1 j' - 1 | K 0 \right) \\
=& - \left[1 + (-)^{\sigma + \sigma' + j + j' - K} \right] \left(j - 1 j' 1 | K 0 \right) \\
=& \left(j - 1 j' 1 | K 0 \right) \begin{cases} -2 & \text{if } (-)^{\sigma + \sigma' + j + j'} = (-)^K \, , \\ 0 & \text{otherwise} \, . \end{cases}
\end{aligned} \tag{6.85}$$

The result is

$$\begin{aligned}
\hat{s}_P^2 \hat{s}_T^2 \bar{\sum_i} \sum_f \sum_\lambda \left| H^{fi}_\lambda \right|^2 =& \frac{16\pi^2}{k^2} \hat{J}_f^2 \sum_K P_K \sum_{\sigma \sigma' j j'}{}' \sum_{S L L' J J'} (-)^{S - J_f + 1} \, \hat{j}\hat{j}' \hat{J}\hat{J}' \hat{L}\hat{L}' e^{i(\sigma_L - \sigma_{L'})} \\
& \times (-i)^{j - j'} T^{\sigma j}_{J_f LSJ} T^{\sigma' j' *}_{J_f L' S J'} \left\{ \begin{array}{ccc} J & J' & K \\ j' & j & J_f \end{array} \right\} \left\{ \begin{array}{ccc} J & J' & K \\ L' & L & S \end{array} \right\} \\
& \times \left(L 0 L' 0 | K 0 \right) \left(j - 1 j' 1 | K 0 \right) \, ,
\end{aligned} \tag{6.86}$$

where $\sum'_{\sigma \sigma' j j'}$ has the condition $(-)^{\sigma + \sigma' + j + j'} = (-)^K$.

The angular momentum algebra can be collected into a coefficient:

$$\begin{aligned}
a_K = & \sum_{\sigma \sigma' j j}{}' \sum_{S L L' J J'} (-)^{S - J_f + 1} \, \hat{j}\hat{j}' \hat{J}\hat{J}' \hat{L}\hat{L}' e^{i(\sigma_L - \sigma_{L'})} (-i)^{j - j'} T^{\sigma j}_{J_f LSJ} T^{\sigma' j' *}_{J_f L' S J'} \\
& \times \left\{ \begin{array}{ccc} J & J' & K \\ j' & j & J_f \end{array} \right\} \left\{ \begin{array}{ccc} J & J' & K \\ L' & L & S \end{array} \right\} \left(L 0 L' 0 | K 0 \right) \left(j 1 j' - 1 | K 0 \right) \, .
\end{aligned} \tag{6.87}$$

Inserting everything into (6.73), where v has been absorbed into the normalization of the scattering wavefunctions, we first integrate over ϕ_q to get a factor of 2π and the move $\mathrm{d}\cos\theta_q$ to the left-hand side to get the differential cross section

$$\begin{aligned}\frac{\mathrm{d}\sigma}{\mathrm{d}\cos\theta_q} =& 4\pi\alpha\frac{2\pi\omega^2\mathrm{d}\omega}{(2\pi)^3 2\omega}2\pi\delta(E_I - E_F - \omega)\bar{\sum_i}\sum_f\sum_\lambda\left|H_\lambda^{fi}\right|^2 \\ =& \alpha\omega f_r\frac{\hat{J}_f^2}{\hat{s}_P^2\hat{s}_T^2}\frac{16\pi^2}{k^2}\sum_K a_K P_K(\cos\theta_q)\ , \end{aligned} \tag{6.88}$$

where $f_r = (1 + \frac{\omega - p_P\cos\theta_q}{M_F})^{-1}$ is the recoil factor, with p_P the projectile momentum and M_F is the mass of the final state bound nucleus. All the $P_K(\cos\theta_q)$ with $K \neq 0$ integrate to 0 (neglecting recoil).

The integrated cross section is then

$$\sigma = \frac{32\pi^2\alpha\omega}{k^2}\frac{\hat{J}_f^2}{\hat{s}_P^2\hat{s}_T^2}a_0\ , \tag{6.89}$$

where

$$\begin{aligned} a_0 =& \sum_{\sigma\sigma' jj}{}' \sum_{SLL'JJ'}(-)^{S-J_f+1}\hat{j}\hat{j}'\hat{J}\hat{J}'\hat{L}\hat{L}'e^{i(\sigma_L-\sigma_{L'})}T^{\sigma j}_{J_f LSJ}T^{\sigma' j'*}_{J_f L'SJ'} \\ & \times\begin{Bmatrix} J & J' & 0 \\ j' & j & J_f\end{Bmatrix}\begin{Bmatrix} J & J' & 0 \\ L' & L & S\end{Bmatrix}(L0L'0|00)\left(j1j'-1|00\right) \\ =& \sum_{\sigma j}\sum_{SLJ}\left|T^{\sigma j}_{J_f LSJ}\right|^2\ . \end{aligned} \tag{6.90}$$

This leaves us with the same result as the γ-decay rate (3.55) but with a sum over initial LSJ channels rather than just J_i and the additional normalization factor $\frac{4\pi}{vk^2}$.

In the long-wavelength limit this becomes

$$\sigma = \frac{32\pi^2\alpha}{k^2}\frac{J_f^2}{\hat{s}_P^2\hat{s}_T^2}\sum_{\sigma j}\frac{\omega^{2j+1}}{[(2j+1)!!]^2}\frac{j+1}{j}\sum_{L_iS_iJ_i}\left|\left\langle\Psi^{J_f\pi_fT_f}\right|\left|M_j^\sigma\right|\left|\Psi^{J_i\pi_iT_i}_{S_iL_i}\right\rangle\right|^2\ , \tag{6.91}$$

matching the literature up to normalization conventions [107, 108].

6.4 Pair Production

If the photon emitted in a γ-decay or radiative capture has high enough energy ($\omega > 2m_e$) then an electron-positron pair may be produced. Diagrammatically this is shown in Figure 6.3 and Figure 6.4. The rate is much lower than photon decays (except in $0^+ \to 0^+$ transitions where γ decays are forbidden [118, 119]) but recent experiments have been able to measure the rate, in particular in radiative capture reactions [120] where additional energy

is provided by the initial kinetic energy. The relevant nuclear operators and kinematics are analogous to electron scattering [56, 121] but with the complication of a larger final phase space.

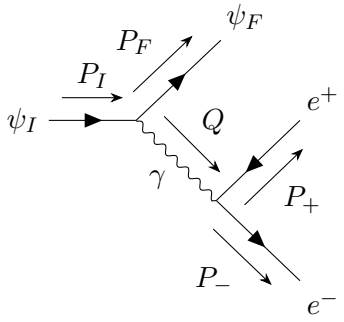

Figure 6.3: The Feynman diagram for the pair production process.

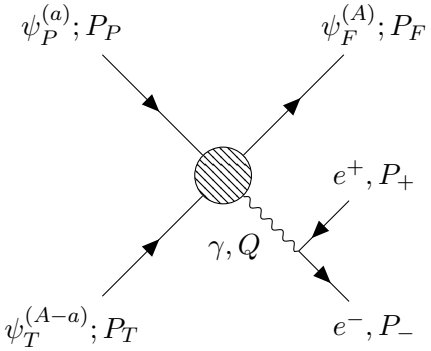

Figure 6.4: The Feynman diagram and kinematics for radiative capture with pair production.

6.4.1 Pair Production in Bound-Bound Decay

This process is simpler to calculate in a bound-bound transition, just as γ-decay (Section 3.1) is simpler than radiative capture (Section 6.3).

We need to calculate the decay rate of a $1 \to 3$ process, i.e.

$$\mathrm{d}\Gamma = \frac{1}{2M_I} \bar{\sum_i} \sum_f \sum_{s_+ s_-} \left| \mathcal{M}_{FI}^{s_+ s_-} \right|^2 \frac{\mathrm{d}^3 p_+}{(2\pi)^3 2E_+} \frac{\mathrm{d}^3 p_-}{(2\pi)^3 2E_-} \frac{\mathrm{d}^3 p_F}{(2\pi)^3 2E_F} \,, \tag{6.92}$$

where $P_+ = (E_+, \vec{p}_+)$ and $P_- = (E_-, \vec{p}_-)$ are respectfully the 4-momenta of the emitted positron and electron and $P_F = (E_F, \vec{p}_F)$ is the 4-momentum of the final state nucleus. The intermediate photon has 4-momentum $Q = (\omega, \vec{q})$.

The amplitude of the diagram in Figure 6.3 is evaluated following the Feynman rules

listed in Section 3.1. We insert the Dirac spinors $\bar{u}^{s-}$ for the outgoing electron and ν^{s+} for the outgoing positron, then insert the propagator $\frac{-i\eta_{\mu\nu}}{Q^2}$ for the exchanged photon between the vertex factors $ie\gamma_\mu$ and $ie\mathcal{J}_\nu$ where we use short-hand for the nuclear current $\mathcal{J}_\nu = \langle f|\,\mathcal{J}_\nu(q)\,|i\rangle$. The amplitude is

$$\mathcal{M}_{s_+s_-} = \bar{u}^{s-}(P_-)\,(ie\gamma_\mu)\left(\frac{-i\eta^{\mu\nu}}{Q^2}\right)(ie\mathcal{J}_\nu)\,v^{s+}(P_+)\;. \tag{6.93}$$

We then insert the appropriate delta functions and normalization factors and integrate over the intermediate 4-momentum Q, i.e.

$$\begin{aligned}&\bar{\sum_i}\sum_{s_+s_-}\sum_f\int\frac{\mathrm{d}^4Q}{(2\pi)^4}\left|\mathcal{M}_{s_+s_-}\right|^2(2\pi)^4\delta(P_I-P_F-Q)(2\pi)^4\delta(Q-P_+-P_-)4E_IE_F\\ =&\bar{\sum_i}\sum_{s_+s_-}\sum_f\left|\mathcal{M}_{s_+s_-}\right|^2(2\pi)^4\delta(P_I-P_+-P_--P_F)4M_IE_F\;.\end{aligned} \tag{6.94}$$

After this step, the symbol Q is defined by the external momenta:

$$Q = P_+ + P_-\;, \tag{6.95}$$

$$Q^2 = 2\left(E_-E_+ - p_-p_+x + m^2\right)\;, \tag{6.96}$$

$$q^2 = p_-^2 + p_+^2 + 2p_-p_+x\;. \tag{6.97}$$

To simplify the expressions we define $x = \cos\theta_{ee} = \hat{p}_+\cdot\hat{p}_-$ and $m = m_e$.

The lepton tensor is computed by via the lepton currents, summing over the final spins, i.e.

$$\begin{aligned}\ell_{\mu\nu} =&\sum_{s\bar{s}}\left(\bar{u}_{s_-}(P_-)\gamma_\mu v_{s_+}(P_+)\right)\left(\bar{v}_{s+}(P_+)\gamma_\nu u_{s_-}(P_-)\right)\\ =&\mathrm{Tr}\left[\gamma_\mu\left(\not{P}_- + m\right)\gamma_\nu\left(\not{P}_+ - m\right)\right]\\ =&4\left[P_{-\mu}P_{+\nu} + P_{-\nu}P_{+\mu} - \eta_{\mu\nu}\left(P_-\cdot P_+ + m^2\right)\right]\;.\end{aligned} \tag{6.98}$$

Folding this with the nuclear current, we get

$$\bar{\sum_i}\sum_{s_+s_-}\sum_f\left|\mathcal{M}_{s_+s_-}\right|^2 = \bar{\sum_i}\sum_f\ell^{\mu\nu}\mathcal{J}_\mu^*\mathcal{J}_\nu\;, \tag{6.99}$$

where the lepton tensor and nuclear current contractions result in

$$\begin{aligned}\frac{1}{4}\ell^{\mu\nu}\mathcal{J}_\mu^*\mathcal{J}_\nu =&\left(P_+\cdot\mathcal{J}\right)\left(P_-\cdot\mathcal{J}^*\right) + \left(P_+\cdot\mathcal{J}^*\right)\left(P_-\cdot\mathcal{J}\right) - \left(\mathcal{J}\cdot\mathcal{J}^*\right)\left(P_+\cdot P_- + m^2\right)\\ =&\frac{Q^4}{q^4}\left|\rho\right|^2\left(E_+E_- + \vec{p}_+\cdot\vec{p}_- - m^2\right) + \left|\mathcal{J}^T\right|^2\left(E_+E_- + m^2 - \frac{\left(\vec{p}_+\cdot\vec{q}\right)\left(\vec{p}_-\cdot\vec{q}\right)}{q^2}\right)\;,\end{aligned} \tag{6.100}$$

where ρ is the charge density and $\vec{\mathcal{J}}^T$ is the transverse current:

$$\vec{\mathcal{J}}^T = \sum_{\lambda=\pm 1} \left(\vec{e}^*_\lambda \cdot \vec{\mathcal{J}}\right) \vec{e}_\lambda \ , \tag{6.101}$$

or equivalently

$$\vec{\mathcal{J}}^T = \left(\vec{e}_x \cdot \vec{\mathcal{J}}\right) \vec{e}_x + \left(\vec{e}_y \cdot \vec{\mathcal{J}}\right) \vec{e}_y \ . \tag{6.102}$$

The result (6.100) is not obvious and comes about through several steps.

- It can be shown that we may make the replacement $\mathcal{J} = (\rho, \vec{\mathcal{J}}) \to \left(\frac{-Q^2}{q^2}\rho, \vec{\mathcal{J}}^T\right)$ via similar arguments to Siegert's theorem i.e. longitudinal components may be related to the time-like component [53]. This is shown later in the manipulations simplifying (6.118) into (6.122).

- Defining $\varrho = \frac{-Q^2}{q^2}\rho$, we have the intermediate result:

$$\begin{aligned}
\frac{1}{4}\ell^{\mu\nu}\mathcal{J}^*_\mu \mathcal{J}_\nu =& 2E_+E_- \left|\varrho\right|^2 \\
&- E_+\varrho\left(\vec{p}_- \cdot \vec{\mathcal{J}}^{T*}\right) - E_-\varrho^*\left(\vec{p}_+ \cdot \vec{\mathcal{J}}^T\right) - E_+\varrho^*\left(\vec{p}_- \cdot \vec{\mathcal{J}}^T\right) - E_-\varrho\left(\vec{p}_+ \cdot \vec{\mathcal{J}}^{T*}\right) \\
&+ \left(\vec{p}_+ \cdot \vec{\mathcal{J}}^T\right)\left(\vec{p}_- \cdot \vec{\mathcal{J}}^{T*}\right) + \left(\vec{p}_+ \cdot \vec{\mathcal{J}}^{T*}\right)\left(\vec{p}_- \cdot \vec{\mathcal{J}}^T\right) \\
&- \left(\left|\varrho\right|^2 - \left|\mathcal{J}^T\right|^2\right)\left(\bar{E}E - \vec{p}_+ \cdot \vec{p}_- - m^2\right) \ .
\end{aligned} \tag{6.103}$$

- The terms which mix ϱ and $\vec{\mathcal{J}}^T$ must vanish as ρ does not change the M of the initial state but $\vec{\mathcal{J}}^T$ does. This is because $\vec{\mathcal{J}}^T$ consists of the operators $\mathcal{J}_\pm$. The terms which mix $\lambda = 1$ and $\lambda = -1$ will also be zero e.g. $\mathcal{J}_+\mathcal{J}^*_-$.

- $\vec{p}_+$ and $\vec{p}_-$ lie in the same plane, so since $\vec{q}$ is along $\hat{z}$ ($p_z\hat{z} = \frac{\vec{p}\cdot\vec{q}}{q^2}\vec{q}$), we may extract the transverse components of the momenta $\vec{p}_T = \vec{p} - \frac{\vec{p}\cdot\vec{q}}{q^2}\vec{q}$, i.e.

$$\vec{p}\cdot\vec{\mathcal{J}}^T = p_x\mathcal{J}_x + p_y \ , \mathcal{J}_y \tag{6.104}$$

and so

$$\left(\vec{p}_+ \cdot \vec{\mathcal{J}}^T\right)\left(\vec{p}_- \cdot \vec{\mathcal{J}}^{T*}\right) + \left(\vec{p}_+ \cdot \vec{\mathcal{J}}^{T*}\right)\left(\vec{p}_- \cdot \vec{\mathcal{J}}^T\right) = \left(\vec{p}_+ \cdot \vec{p}_- - \frac{\left(\vec{p}_+ \cdot \vec{q}\right)\left(\vec{p}_- \cdot \vec{q}\right)}{q^2}\right)\left|\mathcal{J}^T\right|^2 \ . \tag{6.105}$$

The charge density relates directly to the Coulomb operators, i.e.

$$\bar{\sum_i}\sum_f \left|\rho^2\right| = \frac{4\pi}{\hat{J}_i^2}\sum_{J\geq 0}\left|\mathcal{C}_J\right|^2 \equiv \left|\mathcal{M}^C\right|^2 \ , \tag{6.106}$$

while the transverse current relates to the transverse electric and magnetic operators

$$\bar{\sum_i}\sum_f \left|\mathcal{J}^T\right|^2 = \frac{4\pi}{\hat{J}_i^2}\sum_{J\geq 1}\left|\mathcal{T}_J^E\right|^2 + \left|\mathcal{T}_J^M\right|^2 \equiv \left|\mathcal{M}^{EM}\right|^2 \ . \tag{6.107}$$

Putting everything together, we first do the integral over the final nucleus momentum:

$$\mathrm{d}\Gamma = \left(\frac{4\pi\alpha}{Q^2}\right)^2 \frac{\mathrm{d}^3p_+}{(2\pi)^3 2E_+}\frac{\mathrm{d}^3p_-}{(2\pi)^3 2E_-}2\pi\delta(M_I - E_F - E_+ - E_-)\bar{\sum_i}\sum_f \ell^{\mu\nu}\mathcal{J}_\mu^*\mathcal{J}_\nu \ . \tag{6.108}$$

Second, we do the angular integrals. There are four angles determining the directions of the positron and electron momenta. The amplitude only depends on the relative separation angle θ_{ee}. Therefore by measuring the direction of $\vec{p}_+$ relative to $\vec{p}_-$ we can replace the integration $\mathrm{d}\cos\theta_+ \to \mathrm{d}\cos\theta_{ee} = \mathrm{d}x$. The remaining three angles $(\mathrm{d}\phi_+\mathrm{d}\cos\theta_-\mathrm{d}\phi_-)$ then give a constant factor $(8\pi^2)$ in the total rate, i.e.

$$\mathrm{d}\Gamma = \left(\frac{4\pi\alpha}{Q^2}\right)^2 \left(\frac{1}{E_+E_-}\right)\frac{2\pi\mathrm{d}x p_+^2\mathrm{d}p_+}{(2\pi)^3}\frac{4\pi p_-^2\mathrm{d}p_-}{(2\pi)^3}2\pi\delta(M_I - E_F - E_+ - E_-)\bar{\sum_i}\sum_f \ell^{\mu\nu}\mathcal{J}_\mu^*\mathcal{J}_\nu \ . \tag{6.109}$$

Third, we insert the lepton-nuclear tensor contraction and do the integral over $\mathrm{d}p_-$ using the remaining δ. We get a factor of $\frac{\sqrt{p_-^2+m^2}}{p_-} = \frac{E_-}{p_-}$ and a recoil factor $f_r = \left(1 + \frac{E_-}{E_+}\left(1 + \frac{p_+x}{p_-}\right)\right)^{-1}$.We can change integration variables $p_+\mathrm{d}p_+ = E_+\mathrm{d}E_+$, resulting in the differential decay rate:

$$\begin{aligned}\frac{\mathrm{d}\Gamma}{\mathrm{d}x\mathrm{d}E_+} =& \frac{4\alpha^2}{\pi Q^4}p_-p_+f_R\Bigg[\frac{Q^4}{q^4}\left|\mathcal{M}^C\right|^2\left(E_+E_- + p_+p_-x - m^2\right) \\ &+ \left|\mathcal{M}^{EM}\right|^2\left(E_+E_- + m^2 - \frac{(\vec{p}_+\cdot\vec{q})\,(\vec{p}_-\cdot\vec{q})}{q^2}\right)\Bigg] \ .\end{aligned} \tag{6.110}$$

This matches [122] where they make the further change of variables to the dimensionless kinematic variable y (the "asymmetry parameter") defined by:

$$E_+ - E_- = y\omega \ . \tag{6.111}$$

The integral is then presented using $\mathrm{d}y = \frac{\omega}{2}\mathrm{d}E_+$. y can be integrated from $-(1 - \frac{2m_e}{\omega})$ to $1 - \frac{2m_e}{\omega}$, equivalent to integrating E_+ from 0 to $\omega - 2m_e$.

6.4.2 Pair Production in Radiative Capture

When pair production occurs during a radiative capture reaction, i.e. $T(P, e^+e^-)F$ then we must calculate the cross section for a $2 \to 3$ process. The cross section is

$$\mathrm{d}\sigma = \frac{1}{v}\frac{1}{4E_P E_T}\bar{\sum_i}\sum_f\sum_{s_+s_-}\left|\mathcal{M}_{fi}^{s_+s_-}\right|^2\frac{\mathrm{d}^3p_+}{(2\pi)^3 2E_+}\frac{\mathrm{d}^3p_-}{(2\pi)^3 2E_-}\frac{\mathrm{d}^3p_F}{(2\pi)^3 2E_F}\ . \tag{6.112}$$

Following Section 6.4.1, we have

$$\begin{aligned}\mathrm{d}\sigma =& \frac{1}{v}\frac{1}{4E_P E_T}\frac{\mathrm{d}^3p_+}{(2\pi)^3 2E_+}\frac{\mathrm{d}^3p_-}{(2\pi)^3 2E_-}\frac{\mathrm{d}^3p_F}{(2\pi)^3 2E_F}(2\pi)^4\delta^4(P_P + P_T - P_F - P_+ - P_-)8E_P E_T E_F \\ &\times \frac{e^4}{Q^4}\bar{\sum_i}\sum_f \ell^{\mu\nu}\mathcal{J}_\mu\mathcal{J}_\nu^* \\ =& \frac{1}{v}\frac{e^4}{Q^4}\frac{\mathrm{d}^3p_+}{(2\pi)^3 2E_+}\frac{\mathrm{d}^3p_-}{(2\pi)^3 2E_-}2\pi\delta(E_P + E_T - E_F - E_+ - E_-)\bar{\sum_i}\sum_f \ell^{\mu\nu}\mathcal{J}_\mu\mathcal{J}_\nu^*\ .\end{aligned} \tag{6.113}$$

Here again the lepton 4-momenta are $P_\pm = (E_\pm, \vec{p}_\pm)$ and the final nucleus 4-momentum is $P_F = (E_F, \vec{p}_F)$. The lepton tensor (6.98) is again $\ell_{\mu\nu} = 4\left[P_{-\mu}P_{+\nu} + P_{-\nu}P_{+\mu} - \eta_{\mu\nu}\left(P_-\cdot P_+ + m^2\right)\right]$.

The contraction between the lepton tensor and nuclear currents are much more complicated in this case. The kinematics mix in additional nuclear operators, and rather than the two terms in (6.110), the cross section will separate into six terms. Following the notation of [123, 124], we have

$$\frac{1}{4}\bar{\sum_i}\sum_f \ell^{\mu\nu}\mathcal{J}_\mu\mathcal{J}_\nu^* = \sum_{j=1}^{6} v_j R_j\ . \tag{6.114}$$

The expansion of the contraction is done by collecting like terms, in this case we do not make the $\mathcal{J} \to \left(\frac{-Q^2}{q^2}\rho, \vec{\mathcal{J}}^T\right)$ substitution, but rather make use of $\mathcal{J} = (\rho, J_x, J_y, J_z)$ explicitly where $J_z = \frac{\omega}{|\vec{q}|}\rho$. The lepton-nuclear tensor contraction is then

$$\frac{1}{4}\ell^{\mu\nu}\mathcal{J}_\mu\mathcal{J}_\nu^* = \left(P_+\cdot\mathcal{J}\right)\left(P_-\cdot\mathcal{J}^*\right) + \left(P_+\cdot\mathcal{J}^*\right)\left(P_-\cdot\mathcal{J}\right) - \left(\mathcal{J}\cdot\mathcal{J}^*\right)\left(P_+\cdot P_- + m^2\right)\ , \tag{6.115}$$

as in (6.100).

Let's define $A = P_+$ and $B = P_-$ to avoid typing so many subscripts. $Q = A + B$ and we define $C = A - B$ (such that $A = \frac{1}{2}(C + Q)$, $B = \frac{-1}{2}(C - Q)$). This simplifies the equation, i.e.

$$\frac{1}{4}\ell^{\mu\nu}\mathcal{J}_\mu\mathcal{J}_\nu^* = -\left|\mathcal{J}\right|^2\left(A\cdot B + m^2\right) - \frac{1}{2}\left|C\cdot\mathcal{J}\right|^2\ , \tag{6.116}$$

but the evaluation then expands it into something complicated. We write $A = (\alpha, \vec{a}) = (E_+, \vec{p}_+)$ and $B = (\beta, \vec{b}) = (E_-, \vec{p}_-)$ so $\omega = \alpha + \beta$ and $\vec{q} = \vec{a} + \vec{b}$. Finally, $C = (\varsigma, \vec{c}) =$

$(\varsigma, c_x, c_y, c_z)$ where $\varsigma = \alpha - \beta$ and $\vec{c} = \vec{a} - \vec{b}$.

Expanding, we have

$$\begin{aligned}\frac{1}{4}\ell^{\mu\nu}\mathcal{J}_\mu\mathcal{J}_\nu^* = = &-\left(\rho^2 - J_x^2 - J_y^2 - J_z^2\right)\left(\alpha\beta - \vec{a}\cdot\vec{b} + m^2\right) - \frac{1}{2}\Big[\varsigma^2\rho^2 + c_x^2 J_x^2 + c_y^2 J_y^2 + c_z^2 J_z^2 \\ &- \varsigma c_x\left(\rho J_x^* + J_x\rho^*\right) - \varsigma c_y\left(\rho J_y^* + J_y\rho^*\right) - \varsigma c_z\left(\rho J_z^* + J_z\rho^*\right) \\ &+ c_x c_y\left(J_x J_y^* + J_y J_x^*\right) + c_x c_z\left(J_x J_z^* + J_z J_x^*\right) + c_y c_z\left(J_y J_z^* + J_z J_y^*\right)\Big] . \quad (6.117)\end{aligned}$$

We collect like terms (sometimes dropping the $||$ for brevity). R_j here really means $\bar{\sum}_i \sum_f R_j$.

Term 1: ρ^2, J_z^2, ρJ_z^*, $J_z\rho^*$

$$\begin{aligned}v_1 R_1 = &-\left(\rho^2 - J_z^2\right)\left(\alpha\beta - \vec{a}\cdot\vec{b} + m^2\right) - \frac{1}{2}\left(\varsigma^2\rho^2 - \varsigma c_z\rho J_z^* - c_z\varsigma J_z\rho^* + c_z^2 J_z^2\right) \\ = &-\rho^2\left(1 - \frac{\omega^2}{q^2}\right)\left(\alpha\beta - \vec{a}\cdot\vec{b} + m^2\right) - \frac{1}{2}\left(\varsigma - c_z\frac{\omega}{|\vec{q}|}\right)^2\rho^2 . \quad (6.118)\end{aligned}$$

Simplification requires some manipulation. We use $c_z = \frac{\vec{c}\cdot\vec{q}}{|\vec{q}|}$, and some identities:

$$\begin{aligned}\vec{c}\cdot\vec{q} = &b^2 - a^2 \\ = &\beta^2 - \alpha^2 \\ = &\varsigma\omega , \quad (6.119)\end{aligned}$$

$$Q^2 = \omega^2 - q^2 , \quad (6.120)$$

$$\frac{Q^2}{2} = \alpha\beta - \vec{a}\cdot\vec{b} + m^2 . \quad (6.121)$$

We take $R_1 \equiv \rho^2$ and so

$$\begin{aligned}v_1 &= \left(\frac{Q^2}{q^2}\right)\left(\alpha\beta - \vec{a}\cdot\vec{b} + m^2\right) - \frac{1}{2}\left(\varsigma - \frac{\varsigma\omega}{|\vec{q}|}\frac{\omega}{|\vec{q}|}\right)^2 \\ &= \left(\frac{Q^2}{q^2}\right)\left(\frac{Q^2}{2}\right) - \frac{\varsigma^2}{2}\left(-\frac{Q^2}{q^2}\right)^2 \\ &= \left(\frac{Q^4}{q^4}\right)\left(\frac{q^2 - \varsigma^2}{2}\right) \\ &= \left(\frac{Q^4}{q^4}\right)\left(\alpha\beta + \vec{a}\cdot\vec{b} - m^2\right) . \quad (6.122)\end{aligned}$$

This is identical in form to the $\left|\mathcal{M}^C\right|^2$ term in Section 6.4.1).

Term 2: ρJ_x^*, $J_x\rho^*$, $J_z J_x^*$, $J_x J_z^*$

$$\begin{aligned} v_2 R_2 =& -\frac{1}{2}\left[-\varsigma c_x\left(\rho J_x^* + J_x\rho^*\right) + c_z c_x\left(J_z J_x^* + J_x J_z^*\right)\right] \ , \\ v_2 \equiv& -\frac{1}{\sqrt{2}} c_x\left(\alpha - \beta - \frac{\omega}{|\vec{q}|} c_z\right) \ , \qquad (6.123) \\ R_2 \equiv& \mathrm{Re}\left(\rho^*\left(J_+ - J_-\right)\right) \ , \qquad (6.124) \end{aligned}$$

where we've used:

$$\begin{aligned} J_x\rho^* + \rho J_x^* =& 2\mathrm{Re}(J_x\rho^*) \\ =& 2\mathrm{Re}(\frac{-1}{\sqrt{2}}\left(J_+ - J_-\right)\rho^*) \ . \qquad (6.125) \end{aligned}$$

Term 3: ρJ_y^*, $J_y\rho^*$, $J_z J_y^*$, $J_y J_z^*$

$$\begin{aligned} v_3 R_3 =& -\frac{1}{2}\left[-\varsigma c_y\left(\rho J_y^* + J_y\rho^*\right) + c_z c_y\left(J_z J_y^* + J_y J_z^*\right)\right] \ , \\ v_3 \equiv& -\frac{1}{\sqrt{2}} c_y\left(\alpha - \beta - \frac{\omega}{|\vec{q}|} c_z\right) \ , \qquad (6.126) \\ R_3 \equiv& \mathrm{Im}\left(\rho^*\left(J_+ + J_-\right)\right) \ . \qquad (6.127) \end{aligned}$$

Since J_y has the additional factor of i:

$$\begin{aligned} J_y\rho^* + \rho J_y^* =& 2\mathrm{Re}(J_y\rho^*) \\ =& 2\mathrm{Im}(\frac{-1}{\sqrt{2}}\left(J_+ + J_-\right)\rho^*) \ . \qquad (6.128) \end{aligned}$$

J_x, J_y Cross Terms :

The remaining terms are

$$\left(|J_x|^2 + |J_y|^2\right)\left(A\cdot B + m^2\right) - \frac{1}{2}\left(c_x^2|J_x|^2 + c_y^2|J_y|^2 + c_x c_y\left(J_x J_y^* + J_y J_x^*\right)\right) \ . \qquad (6.129)$$

We use

$$\begin{aligned} |J_x|^2 =& \frac{1}{2}\left(|J_+|^2 - J_+ J_-^* - J_- J_+^* + |J_-|^2\right) \ , \qquad (6.130) \\ |J_y|^2 =& \frac{1}{2}\left(|J_+|^2 + J_+ J_-^* + J_- J_+^* + |J_-|^2\right) \ , \qquad (6.131) \\ J_x J_y^* =& \frac{-i}{2}\left(|J_+|^2 + J_+ J_-^* - J_- J_+^* - |J_-|^2\right) \ , \qquad (6.132) \\ J_y J_x^* =& \frac{i}{2}\left(|J_+|^2 - J_+ J_-^* + J_- J_+^* - |J_-|^2\right) \ , \qquad (6.133) \end{aligned}$$

and

$$|J_x|^2 + |J_y|^2 = |J_+|^2 + |J_-|^2 \ , \tag{6.134}$$

$$J_x J_y^* + J_y J_x^* = -\, i \left(J_+ J_-^* - J_- J_+^* \right) \ . \tag{6.135}$$

Then

$$\begin{aligned} & c_x^2 \, |J_x|^2 + c_y^2 \, |J_y|^2 + c_x c_y \left(J_x J_y^* + J_y J_x^* \right) \\ = & \frac{1}{2} \left(c_x^2 + c_y^2 \right) \left(|J_+|^2 + |J_-|^2 \right) \\ & - \frac{1}{2} \left(c_x^2 - c_y^2 \right) \left(J_+ J_-^* + J_- J_+^* \right) \\ & - i c_x c_y \left(J_+ J_-^* - J_- J_+^* \right) \ . \end{aligned} \tag{6.136}$$

Term 4: $|J_+|^2$, $|J_-|^2$

$$\begin{aligned} v_4 R_4 &= \left(|J_+|^2 + |J_-|^2 \right) \left(\alpha\beta - \vec{a} \cdot \vec{b} + m^2 \right) - \frac{1}{2} \cdot \frac{1}{2} \left(c_x^2 + c_y^2 \right) \left(|J_+|^2 + |J_-|^2 \right) \\ &= \left[-\frac{1}{4} \left(c_x^2 + c_y^2 \right) + \alpha\beta - \vec{a} \cdot \vec{b} + m^2 \right] \left[|J_+|^2 + |J_-|^2 \right] \ , \\ v_4 &\equiv -\frac{1}{4} \left(c_x^2 + c_y^2 \right) + \alpha\beta - \vec{a} \cdot \vec{b} + m^2 \ , \end{aligned} \tag{6.137}$$

$$R_4 \equiv |J_+|^2 + |J_-|^2 \ . \tag{6.138}$$

v_4 exactly matches the coefficient in front of $\left| \mathcal{M}^{EM} \right|^2$ in Section 6.4.1, since

$$\begin{aligned} c_x^2 + c_y^2 &= \left| \vec{c} - \frac{\vec{c} \cdot \vec{q}}{q^2} \vec{q} \right|^2 \ , \\ \alpha\beta - \vec{a} \cdot \vec{b} + m^2 - \frac{c_x^2 + c_y^2}{4} &= \alpha\beta + m^2 - \frac{(\vec{a} \cdot \vec{q})(\vec{b} \cdot \vec{q})}{q^2} \ . \end{aligned} \tag{6.139}$$

Term 5: $J_+ J_-^* + J_- J_+^*$

$$\begin{aligned} v_5 R_5 &= \frac{1}{2} \left(c_x^2 - c_y^2 \right) \mathrm{Re} \left(J_+^* J_- \right) \ , \\ v_5 &\equiv \frac{1}{2} \left(c_x^2 - c_y^2 \right) \ , \end{aligned} \tag{6.140}$$

$$R_5 \equiv \mathrm{Re} \left(J_+^* J_- \right) \ . \tag{6.141}$$

Term 6: $J_+J_-^* - J_-J_+^*$

$$\begin{aligned} v_6R_6 =& -\frac{1}{2}\left[-ic_xc_y\left(J_+J_-^* - J_-J_+^*\right)\right] \ , \\ =& -c_xc_y\mathrm{Im}\left(J_+^*J_-\right) \ , \\ v_6 \equiv& -c_xc_y \qquad (6.142) \\ R_6 \equiv& \mathrm{Im}\left(J_+^*J_-\right) \ . \qquad (6.143) \end{aligned}$$

Differential Cross Section The six terms will be inserted in to the differential cross section after shifting to spherical coordinates $\mathrm{d}^3p = p^2\mathrm{d}p\mathrm{d}\Omega$ and using the δ to first do the integral over p_-, then making the change of variables: $p_+\mathrm{d}p_+ = E_+\mathrm{d}E_+$, i.e.

$$\begin{aligned} \mathrm{d}\sigma =& \frac{4}{v}\frac{\alpha^2}{Q^4}f_r\frac{p_-p_+\mathrm{d}E_+\mathrm{d}\Omega_+\mathrm{d}\Omega_-}{(2\pi)^3}\sum_j v_jR_j \ , \\ \frac{\mathrm{d}^5\sigma}{\mathrm{d}E_+\mathrm{d}\Omega_+\mathrm{d}\Omega_-} =& \frac{4\alpha^2}{(2\pi)^3}\frac{f_r}{v}\frac{p_+p_-}{Q^4}\sum_j v_jR_j \ , \qquad (6.144) \end{aligned}$$

where appears the recoil factor $f_r = \left(1 + \left(\frac{E_-}{p_-}\right)\frac{p_- + p_+x - p_P\cos\theta_-}{E_F}\right)^{-1}$.

In radiative capture we have to compute on the matrix elements of the transverse electromagnetic current (i.e. with $\lambda = \pm 1$). Those operators are $X_{jm}^{\sigma\lambda} = \frac{\sqrt{4\pi}}{k}\sqrt{2\pi}\hat{j}\lambda^\sigma)(-i)^j\mathcal{T}_{jm}^\sigma$ where σ denotes electric or magnetic multipoles ($\sigma = 0, 1$ respectively). In pair production we have a virtual photon and hence the polarization can also be $\lambda = 0$. This is apparent due to the presence of $\langle f|\,\rho\,|i\rangle$ terms in the cross section.

To evaluate both ρ and $\mathcal{J}$ terms (and their combinations) we define the operator $\mathcal{N}_{jm}^\mu$ where $\mu = 0$ corresponds to the charge operator ρ. $\mu = \pm 1$ corresponds to the current operator with $\lambda = \pm 1$: $\mathcal{N}_{jm}^\lambda = \sum_\sigma X_{jm}^{\sigma\lambda}$ (H_λ in Section 6.3). We have

$$\begin{aligned} \mathcal{N}_{jm}^0 =& \frac{\sqrt{4\pi}}{k}\sqrt{4\pi}\hat{j}(-i)^j\mathcal{C}_{jm} \ , \qquad (6.145) \\ \mathcal{N}_{jm}^\lambda =& \frac{\sqrt{4\pi}}{k}\sqrt{2\pi}\hat{j}\sum_\sigma \lambda^\sigma(-i)^j\mathcal{T}_{jm}^\sigma \ . \qquad (6.146) \end{aligned}$$

We will have to multiply by a more general D-matrix $D_{m\mu}^j$ where $\mu \in (0, \pm 1)$. If we define the leptonic coordinate system to have an axis perpendicular to both the internal photon and initial velocity, i.e. $\hat{z} = \hat{q}$ and $\hat{y} = \hat{v} \times \hat{q}$ ($\hat{x} = \hat{y} \times \hat{z}$), the necessary rotation is $\mathcal{R}(\phi_q, \theta_q, 0)$ and so $D_{m\mu}^j(-\phi_q, -\theta_q, 0)$ appears. We define

$$N_\mu = \sum_{jm}\mathcal{N}_{jm}^\mu D_{m-\mu}^j(-\phi_q, -\theta_q, 0) \ . \qquad (6.147)$$

j	R_j	$N_\mu N_\kappa^*$
1	ρ^2	$N_0 N_0^*$
2	$\mathrm{Re}(\rho(J_+ - J_-)^*)$	$\mathrm{Re}(N_0(N_+ - N_-)^*)$
3	$\mathrm{Im}(\rho(J_+ + J_-))$	$\mathrm{Im}(N_0(N_+ + N_-)^*)$
4	$J_+^2 + J_-^2$	$N_+ N_+^* + N_- N_-^*$
5	$\mathrm{Re}(J_+ J_-^*)$	$\mathrm{Re}(N_+ N_-^*)$
6	$\mathrm{Im}(J_+ J_-^*)$	$\mathrm{Im}(N_+ N_-^*)$

Table 6.1: Notation for R_j in terms of N.

In the end we will evaluate in terms of the reduced matrix elements

$$\langle J_f | \, |\mathcal{N}_j^\mu| \, |LSJ\rangle = \mathcal{N}^{\mu j}_{J_f LSJ} \, , \tag{6.148}$$

analogous to $X^{\sigma j}_{J_f LSJ}$.

The R_j terms correspond to the combinations in Table 6.1 where

$$N_\mu N_\kappa^* = \bar{\sum_i} \sum_f \langle f | \sum_{jm} D^j_{m-\mu} \mathcal{N}^\mu_{jm} \, |i\rangle \left(\langle f | \sum_{j'm'} D^{j'}_{m'-\kappa} \mathcal{N}^\kappa_{j'm'} \, |i\rangle \right)^* . \tag{6.149}$$

A general expression for $N_\mu N_\kappa^*$ follows from very similar steps to Section 6.3, i.e.

$$\begin{aligned}
N_\mu N_\kappa^* =& \bar{\sum_{m_P m_T}} \sum_{M_f} \left(\langle J_f M_f | \sum_{jm} D^j_{m-\mu} \mathcal{N}^\mu_{jm} \, |s_p m_P s_T m_T\rangle \right) \left(\langle J_f M_f | \sum_{j'm'} D^{j'}_{m'-\kappa} \mathcal{N}^\kappa_{j'm'} \, |s_P m_P s_T m_T\rangle \right)^* \\
=& (\hat{s}_P \hat{s}_T \hat{J}_f)^{-2} \sum_{M_f} \sum_{jm} \sum_{LSJM} \sum_{j'} \sum_{L'J'} \hat{L}\hat{L}' e^{i(\sigma_L - \sigma_{L'})} D^j_{m-\mu} (-)^{m\kappa} D^{j'}_{-m-\kappa} \mathcal{N}^{\mu j}_{J_f LSJ} \mathcal{N}^{\kappa j' *}_{J_f L'SJ'} \\
& \times (L0SM|JM) \left(L'0SM|J'M\right) (JMjm|J_f M_f) \left(J'Mj'm|J_f M_f\right) \\
=& (\hat{s}_P \hat{s}_T \hat{J}_f)^{-2} \sum_{M_f} \sum_{jm} \sum_{LSJM} \sum_{j'} \sum_{L'J'} \hat{L}\hat{L}' e^{i(\sigma_L - \sigma_{L'})} \mathcal{N}^{\mu j}_{J_f LSJ} \mathcal{N}^{\kappa j' *}_{J_f L'SJ'} \\
& \times \sum_K (-)^{m+\kappa} \left(jmj' - m|K0\right) \left(j - \mu j' \kappa | K(\kappa - \mu)\right) D^K_{0(\kappa-\mu)} \\
& \times (L0SM|JM) \left(L'0SM|J'M\right) (JMjm|J_f M_f) \left(J'Mj'm|J_f M_f\right) \\
=& \frac{\hat{J}_f^2}{\hat{s}_P^2 \hat{s}_T^2} \sum_{jj'} \sum_{SLL'JJ'} (-)^{S - J_f - \kappa} \hat{J}\hat{J}' \hat{L}\hat{L}' e^{i(\sigma_L - \sigma_{L'})} \mathcal{N}^{\mu j}_{J_f L'SJ'} \mathcal{N}^{\kappa j' *}_{J_f LSJ} \\
& \times \sum_K \left\{ \begin{array}{ccc} J & J' & K \\ j' & j & J_f \end{array} \right\} \left\{ \begin{array}{ccc} J & J' & K \\ L' & L & S \end{array} \right\} \left(L0L'0|K0\right) \left(j\mu j' - \kappa | K(\mu - \kappa)\right) d^K_{(\mu-\kappa)0}(\theta_q) \, ,
\end{aligned} \tag{6.150, 6.151}$$

where using (A.21), we have $D^K_{0M}(-\phi_q, -\theta_q, 0) = d^K_{0M}(-\theta_q) = d^K_{M0}(\theta_q)$.

The full differential cross section is difficult to compute explicitly for the 5-dimensional

phase space but this can be simplified and made into a form that may be compared to experiment by considering only the case where the photon is perpendicular to the beam such that the electron and positron are in the same plane i.e. $c_z = \frac{\vec{c}\cdot\vec{q}}{q}$,$c_y = \vec{c} - \frac{\vec{c}\cdot\vec{q}}{q^2}\vec{q}$ (as $c_x = 0$ in this situation). In this case, $v_2 = v_6 = 0$, in addition $R_3 = 0$, and so we actually only need c_z^2 and c_y^2. We have

$$\begin{aligned} c_z^2 =& \frac{(\vec{c}\cdot\vec{q})^2}{q^2} \\ =& \frac{((\vec{a}-\vec{b})\cdot(-\vec{a}-\vec{b}))^2}{q^2} \\ =& \frac{(b^2-a^2)^2}{q^2} \ , \end{aligned} \tag{6.152}$$

and

$$\begin{aligned} c_y^2 =& \left|\vec{c} - \frac{\vec{c}\cdot\vec{q}}{q^2}\vec{q}\right|^2 \\ =& c^2 - \frac{(\vec{c}\cdot\vec{q})^2}{q^2} \\ =& a^2 - 2\vec{a}\cdot\vec{b} + b^2 - \frac{(b^2-a^2)^2}{q^2} \ . \end{aligned} \tag{6.153}$$

i	v_i	$v_i(\theta_q = \frac{\pi}{2}, \phi_a = \frac{\pi}{2}, \phi_b = -\frac{\pi}{2})$
1	$\frac{Q^4}{q^4}(\alpha\beta + abx - m^2)$	$\frac{Q^4}{q^4}(\alpha\beta + abx - m^2)$
4	$-\frac{1}{4}\left(c_x^2 + c_y^2\right) + \alpha\beta - abx + m^2$	$-\frac{1}{4}\left(a^2 + b^2 - 2abx - \frac{(b^2-a^2)^2}{q^2}\right) + \alpha\beta - abx + m^2$
5	$\frac{1}{2}\left(c_x^2 - c_y^2\right)$	$-\frac{1}{2}\left(a^2 + b^2 - 2abx - \frac{(b^2-a^2)^2}{q^2}\right)$

Table 6.2: Simplified formulation of kinematic factors v_i corresponding to the ATOMKI experimental setup.

K, M	$d^K_{M0}(\theta)$	$d^K_{0M}(\frac{\pi}{2})$
$0, 0$	1	1
$1, 0$	$\cos\theta$	0
$1, \pm1$	$\mp\frac{1}{\sqrt{2}}\sin\theta$	$\mp\frac{1}{\sqrt{2}}$
$2, 0$	$\frac{1}{2}\left(3\cos^2\theta - 1\right)$	$-\frac{1}{2}$
$2, \pm1$	$\mp\sqrt{\frac{3}{8}}\sin 2\theta$	0
$2, \pm2$	$\sqrt{\frac{3}{8}}\sin^2\theta$	$\pm\sqrt{\frac{3}{8}}$

Table 6.3: Relevant values of the Wigner d-matrix factor [35].

We then can convert the kinematics into a form (Table 6.2) that depends only on the relative angle through $\vec{a}\cdot\vec{b} = |\vec{a}||\vec{b}|\cos\theta_{ee} = abx$ as in Section 6.4.1. Shown in Table 6.3 are

the simplified expressions that result for $d^K_{(\mu-\kappa)0}(\theta_q)$ (which appears in (6.151)).

6.4.3 Hypothetical Intermediate Particles

There have been claims that there are contributions to pair production in radiative capture from BSM bosons. This hypothetical particle has an unknown spin and parity but the presence of a signal could be enhanced by a resonance in the nuclear system, if the corresponding operator has complementary J^π. There have been a number of attempts to understand the observations of experimental anomalies from a particle physics perspective [125–127].

Here we approximate the transition operators in the low-energy limit. In practice the calculation is then to insert a new operator $O^{(X)}$ into the transition strength of the radiative capture (6.91). The label σ would then be dropped and we look at the leading multipole $j = 1$. These operators may be sensitive to the momentum transfer carried by the new particle i.e. $k_X = \sqrt{\omega^2 - m_X^2}$. The total available energy ω is determined by the difference between the initial kinetic energy and final state bound state energy.

For a vector particle, we set the operator proportional to the E1 [128], i.e.

$$O^{(V)} = \epsilon_V M_1^E \frac{k_X}{\omega} \ . \tag{6.154}$$

For a pseudo-scalar, the operator is Σ'' [129] which reduces to S in the long-wavelength limit, i.e.

$$O^{(P)} = \epsilon_P S k_X \ . \tag{6.155}$$

For an axial vector we also get an operator proportional to S [130], i.e.

$$O^{(A)} = \epsilon_A S \sqrt{2 + \frac{m_X^2}{\omega^2}} \ . \tag{6.156}$$

In principle, the couplings ϵ_X would be fitted to match experiments.

Chapter 7

NCSMC Results

Radiative capture reactions are an important pathway by which heavier nuclei can be created in astrophysical environments. For example, $d(p,\gamma)^3$He occurs as a primary step in stellar burning. Using the NCSMC technique we may address radiative capture simultaneously with the nuclear structure of the composite system, elastic scattering, inelastic scattering and reactions involving the same total mass number.

In the $A = 6$ system, we computed ^{4}He(d, γ)^{6}Li. This reaction is an contributor to the prediction of the primordial abundance of ^{6}Li. Accurate determination of the rate requires prediction within the big bang energy window (30 keV - 400 keV), which experimentally hindered by low counting rates, current data require extrapolation to low-energy. In our fully microscopic approach we include previously neglected M1 transitions which enhance the capture probability below 100 keV. Overall, we reduce the uncertainty of the thermonuclear capture rate by a factor of 7

In the $A = 8$ system, we addressed reactions involving $p + {}^7\text{Li} \leftrightarrow {}^8\text{Be} \leftrightarrow n + {}^7\text{Be}$. Recent improvements of the NCSMC have made possible the investigation of reactions such as $^7\text{Li}(p,\gamma)^8\text{Be}$, $^7\text{Be}(n,\gamma)^8\text{Be}$ or $^7\text{Be}(n,p)^7\text{Li}$. These reactions are important channels by which ^{7}Li is created or destroyed. They are the main contributors to the prediction of cosmological lithium abundance of which current estimates differ significantly from measurements [131]. A related reaction which is also accessible with NCSMC is $^7\text{Li}(p,e^+e^-)^8\text{Be}$. A recent experiment at ATOMKI reported an anomaly in the electron-positron spectrum from this reaction [120]. The decay of the two 1^+ excited states of the ^{8}Be to the 0^+ ground state produces the emitted particles. These excited states are just above the $^7\text{Li} + p$ threshold. The spectrum of the particles from the second 1^+ state suggests their production is delayed by an intermediate particle that is not the photon. One possible interpretation of this anomaly is a new boson with mass of 17 MeV [132], which could be a mediator between the visible and dark sectors [127]. Our full ab initio calculation of this reaction has some discrepancy with the data, but is improved compared to previous theoretical calculations (e.g. [122]).

7.1 ^{4}He$(d,\gamma)^6$Li Radiative Capture

There are currently significant discrepancies between theory and experiment in the case of the primordial abundance of ^{6}Li, which is under-predicted by three orders of magnitude [133]. This could be due to systematic discrepancies in extracting the abundances from astronomical observations of metal-poor stars [134, 135]. Another possibility is an inaccurate prediction of the relevant reaction rates as nuclear reaction rates are the main input to models which predict the primordial abundances of elements. Constraining the uncertainties on these reaction rates is an important goal.

7.1.1 The ^{6}Li Composite System and ^{4}He$(d,d)^4$He Elastic Scattering

The NCSMC wavefunction needed for the system is given in terms of ^{6}Li NCSM eigenstates $\left|^6\text{Li}\lambda J^\pi T\right\rangle$ and continuous ^{4}He-d cluster states $\left|\Phi^{J^\pi T}_{\nu r}\right\rangle$ built from ^{4}He (α) and ^{2}H (d) NCSM states, i.e.

$$\left|\Psi^{J^\pi T}\right\rangle = \sum_\lambda c_\lambda \left|^6\text{Li}\lambda J^\pi T\right\rangle + \sum_\nu \int \mathrm{d}r r^2 \frac{\gamma_\nu(r)}{r} \mathcal{A}_\nu \left|\Phi^{J^\pi T}_{\nu r}\right\rangle \ , \tag{7.1}$$

where

$$\left|\Phi^{J^\pi T}_{\nu r}\right\rangle = \left[\left(\left|^4\text{He}\lambda_\alpha J^{\pi_\alpha}_\alpha T_\alpha\right\rangle \left|^2\text{H}\lambda_d J^{\pi_d}_d T_d\right\rangle\right)^{(sT)} Y_\ell(\hat{r}_{\alpha,d})\right]^{(J^\pi T)} \times \frac{\delta(r-r_{\alpha,d})}{r r_{\alpha,d}} \ . \tag{7.2}$$

We use the first 15 NCSM eigenstates of ^{6}Li, the single bound state of ^{4}He (experimentally bound by 19.82 MeV below the $^3\text{He}+p$ threshold) and the single bound state of ^{2}H in combination with ^{2}H "pseudo-states". The pseudo-states are NCSM eigenstates that do not correspond to real bound states, but their inclusion can partially account for the $p+n$ continuum as d is very loosely bound (experimentally the ground state is -2.22 MeV). In total 9 NCSM states are included (3 each from channels $J^\pi = \{1^+, 2^+, 3^+\}$ corresponding to $\{^3S_1 - ^3D_1, ^3D_2, ^3D_3 - ^3G_3\}$ ($S=1$, $L=\{(0,2),(2),(2,4)\}$). The NCSM calculations were up to $N_{max}=12$ and the relative motion between the clusters expanded to $N_{rel}=11$ culminating in an NCSMC calculation with $N_{max}=11$. NCSM calculations were repeated with two choices of 3N force (3N_{loc} [60] and 3N_{lnl} [136]). The first overbinds the ^{6}Li ground state by 250 keV (compared to experiment) and the second underbinds by 590 keV. This difference motivated the choice of 3N_{loc} in the NCSMC predictions.

The ground state energy and the position of the low-lying resonances was predicted with NCSMC (Figure 7.1) with different choices of the nuclear potential. The inclusion of a 3N force improved the $2^+ - 3^+$ splitting, nearly exactly reproducing the 3^+ energy. Despite inclusion of a 3N force, the ground state of ^{6}Li was still overbound by about 350 keV. By adjusting the ground state energy of ^{6}Li in the NCSM (i.e. the values in the $E_{\lambda\lambda'}$ NCSMC kernel) we can accurately reproduce the ground state energy. The 1^+ eigenstates were shifted to reproduce the experimental ^{6}Li ground state energy. This is denoted in the results by NN+3N_{loc}-pheno. This phenomenological approach loosens the first-principles

paradigm to compensate for insufficiencies in the nuclear force as in several previous studies [137–139]. The exact energies and resonance positions are fitted to experiment but the widths, structure and transition strengths are predictions.

As a further benchmark we calculate the elastic scattering cross section $^4\mathrm{He}(d,d)^4\mathrm{He}$ and compare to data. Figure 7.2. Without phenomenological adjustment the results already agree well with experiment.

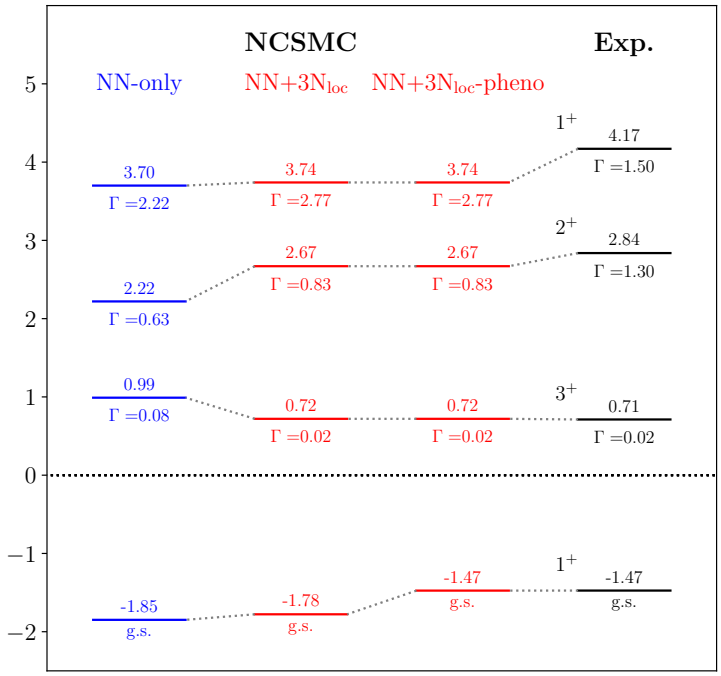

Figure 7.1: Low-lying spectrum of ^{6}Li obtained with the NCSMC at $N_{max} = 11$ using the SRG-evolved N^{3}NLO NN potential [28] (NN-only) with $\lambda = 2$ fm^{-1}, the NN+3n$_{loc}$ [60, 140] without (NN+3N$_{loc}$) and with the phenomenological energy adjustment (NN+3N$_{loc}$-pheno) compared to experiments [141]. The zero energy is taken as the predicted (resp. experimental) $^4\mathrm{He} + d$ threshold for NCSMC (resp. Exp.)

7.1.2 The $^4\mathrm{He}(d,\gamma)^6\mathrm{Li}$ S-factor

The cross-section of the $^4\mathrm{He}(d,\gamma)^6\mathrm{Li}$ reaction is calculated via (6.91). We present the results in terms of the astrophysical S-factor. The S-factor is a rescaling of the cross section to

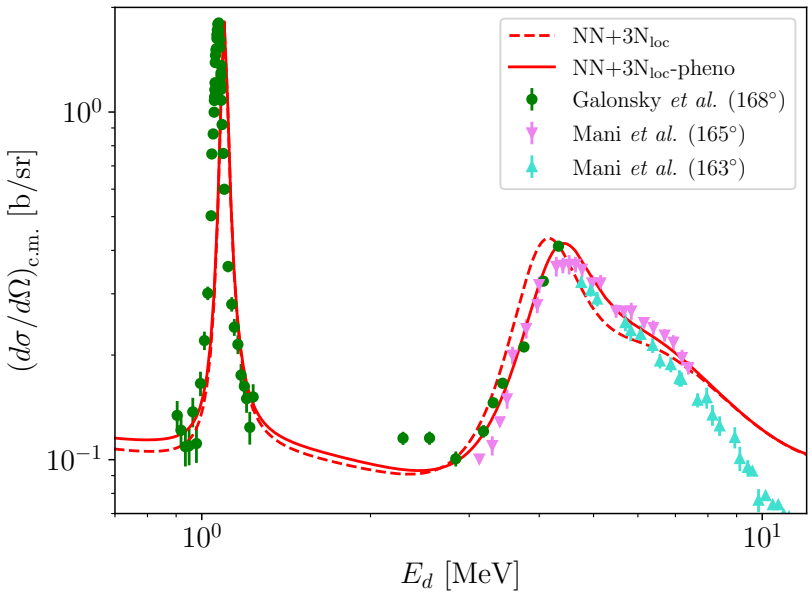

Figure 7.2: NCSMC predictions of ^{4}He$(d,d)^4$He elastic scattering. Both NCSMC predictions obtained without (NN+3N$_{loc}$) and with the phenomenological adjustment (NN+3N$_{loc}$-pheno) reproduce the experimental elastic-scattering ^{4}He$(d,d)^4$He cross section at the deuteron backscattered to the angle $\theta_d = 164°$ [142, 143].

remove the Coulomb repulsion [107], i.e.

$$S(E) = Ee^{2\pi\eta}\sigma(E)\ , \tag{7.3}$$

where η is the Sommerfeld parameter in this case $\eta = \frac{Z_1 Z_2 \alpha}{v} = \frac{\sqrt{3}\alpha}{\sqrt{2E}}$ since $v = \sqrt{2\mu E} = \sqrt{2\left(\frac{2\cdot 4 m_N}{6}\right)E}$.

The predicted S-factor agrees well with data as seen in Figure 7.3. The prediction agrees well with LUNA at low energy already with only the NN potential but fails to reproduce the resonance peaks (3^+ at 0.71 MeV and 2^+ at 2.84 MeV). The resonances are reproduced with the NN+3N$_{loc}$ but the g.s. is overbound. The NN+3N$_{loc}$-pheno achieves both.

The relative importance of the different electromagnetic multipoles (E1,M1,E2) varies with energy. The 3^+ resonance is predominately E2 but the low-energy is a mix of E2 and M1. Previous studies (e.g. [144, 145]) did not include the M1 transitions and we find they have a significant contribution at low-energy. The internal dipole magnetic moments of the ^{6}Li and d contribute to this transition strength and therefore our microscopic model is well-motivated. Phenomenological approaches often find sizable E1 contribution which we refute.

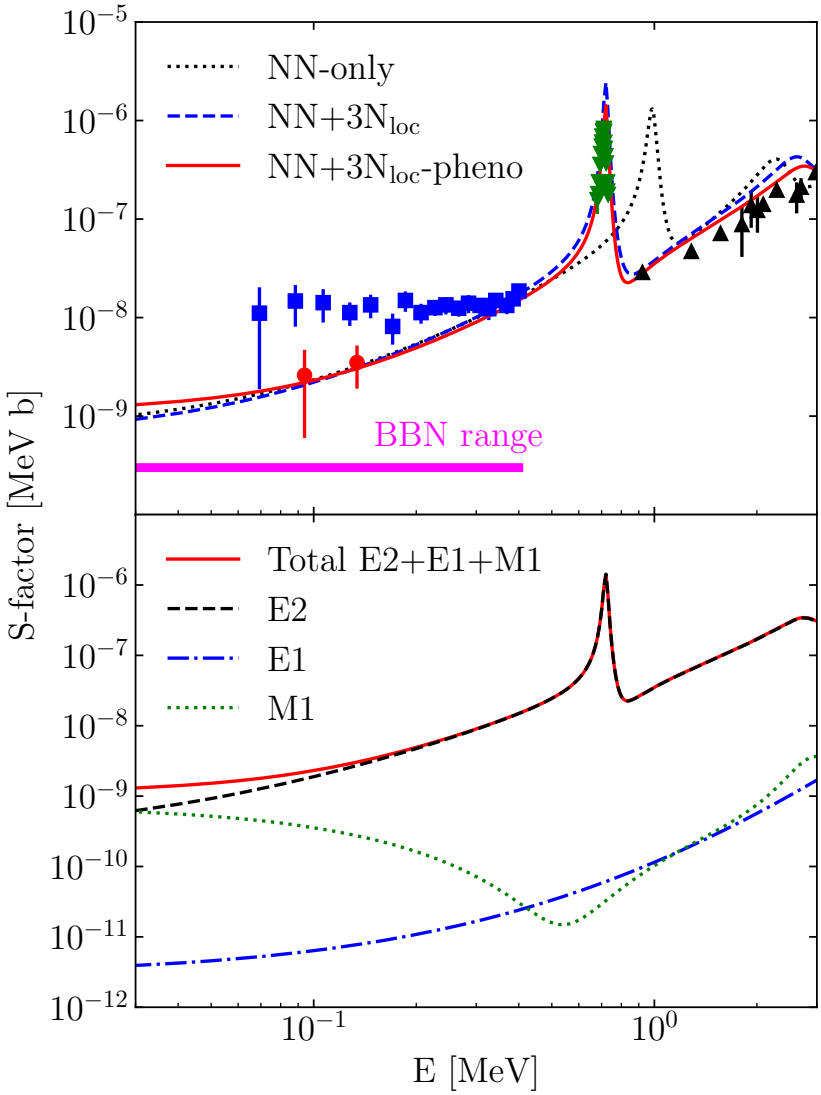

Figure 7.3: Top: Predicted S-factor for the ^{4}He$(d,\gamma)^6$Li compared with data taken from Refs [146] (red circles), [147] (blue squares), [148] (green up-triangles), [149] (black down-triangles). Calculations are obtained using the SRG-evolved N3LO NN potential [28] (NN-only) with $\lambda = 2$ fm^{-2}, the NN+3N$_{loc}$ [60] without (NN+3N$_{loc}$) and with the phenomenological energy adjustment (NN+3N$_{loc}$-pheno). Bottom: E2, E1 and M1 components to the predicted S-factor for the ^{4}He$(d,\gamma)^6$Li obtained with the NN+3N$_{loc}$-pheno.

7.1.3 The Effect of SRG on M1 Contributions

We investigated the effect of consistent SRG evolution of the electromagnetic operators (since we use an SRG evolved potential). Because E1 and E2 operators are long-range, their matrix elements depend mainly on the wavefunctions are large distance and hence the SRG transformation has a negligible impact [74, 150].

The electromagnetic transition strengths in the NCSMC are decomposed into four contributions (6.68). The dominant terms in this case are the $\langle {}^6\mathrm{Li}\lambda' || \mathcal{T}_1^M || {}^6\mathrm{Li}\lambda \rangle$ and $\langle {}^2\mathrm{H}\lambda'_d || \mathcal{T}_1^M || {}^2\mathrm{H}\lambda_d \rangle$ transitions. In fact interference between these cause the minimum near 0.5 MeV and enhancement at low-energy. This emphasizes the fact that a microscopic model is needed to describe this reaction.

We compare in Figure 7.4 calculations obtained where the internal NCSM contributions to the transitions are SRG-evolved (M1) and where they are not evolved (M1 bare). The effect is small, although visible and has a negligible effect on the total S-factor except at the lowest energy.

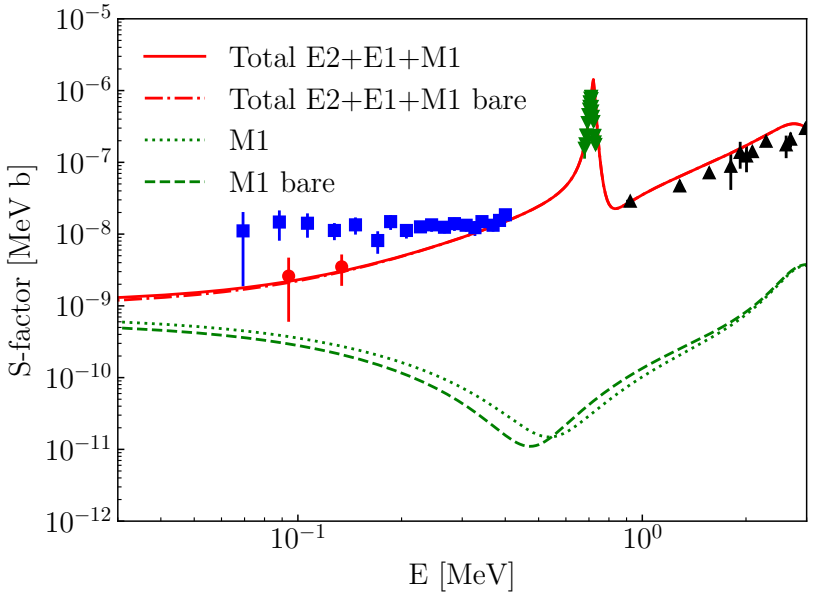

Figure 7.4: Influence of the SRG transformation on the M1 operator. The experimental data follow the same legend as in Fig. 7.3.

7.1.4 Thermonuclear Reaction Rate

From the S-factor (cross section), we obtain a thermonuclear reaction rate for $^4\mathrm{He}(d,\gamma)^6\mathrm{Li}$ and compared this to data (Figure 7.5). Our result falls within the bounds of the NACRE II evaluation with reduced uncertainty by an average factor of 7. The uncertainty in our calculation is estimated based on the truncation error of the model space (N_{max} convergence)

and the choice of 3N force.

The reaction rate requires the folding of the energy-dependent cross section with the Maxwell-Boltzmann energy distribution as a function of temperature. Expressed as the Maxwellian-averaged rate $< \sigma v >$ times the Avogadro number N_A [151]:

$$N_A < \sigma v > = N_A \sqrt{\frac{8}{\pi \mu (k_B T)^3}} \int_0^\infty E \sigma(E) \exp\left[-\frac{E}{k_B T}\right] \mathrm{d}E \,, \tag{7.4}$$

where k_B is the Boltzmann constant, μ the reduced mass and T the temperature. A more typical expression uses T_9, the temperature in units of 10^9 K:

$$N_A < \sigma v > = \frac{3.73 \times 10^9}{\sqrt{\hat{\mu} T_9^3}} \int_0^\infty E \sigma(E) \exp\left[-\frac{11.605 E}{T_9}\right] \mathrm{d}E \,, \tag{7.5}$$

where E and $\sigma(E)$ are in units of MeV and barn respectively, and $\hat{\mu}$ is the reduced mass in atomic mass units. This results in a rate is in units of $\mathrm{cm}^3\ \mathrm{mol}^{-1}\ \mathrm{s}^{-1}$.

We predict an even lower reaction rate than previous predictions, therefore the discrepancy of the predicted ^{6}Li abundance is larger than previously reported.

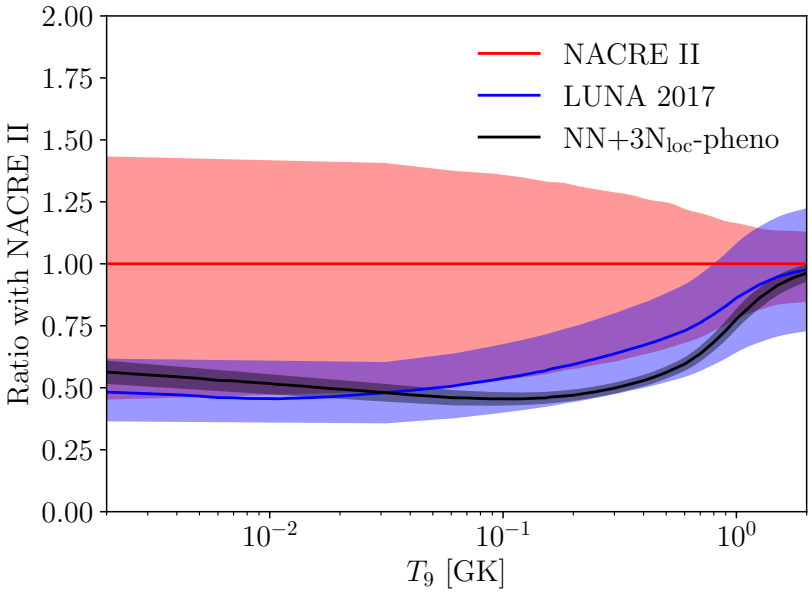

Figure 7.5: Ratio of the predicted thermonuclear reaction rates (black line) for $^4\mathrm{He}(d,\gamma)^6\mathrm{Li}$ with the NACRE-II evaluation (red line) [151] for different temperature T_9 in GK. Our results are also compared with the recent thermonuclear reaction rate derived from the measurements of the LUNA collaboration (blue line) [152]. The shaded areas correspond to the uncertainty of each calculation.

7.2 ^{7}Li$(p,\gamma)^8$Be Radiative Capture

The study of reactions involving ^{7}Li, ^{7}Be and ^{8}Be has several motivations. ^{7}Li has a cosmological abundance problem of smaller in magnitude to that of ^{6}Li and in the opposite direction (the ratio of predicted/measured is about 3). ^{7}Li is stable in contrast to the Beryllium isotopes mentioned. ^{7}Be has a 53 day half-life and therefore is most important in its influence on the ^{7}Li abundance in BBN.

^{8}Be is unstable and is a resonance of $\alpha + \alpha$ at 91.8 keV (with a width of 6 eV). It is a bottleneck of nucleosynthesis and is part of the "triple-alpha" process by which ^{12}C is produced, leading to many of the most important elements for life (e.g.^{16}O). The threshold for $^7\text{Li} + p$ is at 17.2551 MeV below which there are 5 ^{8}Be states ($\alpha + \alpha$ resonances). Reactions of $^7\text{Li} + p$ are enhanced through ^{8}Be resonances above this threshold. There are two 1^+ resonances with only $^7\text{Li} + p$ channels, above which is the $^7\text{Be} + n$ threshold (since ^{7}Be is less bound than ^{7}Li due to Coulomb repulsion). The spectrum becomes extremely complex above this point (see Fig. 7.6).

^{8}Be has recently been brought to attention in experiments. In particular, anomalies were observed in the electron-positron pair production distribution from proton capture on ^{7}Li [120]. These were interpreted as the decay of a new boson. To assist in interpretation of the anomaly, the NCSMC can be applied to calculate radiative capture and the related pair production.

7.2.1 The ^{8}Be Composite System

The NCSMC wavefunction needed for this system is given in terms of ^{8}Be NCSM eigenstates and cluster states composed of ^{7}Li NCSM eigenstates with a single proton and ^{7}Be NCSM eigenstates with a single neutron, i.e.

$$\Psi^{(8)}_{\text{NCSMC}} = \sum_\lambda c_\lambda \left|{}^8\text{Be}, \lambda\right\rangle + \sum_\nu \int \mathrm{d}r \gamma_\nu(r) \hat{\mathcal{A}}_\nu \left|{}^7\text{Li} + p, \nu\right\rangle + \sum_\mu \int \mathrm{d}r \gamma_\mu(r) \hat{\mathcal{A}}_\mu \left|{}^7\text{Be} + n, \mu\right\rangle \ . \tag{7.6}$$

We use the lowest 5 NCSM eigenstates each from ^{7}Li and ^{7}Be. They are mirror nuclei and so the lowest states have the same J^π: $\{\frac{3}{2}^-, \frac{1}{2}^-, \frac{7}{2}^-, \frac{5}{2}^-, \frac{5}{2}^-\}$. We use the 30 lowest NCSM eigenstates of ^{8}Be (15 positive parity and 15 negative parity), covering the energy range of interest.

7.2.2 ^{7}Li, ^{7}Be and ^{8}Be NCSM Results

Our NCSMC calculation requires as input NCSM eigenstates. We used the recently developed nuclear force from chiral EFT NN+3N$_{lnl}$ [136]. This Hamiltonian is fully determined in $A = 2$,3 and 4 systems (nucleon-nucleon scattering and properties of the deuteron, ^{3}H, ^{3}He (including the ^{3}H half-life) and the ^{4}He binding energy). It is SRG-evolved to $\lambda = 2$ fm^{-1}.

This interaction has already been tested in $A = 7, 8$ systems. The predicted excitation

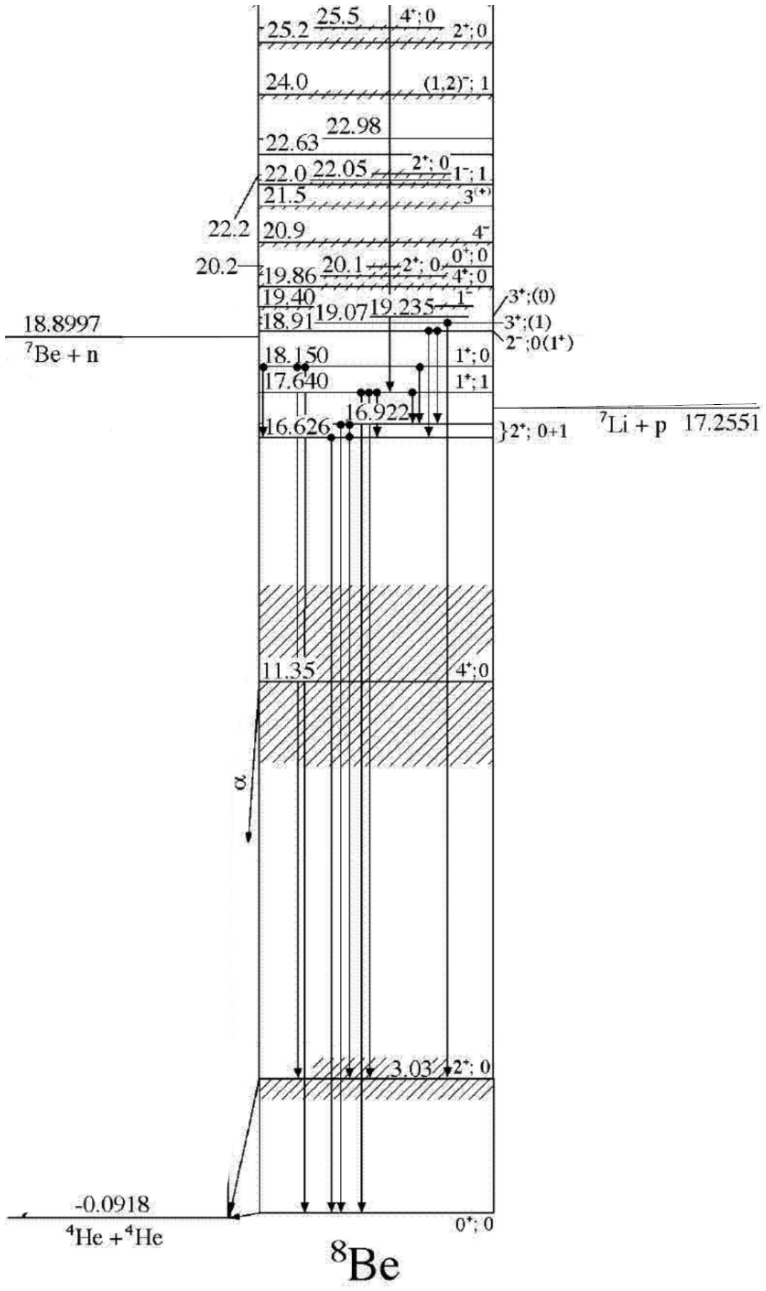

Figure 7.6: The experimental level scheme for ^{8}Be. Adapted from [153].

energies are shown in Figure 7.7. The convergence of the ground state is shown in Figure 7.8.

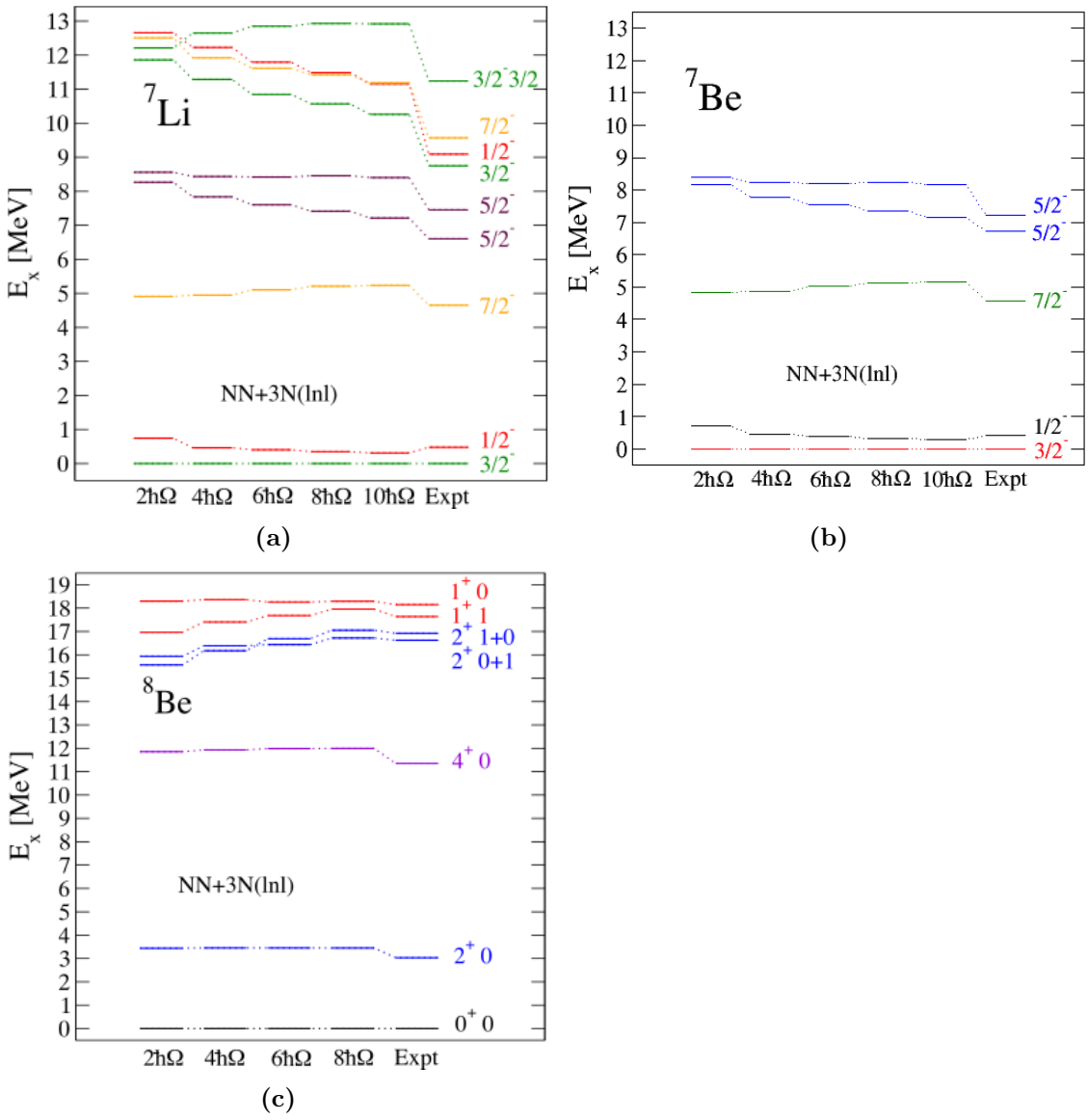

Figure 7.7: Excitation energies from the NCSM for (a) ^{7}Li, (b) ^{7}Be and (c) ^{8}Be using the NN+3N$_{lnl}$ interaction [136]. The lowest states most relevant for input to the NCSMC are in the correct order. Only the lowest 5 states are shown for ^{7}Be.

7.2.3 Resonances and Phase Shifts

As we do not include $|\alpha + \alpha\rangle$ states in our basis we cannot expect to precisely predict the resonance positions below the $^7\text{Li} + p$ threshold. In our calculations these are considered as bound states. However inclusion of some cluster degrees of freedom still improves the

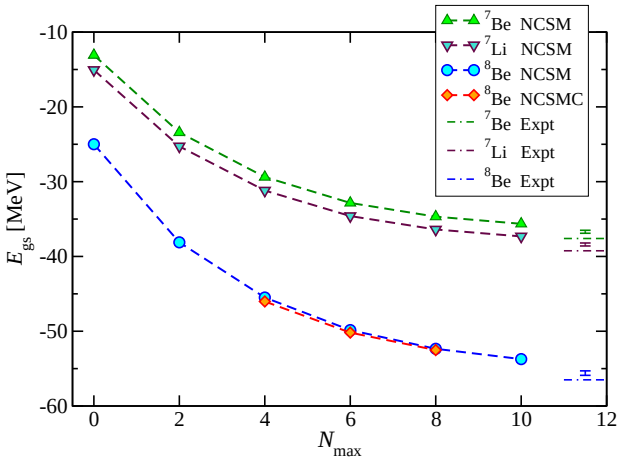

Figure 7.8: The convergence of the ground state energies of ^{7}Li, ^{7}Be and ^{8}Be with the model-space parameter N_{max} using the NN+3N$_{lnl}$ interaction [136].

description of the asymptotics of the wavefunction. The resulting ^{8}Be energies from NCSMC with respect to the $^7\mathrm{Li} + p$ threshold are shown in 7.1. The improved ground state is also added to Figure 7.8 to compare to the NCSM result.

Figure 7.9 shows the eigen-phaseshifts for scattering with $^7\mathrm{Li} + p$ and $^7\mathrm{Be} + n$ channels. Calculations for $N_{max} = 9$ are shown. The eigen-phaseshifts δ are calculated from the eigenvalues $e^{2i\delta}$ of the S-matrix. The S-matrix is computed as a function of the center of mass energy, shown here up to 8 MeV. The maxima in the derivative of the eigen-phaseshifts correspond to resonances. The eigen-phaseshift corresponding to the last 2^+ state, which is bound in experiment (see Table 7.1), shows up as an extremely narrow resonance and can be seen in the bottom-left corner of (a). The next two resonances are 1^+ resonances which correspond to the spin aligned and anti-aligned interactions between the proton and the $\frac{3}{2}^-$ ground state of ^{7}Li. The 1^+ resonances appear clearly in the level-scheme Figure 7.6. New phase shifts occur past the threshold of $^7\mathrm{Be} + n$ which is higher than $^7\mathrm{Li} + p$. We reproduce the 3^+ pair in particular and find many resonances which have not yet been seen in experiment. The data are complex and the TUNL evaluation includes the results of phenomenological R-matrix fits [154].

The convergence of the eigen-phaseshift with N_{max} is shown in Fig. 7.10 . The 1^+ do not change much. The $3^+$is not as well-converged, interestingly there is a crossing at $N_{max} = 9$. The 3^+ resonances are mixed between the $p + {}^7$Li and $n + {}^7$Be mass partitions and the amount of mixing depends on N_{max} as seen in the diagonal phase-shifts (Fig 7.11). The same figure shows that the two 1^+ have different interpretations, corresponding to total channel spin 1 and 2 respectively. We can also extract the isospin character, the first is predominantly $T = 1$ and the second $T = 0$.

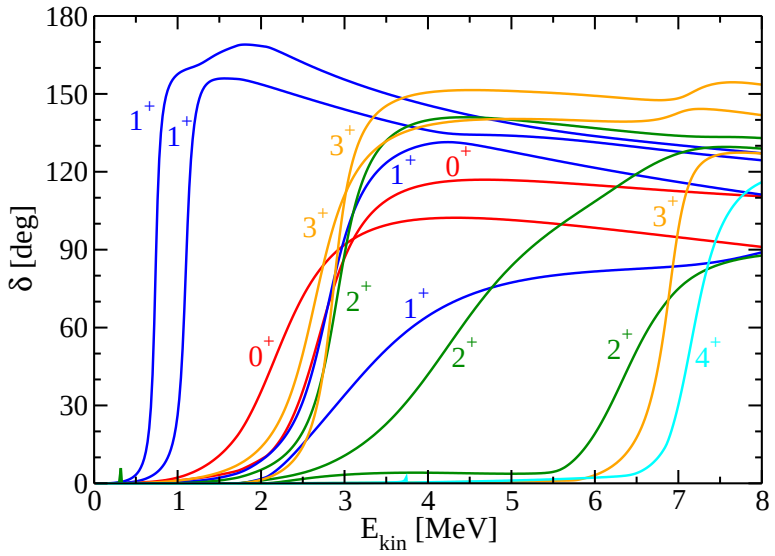

(a)

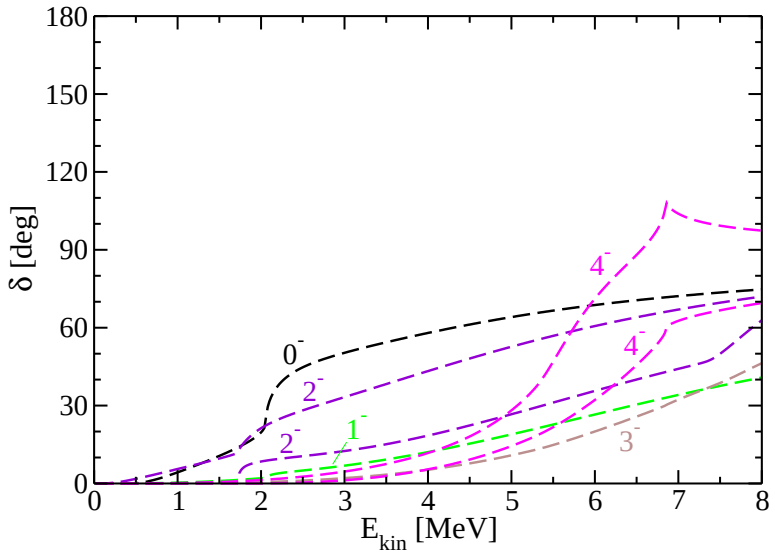

(b)

Figure 7.9: $^7\mathrm{Li} + p$ eigen-phase shifts at $N_{max} = 9$, even (a) and odd (b) parity.

	Energy [MeV]			Excitation Energy [MeV]		
	NCSM	NCSMC	Expt.	NCSM	NCSMC	Expt.
0^+	-15.96	-16.13	-17.25	0.00	0.00	0.00
2^+	-12.51	-12.72	-14.23	3.45	3.41	3.03
4^+	-3.97	-4.31	-5.91	11.99	11.82	11.35
2^+	+0.76	-0.10	-0.63	16.72	16.03	16.63
2^+	+1.09	+0.31	-0.33	17.05	16.44	16.92

Table 7.1: The bound states of ^{8}Be are well reproduced with the NCSMC. One minor exception is that the 3rd 2^+ is slightly above the $^7\mathrm{Li} + p$ threshold.

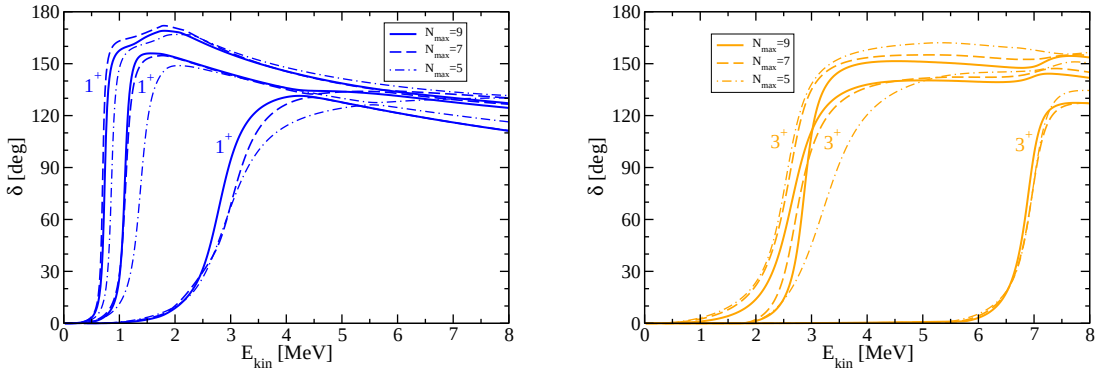

(a) **(b)**

Figure 7.10: Dependence of the $^7\mathrm{Li} + p$ eigen-phase shifts on the NCSMC basis size characterized by N_{max} for the 1^+ (left) and 3^+ (right) resonances. E_{kin} is the kinetic energy of the $^7\mathrm{Li} + p$ in the center of mass frame.

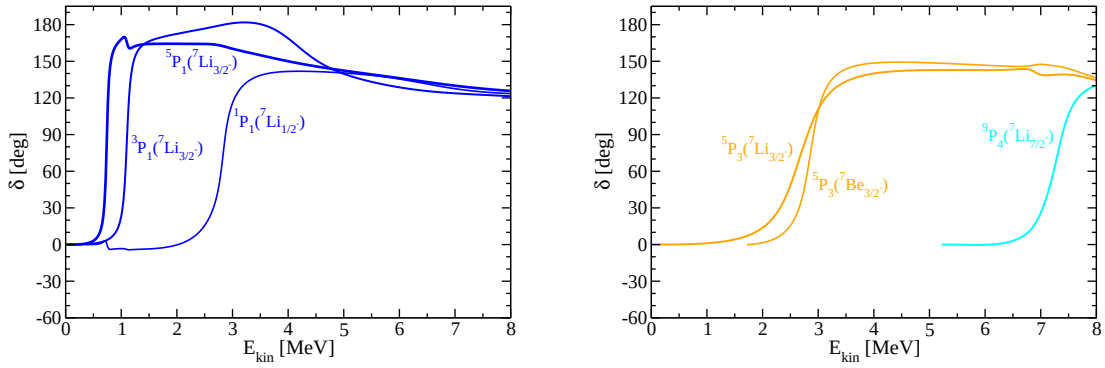

(a) **(b)**

Figure 7.11: Selected P-wave $^7\mathrm{Li} + p$ phase shifts. The $^7\mathrm{Be} + n$ threshold is at 1.64 MeV.

7.2.4 $p + {}^7\mathrm{Li}$ Scattering

The differential and integrated cross sections can be calculated from the full multi-channel S-matrix. These quantities are observables that can be compared to experiments. The cross section is enhanced by the presence of resonances.

Figure 7.12 shows the differential cross section for ${}^7\mathrm{Li}(p,p){}^7\mathrm{Li}$ elastic scattering (meaning ${}^7\mathrm{Li}$ remains in the ground state and so kinetic energy is conserved). The integrated cross section diverges due to the Coulomb repulsion but the differential cross section can be shown at each energy. The dependence of the differential cross-section on N_{max} and the pheno correction is shown. Data from inverse kinematics experiments i.e. $p({}^7\mathrm{Li},{}^7\mathrm{Li})p$ is shown. The lab energy is 5 and 5.44 MeV per nucleon (i.e. ${}^7\mathrm{Li}$ with a beam energy of 35 and 38.1 MeV) [155, 156]. To compare to our calculations dependent on the center of mass energy, we multiply by the ratio with the reduced mass $\frac{7}{8}$: 4.38 and 4.76 MeV. These energies are beyond the point at which phenomenological shifts of the resonances are applied. Our calculations predict a huge number of resonances and their individual contributions to the cross sections has not yet been fully analyzed.

The cross sections for inelastic scattering and transfer reactions are also obtained in our formalism. Results will be compared to data in a future publication.

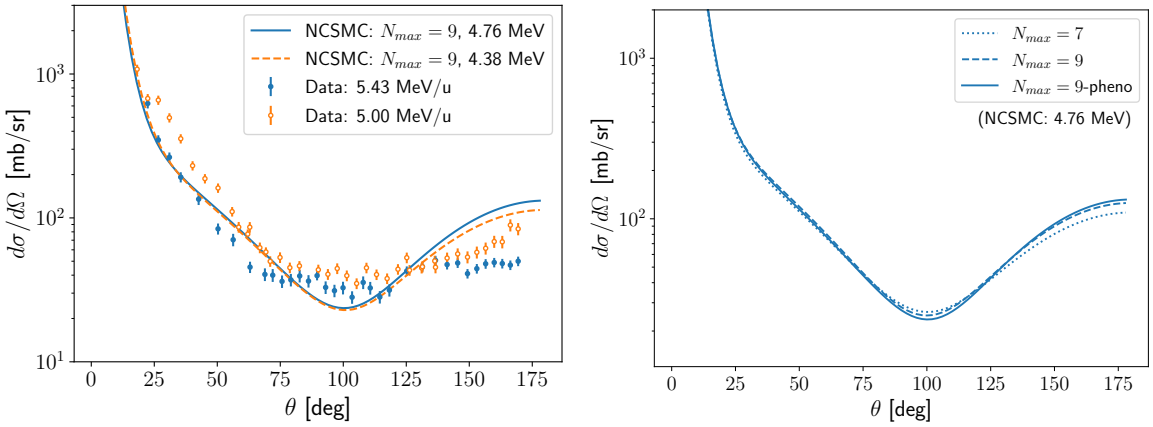

(a) **(b)**

Figure 7.12: The differential cross section for ${}^7\mathrm{Li}(p,p){}^7\mathrm{Li}$ elastic scattering. Θ is the angle between the incoming proton and outgoing proton in the center of mass frame. (a) A comparison between inverse scattering data at 5 and 5.44 MeV/u and NCSMC calculations at the corresponding center of mass energies: $E = 4.38$ and 4.76 MeV. Data from [155, 156]. (b) The convergence of NCSMC calculations at $E = 4.76$ MeV with the input parameter N_{max}.

7.2.5 The ${}^7\mathrm{Li}(p,\gamma){}^8\mathrm{Be}$ Cross Section

Using (6.91) we calculate the radiative capture cross section between the initial cluster scattering state and the first 0^+ and 2^+ ${}^8\mathrm{Be}$ bound states, considering $E1$, $M1$ and $E2$

multipolarities.

For much of the energy range the dominant term in the integrated cross-section is the $E1$ transition strength, corresponding to transitions from the 1^- cluster channels, in the case of transitions to the ground state. However within the 1^+ resonances, the $M1$ transition strength is greatly enhanced. The $E2$ transition strength is negligible at the order of 1%.

In Figure 7.13, we compare the NCSMC predictions of the integrated cross section to an experiment [157]. After phenomenological adjustment the calculations match the data extremely well. The adjustment shifts the position of the peaks but the size of the transition strength is already fairly well predicted, indicating that the *ab initio* wavefunctions are already a reasonably described. We are missing some of the mixing between the T=1 and T=0 resonances, which could be another sign of the insufficiency of the nuclear force.

For completeness, we include the S-factor and phase shifts with the resonances shifted to emphasize the connection between the presence of a resonance and an enhancement in the cross section.

7.2.6 Pair Production and the X17

Attention has been brought to the ^{8}Be system due to recent claims of signals of the discovery of a new BSM particle. Anomalies were observed in the electron-positron pair production from proton capture on ^{7}Li and ^{3}H by the ATOMKI collaboration and interpreted as the decay of a new boson with the mass 17 MeV (hence "X17") [120, 158]. The signal of this new boson is the apparent excess that appears in the data at $\Theta \sim 140^\circ$ in Figure 7.14.

The theory of Section 6.4 has been applied making use of the electromagnetic transition matrix elements calculated with the NCSMC.

Combinations of the E1 and M1 transition strengths can be used to provide an ab initio prediction of the pair distribution. Using the Siegert's theorem, Coulomb matrix elements are replaced with electric multipoles. The E2 is suppressed by additional factors of q and a numerical coefficient $< \frac{1}{100}$.

Unlike [122] we do not fit the E1/M1 ratio but rather predict it. Our prediction is supported by the calculation of radiative capture (Fig. 7.13), the E1 and M1 components are plotted separately in Figure 7.17. In Figure 7.14 the pair production is predicted using approximated transitions, i.e. the bound-bound theory is used as in [122] (but with NCMSC transition strengths inserted into (6.110) with appropriate normalization factors (such that we reproduce the radiative capture cross section through the scaled γ-decay formula)). In this method the 1^+ and 1^- scattering states do not interfere. In Figure 7.14, we compare scaling the predicted curve (as the data is in relative units) to match the data at two different angles characterizing low and high angles. When matched at low angle, the predicted background is much higher than data at high angles. In contrast, when matched at high angle, the predicted background at low angles is lower than the data.

Like in [123] we can include the interference from different partial waves in the scattering

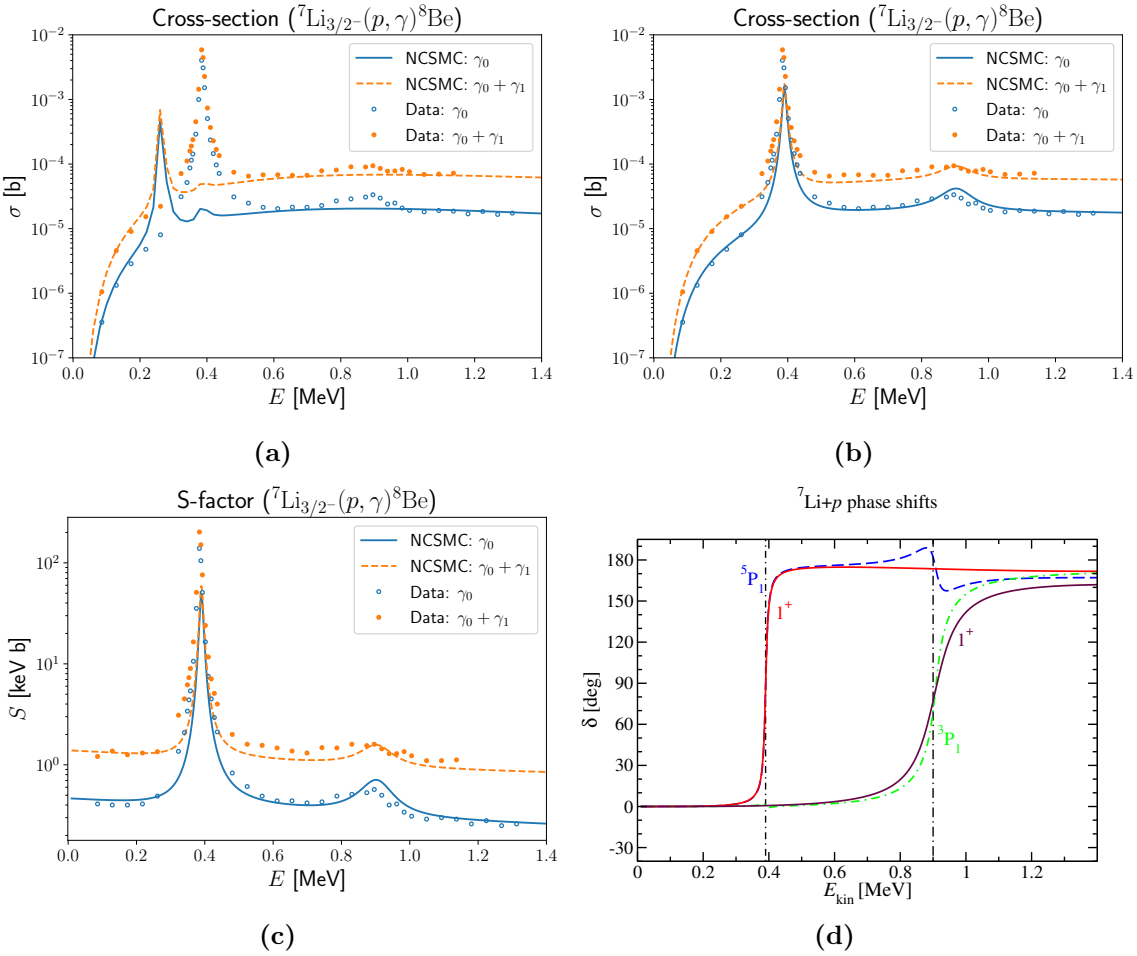

Figure 7.13: The cross-section for $^7\mathrm{Li}(p,\gamma)^8\mathrm{Be}$ capture. (a) The integrated cross section of $^7\mathrm{Li}(p,\gamma)^8\mathrm{Be}$ calculated at $N_{max}=7$ (and without $^7\mathrm{Be}+n$ degrees of freedom). (b) The integrated cross section of $^7\mathrm{Li}(p,\gamma)^8\mathrm{Be}$ calculated at $N_{max}=9$ with phenomenological adjustments. γ_0 is the capture cross-section for proton capture resulting in the ground state of ^{8}Be. γ_1 is the capture cross-section resulting in the first excited state (2^+) of ^{8}Be. Data points are taken from [157]. (c) The $^7\mathrm{Li}(p,\gamma)^8\mathrm{Be}$ astrophysical S-factor (proportional to the cross section in (b) via (7.3)) (d) The phenomenologically adjusted phase shifts at $N_{max}=9$.

state using the full theoretical prediction (6.144). The results are shown in Figure 7.15 and compared against the more approximate method in Figure 7.16. The additional interference terms reduce the cross section at high angles and improve agreement with the data. The difference is less severe when the full range of possible electron-positron energies (in terms of y (6.111)) are included but due to experimental limitations the limited range $-0.5 < y < 0.5$ is better prediction of the observed background rate. This could give some support for the X17 boson claim.

An estimate of the reaction $^7\mathrm{Li}(p, X)^8\mathrm{Be}$ was calculated with three X17 candidates: a pseudoscalar [129], axial vector [130] and vector [126]. The cross section is computed by substituting a leading-order operator in the long-wavelength approximation into the formula for radiative capture (6.91). The results are shown in Figure 7.17.

We estimate the $^7\mathrm{Li}(p, e^+e^-)^8\mathrm{Be}$ cross section by integration of the bound-bound formula. It is essentially proportional to the γ-emitting proton-capture cross section with its magnitude scaled by a factor of $\sim \alpha/2\pi \sim 10^{-3}$. It is understandable that no anomaly would be observed at the first resonance which is swamped by the very high electromagnetic M1 rate. The effect from the hypothetical X17 boson would be expected at second resonance in the case of a pseudoscalar or axial vector character. Any anomaly present between the resonances would be consistent with a vector particle and is the preferred candidate in the most recent ATOMKI publications [159].

The claims of new BSM physics have spurred the development of new experimental programs to search for corroborating evidence. One example at TRIUMF is the DarkLight experiment which will be installed in the new ARIEL e-linac beam hall. Another is the NewJEDI program at several facilities in Europe which has begun taking data.

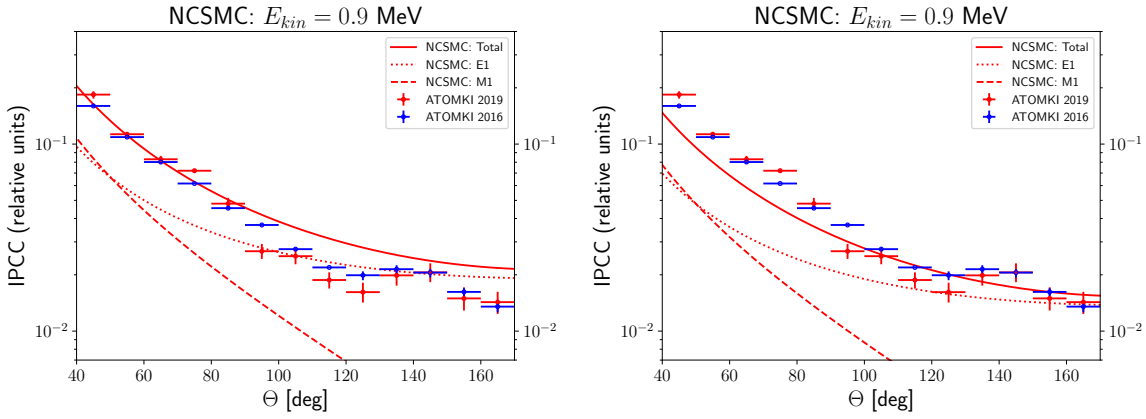

Figure 7.14: The pair creation distribution calculated with NCSMC transition strengths but using the bound-bound formula and compared to the ATOMKI data [160]. The calculation are scaled to match data (a): at 65 degrees, (b): at 105 degrees. The dimensionless parameter y (6.111) is integrated from -0.5 to 0.5 as in [122, 123]. The E1 (1^-) and M1 (1^+) contributions are displayed.

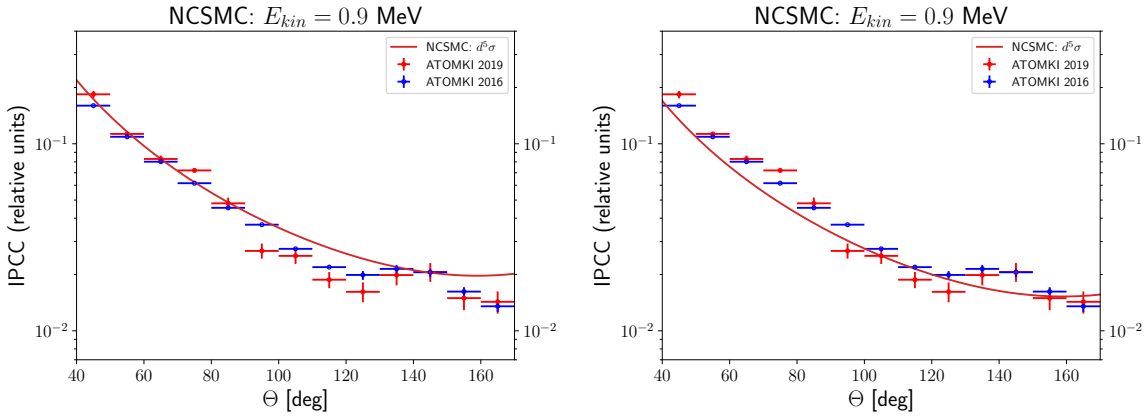

Figure 7.15: The pair creation distribution calculating with the full continuum-bound formula and compared to the ATOMKI data [160]. The calculation are scaled to match data (a): at 65 degrees, (b): at 105 degrees. The dimensionless parameter y (6.111) is integrated from -0.5 to 0.5 as in [122, 123].

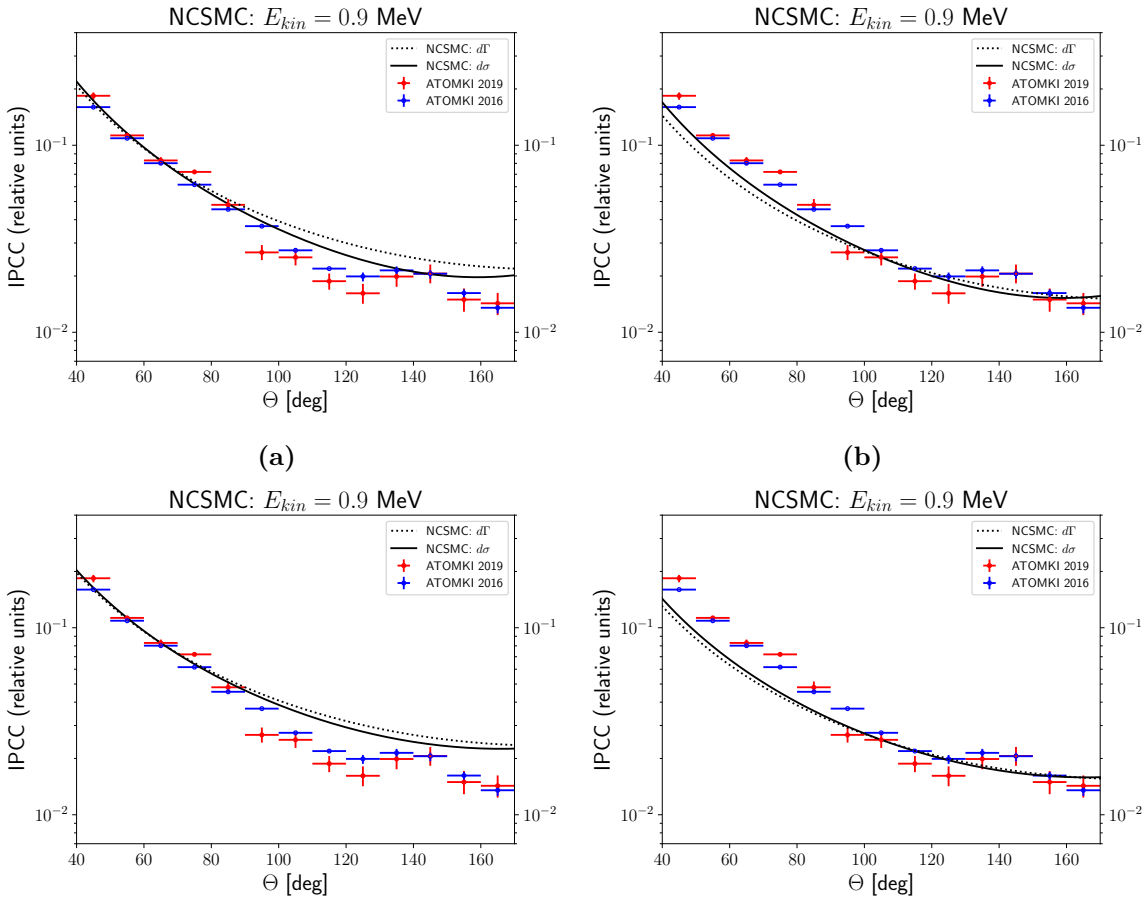

Figure 7.16: The comparison between approximate (Γ) and full calculations (σ). In (a,b) y is integrated from -0.5 to 0.5 and in (c,d) y is integrated from $-(1-\frac{2m_e}{\omega})$ to $1-\frac{2m_e}{\omega}$.

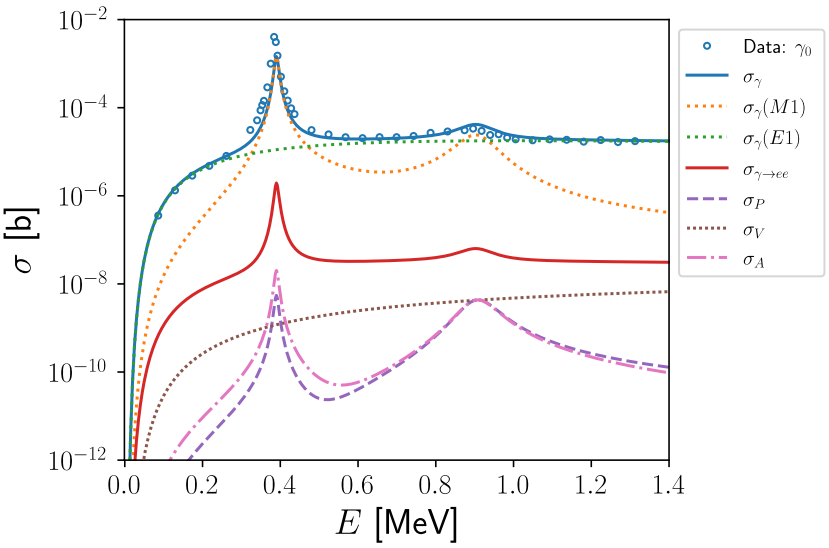

Figure 7.17: The integrated cross section of various X17 candidates vs the standard radiative capture cross section. Interferences between γ and X are not included. The electron-positron integrated cross section is based on a numerical integral of the bound-bound formula. The coupling constants are approximated based on [161], which scales the operators based on the strength of the signal in the 2016/2019 data [160].

Chapter 8

Conclusions

Ab initio techniques in nuclear theory allow accurate predictions of nuclear structure, decays and reactions. The NCSM is one such technique and accurately calculates the spectrum of bound states and β-decay rates in many light nuclei.

Demonstrated in this thesis were predictions for the rates of GT β-decay transitions. Through collaboration with practitioners of more approximate *ab initio* methods, we could compute the nuclear transition rates for nuclei over a much wider range of masses. The inclusion of two-body currents, more sophisticated many-body calculations and consistent SRG evolution resulted in nuclear transition matrix elements that were consistently more agreeable with experiments than the phenomenological shell model. This provided a resolution to the historical discrepancy between theory and experiment in strong GT transitions, removing the necessity of applying a quenching factor to the weak coupling constant g_A.

In the $^6\mathrm{He} \to {}^6\mathrm{Li}$ transition, we demonstrated that there are nuclear structure corrections to the leading-order β-decay operator that must be taken into account in experiments which measure the distribution of the emitted electrons. The level of precision in current and future experiments is such that these higher-order effects will be detected and must not be mistaken for new BSM physics.

In addition, using the NCSM, we provided benchmarks of $0\nu\beta\beta$ nuclear transition matrix elements for several light nuclei, as a test for the *ab initio* methods of coupled-cluster and IMSRG. The NCSM generally supports coupled-cluster calculations which use deformed reference states, while IMSRG matrix elements are often larger. The coupled-cluster and IMSRG methods were used to predict the matrix element for the experimental candidate ^{48}Ca. These methods also provide predictions for ^{76}Ge and in the future will also calculate ^{136}Xe, providing several avenues to study neutrino physics through this decay mode.

Extensions to the NCSM, like NCSMC, provide access to an even greater range of phenomena i.e. scattering and reactions, while simultaneously improving the description of weakly bound states.

In this thesis, we calculated properties of the $^4\mathrm{He} + d$ system, culminating in the prediction of the cross section for the radiative capture reaction $^4\mathrm{He}(d,\gamma)^6\mathrm{Li}$. We revealed that

a fully microscopic approach is needed to achieve the important $M1$ contributions to the cross section. Our calculations provided state of the art predictions for the astrophysical S-factor in the BBN energy range and reduced the uncertainty on predictions of the thermonuclear reaction rate. This result indicates that the uncertainty in this reaction rate is not the reason for the discrepancy between prediction and observation of the cosmological ^{6}Li abundance.

We also calculated properties of the $^7\mathrm{Li} + p$ system, including both ^{8}Be states and the possibility of nucleon exchange to $n + {}^7$Be. The description of ^{8}Be states was improved compared to existing NCSM calculations. In addition, the 1^+ resonances above the $^7\mathrm{Li} + p$ threshold were reproduced. This culminated in the prediction of the radiative capture cross section $^7\mathrm{Li}(p,\gamma)^8\mathrm{Be}$ as well as novel extensions: $^7\mathrm{Li}(p,e^+e^-)^8\mathrm{Be}$ and $^7\mathrm{Li}(p,X)^8\mathrm{Be}$. The standard radiative capture reaction could be calculated in a agreement with experiments. The radiative capture with pair production was first calculated in a simplified bound-to-bound-like formalism summing up separate electric and magnetic contributions in agreement with other theoretical predictions. We demonstrated that a full-continuum calculation that takes into account the interference between different multipoles improves agreement with the observed pair-production distribution in the ATOMKI $^7\mathrm{Li}(p,e^+e^-)^8\mathrm{Be}$ experiments.

The developments in this work leave much room for further study. For example, SRG evolution should be applied to q-dependent β-decay operators and the $0\nu\beta\beta$ contact operator. The more accurate q-dependent multipole operators will be used in future calculations of beta decays and electromagnetic observables. In particular nuclear structure corrections to Fermi decays and GT transitions of heavier nuclei, for example supporting measurements of ^{23}Ne decay [162].

In addition, the calculations of deuteron and proton capture presented here are the starting point towards application of the NCSMC to many more reactions. The $A = 8$ NCSMC calculations presented here contain the information needed to extract the rates of the transfer reactions $^7\mathrm{Li}(p,n)^7\mathrm{Be}$ and $^7\mathrm{Be}(n,p)^7\mathrm{Li}$, which can be compared to experiment. The highly-complex spectrum of ^{8}Be will be investigated through the effects of resonances in scattering and reactions. Finally, the new capability to calculate electron-positron pair production and the emission of hypothetical particles will allow the investigation of similar anomalies in the $^3\mathrm{H}(p,e^+e^-)^4\mathrm{He}$ [163] and $^{11}\mathrm{B}(p,e^+e^-)^{12}\mathrm{C}$ [164] reactions. These calculations of the Standard Model background may form the basis for comparison to the claims of the discovery of new particles.

Bibliography

[1] P. Gysbers, G. Hagen, J. D. Holt, G. R. Jansen, T. D. Morris, P. Navrátil, T. Papenbrock, S. Quaglioni, A. Schwenk, S. R. Stroberg, and K. A. Wendt. Discrepancy between experimental and theoretical β-decay rates resolved from first principles. *Nature Physics*, 15, 2019. → pages v, xiii, xiv, 63, 64, 66, 67, 68

[2] Ayala Glick-Magid, Christian Forssén, Daniel Gazda, Doron Gazit, Peter Gysbers, and Petr Navrátil. Nuclear ab initio calculations of 6he β-decay for beyond the standard model studies. *Physics Letters B*, 832:137259, 2022. → pages v, xiv, xv, 52, 69, 70, 71

[3] S. Novario, P. Gysbers, J. Engel, G. Hagen, G. R. Jansen, T. D. Morris, P. Navrátil, T. Papenbrock, and S. Quaglioni. Coupled-cluster calculations of neutrinoless double-β decay in ^{48}Ca. *Phys. Rev. Lett.*, 126:182502, May 2021. → pages v, vi, xv, 72, 73, 74

[4] C. Hebborn, G. Hupin, K. Kravvaris, S. Quaglioni, P. Navrátil, and P. Gysbers. Ab initio prediction of the $^4\mathrm{He}(d,\gamma)^6\mathrm{Li}$ big bang radiative capture. *Phys. Rev. Lett.*, 129:042503, Jul 2022. → pages v, vi

[5] Jason Crawford. I walk the (beta-stability) line: How counting neutrons explains nuclear waste. https://rootsofprogress.org/nuclear-physics, 2021. Accessed: 2022-10-29. → pages xi, 2

[6] Colorful nuclide chart. https://people.physics.anu.edu.au/~ecs103/chart. Accessed: 2022-10-29. → pages xi, 2

[7] Bruce R. Barrett, Petr Navrátil, and James P. Vary. Ab initio no core shell model. *Progress in Particle and Nuclear Physics*, 69:131 – 181, 2013. → pages 3, 28

[8] J. Carlson, S. Gandolfi, F. Pederiva, Steven C. Pieper, R. Schiavilla, K. E. Schmidt, and R. B. Wiringa. Quantum monte carlo methods for nuclear physics. *Rev. Mod. Phys.*, 87:1067–1118, Sep 2015. → page 3

[9] G. Hagen, T. Papenbrock, D. J. Dean, and M. Hjorth-Jensen. *Ab initio* coupled-cluster approach to nuclear structure with modern nucleon-nucleon interactions. *Phys. Rev. C*, 82:034330, Sep 2010. → page 3

[10] H. Hergert, S.K. Bogner, T.D. Morris, A. Schwenk, and K. Tsukiyama. The in-medium similarity renormalization group: A novel ab initio method for nuclei. *Physics Reports*, 621:165–222, 2016. Memorial Volume in Honor of Gerald E. Brown. → pages 3, 74

[11] David J. Griffiths. *Introduction to Elementary Particles*. Wiley-VCH, Weinheim, Germany, 2nd rev. edition, 2008. → pages xvi, 3, 22, 36, 37, 47, 79, 90

[12] David Morrissey. Course notes - physics 528: Elementary particle physics, 2019. → page 3

[13] Mark A. Srednicki. *Quantum field theory*. Cambridge University Press, Cambridge, 2007. → pages 3, 38

[14] M.E. Peskin and D.V. Schroeder. *An Introduction to Quantum Field Theory*. Advanced book classics. Avalon Publishing, 1995.

[15] Matthew D. Schwartz. *Quantum Field Theory and the Standard Model*. Cambridge University Press, 2013.

[16] C. P. Burgess, Guy D. Moore, and Cambridge Core EBA eBooks Complete Collection. *The standard model: a primer*. Cambridge University Press, Cambridge;New York;, 2007;2006;. → page 3

[17] The standard model of elementary particles. https://en.wikipedia.org/wiki/File:Standard_Model_of_Elementary_Particles.svg, 2019. Accessed: 2022-10-29. → pages xi, 4

[18] Particle data group. https://pdg.lbl.gov/, 2022. → pages xi, 4

[19] Eite Tiesinga, Peter J. Mohr, David B. Newell, and Barry N. Taylor. Codata recommended values of the fundamental physical constants: 2018. *Rev. Mod. Phys.*, 93:025010, Jun 2021. → pages 5, 14, 48

[20] Standard Model - All Feynman diagram vertices, 2021. Accessed: 2023-03-06. → pages xi, 5

[21] Jack Lindon. *Particle Collider Probes of Dark Energy, Dark Matter and Generic Beyond Standard Model Signatures in Events With an Energetic Jet and Large Missing Transverse Momentum Using the ATLAS Detector at the LHC*. PhD thesis, University of Birmingham, 2020. Presented 30 Oct 2020. → pages xi, 5

[22] ATLAS Collaboration. Observation of a new particle in the search for the standard model higgs boson with the atlas detector at the lhc. *Physics Letters B*, 716(1):1–29, 2012. → page 7

[23] CMS Collaboration. Observation of a new boson at a mass of 125 gev with the cms experiment at the lhc. *Physics Letters B*, 716(1):30–61, 2012. → page 7

[24] S. R. Beane, W. Detmold, K. Orginos, and M. J. Savage. Nuclear Physics from Lattice QCD. *Prog. Part. Nucl. Phys.*, 66:1–40, 2011. → page 7

[25] E. Epelbaum, Ulf-G Meibner, and H. . Hammer. Modern theory of nuclear forces. *Reviews of modern physics*, 81(4):1773–1825, 2009. → page 7

[26] V. BERNARD, N. KAISER, and ULF-G. MEIßNER. CHIRAL DYNAMICS IN NUCLEONS AND NUCLEI. *International Journal of Modern Physics E*, 04(02):193–344, jun 1995. → page 8

[27] S. Weinberg. Effective chiral lagrangians for nucleon-pion interactions and nuclear forces. *Nuclear Physics B*, 363(1):3–18, 1991. → page 8

[28] D. R. Entem and R. Machleidt. Accurate charge-dependent nucleon-nucleon potential at fourth order of chiral perturbation theory. *Phys. Rev. C*, 68:041001, Oct 2003. → pages xvi, 8, 110, 112

[29] Evgeny Epelbaum, Hermann Krebs, and Patrick Reinert. High-precision nuclear forces from chiral eft: State-of-the-art, challenges, and outlook. *Frontiers in Physics*, 8, 2020. → pages xii, 8

[30] R. Machleidt and D. R. Entem. Chiral effective field theory and nuclear forces. *Physics Reports*, 503:1–75, June 2011. → page 8

[31] Steven Weinberg. Nuclear forces from chiral lagrangians. *Physics Letters B*, 251(2):288–292, 1990. → page 10

[32] Steven Weinberg. Phenomenological lagrangians. *Physica A: Statistical Mechanics and its Applications*, 96(1):327–340, 1979. → page 10

[33] R. J. Furnstahl, N. Klco, D. R. Phillips, and S. Wesolowski. Quantifying truncation errors in effective field theory. *Phys. Rev. C*, 92:024005, Aug 2015. → page 10

[34] Stefan Schulz. *Four-Nucleon Forces in Ab Initio Nuclear Structure*. PhD thesis, der Technischen Universität Darmstadt, 2018. → page 11

[35] D. A. Varshalovich, A. N. Moskalev, and V. K. Khersonskii. *Quantum Theory of Angular Momentum: Irreducible Tensors, Spherical Harmonics, Vector Coupling Coefficients, 3nj Symbols*. World Scientific, Singapore, 1988. → pages x, 15, 19, 106, 144, 147

[36] David J. Griffiths. *Introduction to Quantum Mechanics*. Pearson Prentice Hall, Upper Saddle River NJ, 2nd edition, 2005. → pages 15, 78, 81

[37] Roger D. Woods and David S. Saxon. Diffuse surface optical model for nucleon-nuclei scattering. *Phys. Rev.*, 95:577–578, Jul 1954. → page 17

[38] Maria Goeppert Mayer and J. Hans D. Jensen. *Elementary Theory of Nuclear Shell Structure*. Wiley, New York, 1955. → page 18

[39] Kenneth S. Krane. *Introductory Nuclear Physics*. John Wiley & Sons, New York, 1988. → page 18

[40] Jouni Suhonen. *From Nucleons to Nucleus: Concepts of Microscopic Nuclear Theory*. Springer, Berlin, Germany, 2007. → pages 19, 20, 148

[41] A. R. Edmonds. *Angular Momentum in Quantum Mechanics*. Princeton University Press, Princeton NJ, 1960. → pages 21, 144

[42] D.J. Rowe and Wood J. L. *Fundamentals of Nuclear Models: Foundational Models*. World Scientific, 2010. → page 25

[43] B. Alex Brown. Lecture notes in nuclear structure physics, 2010. → page 25

[44] Marcos Moshinsky. Transformation brackets for harmonic oscillator functions. *Nuclear Physics*, 13(1):104–116, 1959. → pages 26, 27

[45] G. P. Kamuntavičius, R. K. Kalinauskas, B. R. Barrett, S. Mickevičius, and D. Germanas. The general harmonic-oscillator brackets: compact expression, symmetries, sums and fortran code. *Nuclear physics. A*, 695(1):191–201, 2001. → page 27

[46] P. Navrátil, G. P. Kamuntavičius, and B. R. Barrett. Few-nucleon systems in a translationally invariant harmonic oscillator basis. *Phys. Rev. C*, 61:044001, Mar 2000. → page 27

[47] L. Trlifaj. Simple formula for the general oscillator brackets. *Phys. Rev. C*, 5:1534–1539, May 1972. → page 27

[48] Mark A. Pinsky. *Introduction to Fourier Analysis and Wavelets*. American Mathematical Society, Providence RI, 2002. → page 30

[49] D.H. Gloeckner and R.D. Lawson. Spurious center-of-mass motion. *Physics Letters B*, 53(4):313–318, 1974. → page 30

[50] C. Lanczos. An iteration method for the solution of the eigenvalue problem of linear differential and integral operators. *Journal of Research of the National Bureau of Standards*, 45:255–282, 1950. → page 30

[51] Mark A Caprio, Anna E McCoy, and Patrick J Fasano. Intrinsic operators for the translationally-invariant many-body problem. *Journal of Physics G: Nuclear and Particle Physics*, 47(12):122001, oct 2020. → page 32

[52] Petr Navrátil. Translationally invariant matrix elements of general one-body operators. *Phys. Rev. C*, 104:064322, Dec 2021. → page 33

[53] A. I. Akhiezer, A. G. Sitenko, and V. K. Tarkovskii. *Nuclear Electrodynamics*. Springer-Verlag, Berlin, Germany, 1994. → pages 34, 37, 39, 98, 145, 150

[54] J. D. Walecka. *Theoretical Nuclear and Subnuclear Physics*. World Scientific, Singapore, 2nd edition, 2004. → pages 34, 35, 47, 50, 92, 152

[55] R. P. Feynman. The theory of positrons. *Phys. Rev.*, 76:749–759, Sep 1949. → page 37

[56] T. Jr de Forest and J. D. Walecka. Electron scattering and nuclear structure. *Advances in Physics: A Quarterly Supplement of the Philosophical Magazine*, 15:1–109, Jan 1966. → pages 38, 43, 96

[57] Doron Gazit. *Electro-Weak Interactions in Light Nuclei*. PhD thesis, The Hebrew University, 2008. → pages 44, 51, 64, 150

[58] U. Friman-Gayer, C. Romig, T. Hüther, K. Albe, S. Bacca, T. Beck, M. Berger, J. Birkhan, K. Hebeler, O. J. Hernandez, J. Isaak, S. König, N. Pietralla, P. C. Ries, J. Rohrer, R. Roth, D. Savran, M. Scheck, A. Schwenk, R. Seutin, and V. Werner. Role of chiral two-body currents in ^{6}Li magnetic properties in light of a new precision measurement with the relative self-absorption technique. *Phys. Rev. Lett.*, 126:102501, Mar 2021. → page 45

[59] Doron Gazit, Sofia Quaglioni, and Petr Navrátil. Three-nucleon low-energy constants from the consistency of interactions and currents in chiral effective field theory. *Phys. Rev. Lett.*, 103:102502, Sep 2009. → page 51

[60] Doron Gazit, Sofia Quaglioni, and Petr Navrátil. Erratum: Three-nucleon low-energy constants from the consistency of interactions and currents in chiral effective field theory [phys. rev. lett. 103, 102502 (2009)]. *Phys. Rev. Lett.*, 122:029901, Jan 2019. → pages xvi, 51, 64, 109, 110, 112

[61] P Venkataramaiah, K Gopala, A Basavaraju, S S Suryanarayana, and H Sanjeeviah. A simple relation for the fermi function. *Journal of Physics G: Nuclear Physics*, 11(3):359, mar 1985. → page 52

[62] Ayala Glick-Magid and Doron Gazit. Multipole decomposition of tensor interactions of fermionic probes with composite particles and bsm signatures in nuclear reactions, 2022. → page 52

[63] A.S. Barabash. Average and recommended half-life values for two-neutrino double beta decay. *Nuclear Physics A*, 935:52–64, 2015. → page 52

[64] Andrea Giuliani and Alfredo Poves. Neutrinoless double-beta decay. *Advances in high energy physics*, 2012:1–38, 2012. → page 53

[65] Masaru Doi, Tsuneyuki Kotani, and Eiichi Takasugi. Double Beta Decay and Majorana Neutrino. *Progress of Theoretical Physics Supplement*, 83:1–175, 03 1985. → pages 53, 54

[66] J. Menéndez, A. Poves, E. Caurier, and F. Nowacki. Disassembling the nuclear matrix elements of the neutrinoless $\beta\beta$ decay. *Nuclear Physics A*, 818(3):139–151, 2009. → pages xv, 53, 74

[67] Vincenzo Cirigliano, Wouter Dekens, Jordy de Vries, Michael L. Graesser, Emanuele Mereghetti, Saori Pastore, and Ubirajara van Kolck. New leading contribution to neutrinoless double-β decay. *Phys. Rev. Lett.*, 120:202001, May 2018. → pages 54, 72

[68] V. Cirigliano, W. Dekens, J. de Vries, M. L. Graesser, E. Mereghetti, S. Pastore, M. Piarulli, U. van Kolck, and R. B. Wiringa. Renormalized approach to neutrinoless double-β decay. *Phys. Rev. C*, 100:055504, Nov 2019. → page 54

[69] C. G. Payne. Ab initio theory for two-neutrino and neutrinoless double-beta decay. Master's thesis, University of British Columbia, 2018. → page 54

[70] T Tomoda. Double beta decay. *Reports on Progress in Physics*, 54(1):53, jan 1991. → page 54

[71] R. A. Sen'kov and M. Horoi. Neutrinoless double-β decay of ^{48}Ca in the shell model: Closure versus nonclosure approximation. *Phys. Rev. C*, 88:064312, Dec 2013. → pages xv, 54, 74

[72] R.J. Furnstahl. The renormalization group in nuclear physics. *Nuclear Physics B - Proceedings Supplements*, 228:139–175, 2012. "Physics at all scales: The Renormalization Group" Proceedings of the 49th Internationale Universitätswochen für Theoretische Physik. → pages xii, 56, 58, 61

[73] Angelo Calci. *Evolved Chiral Hamiltonians at the Three-Body Level and Beyond.* PhD thesis, der Technischen Universität Darmstadt, 2014. → page 57

[74] Micah D. Schuster, Sofia Quaglioni, Calvin W. Johnson, Eric D. Jurgenson, and Petr Navrátil. Operator evolution for ab initio theory of light nuclei. *Phys. Rev. C*, 90:011301, Jul 2014. → pages 58, 113

[75] E. R. Anderson, S. K. Bogner, R. J. Furnstahl, and R. J. Perry. Operator evolution via the similarity renormalization group: The deuteron. *Physical Review C*, 82(5), Nov 2010. → page 59

[76] S. K. Bogner, R. J. Furnstahl, and R. J. Perry. Similarity renormalization group for nucleon-nucleon interactions. *Physical Review C*, 75(6), Jun 2007. → page 59

[77] M. R. Bhat. Evaluated Nuclear Structure Data File (ENSDF). In S. M. Qaim, editor, *Nuclear Data for Science and Technology*, page 817. Springer-Verlag, 1992. → pages xiii, 67

[78] G. Martínez-Pinedo, A. Poves, E. Caurier, and A. P. Zuker. Effective g_A in the pf shell. *Phys. Rev. C*, 53:R2602–R2605, Jun 1996. → pages xiii, 67

[79] B. Alex Brown and W. A. Richter. New "USD" Hamiltonians for the *sd* shell. *Phys. Rev. C*, 74:034315, Sep 2006. → pages xiii, 67

[80] C. B. Hinke, M. Böhmer, P. Boutachkov, T. Faestermann, H. Geissel, J. Gerl, R. Gernhäuser, M. Gorska, A. Gottardo, H. Grawe, J. L. Grebosz, R. Krücken, N. Kurz, Z. Liu, L. Maier, F. Nowacki, S. Pietri, Zs. Podolyák, K. Sieja, K. Steiger, K. Straub, H. Weick, H.-J. Wollersheim, P. J. Woods, N. Al-Dahan, N. Alkhomashi, A. Atac, A. Blazhev, N. F. Braun, I. T. Celikovic, T. Davinson, I. Dillmann, C. Domingo-Pardo, P. C. Doornenbal, G. de France, G. F. Farrelly, F. Farinon, N. Goel, T. C. Habermann, R. Hoischen, R. Janik, M. Karny, A. Kaskas, I. M. Kojouharov, Th. Kröll, Y. Litvinov, S. Myalski, F. Nebel, S. Nishimura, C. Nociforo, J. Nyberg, A. R. Parikh, A. Prochazka, P. H. Regan, C. Rigollet, H. Schaffner, C. Scheidenberger, S. Schwertel, P.-A. Söderström, S. J. Steer, A. Stolz, and P. Strmen. Superallowed Gamow-Teller decay of the doubly magic nucleus ^{100}Sn. *Nature*, 486(7403):341–345, jun 2012. → pages xiv, 68

[81] Batist, L., Górska, M., Grawe, H., Janas, Z., Kavatsyuk, M., Karny, M., Kirchner, R., La Commara, M., Mukha, I., Plochocki, A., and Roeckl, E. Systematics of Gamow-Teller beta decay Southeast of ^{100}Sn. *Eur. Phys. J. A*, 46(1):45–53, 2010. → pages xiv, 68

[82] D. Gazda, R. Catena, and C. Forssén. Ab initio nuclear response functions for dark matter searches. *Phys. Rev. D*, 95:103011, May 2017. → page 69

[83] A. Ekström, G. Baardsen, C. Forssén, G. Hagen, M. Hjorth-Jensen, G. R. Jansen, R. Machleidt, W. Nazarewicz, T. Papenbrock, J. Sarich, and S. M. Wild. Optimized chiral nucleon-nucleon interaction at next-to-next-to-leading order. *Phys. Rev. Lett.*, 110:192502, May 2013. → page 69

[84] A. Ekström, G. R. Jansen, K. A. Wendt, G. Hagen, T. Papenbrock, B. D. Carlsson, C. Forssén, M. Hjorth-Jensen, P. Navrátil, and W. Nazarewicz. Accurate nuclear

radii and binding energies from a chiral interaction. *Phys. Rev. C*, 91:051301, May 2015. → page 69

[85] G. Anton, I. Badhrees, P. S. Barbeau, D. Beck, V. Belov, T. Bhatta, M. Breidenbach, T. Brunner, G. F. Cao, W. R. Cen, C. Chambers, B. Cleveland, M. Coon, A. Craycraft, T. Daniels, M. Danilov, L. Darroch, S. J. Daugherty, J. Davis, S. Delaquis, A. Der Mesrobian-Kabakian, R. DeVoe, J. Dilling, A. Dolgolenko, M. J. Dolinski, J. Echevers, W. Fairbank, D. Fairbank, J. Farine, S. Feyzbakhsh, P. Fierlinger, D. Fudenberg, P. Gautam, R. Gornea, G. Gratta, C. Hall, E. V. Hansen, J. Hoessl, P. Hufschmidt, M. Hughes, A. Iverson, A. Jamil, C. Jessiman, M. J. Jewell, A. Johnson, A. Karelin, L. J. Kaufman, T. Koffas, R. Krücken, A. Kuchenkov, K. S. Kumar, Y. Lan, A. Larson, B. G. Lenardo, D. S. Leonard, G. S. Li, S. Li, Z. Li, C. Licciardi, Y. H. Lin, R. MacLellan, T. McElroy, T. Michel, B. Mong, D. C. Moore, K. Murray, O. Njoya, O. Nusair, A. Odian, I. Ostrovskiy, A. Piepke, A. Pocar, F. Retière, A. L. Robinson, P. C. Rowson, D. Ruddell, J. Runge, S. Schmidt, D. Sinclair, A. K. Soma, V. Stekhanov, M. Tarka, J. Todd, T. Tolba, T. I. Totev, B. Veenstra, V. Veeraraghavan, P. Vogel, J.-L. Vuilleumier, M. Wagenpfeil, J. Watkins, M. Weber, L. J. Wen, U. Wichoski, G. Wrede, S. X. Wu, Q. Xia, D. R. Yahne, L. Yang, Y.-R. Yen, O. Ya. Zeldovich, and T. Ziegler. Search for neutrinoless double-β decay with the complete exo-200 dataset. *Phys. Rev. Lett.*, 123:161802, Oct 2019. → page 72

[86] M. Agostini, A. M. Bakalyarov, M. Balata, I. Barabanov, L. Baudis, C. Bauer, E. Bellotti, S. Belogurov, A. Bettini, L. Bezrukov, D. Borowicz, V. Brudanin, R. Brugnera, A. Caldwell, C. Cattadori, A. Chernogorov, T. Comellato, V. D'Andrea, E. V. Demidova, N. Di Marco, A. Domula, E. Doroshkevich, V. Egorov, R. Falkenstein, M. Fomina, A. Gangapshev, A. Garfagnini, M. Giordano, P. Grabmayr, V. Gurentsov, K. Gusev, J. Hakenmüller, A. Hegai, M. Heisel, S. Hemmer, R. Hiller, W. Hofmann, M. Hult, L. V. Inzhechik, J. Janicskó Csáthy, J. Jochum, M. Junker, V. Kazalov, Y. Kermaïdic, T. Kihm, I. V. Kirpichnikov, A. Kirsch, A. Kish, A. Klimenko, R. Kneißl, K. T. Knöpfle, O. Kochetov, V. N. Kornoukhov, P. Krause, V. V. Kuzminov, M. Laubenstein, A. Lazzaro, M. Lindner, I. Lippi, A. Lubashevskiy, B. Lubsandorzhiev, G. Lutter, C. Macolino, B. Majorovits, W. Maneschg, M. Miloradovic, R. Mingazheva, M. Misiaszek, P. Moseev, I. Nemchenok, K. Panas, L. Pandola, K. Pelczar, L. Pertoldi, P. Piseri, A. Pullia, C. Ransom, S. Riboldi, N. Rumyantseva, C. Sada, E. Sala, F. Salamida, C. Schmitt, B. Schneider, S. Schönert, A.-K. Schütz, O. Schulz, M. Schwarz, B. Schwingenheuer, O. Selivanenko, E. Shevchik, M. Shirchenko, H. Simgen, A. Smolnikov, L. Stanco, D. Stukov, L. Vanhoefer, A. A. Vasenko, A. Veresnikova, K. von Sturm, V. Wagner, A. Wegmann, T. Wester, C. Wiesinger, M. Wojcik, E. Yanovich, I. Zhitnikov, S. V. Zhukov, D. Zinatulina, A. Zschocke, A. J. Zsigmond, K. Zuber, G. Zuzel, and GERDA Collaboration. Probing majorana neutrinos with double-β decay. *Science*, 365(6460):1445–1448, 2019.

[87] S. I. Alvis, I. J. Arnquist, F. T. Avignone, A. S. Barabash, C. J. Barton, V. Basu, F. E. Bertrand, B. Bos, M. Busch, M. Buuck, T. S. Caldwell, Y-D. Chan, C. D. Christofferson, P.-H. Chu, M. Clark, C. Cuesta, J. A. Detwiler, Yu. Efremenko, H. Ejiri, S. R. Elliott, T. Gilliss, G. K. Giovanetti, M. P. Green, J. Gruszko, I. S. Guinn, V. E. Guiseppe, C. R. Haufe, R. J. Hegedus, L. Hehn, R. Henning,

D. Hervas Aguilar, E. W. Hoppe, M. A. Howe, M. F. Kidd, S. I. Konovalov, R. T. Kouzes, A. M. Lopez, R. D. Martin, R. Massarczyk, S. J. Meijer, S. Mertens, J. Myslik, G. Othman, W. Pettus, A. Piliounis, A. W. P. Poon, D. C. Radford, J. Rager, A. L. Reine, K. Rielage, N. W. Ruof, B. Shanks, M. Shirchenko, D. Tedeschi, R. L. Varner, S. Vasilyev, B. R. White, J. F. Wilkerson, C. Wiseman, W. Xu, E. Yakushev, C.-H. Yu, V. Yumatov, I. Zhitnikov, and B. X. Zhu. Search for neutrinoless double-β decay in ^{76}Ge with 26 kg yr of exposure from the majorana demonstrator. *Phys. Rev. C*, 100:025501, Aug 2019. → page 72

[88] I. Ogawa, R. Hazama, H. Miyawaki, S. Shiomi, N. Suzuki, Y. Ishikawa, G. Kunitomi, Y. Tanaka, M. Itamura, K. Matsuoka, S. Ajimura, T. Kishimoto, H. Ejiri, N. Kudomi, K. Kume, H. Ohsumi, and K. Fushimi. Search for neutrino-less double beta decay of 48ca by caf2 scintillator. *Nuclear Physics A*, 730(1):215–223, 2004. → page 72

[89] K. Tetsuno, S. Ajimura, K. Akutagawa, T. Batpurev, W. M. Chan, K. Fushimi, R. Hazama, T. Iida, Y. Ikeyama, B. T. Khai, T. Kishimoto, K. K. Lee, X. Li, K. Matsuoka, K. Matsuoka, K. Mizukoshi, Y. Mori, K. Nakajima, P. Noithong, M. Nomachi, I. Ogawa, H. Ohsumi, K. Ozawa, K. Shimizu, M. Shokati, F. Soberi, K. Suzuki, Y. Takemoto, Y. Takihira, Y. Tamagawa, M. Tozawa, V. T. T. Trang, S. Umehara, K. Yamamoto, S. Yoshida, A : CANDLES collaboration, A(*) : CANDLES collaboration, low temperature group, I Kim, D H Kwon, H L Kim, H J Lee, M K Lee, Y H Kim, and B : low temperature group. Status of 48ca double beta decay search and its future prospect in candles. *Journal of Physics: Conference Series*, 1468(1):012132, feb 2020. → page 72

[90] G Hagen, T Papenbrock, M Hjorth-Jensen, and D J Dean. Coupled-cluster computations of atomic nuclei. *Reports on Progress in Physics*, 77(9):096302, sep 2014. → page 72

[91] John D. Watts, Jürgen Gauss, and Rodney J. Bartlett. Coupled-cluster methods with noniterative triple excitations for restricted open-shell hartree–fock and other general single determinant reference functions. energies and analytical gradients. *The Journal of Chemical Physics*, 98(11):8718–8733, 1993. → page 72

[92] John D. Watts and Rodney J. Bartlett. Economical triple excitation equation-of-motion coupled-cluster methods for excitation energies. *Chemical Physics Letters*, 233(1):81–87, 1995. → page 72

[93] K. Hebeler, S. K. Bogner, R. J. Furnstahl, A. Nogga, and A. Schwenk. Improved nuclear matter calculations from chiral low-momentum interactions. *Phys. Rev. C*, 83:031301, Mar 2011. → pages xv, 73

[94] J. M. Yao, B. Bally, J. Engel, R. Wirth, T. R. Rodríguez, and H. Hergert. Ab initio treatment of collective correlations and the neutrinoless double beta decay of ^{48}Ca. *Phys. Rev. Lett.*, 124:232501, Jun 2020. → pages xv, 72, 74, 75

[95] L. Coraggio, A. Gargano, N. Itaco, R. Mancino, and F. Nowacki. Calculation of the neutrinoless double-β decay matrix element within the realistic shell model. *Phys. Rev. C*, 101:044315, Apr 2020. → pages xv, 74

[96] Fedor Šimkovic, Vadim Rodin, Amand Faessler, and Petr Vogel. $0\nu\beta\beta$ and $2\nu\beta\beta$ nuclear matrix elements, quasiparticle random-phase approximation, and isospin symmetry restoration. *Phys. Rev. C*, 87:045501, Apr 2013. → pages xv, 74

[97] J. Barea, J. Kotila, and F. Iachello. $0\nu\beta\beta$ and $2\nu\beta\beta$ nuclear matrix elements in the interacting boson model with isospin restoration. *Phys. Rev. C*, 91:034304, Mar 2015. → pages xv, 74

[98] Nuria López Vaquero, Tomás R. Rodríguez, and J. Luis Egido. Shape and pairing fluctuation effects on neutrinoless double beta decay nuclear matrix elements. *Phys. Rev. Lett.*, 111:142501, Sep 2013. → pages xv, 74

[99] J. M. Yao, L. S. Song, K. Hagino, P. Ring, and J. Meng. Systematic study of nuclear matrix elements in neutrinoless double-β decay with a beyond-mean-field covariant density functional theory. *Phys. Rev. C*, 91:024316, Feb 2015. → pages xv, 74

[100] A. A. Kwiatkowski, T. Brunner, J. D. Holt, A. Chaudhuri, U. Chowdhury, M. Eibach, J. Engel, A. T. Gallant, A. Grossheim, M. Horoi, A. Lennarz, T. D. Macdonald, M. R. Pearson, B. E. Schultz, M. C. Simon, R. A. Senkov, V. V. Simon, K. Zuber, and J. Dilling. New determination of double-β-decay properties in ^{48}Ca: High-precision $Q_{\beta\beta}$-value measurement and improved nuclear matrix element calculations. *Phys. Rev. C*, 89:045502, Apr 2014. → pages xv, 74

[101] Y. Iwata, N. Shimizu, T. Otsuka, Y. Utsuno, J. Menéndez, M. Honma, and T. Abe. Large-Scale Shell-Model Analysis of the Neutrinoless $\beta\beta$ Decay of ^{48}Ca. *Phys. Rev. Lett.*, 116:112502, Mar 2016. → pages xv, 74

[102] Robert Roth. Importance truncation for large-scale configuration interaction approaches. *Phys. Rev. C*, 79:064324, Jun 2009. → pages xv, 75

[103] M. Heinz, A. Tichai, J. Hoppe, K. Hebeler, and A. Schwenk. In-medium similarity renormalization group with three-body operators. *Phys. Rev. C*, 103:044318, Apr 2021. → page 75

[104] C. Matei, L. Buchmann, W. R. Hannes, D. A. Hutcheon, C. Ruiz, C. R. Brune, J. Caggiano, A. A. Chen, J. D'Auria, A. Laird, M. Lamey, ZH. Li, WP. Liu, A. Olin, D. Ottewell, J. Pearson, G. Ruprecht, M. Trinczek, C. Vockenhuber, and C. Wrede. Measurement of the cascade transition via the first excited state of ^{16}O in the ^{12}C$(\alpha,\gamma)^{16}$O reaction, and its s factor in stellar helium burning. *Phys. Rev. Lett.*, 97:242503, Dec 2006. → page 77

[105] P. Navrátil, S. Quaglioni, G. Hupin, C. Romero-Redondo, and A. Calci. Unified ab initio approaches to nuclear structure and reactions. *Physica Scripta*, 91(5):053002, May 2016. → page 77

[106] Rubin H. Landau. *Quantum Mechanics II: A Second Course in Quantum Theory.* Wiley, New York, 2nd edition, 1996. → pages 78, 83, 151

[107] Ian J. Thompson and Filomena M. Nunes. *Nuclear Reactions for Astrophysics: Principles, Calculation and Applications of Low-Energy Reactions.* Cambridge University Press, Cambridge, UK, 2009. → pages 81, 82, 95, 111

[108] P. Descouvemont. *Theoretical Models for Nuclear Astrophysics*. Nova Science, Hauppauge NY, 2003. → pages 81, 95

[109] P Descouvemont and D Baye. The r-matrix theory. *Reports on Progress in Physics*, 73(3):036301, feb 2010. → pages 82, 83

[110] Chloë Hebborn. *Study of the eikonal approximation to model exotic reactions*. PhD thesis, École Polytechnique de Bruxelles, 2020. → page 83

[111] Simone Baroni, Petr Navrátil, and Sofia Quaglioni. Unified ab initio approach to bound and unbound states: No-core shell model with continuum and its application to ^{7}He. *Phys. Rev. C*, 87:034326, Mar 2013. → pages 83, 86, 88

[112] Sofia Quaglioni and Petr Navrátil. Ab initio many-body calculations of nucleon-nucleus scattering. *Phys. Rev. C*, 79:044606, Apr 2009. → page 85

[113] Petr Navratil and Sofia Quaglioni. Ab initio nuclear reaction theory with applications to astrophysics, 2022. → page 86

[114] M. Hesse, J.-M. Sparenberg, F. Van Raemdonck, and D. Baye. Coupled-channel r-matrix method on a lagrange mesh. *Nuclear Physics A*, 640(1):37–51, 1998. → page 87

[115] M. Hesse, J. Roland, and D. Baye. Solving the resonating-group equation on a lagrange mesh. *Nuclear Physics A*, 709(1):184–200, 2002. → page 87

[116] Daniel Baye. Complements de physique nucleaire, 2006. → page 89

[117] M. Jacob and G. C. Wick. On the general theory of collisions for particles with spin. *Annals of physics*, 281(1-2):774–799, 2000. → page 92

[118] J. D. Walecka. Electron scattering from a quantized liquid drop. *Phys. Rev.*, 126:653–662, Apr 1962. → page 95

[119] J.L Friar. Low-energy theorems for nuclear compton and raman scattering and $0^+ \to 0^+$ two-photon decays in nuclei. *Annals of Physics*, 95(1):170–201, 1975. → page 95

[120] A. J. Krasznahorkay, M. Csatlós, L. Csige, Z. Gácsi, J. Gulyás, M. Hunyadi, I. Kuti, B. M. Nyakó, L. Stuhl, J. Timár, T. G. Tornyi, Zs. Vajta, T. J. Ketel, and A. Krasznahorkay. Observation of anomalous internal pair creation in ^{8}Be: A possible indication of a light, neutral boson. *Phys. Rev. Lett.*, 116:042501, Jan 2016. → pages 95, 108, 115, 122

[121] J. D. Walecka. *Electron Scattering for Nuclear and Nucleon Structure*. Cambridge University Press, Cambridge, UK, 2001. → page 96

[122] A. C. Hayes, J. Friar, G. M. Hale, and G. T. Garvey. Angular correlations in the e^+e^- decay of excited states in ^{8}Be. *Phys. Rev. C*, 105:055502, May 2022. → pages xviii, 99, 108, 122, 125

[123] M. Viviani, E. Filandri, L. Girlanda, C. Gustavino, A. Kievsky, L. E. Marcucci, and R. Schiavilla. $x17$ boson and the $^3\mathrm{H}(p, e^+e^-)^4\mathrm{He}$ and $^3\mathrm{He}(n, e^+e^-)^4\mathrm{He}$ processes: A theoretical analysis. *Phys. Rev. C*, 105:014001, Jan 2022. → pages xviii, 100, 122, 125

[124] M. Viviani. Private Communication, 2022. → page 100

[125] Daniele S. M. Alves. Signals of the qcd axion with mass of 17 MeV/c^2: Nuclear transitions and light meson decays. *Phys. Rev. D*, 103:055018, Mar 2021. → page 107

[126] Xilin Zhang and Gerald A. Miller. Can a protophobic vector boson explain the atomki anomaly? *Physics Letters B*, 813:136061, 2021. → page 124

[127] Jonathan L. Feng, Bartosz Fornal, Iftah Galon, Susan Gardner, Jordan Smolinsky, Tim M. P. Tait, and Philip Tanedo. Particle physics models for the 17 mev anomaly in beryllium nuclear decays. *Phys. Rev. D*, 95:035017, Feb 2017. → pages 107, 108

[128] Jonathan L. Feng, Tim M. P. Tait, and Christopher B. Verhaaren. Dynamical evidence for a fifth force explanation of the atomki nuclear anomalies. *Phys. Rev. D*, 102:036016, Aug 2020. → page 107

[129] T. W. Donnelly, S. J. Freedman, R. S. Lytel, R. D. Peccei, and M. Schwartz. Do axions exist? *Phys. Rev. D*, 18:1607–1620, Sep 1978. → pages 107, 124

[130] Jonathan Kozaczuk, David E. Morrissey, and S. R. Stroberg. Light axial vector bosons, nuclear transitions, and the ^{8}Be anomaly. *Phys. Rev. D*, 95:115024, Jun 2017. → pages 107, 124

[131] Rafael S. de Souza, Tan Hong Kiat, Alain Coc, and Christian Iliadis. Hierarchical bayesian thermonuclear rate for the 7be(n,p)7li big bang nucleosynthesis reaction. *The Astrophysical Journal*, 894(2):134, May 2020. → page 108

[132] Xilin Zhang and Gerald A. Miller. Can nuclear physics explain the anomaly observed in the internal pair production in the Beryllium-8 nucleus? *Phys. Lett. B*, 773:159–165, 2017. → page 108

[133] Brian D. Fields. The primordial lithium problem. *Annual Review of Nuclear and Particle Science*, 61(1):47–68, 2011. → page 109

[134] M. Asplund, D. L. Lambert, P. E. Nissen, F. Primas, and V. V. Smith. Lithium isotopic abundances in metal-poor halo stars. *The Astrophysical Journal*, 644(1):229–259, jun 2006. → page 109

[135] R. H. Cyburt, B. D. Fields, K. A. Olive, and T.-H. Yeh. Big bang nucleosynthesis: Present status. *Rev. Mod. Phys.*, 88:015004, Feb 2016. → page 109

[136] V. Somà, P. Navrátil, F. Raimondi, C. Barbieri, and T. Duguet. Novel chiral hamiltonian and observables in light and medium-mass nuclei. *Phys. Rev. C*, 101:014318, Jan 2020. → pages xvii, 109, 115, 117, 118

[137] Angelo Calci, Petr Navrátil, Robert Roth, Jérémy Dohet-Eraly, Sofia Quaglioni, and Guillaume Hupin. Can ab initio theory explain the phenomenon of parity inversion in ^{11}Be? *Phys. Rev. Lett.*, 117:242501, Dec 2016. → page 110

[138] J. Dohet-Eraly, P. Navrátil, S. Quaglioni, W. Horiuchi, G. Hupin, and F. Raimondi. ^{3}He (α , γ)^{7}Be and ^{3}H (α , γ)^{7}Li astrophysical S factors from the no-core shell model with continuum. *Physics Letters B*, 757:430–436, June 2016.

[139] F. Raimondi, G. Hupin, P. Navrátil, and S. Quaglioni. Deuteron-induced nucleon transfer reactions within an ab initio framework: First application to p-shell nuclei. *Phys. Rev. C*, 93:054606, May 2016. → page 110

[140] U. van Kolck. Few-nucleon forces from chiral lagrangians. *Phys. Rev. C*, 49:2932–2941, Jun 1994. → pages xvi, 110

[141] D.R. Tilley, C.M. Cheves, J.L. Godwin, G.M. Hale, H.M. Hofmann, J.H. Kelley, C.G. Sheu, and H.R. Weller. Energy levels of light nuclei a=5, 6, 7. *Nuclear Physics A*, 708(1):3–163, 2002. → pages xvi, 110

[142] A. Galonsky, R. A. Douglas, W. Haeberli, M. T. McEllistrem, and H. T. Richards. Deuteron-helium differential scattering cross sections. *Phys. Rev.*, 98:586–590, May 1955. → pages xvi, 111

[143] G.S. Mani and A. Tarratts. Elastic scattering of deuterons by alpha particles. *Nuclear Physics A*, 107(3):624–638, 1968. → pages xvi, 111

[144] D Baye and E M Tursunov. Isospin-forbidden electric dipole capture and the $\alpha(d,\gamma)$6li reaction. *Journal of Physics G: Nuclear and Particle Physics*, 45(8):085102, jun 2018. → page 111

[145] A. M. Mukhamedzhanov, Shubhchintak, and C. A. Bertulani. Primordial $\alpha + d \rightarrow^6$ Li + γ reaction and second lithium puzzle. *Phys. Rev. C*, 93:045805, Apr 2016. → page 111

[146] M. Anders, D. Trezzi, R. Menegazzo, M. Aliotta, A. Bellini, D. Bemmerer, C. Broggini, A. Caciolli, P. Corvisiero, H. Costantini, T. Davinson, Z. Elekes, M. Erhard, A. Formicola, Zs. Fülöp, G. Gervino, A. Guglielmetti, C. Gustavino, Gy. Gyürky, M. Junker, A. Lemut, M. Marta, C. Mazzocchi, P. Prati, C. Rossi Alvarez, D. A. Scott, E. Somorjai, O. Straniero, and T. Szücs. First direct measurement of the ^{2}H$(\alpha,\gamma)^6$Li cross section at big bang energies and the primordial lithium problem. *Phys. Rev. Lett.*, 113:042501, Jul 2014. → pages xvi, 112

[147] J. Kiener, H. J. Gils, H. Rebel, S. Zagromski, G. Gsottschneider, N. Heide, H. Jelitto, J. Wentz, and G. Baur. Measurements of the coulomb dissociation cross section of 156 mev ^{6}Li projectiles at extremely low relative fragment energies of astrophysical interest. *Phys. Rev. C*, 44:2195–2208, Nov 1991. → pages xvi, 112

[148] P. Mohr, V. Kölle, S. Wilmes, U. Atzrott, G. Staudt, J. W. Hammer, H. Krauss, and H. Oberhummer. Direct capture in the 3^+ resonance of ^{2}H$(\alpha,\gamma)^6$li. *Phys. Rev. C*, 50:1543–1549, Sep 1994. → pages xvi, 112

[149] R. G. H. Robertson, P. Dyer, R. A. Warner, R. C. Melin, T. J. Bowles, A. B. McDonald, G. C. Ball, W. G. Davies, and E. D. Earle. Observation of the capture reaction ^{2}H$(\alpha, \gamma)^6$Li and its role in production of ^{6}Li in the big bang. *Phys. Rev. Lett.*, 47:1867–1870, Dec 1981. → pages xvi, 112

[150] Micah D. Schuster, Sofia Quaglioni, Calvin W. Johnson, Eric D. Jurgenson, and Petr Navrátil. Operator evolution for ab initio electric dipole transitions of ^{4}He. *Phys. Rev. C*, 92:014320, Jul 2015. → page 113

[151] Y. Xu, K. Takahashi, S. Goriely, M. Arnould, M. Ohta, and H. Utsunomiya. Nacre ii: an update of the nacre compilation of charged-particle-induced thermonuclear reaction rates for nuclei with mass number a¡16. *Nuclear Physics A*, 918:61–169, 2013. → pages xvii, 114

[152] D. Trezzi, M. Anders, M. Aliotta, A. Bellini, D. Bemmerer, A. Boeltzig, C. Broggini, C.G. Bruno, A. Caciolli, F. Cavanna, P. Corvisiero, H. Costantini, T. Davinson, R. Depalo, Z. Elekes, M. Erhard, F. Ferraro, A. Formicola, Zs. Fülop, G. Gervino, A. Guglielmetti, C. Gustavino, Gy. Gyürky, M. Junker, A. Lemut, M. Marta, C. Mazzocchi, R. Menegazzo, V. Mossa, F. Pantaleo, P. Prati, C. Rossi Alvarez, D.A. Scott, E. Somorjai, O. Straniero, T. Szücs, and M. Takacs. Big bang 6li nucleosynthesis studied deep underground (luna collaboration). *Astroparticle Physics*, 89:57–65, 2017. → pages xvii, 114

[153] TUNL Nuclear Data Evaluation Project. Energy Level Diagram ^{8}Be. https://nucldata.tunl.duke.edu/nucldata/figures/08figs/08_04_2004.pdf, 2004. → pages xvii, 116

[154] D.R. Tilley, J.H. Kelley, J.L. Godwin, D.J. Millener, J.E. Purcell, C.G. Sheu, and H.R. Weller. Energy levels of light nuclei a=8,9,10. *Nuclear Physics A*, 745(3):155–362, 2004. → page 118

[155] A. Pakou, F. Cappuzzello, N. Keeley, L. Acosta, C. Agodi, X. Aslanoglou, S. Calabrese, D. Carbone, M. Cavallaro, A. Foti, G. Marquínez-Durán, I. Martel, M. Mazzocco, C. Parascandolo, D. Pierroutsakou, K. Rusek, O. Sgouros, V. Soukeras, E. Strano, V. A. B. Zagatto, and K. Zerva. Global description of the $^7\mathrm{Li} + p$ reaction at 5.44 mev/u in a continuum-discretized coupled-channels approach. *Phys. Rev. C*, 96:034615, Sep 2017. → pages xvii, 121

[156] A. Pakou, V. Soukeras, F. Cappuzzello, L. Acosta, C. Agodi, X. Aslanoglou, S. Calabrese, D. Carbone, M. Cavallaro, A. Foti, N. Keeley, G. Marquinez-Duran, I. Martel, M. Mazzocco, C. Parascandolo, D. Pierroutsakou, K. Rusek, O. Sgouros, E. Strano, and V. A. B. Zagatto. Probing the cluster structure of ^{7}Li via elastic scattering on protons and deuterons in inverse kinematics. *Phys. Rev. C*, 94:014604, Jul 2016. → pages xvii, 121

[157] D. Zahnow, C. Angulo, C. Rolfs, S. Schmidt, W. H. Schulte, and E. Somorjai. The s(e) factor of7li(p, γ)8be and consequences for s(e) extrapolation in7be(p, γ0)8b. *Zeitschrift für Physik A Hadrons and Nuclei*, 351(2):229–236, Jun 1995. → pages xvii, 122, 123

[158] A. J. Krasznahorkay, M. Csatlós, L. Csige, J. Gulyás, A. Krasznahorkay, B. M. Nyakó, I. Rajta, J. Timár, I. Vajda, and N. J. Sas. New anomaly observed in ^{4}He supports the existence of the hypothetical x17 particle. *Phys. Rev. C*, 104:044003, Oct 2021. → page 122

[159] N. J. Sas, A. J. Krasznahorkay, M. Csatlós, J. Gulyás, B. Kertész, A. Krasznahorkay, J. Molnár, I. Rajta, J. Timár, I. Vajda, and M. N. Harakeh. Observation of the x17 anomaly in the ^{7}li(p,$e^{+}e^{-}$)^{8}be direct proton-capture reaction, 2022. → page 124

[160] Firak, D. S., Krasznahorkay, A. J., Csatlós, M., Csige, L., Gulyás, J., Koszta, M., Szihalmi, B., Timár, J., Nagy, Á., Sas, N. J., and Krasznahorkay, A. Confirmation of the existence of the x17 particle. *EPJ Web Conf.*, 232:04005, 2020. → pages xviii, 125, 127

[161] Johannes Backens and Marc Vanderhaeghen. X17 discovery potential in the $\gamma n \to e^{+}e^{-}n$ process at electron scattering facilities. *Phys. Rev. Lett.*, 128:091802, Mar 2022. → pages xviii, 127

[162] Yonatan Mishnayot, Ayala Glick-Magid, Hitesh Rahangdale, Guy Ron, Doron Gazit, Jason T. Harke, Micha Hass, Ben Ohayon, Aaron Gallant, Nicholas D. Scielzo, Sergey Vaintruab, Richard O. Hughes, Tsviki Hirsch, Christian Forssén, Daniel Gazda, Peter Gysbers, Javier Menéndez, Petr Navrátil, Leonid Weissman, Arik Kreisel, Boaz Kaizer, Hodaya Daphna, and Maayan Buzaglo. Constraining new physics with a novel measurement of the ^{23}Ne β-decay branching ratio, 2021. → page 129

[163] A. J. Krasznahorkay, M. Csatlos, L. Csige, J. Gulyas, M. Koszta, B. Szihalmi, J. Timar, D. S. Firak, A. Nagy, N. J. Sas, and A. Krasznahorkay. New evidence supporting the existence of the hypothetic x17 particle, 2019. → page 129

[164] A. J. Krasznahorkay, A. Krasznahorkay, M. Begala, M. Csatlós, L. Csige, J. Gulyás, A. Krakó, J. Timár, I. Rajta, I. Vajda, and N. J. Sas. New anomaly observed in ^{12}C supports the existence and the vector character of the hypothetical X17 boson. *Phys. Rev. C*, 106:L061601, Dec 2022. → page 129

[165] Morris E. Rose. *Elementary theory of angular momentum*. Wiley, New York, 1957. → page 144

[166] L. C. Biedenharn, James D. Louck, and Cambridge Core EBA eBooks Complete Collection. *Angular momentum in quantum physics: theory and application*, volume 8. Cambridge University Press, New York, NY, USA;Cambridge, [Cambridgeshire];, 1984. → page 144

[167] Chien-Yeah Seng. Private Communication, 2022. → page 150

[168] T. W. Donnelly and W. C. Haxton. Multipole operators in semileptonic weak and electromagnetic interactions with nuclei: Harmonic oscillator single-particle matrix elements. *Atomic data and nuclear data tables*, 23(2):103–176, 1979. → page 152

[169] Wick Haxton and Cecilia Lunardini. Sevenoperators, a mathematica script for harmonic oscillator nuclear matrix elements arising in semileptonic electroweak interactions. *Computer Physics Communications*, 179(5):345–358, 2008. → page 152

Appendix A

Preliminary Material

This section compiles useful definitions and identities. Further properties of CGs, $3nj$s and D-matrices are tabulated in [35, 41, 165, 166].

A.1 Pauli Matrices

We use the convention:

$$\sigma_x = \begin{pmatrix} 0 & 1 \\ 1 & 0 \end{pmatrix} \tag{A.1}$$

$$\sigma_y = \begin{pmatrix} 0 & -i \\ i & 0 \end{pmatrix} \tag{A.2}$$

$$\sigma_z = \begin{pmatrix} 1 & 0 \\ 0 & -1 \end{pmatrix} \tag{A.3}$$

A.2 Angular Momentum Coupling

A.2.1 Properties of Clebsch-Gordan Coefficients

The orthogonality property:

$$\sum_{m_1 m_2} (j_1 m_1 j_2 m_2 | jm) \left(j_1 m_1 j_2 m_2 | j' m'\right) = \delta_{jj'} \delta_{mm'} \ . \tag{A.4}$$

The completeness property:

$$\sum_{jm} (j_1 m_1 j_2 m_2 | jm) \left(j_1 m_1' j_2 m_2' | jm\right) = \delta_{m_1 m_1'} \delta_{m_2 m_2'} \ . \tag{A.5}$$

The entries may be reordered by

$$(j_1 m_1 j_2 m_2|jm) = (-)^{j_2+m_2} \frac{\hat{j}}{\hat{j}_1} (j_2 - m_2 jm|j_1 m_1) \tag{A.6}$$

$$= (-)^{j_1-m_1} \frac{\hat{j}}{\hat{j}_2} (jmj_1 - m_1|j_2 m_2) \tag{A.7}$$

$$= (-)^{j_1+j_2-j} (j_2 m_2 j_1 m_1|jm) \ . \tag{A.8}$$

Some particularly useful values (from [53]):

$$\begin{aligned} ((j-1)01\lambda|j\lambda) =& \sqrt{\frac{j+1}{2(2j-1)}} \ , \\ (j01\lambda|j\lambda) =& -\frac{\lambda}{\sqrt{2}} \ , \\ ((j+1)01\lambda|j\lambda) =& \sqrt{\frac{j}{2(2j+3)}} \ . \end{aligned} \tag{A.9}$$

A.2.2 Definitions and Properties of $3nj$ Symbols

The $3j$ symbol is defined in terms of the CG coefficients:

$$\begin{pmatrix} j_1 & j_2 & j_3 \\ m_1 & m_2 & m_3 \end{pmatrix} = (-)^{j_1-j_2-m_3} \hat{j}_3^{-1} (j_1 m_1 j_2 m_2|j_3 - m_3) \ . \tag{A.10}$$

Explicitly the $6j$ is defined by a sum over four CGs:

$$\begin{aligned} \begin{Bmatrix} j_1 & j_2 & j_{12} \\ j_3 & j & j_{23} \end{Bmatrix} = \frac{(-)^{j_1+j_2+j_3+j}}{\hat{j_{12}}\hat{j_{23}}} \sum_{m_1 m_2} & (j_1 m_1 j_2 m_2|j_{12} m_{12}) (j_{12} m_{12} j_3 m_3|jm) \\ & \times (j_2 m_2 j_3 m_3|j_{23} m_{23}) (j_1 m_1 j_{23} m_{23}|jm) \ , \end{aligned} \tag{A.11}$$

but it also appears in the appropriate sum over three CGs:

$$\begin{aligned} (-)^{j_1+j_2+j_3+j} \hat{j_{12}}\hat{j_{23}} \begin{Bmatrix} j_1 & j_2 & j_{12} \\ j_3 & j & j_{23} \end{Bmatrix} (j_1 m_1 j_{23} m_{23}|jm) = \\ \sum_{m_2} (j_1 m_1 j_2 m_2|j_{12} m_{12}) (j_{12} m_{12} j_3 m_3|jm) (j_2 m_2 j_3 m_3|j_{23} m_{23}) \ . \end{aligned} \tag{A.12}$$

The $9j$ symbol is defined by:

$$\left\{ \begin{array}{ccc} j_1 & j_2 & j_{12} \\ j_3 & j_4 & j_{34} \\ j_{13} & j_{24} & j \end{array} \right\} = \sum_{m_1 m_2} \sum_{m_3 m_4} \sum_{m_{12} m_{34}} \sum_{m_{13} m_{24} m} \left(\begin{array}{ccc} j_1 & j_2 & j_{12} \\ m_1 & m_2 & m_{12} \end{array} \right) \left(\begin{array}{ccc} j_3 & j_4 & j_{34} \\ m_3 & m_4 & m_{34} \end{array} \right)$$
$$\times \left(\begin{array}{ccc} j_{13} & j_{24} & j \\ m_{13} & m_{24} & m \end{array} \right) \left(\begin{array}{ccc} j_1 & j_3 & j_{13} \\ m_1 & m_3 & m_{13} \end{array} \right) \left(\begin{array}{ccc} j_2 & j_4 & j_{24} \\ m_2 & m_4 & m_{24} \end{array} \right) \left(\begin{array}{ccc} j_{12} & j_{34} & j \\ m_{12} & m_{34} & m \end{array} \right) . \tag{A.13}$$

When one of the elements of a $9j$ is zero, we can reduce it to a $6j$, i.e.

$$\left\{ \begin{array}{ccc} j_1 & j_2 & j_{12} \\ j_3 & j_4 & j_{34} \\ j_{13} & j_{24} & 0 \end{array} \right\} = \delta_{j_{12} j_{34}} \delta_{j_{13} \delta_{24}} \hat{j}_{12}^{-1} \hat{j}_{13}^{-1} (-)^{j_{12}+j_{13}+j_2+j_3} \left\{ \begin{array}{ccc} j_1 & j_2 & j_{12} \\ j_4 & j_3 & j_{13} \end{array} \right\} . \tag{A.14}$$

A $6j$ can be reduced , i.e.

$$\left\{ \begin{array}{ccc} j_1 & j_2 & j_3 \\ 0 & j_3' & j_2' \end{array} \right\} = \frac{(-)^{j_1+j_2+j_3}}{\hat{j}_2 \hat{j}_3} \delta_{j_2 j_2'} \delta_{j_3 j_3'} \Delta(j_1 j_2 j_3) , \tag{A.15}$$

which introduces the triangular delta, defined as

$$\Delta(j_1 j_2 j_3) = \begin{cases} 1 & \text{if } |j_1 - j_2| \leq j_3 \leq j_1 + j_2 \\ 0 & \text{otherwise} \end{cases} . \tag{A.16}$$

Sometimes angular momentum coupling is expressed in terms of the Racah symbols:

$$W(j_1 j_2 l_2 l_1; j_3 l_3) = (-)^{j_1+j_2+l_1+l_2} \left\{ \begin{array}{ccc} j_1 & j_2 & j_3 \\ l_1 & l_2 & l_3 \end{array} \right\} . \tag{A.17}$$

A.3 Rotations and Wigner D-matrices

A rotation of the coordinate axes by the Euler angles α, β, γ induces a unitary transformation on angular momentum eigenstates $|jm\rangle$. The rotation $\mathcal{R}(\alpha, \beta, \gamma)$ corresponds to a rotation about the z axis by the angle α, then about the new y' axis by β, and then about the new z'' axis by γ (all right-hand rotations). This is equivalent to the following sequence of rotations about the original axes: first γ about z, then β about y and then α about z. These steps correspond to the operator:

$$\begin{aligned} \mathcal{R}(\alpha, \beta, \gamma) =& e^{-i\gamma J_{z''}} e^{-i\beta J_{y'}} e^{-i\alpha J_z} \\ =& e^{-i\alpha J_z} e^{-i\beta J_y} e^{-i\gamma J_z} \end{aligned} \tag{A.18}$$

where J_ξ is the angular momentum projection operator for the axis ξ (following the conventions of [35]). The inverse of the rotation is:

$$\mathcal{R}^{-1}(\alpha,\beta,\gamma) = \mathcal{R}^\dagger(\alpha,\beta,\gamma) = \mathcal{R}(-\gamma,-\beta,-\alpha)\ . \tag{A.19}$$

The Wigner D-matrix is the matrix element of the rotation operator, i.e.

$$\left\langle j'm'\right| \mathcal{R}(\alpha,\beta,\gamma)\left|jm\right\rangle = \delta_{j'j} D^j_{m'm}(\alpha,\beta,\gamma) \tag{A.20}$$

where

$$D^j_{m'm}(\alpha,\beta,\gamma) = e^{-im'\alpha} d^j_{m'm}(\beta) e^{-im\gamma} \tag{A.21}$$

with the "small d-matrix" defined by

$$d^j_{m'm}(\beta) = \left\langle jm'\right| e^{-i\beta J_y}\left|jm\right\rangle = D^j_{m'm}(0,\beta,0)\ . \tag{A.22}$$

It follows from (A.19) that

$$D^{j*}_{m'm}(\alpha,\beta,\gamma) = D^j_{m'm}(-\gamma,-\beta,-\alpha)\ . \tag{A.23}$$

The conjugate is also related by the identities

$$D^j_{mk}(\alpha,\beta,\gamma) = (-)^{m-k}\, D^{j*}_{-m-k}(\alpha,\beta,\gamma);, \tag{A.24}$$

$$D^{j*}_{mk}(\alpha,\beta,\gamma) = (-)^{m-k}\, D^{j}_{-m-k}(\alpha,\beta,\gamma)\ . \tag{A.25}$$

When both indices are set to zero, the D-matrix elements are given by ordinary Legendre polynomials, i.e.

$$D^j_{00}(\alpha,\beta,\gamma) = d^j_{00}(\beta) = P_j(\cos\beta)\ . \tag{A.26}$$

The D-matrices relate quantum states in the rotated frame to a linear combination of states in the original frame, i.e.

$$\mathcal{R}(\alpha,\beta,\gamma)\left|jm\right\rangle = \sum_{m'} D^j_{m'm}(\alpha,\beta,\gamma)\left|jm'\right\rangle\ . \tag{A.27}$$

The wavefunction in the rotated frame $\psi_{jm}(r,\theta',\phi',\sigma')$ is related to $\psi_{jm}(r,\theta,\phi,\sigma)$ in the original frame by

$$\psi_{jm}(r,\theta',\phi',\sigma') = \sum_{m'} D^j_{m'm}(\alpha,\beta,\gamma)\psi_{jm'}(r,\theta,\phi,\sigma) \tag{A.28}$$

Here θ,ϕ and θ',ϕ' are the polar coordinates in the initial and rotated frames (and σ and σ' are the initial and rotated spin variables respectively). A spherical tensor operator

transforms as

$$\mathcal{R}(\alpha,\beta,\gamma)O_{jm}\mathcal{R}^{\dagger}(\alpha,\beta,\gamma)=\sum_{m'}D^{j}_{m'm}(\alpha,\beta,\gamma)O_{jm'}\ . \tag{A.29}$$

D-matrices (with the same angles) can be combined by the product rules:

$$D^{j}_{mk}D^{j'}_{m'k'}=\sum_{J=|j-j'|}^{j+j'}\left(jmj'm'|J(m+m')\right)\left(jkj'k'|J(k+k')\right)D^{J}_{(m+m')(k+k')}\ , \tag{A.30}$$

$$D^{j}_{mk}D^{j'*}_{m'k'}=\sum_{J=|j-j'|}^{j+j'}(-)^{m'-k}\left(jmj'-m'|J(m-m')\right)\left(jkj'-k'|J(k-k')\right)D^{J}_{(m-m')(k-k')}\ . \tag{A.31}$$

A.4 Useful Functions

Explicitly the radial harmonic oscillator wavefunctions are given by

$$R_{nl}(r,b)=\sqrt{\frac{2\Gamma(n+1)}{(b^2)^{l+\frac{3}{2}}\Gamma(n+l+\frac{3}{2})}}r^{l}\exp\left(-\frac{r^2}{2b^2}\right)L_n^{l+\frac{1}{2}}\left(\frac{r^2}{b^2}\right)\ , \tag{A.32}$$

where $b=\sqrt{\frac{\hbar}{m_N\Omega}}$ is the oscillator length, Γ is the Euler gamma function and $L_n^{l+\frac{1}{2}}$ is a generalized Laguerre polynomial.

The first three associated Laguerre polynomials are

$$L_0^{l+\frac{1}{2}}(x)=1\ , \tag{A.33}$$

$$L_1^{l+\frac{1}{2}}(x)=l-x+\frac{3}{2}\ , \tag{A.34}$$

$$L_2^{l+\frac{1}{2}}(x)=\frac{1}{2}\left[(l+\frac{3}{2})(l+\frac{5}{2})-2(l+\frac{5}{2})x+x^2\right]\ . \tag{A.35}$$

Further polynomials can be derived via the recursion relation [40]:

$$L_n^{l+\frac{1}{2}}(x)=L_n^{l+\frac{3}{2}}(x)-L_{n-1}^{l+\frac{3}{2}}(x)\ . \tag{A.36}$$

Appendix B

The Connection between QED and Nucleon Currents

B.1 Relativistic Formalism

We use the metric:

$$\eta = \begin{pmatrix} 1 & & & \\ & -1 & & \\ & & -1 & \\ & & & -1 \end{pmatrix} . \tag{B.1}$$

The 4-momentum of a particle is $P = (E, \vec{p})$ where the energy is the first component $E = P^0$ and the other components are the 3-momentum $\vec{p}$. The square of the 4-momentum is the squared mass for observable "on-shell" particles, i.e.

$$P^2 = P^\mu P_\mu = P_\nu \eta^{\mu\nu} P_\mu = E^2 - p^2 = m^2 . \tag{B.2}$$

We use the following convention for Dirac gamma matrices (where each block is a 2×2 matrix ($1 = I_{2\times 2}$, σ_i are Pauli matrices)):

$$\gamma^0 = \begin{pmatrix} 1 & 0 \\ 0 & -1 \end{pmatrix} , \tag{B.3}$$

$$\vec{\gamma} = \gamma^0 \begin{pmatrix} 0 & \vec{\sigma} \\ \vec{\sigma} & 0 \end{pmatrix} , \tag{B.4}$$

$$\gamma_5 = \begin{pmatrix} 0 & 1 \\ 1 & 0 \end{pmatrix} . \tag{B.5}$$

We can also form the anti-symmetric tensor:

$$\sigma^{\mu\nu} = \frac{i}{2}\left(\gamma^\mu\gamma^\nu - \gamma^\nu\gamma^\mu\right) . \tag{B.6}$$

Any 4×4 matrix can be constructed as a linear combination of 1, γ^5, γ^μ, $\gamma^\mu\gamma^5$ and $\sigma^{\mu\nu}$. We sandwich them between 4-component Dirac spinors to create scalars, pseudoscalars, vectors, axial-vectors, and anti-symmetric tensors respectively. For example, a lepton vector current is: $\ell^\mu = \bar{u}\gamma^\mu u$.

B.2 Non-relativistic Expansion of Dirac Spinors

In QED, fermions are 4-component spinors. However, in non-relativistic quantum mechanics we have a 2-component spinor χ. A Dirac spinor of mass M takes the form:

$$u(p,\sigma) = \sqrt{E+M}\begin{pmatrix} \chi_\sigma \\ \frac{\vec{\sigma}\cdot\vec{p}}{E+M}\chi_\sigma \end{pmatrix} . \tag{B.7}$$

We use the notation $\bar{u} = u^\dagger\gamma_0$ and with this convention $u^\dagger u = 2E$ ($\bar{u}u = 2M$). We can take the non-relativistic limits of matrix elements between $\bar{u}(p',s')$ and $u(p,s)$ by expanding in powers of inverse mass [57, 167] as shown in Table B.1. We neglect terms of order $\mathcal{O}(\frac{1}{M^2})$ and define $q = p - p'$.

$\bar{u}(p',s')\,(\cdots)\,u(p,s)$	$2M\chi^\dagger_{s'}\,(\cdots)\,\chi_s$
1	1
γ_5	$\frac{\vec{\sigma}\cdot\vec{q}}{2M}$
γ^0	1
$\vec{\gamma}$	$\frac{\vec{p}+\vec{p}'}{2M} + \frac{i(\vec{q}\times\vec{\sigma})}{2M}$
$\gamma^0\gamma_5$	$\frac{\vec{\sigma}\cdot(\vec{p}+\vec{p}')}{2M}$
$\vec{\gamma}\gamma_5$	$\vec{\sigma}$
$\frac{1}{M}\sigma^{0i}$	0
$\frac{1}{M}\sigma^{ij}$	$\frac{\epsilon^{ijk}\sigma^k}{M}$
$\frac{1}{M}\sigma^{0i}\gamma_5$	$\frac{i\sigma^i}{M}$
$\frac{1}{M}\sigma^{ij}\gamma_5$	0

Table B.1: Equivalent matrix elements between Dirac spinors (left) and those taken in the nonrelativistic limit (right).

B.3 Nucleon Currents

Following [53], we can model the nucleon as a Dirac spinor but the vector interaction must include two form factors $F_1(q^2)$ and $F_2(q^2)$. For protons: $F_{1p}(0) = F_{2p}(0) = 1$, while for neutrons: $F_{1n}(0) = 0$, $F_{2n}(0) = 1$. The single-nucleon vertex for a vector interaction (e.g.

with a photon) is

$$\gamma_\mu^V = F_1\gamma_\mu + i\frac{\kappa}{2m_N}F_2\sigma^{\mu\nu}q_\mu \,, \tag{B.8}$$

where κ is the anomalous magnetic moment. In principle κ is non-zero for electrons as well due to QED corrections but is very small [106].

The form factors are often rearranged into the linear combinations $G_E = F_1 - \frac{\kappa q^2}{4m_N^2}F_2$ and $G_M = F_1 + \kappa F_2$. To leading order in $\frac{q^2}{m_N^2}$, $G_{Ep} = 1$, $G_{En} = 0$, $G_{Mp} = g_p = 1 + \kappa_p$, $G_{Mn} = g_n = \kappa_n$. In the isospin picture, the form factors have isoscalar and isovector components $F_i = \frac{1}{2}\left(F_i^S + \tau_z F_i^V\right)$, and so $F_1^S = F_1^V = 1$, $F_2^S = g_p + g_n = 0.88$, and $F_2^V = g_p - g_n = 4.706$.

We treat the nucleons as non-relativistic point particles with spin and a non-zero anomalous magnetic moment. Using the expansion above in Section B.2, we can attach the form factors to the multipole operators. We have a clear correspondence between $e\gamma_0^V$ and the charge operator, i.e.

$$\frac{1}{2m_N}\bar{u}(p',s')e\gamma_0^V u(p,s) \simeq eF_1\chi_{s'}^\dagger\chi_s \tag{B.9}$$

$$= e\frac{1+\tau_z}{2}\chi_{s'}^\dagger\chi_s \,, \tag{B.10}$$

whereas $e\vec{\gamma}^V$ gives the convection current and magnetization (as in Section 2.10):

$$\frac{1}{2m_N}\bar{u}(p',s')e\vec{\gamma}^V u(p,s) \simeq \chi_{s'}^\dagger\left[F_1\left(\frac{\vec{p}+\vec{p}'}{2m_N} + \frac{i\left(\vec{q}\times\vec{\sigma}\right)}{2m_N}\right) + \frac{i\kappa}{2m_N}F_2\vec{q}\times\vec{\sigma}\right]\chi_s \tag{B.11}$$

$$= e\frac{1+\tau_z}{2}\chi_{s'}^\dagger\chi_s\frac{\vec{p}+\vec{p}'}{2m_N} + \chi_{s'}^\dagger\left[\mu\vec{\nabla}\times\vec{\sigma}\right]\chi_s \,. \tag{B.12}$$

A free nucleon is a spinor times a plane wave. The nucleons in nuclei can be decomposed into linear combinations of these states. The vector current density $\mathcal{J}_\mu^V(\vec{r})$ is evaluated by inserting γ_μ^V between those basis states. The spatial dependence can be organized into multipole operators and we must attach the appropriate form factors.

For $\mu = 0$ we may write

$$\rho(q) = \int \mathrm{d}^3r \sum_{JM} C_{JM}^V(q,r)$$

$$\mathcal{C}_{JM}^V(q,r) = M_{JM}(q,r)F_1(q^2) \,. \tag{B.13}$$

For $\mu \in (x,y,z)$, we decompose into the longitudinal and transverse multipoles (as in

Section 3.1.1). Schematically (dropping q, r and JM):

$$\mathcal{L}^V = -\frac{Q}{q}F_1 M \ , \tag{B.14}$$

$$\mathcal{T}^{V,E} = \frac{q}{m_N}\left[F_1\Delta' + \frac{G_M}{2}\Sigma\right] \ , \tag{B.15}$$

$$\mathcal{T}^{V,M} = -i\frac{q}{m_N}\left[F_1\Delta - \frac{G_M}{2}\Sigma'\right] \ , \tag{B.16}$$

where we use the short-hand multipole operators listed in Section B.4.

The nucleon axial-vector current is:

$$\gamma^A_\mu = F_A\gamma_\mu\gamma_5 - iF_P q_\mu\gamma_5 \ , \tag{B.17}$$

where $F_A(0) = g_A$ and the pseudo-scalar form factor is determined via $F_P = \frac{2m_N F_A}{q^2+m_\pi^2}$ due to the Goldberger-Treiman relation [54]. And so we have the operators:

$$\mathcal{C}^A = -\frac{iq}{M}\left[F_A\Omega - \frac{1}{2}\left(F_A - \frac{Q}{2m_N}F_P\right)\Sigma''\right] \ , \tag{B.18}$$

$$\mathcal{L}^A = i\left[F_A + \frac{q^2}{2m_N}F_P\right]\Sigma'' \ , \tag{B.19}$$

$$\mathcal{T}^{A,E} = iF_A\Sigma' \ , \tag{B.20}$$

$$\mathcal{T}^{A,M} = F_A\Sigma \ . \tag{B.21}$$

B.4 Seven Multipole Operators

Single-particle multipole operators can be expressed as product of form factors and the following seven operators [168, 169]:

1.
$$M_{JM}(q,r) \ , \tag{B.22}$$

2.
$$\Delta_{JM}(q,r) = \vec{M}_{JJM}(q,r)\cdot\frac{\vec{\nabla}}{q} \ , \tag{B.23}$$

3.
$$\Delta'_{JM}(q,r) = -i\left(\frac{\vec{\nabla}}{q}\times\vec{M}_{JJM}(q,r)\right)\cdot\frac{\vec{\nabla}}{q} \ , \tag{B.24}$$

4.
$$\Sigma_{JM}(q,r) = \vec{M}_{JJM}(q,r)\cdot\vec{\sigma} \ , \tag{B.25}$$

5.

$$\Sigma'_{JM}(q,r) = -i\left(\frac{\vec{\nabla}}{q} \times \vec{M}_{JJM}(q,r)\right) \cdot \vec{\sigma}\ , \tag{B.26}$$

6.

$$\Sigma''_{JM}(q,r) = \left(\frac{\vec{\nabla}}{q} M_{JM}\right) \cdot \vec{\sigma}\ , \tag{B.27}$$

7.

$$\Omega_{JM}(q,r) = M_{JM}(q,r)\vec{\sigma} \cdot \frac{\vec{\nabla}}{q}\ , \tag{B.28}$$

where $M_{JM}(q,r) = j_J(qr)Y_{JM}(\Omega_r)$ and $\vec{M}_{JLM}(q,r) = j_L(qr)\vec{Y}_{JLM}(\Omega_r)$ and the gradient $\vec{\nabla}$ is with respect to $\vec{r}$.

In some situations it is useful to form the combination:

$$\Omega'_{JM} = M_{JM}\vec{\sigma} \cdot \vec{\nabla} + \frac{1}{2}\Sigma''_{JM}\ . \tag{B.29}$$